

***From Single Cells to Microtissues:  
Using Advanced Culture Techniques to Create a Better  
Understanding of Microplastic Toxicity***

Von der Fakultät für Ingenieurwissenschaften  
der Universität Bayreuth  
zur Erlangung der Würde eines  
**Doktor-Ingenieur (Dr.-Ing.)**  
genehmigte Dissertation

von

M. Sc. Matthias Sebastian Völkl

aus

Bayreuth

Erstgutachterin: Frau Prof. Dr. Ruth Freitag

Zweitgutachterin: Frau Prof. Dr. Heike Feldhaar

Tag der mündlichen Prüfung: 09.08.2023

Lehrstuhl Bioprozesstechnik

Universität Bayreuth

2023



# Table of contents

Danksagung .....	I
Preamble .....	III
List of Abbreviations.....	IV
Kurzfassung .....	1
Abstract .....	4
1. Introduction.....	7
1.1. Usage of cell cultivation in microplastic research .....	8
1.2. Particle-cell interaction – what is known from the literature.....	8
1.3. Biological effects of MP on a cellular level.....	13
1.4. Relevant fundamentals for cell culture assays used in this work .....	14
1.5. Polarisation of macrophages.....	19
1.6. Primary cells in microplastic research .....	19
1.7. Usage of more complex three-dimensional cell cultivation in microplastic research .....	20
1.8. Model organisms in microplastic research.....	22
1.8.1. Unicellular organisms in microplastic research.....	22
1.8.2. Terrestrial model organisms.....	23
1.9. Objective of this work .....	24
2. Methods .....	26
2.1. Flow cytometry.....	26
2.2. Characterisation of the used particles in this study .....	26
2.3. Cell lines used in this work .....	28
2.4. Cryopreservation and thawing of cells.....	29
2.5. Estimation of the cell count and viability.....	30
2.6. Polarisation of macrophages.....	30
2.7. Isolation and cultivation of primary <i>E.fetida</i> cells.....	31
2.8. Transwell seeding .....	31
2.9. Spheroid formation .....	32

2.10.	Agarose micro-array embedding.....	33
2.11.	Gelatine Capsules Embedding .....	34
2.12.	Cell Assays .....	34
2.12.1.	MTT Assay.....	34
2.12.2.	Proliferation assay by cell count.....	35
2.12.3.	ROS Assay .....	35
2.12.4.	CFSE staining.....	36
2.12.5.	CTV staining .....	36
2.12.6.	LDH assay.....	37
2.12.7.	COMET Assay .....	37
2.12.8.	Enzyme-Linked Immunosorbent-Assay .....	38
2.12.9.	Lucifer Yellow Assay .....	39
2.13.	Ribonucleic acid Sequencing .....	39
2.14.	Particle distribution during cell division .....	40
2.15.	Analysis of particle excretion after ingestion .....	40
2.16.	Single-cell sorting .....	40
2.17.	Protist cultivation .....	41
2.18.	Statistics.....	43
2.19.	Licence agreements.....	43
3.	Biological interactions and effects of microplastic on a cellular level .....	44
3.1.	Quantitative PCI analysis and the dependency of macrophages' polarisation state .....	44
3.1.1.	Quantification of PCI with the flow cytometry.....	45
3.1.2.	Influence of polarisation state of macrophages on the PCI .....	47
3.1.3.	Summary and conclusion .....	50
3.2.	Particle distribution after ingestion of MPP .....	51
3.3.	Cellular effects induced by MPP.....	57
3.3.1.	Influence of the PCI .....	57
3.3.2.	Influence of the particle size .....	60



3.3.3.	Influence of the protein corona design .....	67
3.3.4.	Influence of monomer residues .....	69
3.3.5.	Influence of the polymer type .....	70
3.3.6.	Influence of artificial ageing of particles .....	73
3.3.7.	Influence of paint microparticle fractions .....	92
3.3.8.	Summary and conclusion .....	94
3.4.	Excretion behaviour of ingested particles .....	96
4.	Effects of MP on microtissue .....	100
4.1.	Effects of microplastic in the transwell assay .....	100
4.1.1.	Influence of microplastic on the epithelial monolayer integrity .....	101
4.1.2.	Migration of particles through an epithelial layer .....	102
4.2.	Interactions of microplastic with spheroid microtissue .....	105
4.2.1.	Establishment of spheroid cultivation .....	105
4.2.2.	Interaction of spheroids with MPP .....	109
4.2.3.	Establishment of spheroid analysis using thin sectioning .....	111
4.2.4.	Co-cultivation of spheroids with macrophages .....	113
4.3.	Summary and conclusion .....	115
5.	The effect of MP on primary intestinal cells from <i>E. fetida</i> .....	116
6.	Effects of MP on unicellular organisms .....	118
6.1.	Ingestion of particles in protists .....	119
6.2.	Analysis of the uptake mechanism in <i>A. proteus</i> .....	121
6.3.	Possible transfer of microplastic through trophic levels via a simplified food chain .....	123
6.4.	Summary and Conclusion .....	126
7.	Summary and outlook .....	128
8.	Appendix .....	131
8.1.	Data availability for RNA <sub>seq</sub> raw data .....	131
8.2.	Supplementary figures and tables .....	131
9.	Lists .....	138

9.1.	List of Figures.....	138
9.2.	List of Schemes.....	139
9.3.	List of Tables.....	141
9.4.	List of Equations .....	141
10.	Materials, Devices and Software.....	142
10.1.	Buffers and Solutions .....	142
10.2.	Cells and organisms .....	143
10.3.	Particles used in this study .....	144
10.4.	Chemicals, Reagents and Kits .....	146
10.5.	Accessories .....	150
10.6.	Devices and Equipment.....	151
10.7.	Software .....	153
11.	List of publications.....	154
12.	References.....	155

## Danksagung

Ich möchte mich an dieser Stelle bei allen bedanken, die mich während meiner Promotionszeit unterstützt haben.

In erster Linie gilt mein Dank Frau Prof. Dr. Ruth Freitag, für die Möglichkeit meine Promotion am Lehrstuhl Bioprozesstechnik zu absolvieren. Dank Ihrer hervorragenden Betreuung und hilfsbereiten Art, war die Zeit am Lehrstuhl äußerst angenehm und lehrreich.

Ein weiterer großer Dank gilt Frau Dr. Valérié Jérôme. Auf ihre Ideen, konstruktiven Gespräche und Hilfe im Labor sowie bei der Lehre konnte ich mich immer verlassen.

Besonderer Dank gilt auch Prof. Dr. Thomas Scheibel und Julia Jasinski für die hervorragende Zusammenarbeit als ProjektpartnerInnen.

Ich bedanke mich außerdem beim gesamten Team und Projekt SFB Mikroplastik. Spezieller Dank gilt Prof. Dr. Heike Feldhaar, Prof. Dr. Christian Laforsch, Prof. Dr. Holger Kress, Prof. Dr. Andreas Greiner, Dr. Alfons Weig und allen weiteren Projektpartnern für die hervorragende Zusammenarbeit sowie die konstruktive Unterstützung in fachlichen Gesprächen und beim Veröffentlichen von Daten. Ich bedanke mich bei Melanie Pöhlmann, die als Koordinatorin des SFB Mikroplastik mit Rat und Tat zur Seite stand.

Ein herzliches Dankeschön auch an alle DoktorandInnen, mit denen ich die Gelegenheit hatte zusammenzuarbeiten. Insbesondere bei Anja Ramsperger (Konfokalbilder) und Thomas Witzmann für die Arbeit am Beadvergleichsprojekt, bei Simon Riedl (Etablierung der Kultivierung) und Anja Holzinger (Isolierung der Därme) für die Zusammenarbeit in der Primärzellkultivierung, bei Nora Meides für die Alterung der Partikel, bei Sven Ritschar für die Zusammenarbeit am Kryotom und den Sphäroiden, bei Yuanhu Zhang und Ann-Katrin Müller für die Bereitstellung von Partikeln sowie bei Simona Mondellini und Michael Schwarzer für Bereitstellung von Paramecien. Zusätzlich danke Teresa Menzel, Johanna Schmidtmann und Sebastian Weigert für die schöne Zeit im Projekt auch neben fachlichen Gesprächen.

Ein besonderer Dank gilt auch an alle Studierenden, die ich im Rahmen meiner Arbeit betreuen durfte, und mir in der Erstellung von Daten behilflich waren. Namentlich zu erwähnen sind hier Ali Abu-Abed (gealtertes Mikroplastik), Christoph Rudisch (Polarisation von Makrophagen), Hanin Alkhanis (PLA Zytotoxizität), Johanna Fritsche (Polarisation von Makrophagen), Jokim Zubizaretta (3D Druck), Rafael Kaiser (Ausscheidung von Mikroplastik), Razan Salhany (MTT Daten), Sarah Tauman (gealterte Partikel), Sathish Govindaraju (PLA Zytotoxizität), Sebastian Reich (gealterte Partikel), Sophia Fassold (gealterte Partikel), Stefan Eder (Amöben), Tasmai Paul (Monomerresidues) und Tomas Penaherrera (Sphäroide).

Ein großer Dank geht auch an meinen Bürokollegen Moritz Helm und an Daniel Keim für die täglichen 11:15 Termine. Vielen Dank auch an alle weiteren Doktoranden am Lehrstuhl, Thomas Steiner, Stanislava Mlinar, Songyan Ben Huang, Leif Meyer, Elisabeth Ranze und Meshack Simeon für die immer gute Zusammenarbeit. Ich bedanke mich bei Andrea Schott für ihre Arbeit im Labor sowie bei Edith Hübner und Kristina Thompson für die zügige Bearbeitung aller größeren oder kleineren Probleme und für die zuverlässige Zusammenarbeit.

Abschließend möchte ich mich bei meiner Familie und Freunden bedanken. In erster Linie bei meiner Mutter, die mich in jeder erdenklichen Weise und zu jeder Zeit unterstützt hat. Ich denke zu guter Letzt auch an meinen Vater, der in mir das wissenschaftliche Interesse und die Lust am Forschen geweckt hat und immer für mich da war.

## Preamble

Overall, the still relatively young research field of MP is mainly restricted to monitoring analytics, quantitatively estimating environmental pollution, and identifying the relevant entry paths. In ecotoxicological analysis, mostly pristine polymers are used. A fundamental understanding of physical, chemical and biological mechanisms is still heavily lacking. Various perspectives furthermore influence others highly. Overarching, interdisciplinary research is of great value in advancing MP research. Therefore, the *Collaborative Research Centre (CRC) 1357 Microplastics* was applied at the University of Bayreuth in 2018. The main aim of the CRC is to investigate the MP load on organisms, the behaviour and migration of MP under different environmental compartments, as well as the ageing and change of MP under the influence of various environmental conditions. Another focus is the development of novel plastics that contribute to sustainable polymer chemistry. Central points of MP pollution are split into three superordinate project areas:

Project area A: Biological Effects

Project area B: Behaviour and migration

Project area C: Degradation and development of novel plastics

The individual project areas are divided into further sub-projects, whereby networked, intradisciplinary cooperation of the individual sub-projects is promoted. This project was integrated into project area “A” as subproject “A05”. Together with the cooperation partner, the chair “Biomaterials”, the “effects of microplastic particles on a cellular level” were analysed. The co-PhD in the project, Julia Jasinski, born Rudolph, was mainly responsible for the interaction, uptake and intracellular distribution while the cytotoxic effects, primary cell isolation and testing, formation of micro tissue and the transfer to unicellular, environmentally relevant organisms were mainly focused on in this work. High interaction and cooperation were requested and promoted. Especially since various results are highly complementary, most projects were treated as cooperation. In the result paragraphs, the respective cooperation partners and their contributions to the results will be named individually.

## List of Abbreviations

°	degree
3D	three dimensional
<i>A. proteus</i>	<i>Amoeba proteus</i>
A	ampere
a.u	arbitrary unit
ANOVA	Analysis of Variance
ARG1	Arginase 1
ATCC	American Type Culture Collection
C	Celsius
CA	cellulose acetate
CASI	cytofluorimetric analysis of spheroid invasion
CCL	chemokine ligand
CD	cluster of differentiation
CFSE	Carboxyfluorescein succinimidyl ester
CLSM	confocal laser scanning microscopy
CRC	Collaborative Research Centre
CTV	Cell trace violet
Da	Dalton
DCF	2',7'-dichlorofluorescein
DLS	Dynamic light scattering
DMEM	Dulbecco's Modified Eagle Media
DMSO	Dimethylsulfoxide
DNA	desoxyribonucleic acid
DPBS	Dulbecco's Phosphate Buffered Saline
EDTA	Ethylenediaminetetraacetic acid
<i>E. fetida</i>	<i>Eisenia fetida</i>
ELISA	enzyme-linked immunosorbent assay
Em	Emission
ER	endoplasmic reticulum
Ex	excitation
FACS	fluorescence-activated cell sorting
FC	flow cytometry
FCS	fetal calf serum

FDR	false discovery rate
FIZZ1	Resistin-like molecule alpha
FITC	Fluoresceinisothiocyanat
FSC	forward scatter
g	gram
<i>g</i>	gravity
GO	gene ontology
GSEA	gene set enrichment analysis (
h	hours
HBSS	Hanks Balanced Salt Solution
H <sub>2</sub> DCFDA	dichlorofluorescin diacetate
IFN	interferon
IL	Interleukin
iNOS	inducible nitric oxide synthase
KEGG	Kyoto Encyclopedia of Genes and Genomes
L	Liter
LBSS	Lumbricus Balanced Salt Solution
LDH	Lactate dehydrogenase
LPS	lipopolysaccharides
LY	Lucifer yellow
M	metre
M	Molar
MEM	minimum essential media
MFI	median fluorescence intensity
M-HBSS	modified Hanks Balanced Salt Solution
min	minute
Mn	number average molar mass
MP	Microplastic
MPP	Microplastic particles
MTT	3-(4,5-Dimethylthiazol-2-yl)-2,5-diphenyltetrazoliumbromid
NES	normalised enrichment score
O.C.T. compound	optimum cutting temperature compound
<i>P. caudatum</i>	<i>Paramecium caudatum</i>
PCI	particle-cell interaction
PE	polyethene

PET	polyethylene terephthalate
PFA	paraformaldehyde
PLA	polylactic acid
PP	polypropylene
PS	polystyrene
PSTGA	Penicillin, Streptomycin, Tetracyclin, Gentamicin, Amphotericin B
PVC	polyvinyl chloride
RNA	Ribonucleic acid
rpm	rounds per minute
ROS	reactive oxygen species
RPMI1640	Roswell Park Memorial Institute-1640
RT	room temperature
sec	second
SDM	Schneider's Drosophila Media
SSC	side scatter
SLA	stereolithography
<i>T. pyriformis</i>	<i>Tetrahymena pyriformis</i>
TGF	Transforming growth factor
TMB	3,3',5,5'-tetramethylbenzidine
TNF	tumour necrosis factor
V	Volt
v/v	volume/volume
VEGF	Vascular endothelial growth factor
w/v	weight/volume



## Kurzfassung

In dieser Arbeit wird das potenzielle Risiko von Mikroplastik auf zellulärer Ebene in zunehmender Komplexität analysiert. Hierfür werden zunächst kritische Parameter von Mikroplastikpartikeln bezüglich der intrazellulären Verteilung, Auslösung von Effekten und einer möglichen Ausscheidung in Standardzellkulturansätzen identifiziert. Ausgewählte Charakteristika von Mikroplastikpartikeln sind hierbei Oberflächenladung und chemische Modifikationen, Größe, Form, Polymerart oder Monomer-Rückständen. Eine erste Konvergenz zu realistischeren Ansätzen wird durch eine künstliche Laboralterung dieser Partikel und die Verwendung von aus handelsüblichen Wandfarben extrahierten Partikelfractionen erreicht. Anschließend wird die Komplexität des Zellkultursystems von herkömmlichen Standardsystemen auf 3D-Mikrogewebeansätze erhöht. Transwell-Systeme und die Kultivierung von Sphäroiden werden verwendet, um die Wirkung von Mikroplastik auf die Bildung dieser Mikrogewebe zu analysieren. Darüber hinaus wird das Penetrationsverhalten von Partikeln in vollständig gebildeten Mikrogeweben analysiert. Primärzellen von *Eisenia fetida* als Modellorganismus werden anschließend verwendet, um zelluläre Erkenntnisse leichter auf die organismische Ebene zu übertragen. Abschließend werden einzellige Organismen (*Amoeba proteus* und *Tetrahymena pyriformis*) als Repräsentanten der unteren Trophieebenen verwendet, um den Mechanismus des Aufnahmeverhalten von Mikroplastikpartikeln in diesen zu bestimmen und einen möglichen Transfer über eine vereinfachte Nahrungskette zu analysieren.

Die Identifizierung der kritischen Parameter für Mikroplastikpartikel wurde mithilfe von Standard-Zellkulturtests durchgeführt, um potenzielle zytotoxische, genotoxische und entzündliche Reaktionen sowie oxidativen Stress zu screenen. Neben der Abhängigkeit des Zellphänotyps erwiesen sich Parameter, die die Partikel-Zell-Interaktion beeinflussen, als besonders einflussreich. Dies wurde durch Verwendung von Partikeln mit hoher Oberflächenladung (hohe Partikel-Zell-Interaktion) und niedriger Oberflächenladung (niedrige Partikel-Zell-Interaktion), aber ansonsten gleichen Eigenschaften, verifiziert. Die gemessenen Effekte waren signifikant größer für die erhöhte Interaktionsrate. Insbesondere die Oberflächenladung, Protein-Oberflächen-Korona und Größenbereiche, die die Aufnahmewahrscheinlichkeit beeinflussen, erwiesen sich daher als kritisch für die nachfolgenden Effekte. Gemessene Effekte traten jedoch nur bei relativ hohen Partikelkonzentrationen (250 µg/mL) auf.

Bei Verwendung künstlich gealterter Partikel (durch UV-Bestrahlung) oder Partikelfractionen aus Wandfarben konnte eine Zytotoxizität bereits bei wesentlich niedrigeren Konzentrationen beobachtet werden (2 – 20 µg/mL). Als Hauptfaktoren hierfür konnte die Morphologie der Partikel (z.B. schärfere Kanten) und eine erhöhte Reaktivität auf der Oberfläche der Partikel aufgrund der UV-Bestrahlung

während der künstlichen Alterung identifiziert werden. Im Gegensatz dazu, war das Entzündungsniveau bei Zellen, die mit fabrikneuen Partikeln behandelt wurden, höher. RNA-Sequenzierungen konnten diese Ergebnisse verifizieren und einen Einblick in mögliche Mechanismen geben (Aufnahmewege, spezifischere Entzündungsreaktion für fabrikneue Partikel, akut-zytotoxische Reaktionswege für gealterte Partikel).

Verteilungs- und Ausscheidungsstudien zeigten eine unspezifische Verteilung während der Zellteilung und keine aktive Ausscheidung in einer Kultivierungsdauer von 72 Stunden. Dies legt nahe, dass eine intrazelluläre Anreicherung der Partikel möglich ist.

Der Einfluss von Mikroplastikpartikeln auf die Integrität einer epithelialen Membran wurde mittels Transwell-Inserts analysiert. Der Effekt der Partikel auf die Funktionalität der Membran war jedoch vernachlässigbar, was mutmaßlich mit der geringen Partikel-Zell Interaktion in den verwendeten Epithelzelllinien zusammenhängt. Die Etablierung eines Penetrations-Assays mit diesem System war aufgrund eines Mangels an Partikeln, die die Membran selbst ohne Zellen durchdringen konnten, nicht möglich.

Die Analyse an Sphäroiden hingegen lieferte mehr Einblicke auf die Interaktion von Mikroplastik und Mikrogewebe. Die Bildung dieser Zellaggregate wurde signifikant gestört, wenn Partikel während der initialen Wachstumsphase hinzugefügt wurden. Hierbei zeigten erneut künstlich gealterte Partikel einen größeren Effekt im Vergleich zu unveränderten Partikeln. Partikel, die nach vollständiger Etablierung des Gewebes hinzugefügt wurden, konnten in die Sphäroide eindringen und mittels etablierten Analyse-Workflow nachgewiesen werden. Abschließend wurde eine Ko-Kultivierungsmethode für Makrophagen und Sphäroide etabliert, um sich der natürlichen Umgebung weiter anzunähern.

Primäre Darmzellen von *E. fetida* wurden verwendet, um Erkenntnisse aus der Zelllinienkultivierung auf primäre Zellen zu übertragen und Schlussfolgerungen für die organismische Ebene zu ziehen. Dabei stellte sich die Partikelgröße erneut als entscheidender Faktor für die Partikel-Zell Interaktion heraus. Es konnte jedoch keine akute Zytotoxizität in den primären Zellen als Reaktion auf Mikroplastikpartikel beobachtet werden, was wahrscheinlich mit der geringen Wechselwirkungsrate und dem epithelialen Phänotyp zusammenhängt, wie zuvor identifiziert. Die Möglichkeit langfristiger Auswirkungen oder einer Anhäufung auf Gewebeebene kann jedoch nicht ausgeschlossen werden, da gezeigt wurde, dass Partikel in Mikrogewebe eindringen können. Basierend auf den Ergebnissen dieser Studie war es allerdings nicht möglich, eine Verbindung zwischen den zellulären und organismischen Ebenen herzustellen.

Die Analyse von Einzellern lieferte weitere Einblicke in eine mögliche Bioakkumulation und Biomagnifikation. *T. pyriformis* zeigte eine schnelle und größenabhängige Aufnahme (Partikel < 6 µm). *A. proteus* nahm Partikel ≤ 6 µm auf. Während *T. pyriformis* als Filtrierer die Partikel unspezifisch aufnahm, konnte für die Amöbe als Aufnahmemechanismus die Pinocytose identifiziert werden. Darüber hinaus könnten Partikel indirekt von *A. proteus* aufgenommen werden, wenn sie Mikroplastik-belastete Beute in einem vereinfachten Nahrungsnetzwerk fressen. Es wurde weiterhin festgestellt, dass der Aufnahmemechanismus den Verbleib der Partikel innerhalb der Amöbe signifikant beeinflusste. Direkt durch Pinocytose aufgenommene Partikel blieben bis zu 14 Tage in den Organismen erhalten, während durch belastete Beute phagozytisch aufgenommene Mikropartikel aktiv ausgeschieden wurden, was auf das Vorhandensein von selektiven intrazellulären Mechanismen hinweist. Daher ist eine mögliche Bioakkumulation auf den unteren trophischen Ebenen wahrscheinlich und hängt stark von der Partikelgröße und dem Aufnahmemechanismus ab.

Als kritische Parameter für Laborpartikel wurden Eigenschaften identifiziert, welche die Partikel-Zell Interaktionen fördern. Für weitere Forschungsansätze zur Risikobewertung von Mikroplastik wird insbesondere die Verwendung von umweltrelevanten Mikroplastikpartikeln dringend empfohlen, da Reaktionen und Mechanismen stark von Laborpartikeln abweichen. Die Verwendung von komplexeren 3D-Zellkultivierungen zeigte die Möglichkeit des Eindringens von Partikeln in Mikrogewebe auf. Darüber hinaus wurden keine Exkretionsmechanismen in Säugetierzellen gefunden, was eine Anreicherung von Partikeln in Organismen oder Geweben wahrscheinlich macht. Studien an Organismen auf den unteren trophischen Ebenen zeigten eine erhöhte Akkumulation von Partikeln in einer besonders kritischen Größe (< 6 µm) für Säugetierzellen. Da die Übertragung dieser Partikel entlang der Nahrungskette wahrscheinlich ist, könnte eine höhere Aufnahme kleiner Partikel möglich sein, was das Risiko einer Biomagnifikation erhöht. Daher liefert diese Arbeit weitere Erkenntnisse zur Bewertung des Risikos von Mikroplastik auf zellulärer Ebene und ermöglicht Schlussfolgerungen für höhere Organismen.

## Abstract

This work evaluates the potential risk of hazardous effects of microplastic on a cellular level in increasing complexity. First, critical parameters of microplastic particles are identified in standard cell cultivation. In this process, the pathway of an ingested particle concerning its intracellular distribution, effect triggering, and excretion is analysed. Hereby, the multi-parameter characteristics of microparticles, like surface charge and modifications, size, shape, polymer type, or monomer residues, are considered. The first convergence towards a realistic approach is the usage of artificial weathered model particles and particles extracted from commercially available wall paints. Following this, the cell cultivation system complexity increases from standard systems to 3D microtissue approaches. Transwell systems and the cultivation of spheroids are used to analyse the effect of microplastic on the formation of these microtissues. Furthermore, the penetration behaviour of particles into fully formed microtissues is tracked. Primary cells from *Eisenia fetida*, as a model organism, are subsequently used to transfer cellular findings to the organismic level. Finally, unicellular organisms (*Amoeba proteus* and *Tetrahymena pyriformis*), as representatives of the lower trophic levels, are used to study the uptake behaviour of microparticles, their ingestion pathway and a possible transfer across a simplified food web.

The identification of particular critical parameters for microplastic particles was performed by using standard cell culture assays to investigate potential cytotoxicity, oxidative stress, genotoxicity, and inflammatory responses. Next to the dependency of the cell phenotype, parameters influencing the particle-cell interaction proved notably important. This was verified using particles with a high surface charge (high particle-cell interaction) and a low surface charge (low particle-cell interaction) but otherwise with the same characteristics. Measured effects were significantly larger for the increased interaction rate. In particular, the surface charge, protein surface corona, and size range, as parameters affecting the uptake probability, proved critical for subsequent effects. Nevertheless, effects were only observed for relatively high concentrations (250 µg/mL).

However, when using artificially aged particles (via UV-irradiation) or paint particle fractions, cytotoxicity could be observed for significantly lower concentrations (2 – 20 µg/mL). The morphology of the particles (e.g. sharper edges) and an increased reactivity on the particle's surface due to the UV irradiation could be identified as the main influencing factors. Interestingly though, the inflammation level was higher for cells treated with pristine particles. RNA sequencing could confirm these findings and provide a glimpse into possible mechanisms (uptake pathways, specific inflammation pathways for pristine particles, acute-cytotoxic reactions for aged particles).

Further distribution and excretion studies revealed an unspecific distribution during the cell division and no active excretion during 72 h of cultivation. These findings led to the assumption that an intracellular accumulation of particles is likely.

Afterwards, the cell cultivation system was expanded from 2D to 3D systems. The influence of microplastic particles on the integrity of an epithelial membrane was hereby analysed using transwell inserts. However, the effect of the particles was negligible, which was likely connected to the low interaction rate between epithelial cells and particles. Due to a lack of particles penetrating the membrane even without cells, establishing a penetration assay with the same system was not possible. Contrarily, the usage of spheroids provided more insights. The formation of these microtissues was significantly disturbed when adding particles during the initial growth phase. Again, artificially aged particles showed a higher effect compared to pristine ones. Particles added after the full establishment penetrated the spheroid and could be detected by an established analysis workflow. Finally, a co-cultivation method for macrophages and the spheroids was established to converge closer to the *in vivo* environment.

Primary intestinal cells from *Eisenia fetida* were used to transfer previous findings from the cell cultivation to primary cells and to draw conclusions for the organismic level. Notably, particle size was again a crucial factor for the interaction. However, acute cytotoxicity could not be observed in the primary cells in response to particles, which can be associated with the comparable low interaction rate of the epithelial phenotype, as identified previously. The possibility of long-term effects or accumulation at a tissue level cannot be dismissed, as it was demonstrated that particles could penetrate microtissues. Nonetheless, based on this study's findings, it was not possible to establish a link between the cellular and organismic levels.

The analysis of unicellular organisms revealed further insight into bioaccumulation and biomagnification on the lower trophic levels. *Tetrahymena pyriformis* showed a fast and size-dependent uptake (particles < 6 µm). *Amoeba proteus* ingested particles ≤ 6 µm. While *T. pyriformis*, as filter feeder, ingested particles unspecifically, pinocytosis was identified as the main uptake mechanism for the amoeba. Furthermore, particles could be indirectly ingested by *A. proteus* when feeding microplastic-burdened prey in a simplified food web. These uptake mechanisms, in return, significantly influenced the fate of the particles ingested by the amoeba. Directly ingested particles remained for up to 14 days, while phagocytic ingested MP through burdened prey was actively excreted, suggesting the presence of selective intracellular mechanisms. Either way, a possible bioaccumulation on lower trophic levels is likely and highly dependent on the particle size and the uptake mechanism.

As especially critical parameters for pristine particles, particle-cell-interaction promoting properties could be identified. Further combining the results from this study, especially the usage of environmentally relevant microplastic particles, is highly recommended for research purposes due to their highly deviating effects compared to pristine ones. More complex 3D cell cultivation revealed the possibility of particles penetrating microtissues. Moreover, no excretion mechanisms in mammalian cells were found, making an accumulation of particles in organisms likely. Studies on organisms at the lower trophic levels revealed a further possible accumulation of particles in an especially critical size ( $< 6 \mu\text{m}$ ) for mammalian cells. Since the transfer of these particles along the food web is likely, a higher uptake of small particles might be possible, increasing the risk of biomagnification. Therefore, this work could provide further insight to assess the risk of microplastic on a cellular level and draw conclusions for higher organisms.

# 1. Introduction

For 70 years, plastic has been an indispensable part of everyday life as a mass product. Despite this lengthy time as a consumer product, there is still no widespread recycling of plastic. While only 9% of the plastic produced is reused, 79% ends up in landfills or the environment <sup>[1]</sup>. By 2050, the accumulation of waste in the environment is expected to increase from 6300 million tons in 2017 to 12000 million tons <sup>[1]</sup>. In addition to macroplastics, known as, e.g. packaging material, environmental pollution with microplastics (MP) is also a converging problem. While the first scientific notation of MP was only in 2004 in the highly regarded paper “Lost at Sea: Where is all the plastic?” by Thompson et al. <sup>[2]</sup>, the scientific, political and public attention has risen largely till today <sup>[3]</sup>. However, an all-inclusive definition of the term microplastic is still being discussed. Frias and Nash proposed in 2019 the following: “Microplastics are any synthetic solid particle or polymeric matrix, with regular or irregular shape and with size ranging from 1 µm to 5 mm, of either primary or secondary manufacturing origin, which are insoluble in water” <sup>[4]</sup>. The MP burden is hereby split into two main categories, primary and secondary MP. Primary MP is purposely produced by humans, e.g., plastic pellets, as an ingredient in personal care products or as matrix addition in wall paint, and others <sup>[5]</sup>. Secondary MP arises from the decomposition of macroplastic through UV radiation, abrasion or bacterial degradation <sup>[6]</sup>. MP accumulates in the environment and can nowadays be found in all environmental compartments like marine and freshwater systems, terrestrial, air and even in isolated areas like glaciers, the arctic sea or the highest mountains as described by various reviews <sup>[7–9]</sup>. Consequently, organisms in the respective compartment must deal with this new environmental pollutant. Especially for the marine and aquatic environment, various studies regarding either small model organisms like the water flea *Daphnia magna* or the zebrafish *Danio rerio* or larger organisms like, e.g. marine fish or seals were analysed and summarised in various reviews <sup>[10–13]</sup>. Evidence shows that the ingestion of MP by aquatic organisms has the potential to induce different adverse effects, such as impairment of food consumption or effects on growth as well as disordered reproduction in small organisms, using vertebrates and invertebrates <sup>[14–19]</sup>. In larger animals, MP accumulation, the introduction of endocrine disruptor chemicals (EDC) and a possible vector function for pathogens and following infectious diseases are considered threads, as summarised in a recent review <sup>[20]</sup>. Recently, a new disease could be correlated explicitly to the MP burden in sea birds, the so-called plasticosis, a fibrosis type <sup>[21]</sup>. The accumulation in the food chain can further be observed for terrestrial organisms <sup>[22,23]</sup>, and implementing this, the MP burden is also a relevant factor for human health<sup>[24]</sup>. According to a study by the *World Wide Fund for Nature*, a person consumes an average of up to 5 g MP per week by diet or respiration <sup>[25]</sup>. Other studies estimate about 200,000 particles/year as uptake of a typical human, noting that due to methodical limitations, an underestimation of smaller particles is likely <sup>[26]</sup>. MP has

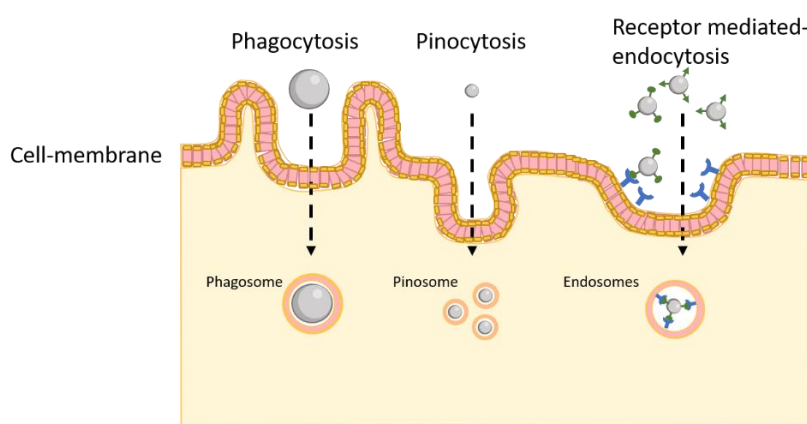
already been found in the human placenta, faeces, lung tissue, and blood [27–30]. These findings, therefore, advocate for an accurate analysis from scratch of MP pollution regarding distribution and degradation in the environment, uptake and accumulation throughout the food chain, toxicity assessment of MP for organisms and ultimately, the effect of MP on humans.

### 1.1. Usage of cell cultivation in microplastic research

One possibility to analyse the effect of contaminants is the usage of animal experiments, which are mostly conducted with mice. Various *in vivo* studies of the effect of MP on this model organism have been carried out in the last few years [31–37]. Consistent findings included effects on the gut epithelium and the microbiota, immunotoxicity, the formation of reactive oxygen species (ROS) and hepatotoxic effects. Furthermore, a vector function of microplastic particles (MPP) for pathogens is often named. Analysing the impact of MP on mammals *in vivo*, though, is, on the one hand, more challenging to analyse due to higher legal restrictions and the dependency on more complex *in vivo* analysis. On the other hand, ethical and moral questions need to be asked when performing animal experiments. Therefore, animal and human cell cultivation have become very beneficial for diverse biotechnology, medicine and veterinary applications. Cell cultivation became an indispensable tool to study intra- or intercellular responses and to serve as *in vitro* model for research [38]. Due to its usage in risk assessment and toxicological research for the past 40 years, it is qualified for reliability and comparability, benefitting from a vast trove of experience [39,40]. Cell culture is, therefore, an obvious application for the analysis of the toxicity of MP, and publications have drastically increased in the last couple of years [41].

### 1.2. Particle-cell interaction – what is known from the literature

Cytotoxic effects are often only triggered after the interaction of the pollutant and a cell. An interaction or ingestion of the particle inside a cell can be crucial for later analysis. Three principal uptake mechanisms exist for cells (Scheme 1).



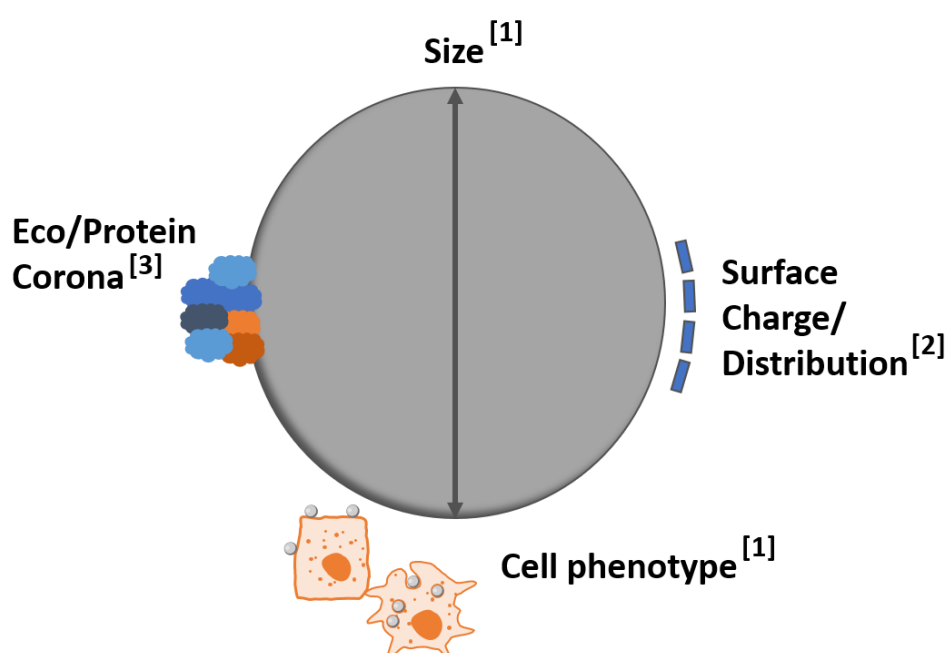
**Scheme 1** Uptake mechanism of particles in mammalian cells



Phagocytosis is mainly observed in specialised cells like macrophages, describing the active ingestion of particular matter, bacteria, small cells or remains of, e.g. dead cells. This uptake pathway is critical for controlling and degrading infectious agents and senescent cells and is mainly restricted to particular matter  $> 0.5 \mu\text{m}$  <sup>[42–44]</sup>. After ingestion via phagocytosis, a phagosome is formed, where the ingested matter is digested by an acidified compartment. Subsequently, it fuses with the lysosome to develop into phagolysosomes, eliminating the respective extracellular matter <sup>[45]</sup>. A second endocytotic uptake mechanism is via pinocytosis. Pinocytosis refers to the uptake of fluids or small particles ( $< 0.5 \mu\text{m}$ ) and can be performed by most cells <sup>[46–48]</sup>. The engulfed fluid is encapsulated by a pinosome, which is formed by pinching the cell membrane inward. Receptor-mediated endocytosis is the third main method of endocytosis. Similar to pinocytosis, mainly solutes and small particular matter is engulfed. Additionally, specific receptors are involved in selecting molecules. It can be principally differentiated between clathrin-mediated, caveolin-mediated and clathrin- and caveolin-independent endocytosis, each specialised for different functions of the cells <sup>[48,49]</sup>.

Consequently, the uptake mechanism depends on the size of particles, their interaction with (specific) receptors to the cellular membrane, and the cell phenotype <sup>[42,49–51]</sup>. Particle properties, e.g. hydrophobicity/hydrophilicity, surface charge or modification and physical properties (size and shape), are hereby essential for the interaction and uptake of cell particles <sup>[49]</sup>.

Therefore, the particle-cell interaction (PCI) for selected particle parameters has been investigated (Scheme 2).



**Scheme 2 Investigated parameters influencing the PCI and ingestion in cooperation projects**

[1] Investigated in Rudolph, Völkl et al. (2021); [2] Investigated in Ramsperger, Jasinski, Völkl et al. (2022); [3] Investigated in Jasinski et al. (2022)

These analyses were mainly done with and by cooperation partners and were published in the shared publications Rudolph and Völkl et al. (2021), Ramsperger, Jasinski and Völkl et al. (2022) and Jasinski et al. (2022). In the following, the main results of these papers regarding the PCI and uptake will be summarised. One main advantage of these cooperations was hereby the usage of the same particles and cell lines. Therefore, results from these ingestion studies can be easily viewed in context with results from this work. The abbreviation PCI will be used when ingestion was not verified by the applied method but only an interaction, which can be an ingested particle or an adherence to the cell membrane.

In Rudolph, Völkl et al. (2021), Julia Jasinski, born Rudolph, analysed the influence of the particle size and cell phenotype on the PCI by flow cytometry (FC). Polystyrene (PS) particles in a size range between 0.2 and 6  $\mu\text{m}$  were used (0.2, 0.5, 1, 2, 3, 6  $\mu\text{m}$ ). Differences in the PCI could be observed between all used cell lines (J774A.1 and ImKC as macrophages, BNL CL.2 and STC-1 as epithelial cells) (Figure S1 and Figure S2). Phenotype-specific differences were expected (macrophages >> epithelial cells), which can easily be explained by the natural purpose of the cells (macrophages as scavenger cells, epithelial cells with a barrier function).

Interestingly, significant differences among the respective macrophages (Figure S1) and epithelial cell lines (Figure S2) were also found. While the J774A.1 cell line showed overall the highest PCI, the increased PCI compared to ImKC might be related to various reasons. One explanation is the size of both macrophages. J774A.1 cells proved to be around 1.5 times larger (20 – 25  $\mu\text{m}$ ) compared to ImKC ( $\approx$  15  $\mu\text{m}$ ). Bigger cells have more volume to incorporate particles. Since, especially for particles between 1 – 3  $\mu\text{m}$ , cells were highly interacting with the particles, more volume corresponds to potentially more PCI. Another reason might be the phenotype of the J774A.1 cells. While this cell line was isolated from the ascites, which had the purpose of so-called wandering macrophages, ImKC cells are immortalised resident Kupffer cells. J774A.1 might be more active at moving around the plate and, therefore, might be in more contact with particles. Kupffer cells, on the other hand, are known to be more specialised in the clearance of small, particular matter on the nanometer scale <sup>[52,53]</sup>. This might influence the uptake rate in the here measured low micron-sized particle range. Next to the phenotype-specific differences, a size dependency of MP uptake was also found. While a high amount of 1 – 3  $\mu\text{m}$  particles showed interaction, 6  $\mu\text{m}$  particles, as the largest particle size analysed, only showed a low interaction rate, which was true for both macrophage cell lines. The natural purpose of macrophages can again explain this observed size dependency. One of their main functions *in vivo* is the clearance of bacterial infection <sup>[54]</sup>. Most bacteria are in a size range of 1 – 4  $\mu\text{m}$  <sup>[55]</sup>, which corresponds well to the high interaction with particles in this size range. Larger particles, on the other hand, are more difficult to ingest and exhibit a higher volume resulting again in fewer PCI possibilities

for the cells. As shown in the literature <sup>[44,56–58]</sup>, the uptake of larger particles often depends on special surface modifications, e.g. IgG-opsonisation, and only low ingestion rates were visible.

Furthermore, a concentration-dependent PCI was observed. This was expected since more particles were available per cell, increasing the PCI probability. Interestingly, macrophages did not seem to stop ingesting particles after a certain amount of PCI, but most cells showed  $PCI > 20$  if only enough particles were added.

Both epithelial cell lines showed a significantly lower PCI compared to the macrophages. Nevertheless, significant differences between both epithelial cell lines were visible (Figure S2). While STC-1 only showed low PCI for all particle sizes, BNL CL.2 cells showed a size-depending pattern of PCI. Especially for the smaller particles, various PCI could be observed, while only sporadic 6  $\mu\text{m}$  particles were interacted with. Although BNL CL.2 cells have been previously described as non-phagocytotic <sup>[56,57]</sup>, ingestion via macropinocytosis is possible for particles up to 5  $\mu\text{m}$  <sup>[47]</sup>, which might explain the PCI found for BNL CL.2 cells. Especially for liver cells, macropinocytosis is essential for the clearance of apoptotic or necrotic cells <sup>[58]</sup>, while for STC-1, comparative literature showed particle ingestion only for 0.12  $\mu\text{m}$  <sup>[59,60]</sup>.

To further verify if particles were indeed fully ingested or only stuck to the cell membrane, confocal laser scanning microscopy (CLSM) was used to complement this information. This method captures fluorescent 2D images at different depths in a cell and subsequently enables the reconstruction of three-dimensional (3D) structures. The FC data findings could be confirmed (Figure S3). While both macrophage cell lines did seem to ingest most of the interacting particles, the epithelial cells showed less interaction and often no engulfment of interacting particles. Using these complementary methods, a quantitative (FC) and qualitative (CLSM) measurement of PCI and ingestion of particles in the four used cell lines, dependent on size, phenotype and concentration, could be accomplished.

As an additional particle parameter, the surface charge is a known property from nanoparticle studies affecting the PCI and ingestion <sup>[51]</sup>. In Ramsperger, Jasinski and Völkl et al. (2022), the influence of particles with a different surface charge and distribution (MP<sub>polyscience</sub>,  $\zeta$ -Potential  $\approx -30$  mV, homogeneously distributed; MP<sub>micromod</sub>,  $\zeta$ -Potential  $\approx -1.5$  mV, heterogeneous distribution) on the PCI with the already established macrophage cell lines (ImKC and J774A.1) was investigated. PCI and the ingestion rate were significantly higher for MP<sub>polyscience</sub> compared to MP<sub>micromod</sub>. This was found for both cell lines. An increase of 150 (for J774A.1) to 260 (for ImKC) times higher PCI and an 80 (for J774A.1) to 360 times (for ImKC) higher internalisation rate of MP<sub>polyscience</sub> could be found when compared to MP<sub>micromod</sub>. This finding confirms the hypothesis that the surface charge is highly significant for the internalisation of MP, which was approved mainly for nanoparticles previously <sup>[51,61]</sup>. The pattern of a

more anionic surface getting internalised higher than non-ionic or positively charged ones is also comparable to the nanoparticle scale <sup>[61,62]</sup>. Again, the biological function of the used macrophages might be one of the influencing factors. The  $\zeta$ -potential of the cell wall of common bacteria was measured at - 22 mV at pH 7.0 <sup>[63]</sup>. This charge range is comparable to the surface charge of MP<sub>polyscience</sub> in cell culture media. The non-charged particular matter might, therefore, not be recognised by macrophages. Additionally, the PCI and uptake depends on the formation of an eco or protein-corona <sup>[64]</sup>, which in return depends on the surface properties and modifications <sup>[65–69]</sup>. Relevant to this experimental setup, the formation of the protein corona in the cell culture media with fetal calf serum is also influenced by the initial surface charge of the particles <sup>[70]</sup>. This is shown by the significantly greater change in the  $\zeta$ -potential for MP<sub>polyscience</sub> after incubation in full growth media compared to MP<sub>micromod</sub> (polyscience  $\approx \Delta|50 \text{ mV}|$  compared to micromod  $\approx \Delta|0 \text{ mV}|$ ). A more pronounced formation of the protein corona is, therefore, likely. This, in return, could have impacted the uptake and PCI.

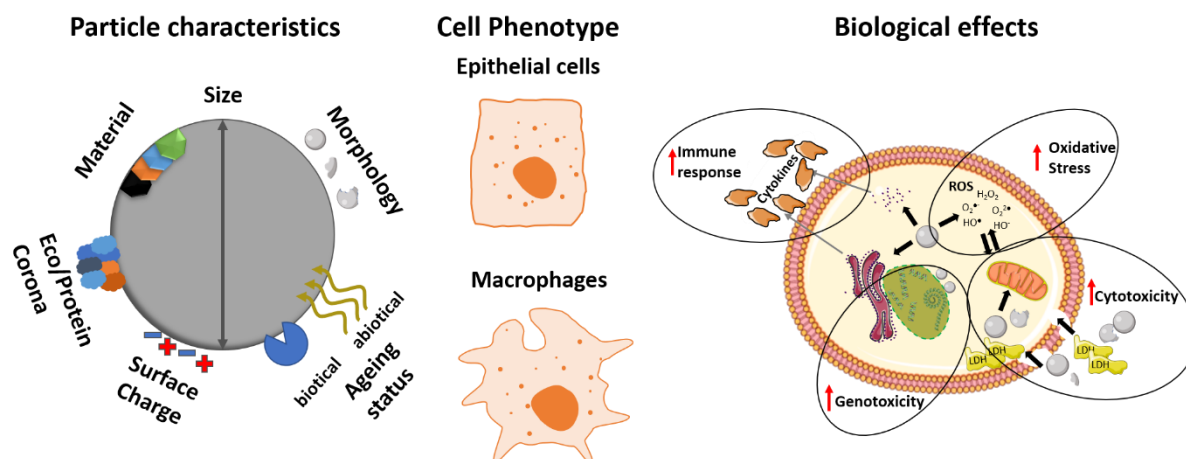
A deeper analysis of the influence of the protein corona was done in the study “Tailor-Made Protein Corona Formation on Polystyrene Microparticles and its Effect on Epithelial Cell Uptake” by Jasinski et al. (2022). It has to be noted that while in the previous studies, macrophages were used, the main interest in this study was on the effects on the epithelial cells (STC-1 and BNL CL2). PS particles (0.2  $\mu\text{m}$  and 3  $\mu\text{m}$ ) were pre-coated with bovine serum albumin (BSA), myoglobin,  $\beta$ -lactoglobulin, lysozyme, or fibrinogen before incubating the particles in full cell culture medium with 10 % (v/v) FCS. The pre-coating step influenced the protein corona formation, and the primary protein layer could still be found by Liquid-Chromatography-Mass spectrometry/ Mass spectrometry. When incubated in full growth media, the surface charge converged to around - 25 mV for 0.2  $\mu\text{m}$  particles and - 35 mV for 3  $\mu\text{m}$  particles, no matter the coating. Nevertheless, the pre-coating significantly influenced the PCI and ingestion rate for four cell lines (ImKC, J774A.1, BNL CL.2, STC-1). While 0.2  $\mu\text{m}$  particles coated with lysozyme or myoglobin were taken up at a higher rate than control particles, fibrinogen pre-coating reduced the interaction rate. Whereas the pre-coating highly influenced the 0.2  $\mu\text{m}$  particles, 3  $\mu\text{m}$  particles did not show high increases in PCI. Fibrinogen-coated 3  $\mu\text{m}$  particles, though, were taken up less. In summary, it could be shown that the pre-coating of particles significantly affects the protein corona formation and the PCI and ingestion rate with the used cell lines, which in turn confirms the hypothesis of the PCI-affecting protein corona.

### 1.3. Biological effects of MP on a cellular level

After the interaction or uptake of MPP with cells, particles might damage or disturb the normal metabolism of cells. Various studies worked with murine [71–75] and human cell lines [76–87] from different tissues, organs and phenotypes, analysing distinct biological effects of MP and review summarising the data [24,88–92], are stretching the importance of cell culture application and further expansion of data. As recently reviewed, established effects of MP on mammalian cells involve mainly cytotoxicity, oxidative stress, genotoxicity and inflammatory response [93]. Most of these studies concluded that MPP are not as harmful as feared and exert effects only at concentrations above the current environmental ones. However, most prior *in vitro* studies used pristine PS beads due to their defined size distribution and easily accessible surface chemistry (i.e., functionalisation) [94,95]. Both parameters have further been demonstrated to be highly important for PCI [64,96,97]. Considerably less is known about other petroleum-based polymer microparticles such as polyethene (PE), polyvinyl chloride (PVC), and the biologically degradable polylactic acid (PLA) [89,91,98]. Previously published works indeed used different polymer microparticles like PVC, polyethylene terephthalate (PET), polypropylene (PP), and PE, [73,79,98,99] but the particles were comparably large and polydisperse (between 1 – 100 µm), making a comparison to smaller, monodisperse PS particles difficult. However, different polymers might trigger different results due to different surface chemistry and composition of the particles. As a result, the influence of the MP material has not yet been sufficiently researched.

Furthermore, environmentally found particles differ greatly from the pristine test particles [100]. Particles exposed to the environment are degraded by mechanical stress or photo- and biotic-degradation [6,101,102]. This disruptive process, often referred to as “ageing” or “weathering”, produces secondary microplastic with heterogeneous morphological structures and complex surface characteristics (physical and chemical) [94,103,104]. It has been shown that these weathered MP are more harmful than laboratory ones to a range of model organisms (e.g., bacteria, algae, fish) [77,105–109]. However, for mammalian cells, only a few reports are available. Increased toxicity of photo-oxidised particles compared to pristine ones was shown for human intestinal epithelial (Caco-2) and lung epithelial (A549) cells [110,111]. In both reports, a correlation between the weathering time and the oxidative potential of the particles was shown, which in turn correlates with their increased cytotoxicity. On the other hand, a decreased cytotoxicity for weathered MP compared to milled ones was shown for large PS and PP fragments (100 µm) [112]. This leaves a distinct lack of reports in the highly important area of environmental particles.

Overall the research of MP with cell cultures proves as a multi-parametrical problem (Scheme 3), with a lack of a systematic, well-characterised in-depth analysis of comparable and environmentally relevant MPP.



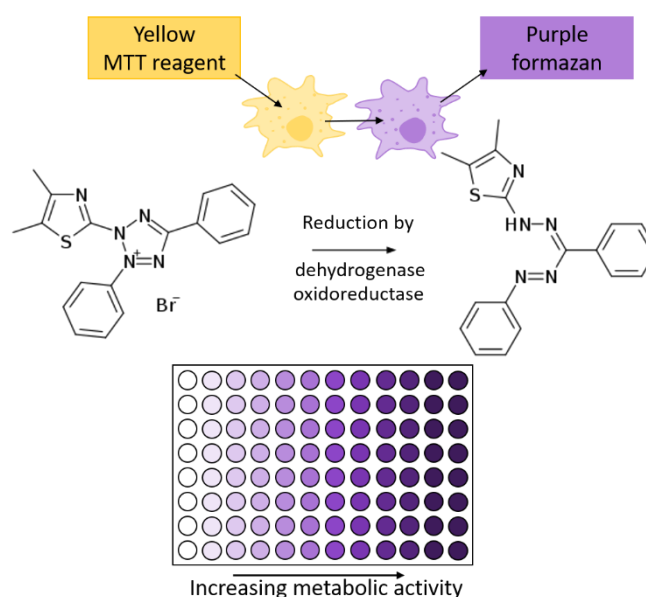
*Scheme 3 Multiparametric problem situation of MP on mammalian cells*

#### 1.4. Relevant fundamentals for cell culture assays used in this work

Various standardised and well-established assays exist to analyse the impact of potentially hazardous materials in cell culture systems. By using such assays, the comparison and reproducibility of results is easier and more expressive due to a comprehensive existing data set in the literature. The following paragraphs will explain the principles of the most common assays used in this work.

##### *Metabolic activity assay for cells*

The 3-(4,5-Dimethylthiazol-2-yl)-2,5-diphenyltetrazoliumbromid (MTT) assay is a colourimetric assay based on the reduction of a yellow solution of MTT to violet formazan crystals via active metabolic cells. The more active the cells are, the higher the conversion rate and, in return, the viability of the cells (Scheme 4).



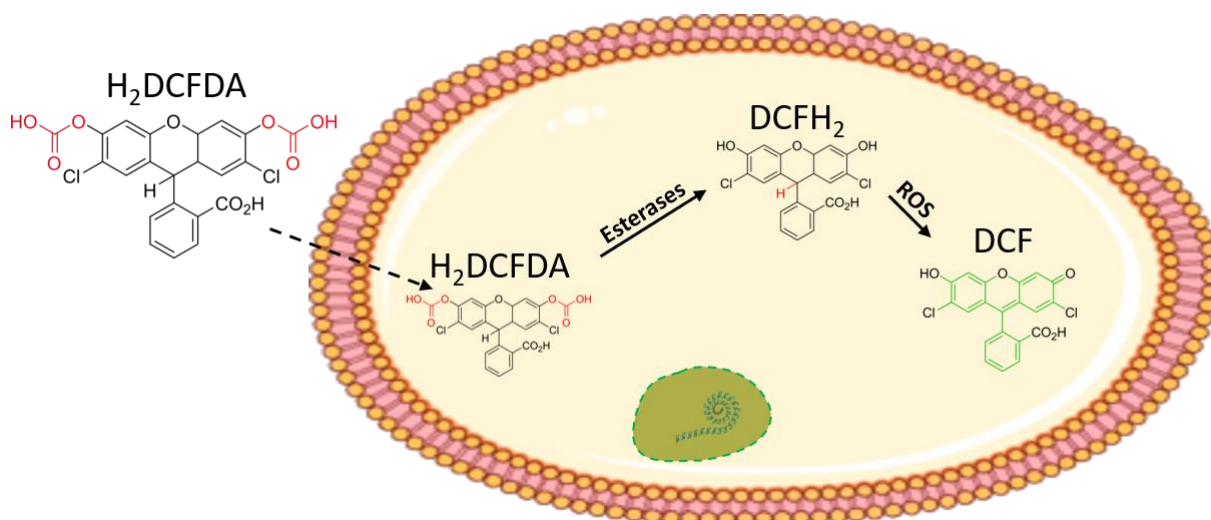
*Scheme 4 Principle of the MTT assay*

The reduction is mediated by oxidoreductases, dehydrogenases and electron donors during the glycolytic pathway <sup>[113,114]</sup>. Next to the mitochondria, other intracellular organelles like the Endoplasmatic Reticulum, cytosolic lipid droplets and others contribute to the MTT reduction <sup>[114]</sup>. The MTT assay is, therefore, more than a mere representation of the mitochondrial activity but allows a good overview of the overall cell viability <sup>[114]</sup>. The MTT assay is a recognised method to assess the effect of MPP and was used in various publications for this work <sup>[71,115–118]</sup> and by other groups <sup>[73,79,80,119]</sup>.

#### *H<sub>2</sub>DCFDA conversion assay to detect ROS*

Oxidative stress is induced by reactive species derived from oxygen and nitrogen. Prominent representatives of the ROS family are superoxides ( $O_2^{\bullet-}$ ), hydrogen peroxide ( $H_2O_2$ ), hydroxyl radicals ( $\bullet OH$ ), ozone ( $O_3$ ) and singlet oxygen ( $^1O_2$ ) <sup>[120]</sup>. Reactive species are usually a byproduct of the metabolism and derive at different stages in the respiratory chain through leakages of electrons <sup>[120,121]</sup>. While a basal level of ROS is necessary for cell signalling and homeostasis <sup>[122,123]</sup>, an unbalanced amount might lead to oxidative stress causing severe damage to organelles and proteins <sup>[124–127]</sup>. In the case of MPP, ROS are among the highlighted potential stresses <sup>[87,128]</sup>. Reactive groups on the surface of the particles, either added intentionally for functionalisation purposes or by ageing of the particle <sup>[6]</sup>, might induce an uncontrolled overproduction of intracellular ROS.

Intracellular ROS is often labelled with the non-fluorescent membrane-permeable dye dichlorofluorescein diacetate ( $H_2DCFDA$ ) <sup>[129]</sup>, which is converted into fluorescent 2',7'-dichlorofluorescein (DCF) upon oxidation by intracellular ROS (Scheme 5).

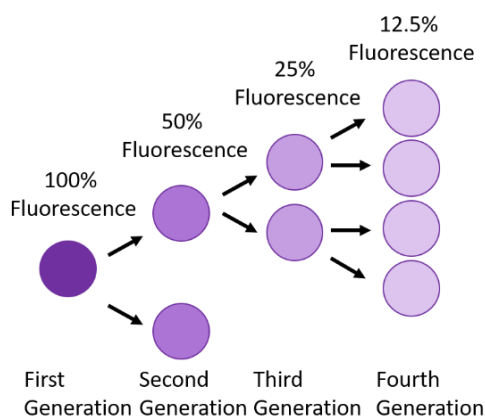


*Scheme 5 Principle of the  $H_2DCFDA$  conversion assay*

### *Proliferation tracking*

Proliferation is one of the fundamental processes in cells. Therefore, tracking the proliferation is an important marker in drug screening or cytotoxicity assessment <sup>[130]</sup>. It can be measured by dye dilution assays or by counting the cell number manually.

Cell trace violet (CTV) is a cell-permeable staining dye to track cell division without interfering with cell viability or well-being <sup>[131,132]</sup>. The staining dye contains a non-fluorescent succinimidyl ester molecule, which binds to amine groups inside the cells, resulting in long-term dye retention. Cellular esterases convert this non-fluorescent molecule to a fluorescent derivate upon cell entry. After cell division, daughter cells contain roughly half of the fluorescent labelling (Scheme 6), allowing to trace cell division with the FC.



*Scheme 6 Function of the CTV dye for tracking cell proliferation*

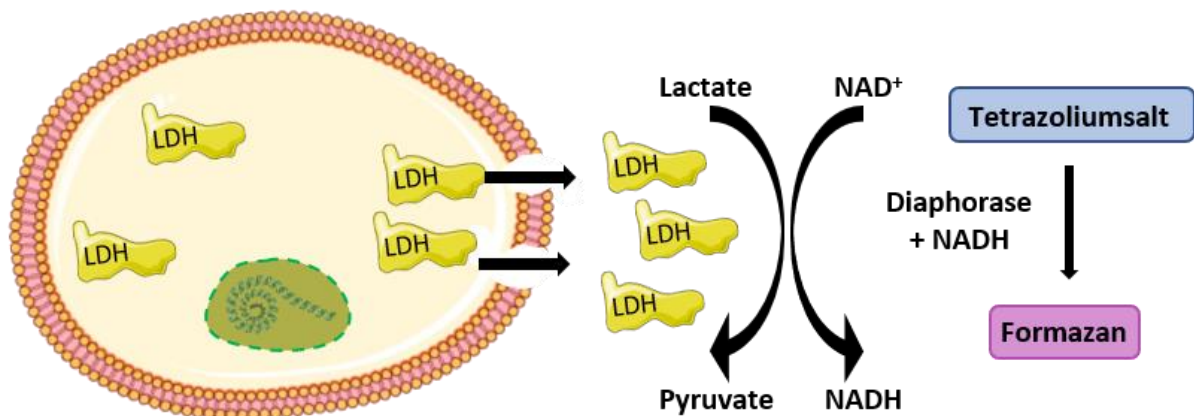
Carboxyfluorescein succinimidyl ester (CFSE) labelling works by the same principle as CTV <sup>[131]</sup>. The membrane-permeable CFSE binds covalently to the amine groups of intracellular proteins to form fluorescent conjugates. When labelled cells divide, their progeny contain half the number of tagged proteins. Hence each cell division can be assessed by measuring the corresponding decrease in cell fluorescence using FC.

### *LDH Assay for measuring membrane integrity*

Lactate dehydrogenase (LDH) is a cytosolic enzyme present in many different cell types and is a well-defined and reliable indicator of cytotoxicity <sup>[133]</sup>. When the plasma membrane of a cell is damaged, LDH is released into the surrounding culture medium. To measure the amount of LDH released, a coupled enzymatic reaction can be performed, in which LDH catalyzes the conversion of lactate to pyruvate via NAD<sup>+</sup> reduction to NADH. The resulting NADH is then oxidised by diaphorase, causing a reduction of a tetrazolium salt to a red formazan product which can be detected spectroscopically



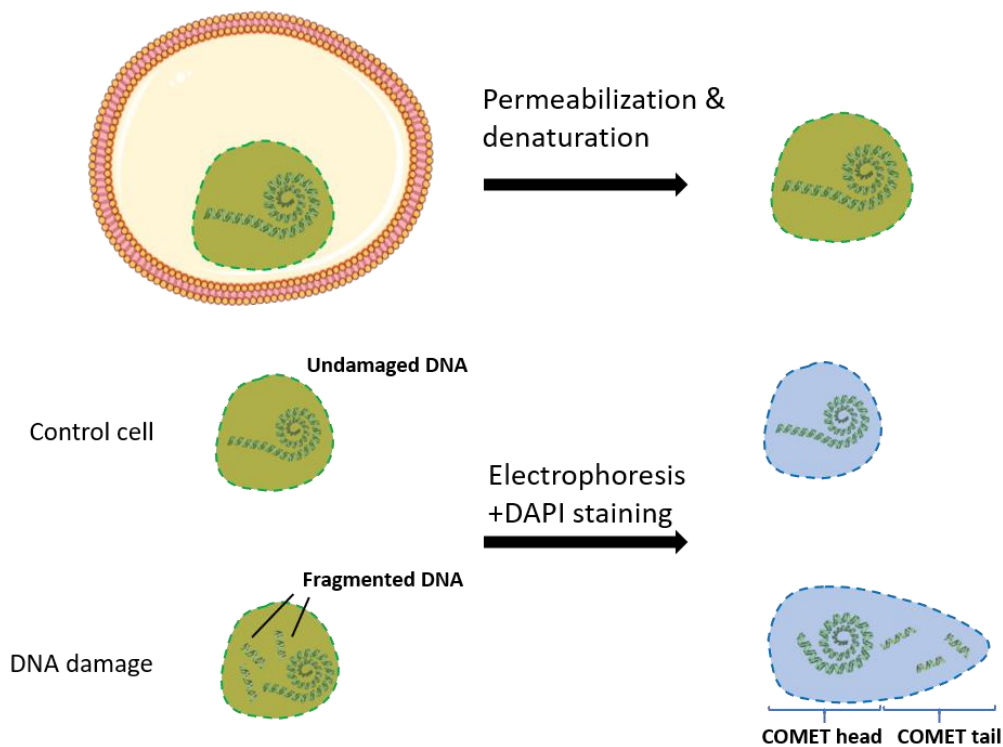
(Scheme 7). The degree of formazan formation is directly proportional to the quantity of LDH released into the medium, serving as an indicator of cytotoxicity.



*Scheme 7 Principle of the LDH assay*

#### *COMET assay to evaluate the genotoxic potential*

The COMET assay was first developed by Ostling and Johanson <sup>[134]</sup>. It is an established method to detect DNA damage in single cells using denaturing electrophoresis <sup>[135]</sup>. The assay measures strand breaks in the DNA, estimating the following genotoxic potential (Scheme 8).

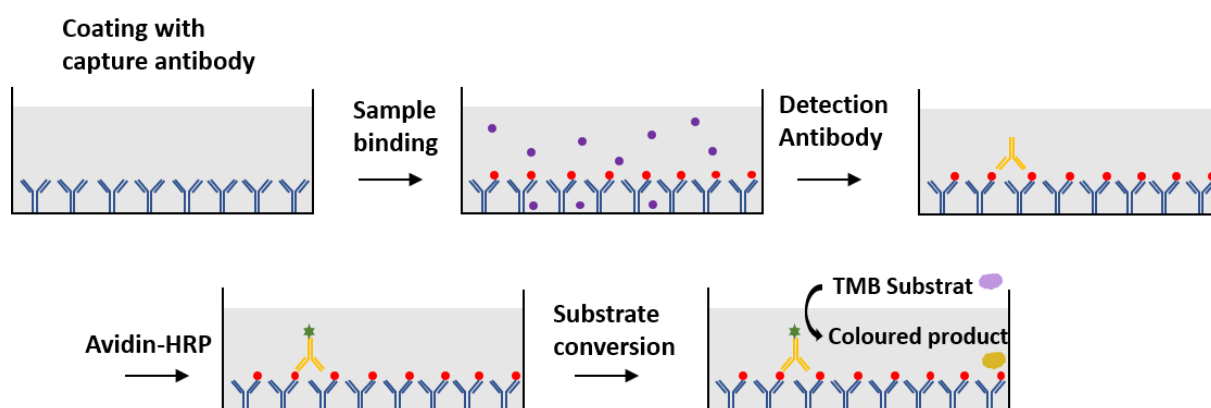


*Scheme 8 Principle of the COMET assay*

In this method, cells are embedded in agarose on a microscopic slide and lysed by a detergent to form nucleoids containing the supercoiled DNA. Via electrophoresis, comet structures arise in the case of fragmented DNA due to an easier “movement” in the agarose gel during electrophoresis. These structures are subsequently stained with a DNA dye (e.g. 4',6-Diamidino-2-phenylindol (DAPI) or HOECHST). The DNA damage can be determined by calculating the COMET tail percentage, either manually scoring or automatically by imaging software.

### *Enzyme-linked immunosorbent assay*

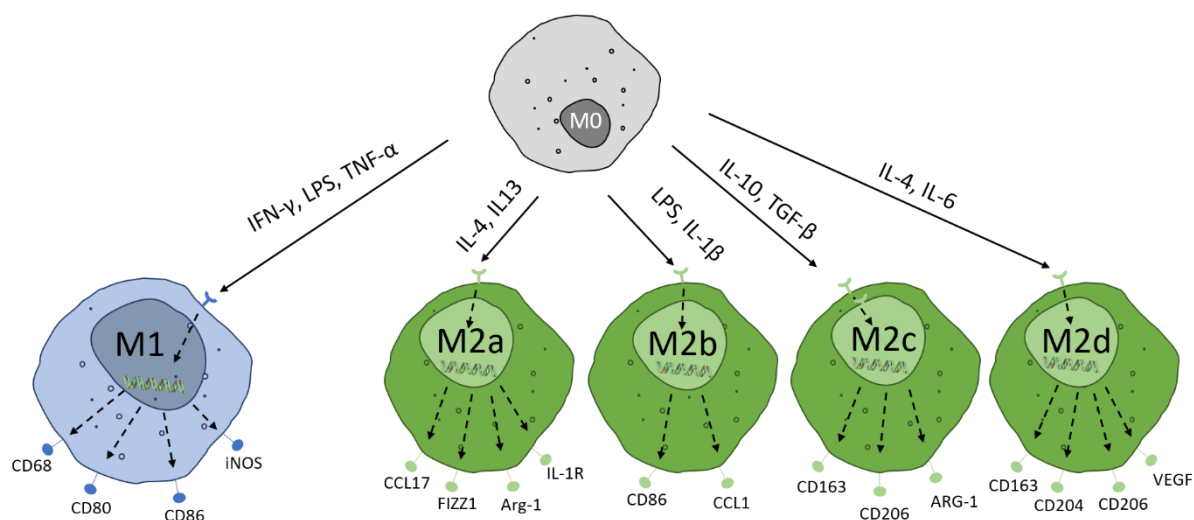
The enzyme-linked immunosorbent assay (ELISA) is an antibody-based assay that identifies and quantifies biological molecules (e.g. proteins or cytokines). The benefits of ELISA are its high specificity, high resolution, and low detection limit <sup>[136]</sup>. The system used is a so-called sandwich ELISA (Scheme 9). In this assay, the plate is first coated by a capture antibody to specifically bind the desired molecule (in this case, TNF- $\alpha$ ). Afterwards, the addition of a TNF- $\alpha$  detection antibody forms the eponymous antibody-antigen-antibody “sandwich” structure. Adding avidin-horseradish peroxidase, which binds specifically to the detection antibody, 3,3',5,5'-tetramethylbenzidine (TMB) substrate produces a blue colour in the concentration of TNF- $\alpha$  in the sample. Finally, the stop solution ends the enzymatic conversion and changes the colour from purple to yellow. The sample concentration can be measured using spectroscopical methods. The TNF- $\alpha$  cytokine response to the treatment with MPP was measured since MPP are assumed to provoke an inflammatory response <sup>[137]</sup>. TNF- $\alpha$  is hereby one of the main cytokines in the cell-mediated inflammatory response <sup>[138]</sup>.



*Scheme 9 Principle of the ELISA sandwich assay*

## 1.5. Polarisation of macrophages

The cell phenotype is an important parameter when using cell lines *in vitro*. In the case of macrophages, their high plasticity and reactivity are some of their main characteristics. *In vivo* and *in vitro*, undifferentiated macrophages (M0) are able to exhibit two different functional phenotypes, the classical proinflammatory M1 state and the alternative, anti-inflammatory M2 state [139]. These states are activated by environmental clues or the excretion of stimulating factors [140,141]. *In vivo*, M1 macrophages usually form the first immune response at the beginning of an infection and recruit and maintain inflammation as a response [142]. M2 macrophages are recruited to diminish inflammation and contribute to tissue regeneration [143]. In the case of M2 activation, 4 sub-types with different specifications exist (M2a – wound healing, M2b – immunoregulation, M2c – immunosuppression and phagocytosis of apoptotic cells, M2d – tumour-associated macrophage). *In vivo* as well as *in vitro*, M1 macrophages are stimulated by, e.g. interferon (IFN)- $\gamma$ , tumour necrosis factor (TNF)- $\alpha$  or lipopolysaccharides (LPS). M2 activation is mainly driven by Interleukin (IL)-4, IL-10 and IL-13 [139–141]. After activation, a signal pathway is activated, and various specific surface markers are expressed (Scheme 10), accompanied by an overproduction of ROS (especially for M1 polarisation) [144–146].



**Scheme 10 Model for the polarisation of macrophages and expression of selected, polarisation-specific surface markers**

TGF = Transforming growth factor; CD = cluster of differentiation, iNOS = inducible nitric oxide synthase, CCL = chemokine ligand, FIZZ1 = Resistin-like molecule alpha, ARG1 = Arginase 1, VEGF = Vascular endothelial growth factor

## 1.6. Primary cells in microplastic research

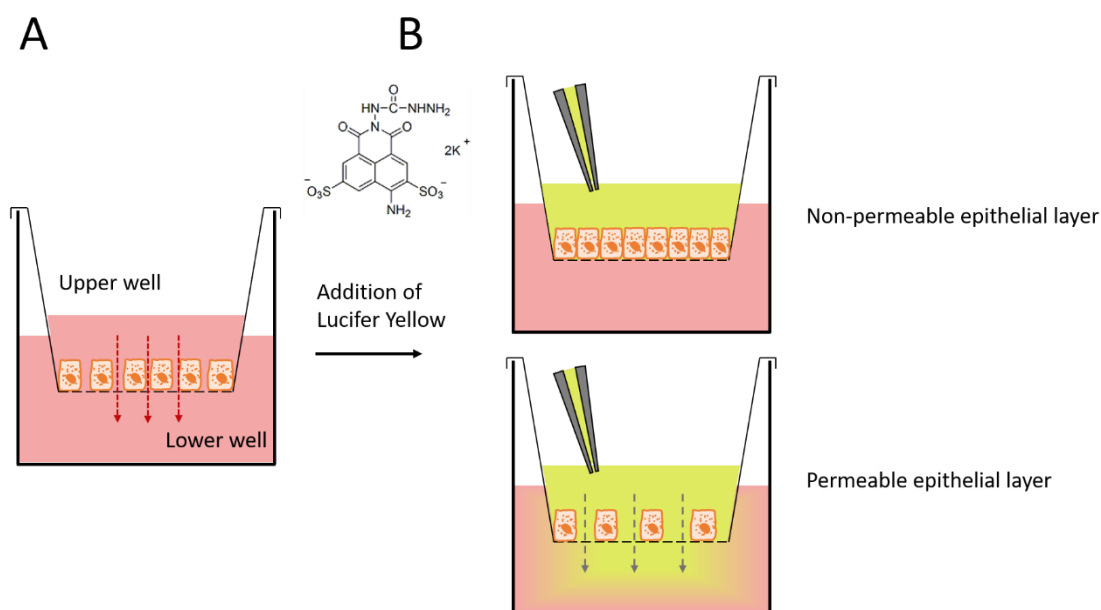
Primary cells are one common approach to increase the nativeness of used cells further. Primary cells are usually freshly isolated from the tissue of a multicellular organism. They can be obtained from a specific tissue, better representing the respective physiological and characteristic biological and cellular functions than immortalised cell lines [147–150]. Especially for transferring results from cell culture experiments to *in vivo* studies and understanding possible mechanisms, the functionality of

primary cells shines. Besides, using primary cells also has disadvantages. Compared to cell lines, they are harder to assess since they need to be freshly isolated, and their cultivation stability is lower. Assay reproducibility is often challenging due to batch-to-batch variation, and obtaining sufficient cells per batch highly depends on the used organism and tissue <sup>[151]</sup>. Nevertheless, using primary cells would be an excellent, complementary method in the MPP research field, especially when analysing critical parameters or gaining knowledge on a more mechanistic level. Despite that, only few researchers have used primary cells for MP research. Some analyses with primary mouse cells were conducted <sup>[152,153]</sup>, as well as with fish <sup>[154,155]</sup> and human cells <sup>[155,156]</sup>. All studies confirmed the uptake of micro- and nanoplastic in the respective primary cells. Especially the phenotype-specific mechanisms were affected. E.g. human Leydig cells showed reduced testosterone production <sup>[152]</sup>, Jung et al. found a cell type-dependent cytotoxicity for three different human brain cells <sup>[153]</sup>, and trout B cells showed less development potential after treatment with MPP <sup>[154]</sup>. However, compared to the growing amount of produced data on model organisms or cell lines, results generated with primary cells are still heavily lacking.

### **1.7. Usage of more complex three-dimensional cell cultivation in microplastic research**

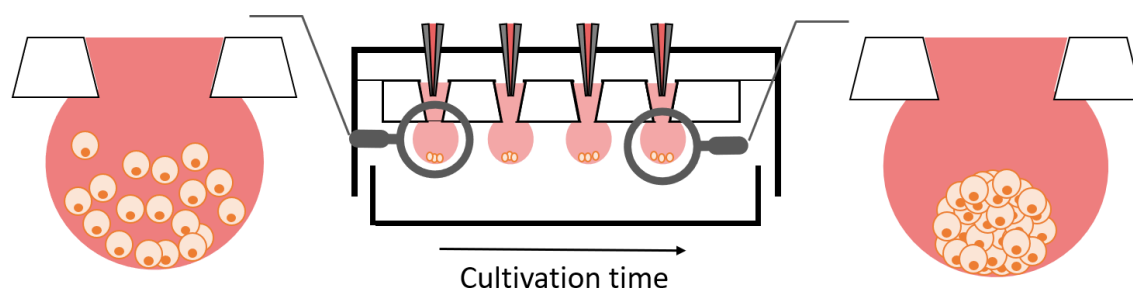
Another common approach to converge laboratory studies to more realistic conclusions is 3D cell cultivation. While cell lines are handy for generating an overview and analysing numerous parameters quickly <sup>[41]</sup>, there are still limitations (cell sources might be cancerogenic or tumour-derived, nonhomeostatic and nonphysiological culture conditions) <sup>[40]</sup>. It requires high effort when comparing *in vitro* and *in vivo* data, mainly due to the lack of a 3D microenvironment <sup>[157]</sup>. This 3D environment is highly important when estimating toxic effects since it converges experiments into a more realistic approach. To tackle this significant drawback, establishing 3D *in vitro* cultivation systems have become more important for risk assessment studies in the last couple of years <sup>[158,159]</sup>.

One approach to realise 3D cell culture is the usage of so-called transwell systems (Scheme 11A). Transwell assays are usually permeable membrane inserts with pore sizes between 0.4 – 8 µm, used for cell migration or invasion and permeability assays of mostly endothelial cells <sup>[160–162]</sup>. Some studies using transwell insert for the research of MP have been conducted <sup>[163–170]</sup>. Especially the impact of MP on the intestinal barrier and endothelial dysfunctions was analysed. The main findings included inflammation and enervated membrane integrity, with no acute toxicity. Most studies, though, found a translocation across the membrane, depending on size (smaller size → more translocation) and concentration (higher concentration → more translocation). One commonly used approach in the permeability analysis of epithelial barriers is the lucifer yellow (LY) assay <sup>[171–173]</sup>. LY is a non-membrane permeable, fluorescent molecule used to analyse the permeability and, thereby, the formation of a closed epithelial layer in the transwell assay (Scheme 11B).



**Scheme 11 Principle of the transwell system and the lucifer yellow assay**

Another approach in 3D cell cultivation is the usage of spheroids. Spheroids are spherical, 3D aggregations of cells with low structural complexity but can be established relatively quickly due to the relative simplicity of the cultivation <sup>[174]</sup>. They typically reach a diameter between 100 – 500  $\mu\text{m}$  connecting several thousand cells. Spheroids can be grown either by the addition of scaffolds or with scaffold-free techniques, e.g. the hanging drop method (Scheme 12) <sup>[175]</sup>.



**Scheme 12 Model for the spheroid cultivation in the hanging drop model**

Hereby, gravity is harnessed to promote the formation of cell aggregates in hanging droplets of the medium. Simple adaptations of standard cell culture materials and highly specialised plates can be used for the initial formation <sup>[176–178]</sup>. In biomedical research, spheroids are often used to provide tumour models for the analysis of cell-cell interaction or as a simplified model for tissue engineering <sup>[174,179,180]</sup>. Despite the great possibilities, spheroids or similarly constructed organoids have not been used often in MP research, with only a few studies available. Hua et al. found a negative impact on human forebrain organoid development when exposed to 1 and 10  $\mu\text{m}$  PS particles <sup>[181]</sup>. For liver organoids (slightly more complex microtissues than spheroids), induced hepatotoxicity was found when exposed to 1  $\mu\text{m}$  PS particles <sup>[84,182,183]</sup>. Lipid metabolism, increased ROS generation and inflammation,

as well as transcriptomic changes, were found, with all studies stressing the importance of the novel 3D approach. Despite the first efforts of implementing the 3D cell cultivation in the MP research, a high development potential exists, with the perspective of new, more reliable and physiologically relevant data.

### **1.8. Model organisms in microplastic research**

Finally, despite *in vitro* analysis having shown benefits, it misses the holism of an organism and the overarching, often highly complex reaction to pollutants. It is felt that “as much as *in vitro* can obviate *in vivo* to a great extent, still an element of whole animal study is essential” <sup>[184]</sup>. Various model organisms exist, from terrestrial to aquatic environments and vertebrates as well as invertebrates <sup>[185]</sup>. In microplastic research, the most used organisms stem from marine environments <sup>[186]</sup>. Prokić et al. stated in a comprehensive review that a “develop[ment] of new model organisms and non-invasive methods for MPs studies are necessary”. Especially for the terrestrial sector, only a few model organisms are considered <sup>[186]</sup>, with some of the most frequently used terrestrial model organisms being different earthworm species.

#### **1.8.1. Unicellular organisms in microplastic research**

Unicellular organisms, e.g. bacteria, algae or fungi, might act as a conjunction between the organismic and cell culture levels. They play an essential role in the low trophic levels of the food chain, are present in every compartment of the earth and interact in various ways with most higher organisms. Unicellular organisms demonstrate key features like locomotion, feeding and reproduction, connecting larger and more complex systems with cellular mechanisms. Larger unicellular organisms are essential in aquatic ecosystems as primary bacterial consumers <sup>[187]</sup>. Hence, they link bacterial production with higher trophic levels <sup>[188]</sup>. An imbalance in their population could, therefore, possibly alter entire communities. Investigating the possible effects of MP exposure on eukaryotic unicellular organisms, like, e.g. protists, should therefore be nearby, though they are still only scarcely researched. Recent investigations confirmed size-dependent uptake and toxicity of MP in, e.g. microzooplankton, like rotifers. It was shown that MP ingestion adversely affects their feeding activity, oxidative status and gene expression <sup>[189–191]</sup>. Athey et al. <sup>[192]</sup> also showed that the tintinnid *Favella spp.* quickly ingests MP, and those particles are transferred via predation to estuarine fish larvae (*Menidia beryllina*). Some studies used protists feeding unspecific and therefore are likely interacting with MP<sup>[193–196]</sup>.

Another often non-selective, unicellular predator is the group of protozoa. They feed on particulate matter, algae, bacteria or other smaller protists, though food choice highly depends on availability <sup>[197]</sup>. Given MP abundance in virtually all compartments, these particles are available for a wide range of these suspensive- and filter feeders <sup>[194]</sup>. Since various protozoa display this feeding behaviour and

since a large amount of MP in a smaller size range ( $< 50 \mu\text{m}$ ) is available <sup>[198,199]</sup>, they likely ingest MP. Therefore, research on the foot of the food webs is quite important since it gains knowledge about possible bioaccumulation or transfers to predators (for instance, amoeba), and hence to higher trophic levels <sup>[188]</sup>. *Amoeba proteus* is a predator that feeds on other protists slow enough to be engulfed by its pseudopods or via pinocytosis. Due to their capability of different ingestion methods and relatively large size ( $200 - 800 \mu\text{m}$ ), the likeliness of interaction with MP and a following transfer to higher trophic levels is elevated. Nevertheless, no literature is available on the interaction of microplastic and amoeba, representing a huge lack of knowledge in these trophic levels.

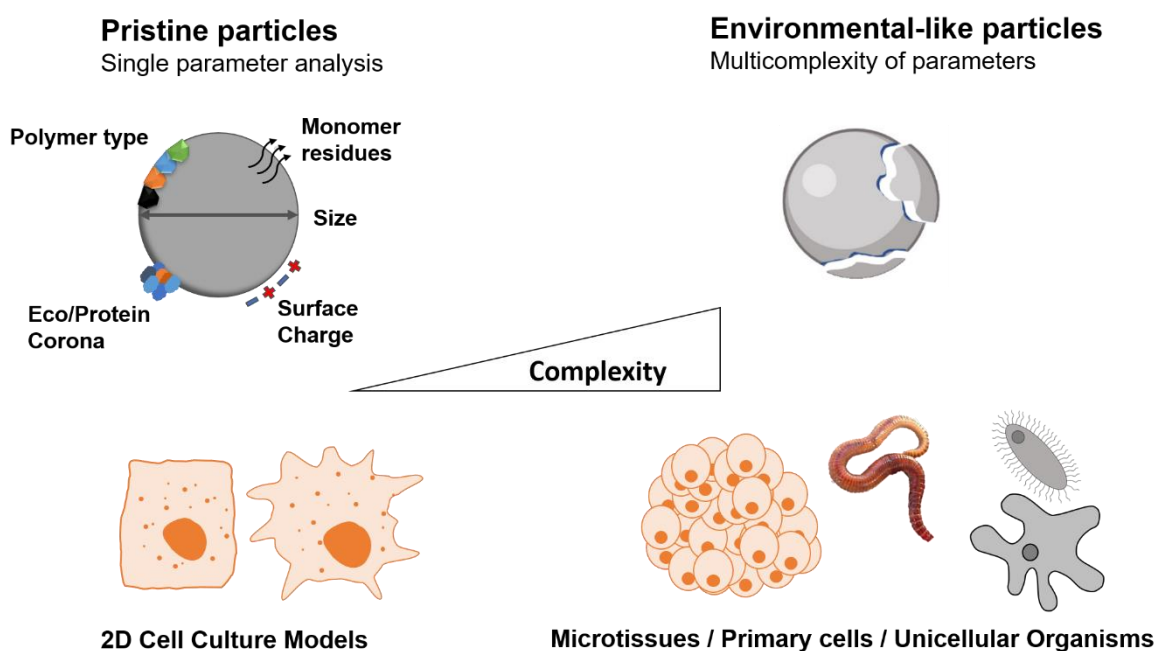
### 1.8.2. Terrestrial model organisms

Earthworms compose about 80 % of the terrestrial biomass, playing an essential role in the decomposition of organic matter, form a vital link in the food chain and improve soil quality through their feeding, burrowing and casting activities <sup>[200]</sup>. Due to their significant influence on the soil and in return, the soil composition influencing the organism highly, earthworms have been extensively used in ecotoxicological studies <sup>[200–202]</sup>. Consequently, earthworms were also used in the research with MP, as pictured by various reviews in the last years <sup>[203–207]</sup>. The used earthworms were affected by various standard ecotoxicological markers (e.g. the growth rate, behaviour, oxidative response, gene expression and gut microbiota). In, e.g. *Eisenia fetida*, MP exposure led mainly to an increase in the organisms' oxidative stress levels, while other tests, like effects on survival or reproducibility, did not show significant results <sup>[208–212]</sup>. However, the endpoint analysis of various ecotoxicological assays does not consider the mechanisms behind the observed effects. Highly complementary *in vitro* and *in vivo* assays might be used to tackle this downfall. Despite this, no literature considers primary earthworm cells and the effect of MP. Though, possibilities for *E. fetida in vitro* assays exist. One possibility is the isolation of coelomocytes, the immune cells of earthworms. Various protocols exist for isolating coelomocytes, e.g. mechanically, by ultrasound or electrically <sup>[213–215]</sup>. The relatively easy assessability and established method make coelomocytes an often-used analysis tool for ecotoxicological studies. MP effects, though, are possibly more directed to the intestinal tissue, where the particles initially encounter the earthworm after uptake via soil. Just recently, an isolation and cultivation protocol for primary cells of the intestinal tissue of *E.fetida* was established, allowing the cultivation of primary cells for up to six days and providing a tool for ecotoxicological assays, which might be applied to MP as well <sup>[118]</sup>.

## 1.9. Objective of this work

The above-mentioned increasing distribution of MP in all environmental compartments faces the inevitable consequences of interaction, accumulation, or even toxic effects in uni- and multicellular organisms. Via ingestion by, e.g. diet or inhalation, organisms and their tissue or epithelial layer get in contact with the intruding particles. Via cellular uptake or piercing through tissue, particles can be distributed in the whole organism causing numerous hazardous effects. Therefore, this work tries to investigate some of these concerns (Scheme 13).

c



*Scheme 13 Objectives of this work*

In the first step, the multi-parametric problem of MP should be dealt with. Thus, the influence of key parameters of MPP, like size, shape, material, surface charge and modifications, or monomer residues, are investigated with standard cytotoxicity assays to identify critical parameters on a cellular level. Macrophages and epithelial cell lines are used to cover the key cell phenotypes that might encounter MPP *in vivo*. Intracellular localisation, the distribution during mitosis and the excretion of MPP are considered to investigate a possible accumulation in specific tissues or cells. After answering these key questions with pristine, well-characterised particles and the basic model cell systems, results are transferred to more complex systems. First, environmentally more relevant MPP will be used. Particles will be artificially aged to simulate the impact of the environment on particles. Effects triggered by these aged particles will then be compared to the impact of the pristine particle. Using particles extracted from commercially available wall paints further increases environmental relevance. Subsequently, the cell systems will be constructed more complexly to establish epithelial layers or



micro-tissue formation. Based on these more complex cellular systems, penetration of particles through epithelial layers or into tissues might be analysed. After using murine cell lines, primary cells from environmentally relevant model organisms will be used to verify if investigated effects on a cellular level can be transferred to effects on an organismic level. Therefore, primary intestinal cells from *E. fetida* will be isolated and used to compare found results on an organismic level with potential effects on a cellular level. Finally, unicellular organisms will be taken into the equation, and the ingestion and possible transfer across a simplified food web will be analysed. In summary, the multi-parametric problem of MP burden on a cellular level should be investigated in increasing complexity to unravel critical key parameters step by step and transfer findings from a cellular level to more complex layers.

## 2. Methods

This chapter illustrates the methods used in this work. Detailed material information is added in Chapter 10.

### 2.1. Flow cytometry

Standard flow cytometry analysis was performed using a Cytomics FC500 equipped with a 405 and 488 nm laser. For each sample, at least 30,000 events were measured. If more cells were analysed, it would be specially noted. For standard analysis, seeded cells were washed twice with DPBS, detached by trypsinisation or citric acid treatment as described in 2.3 and suspended in 1 mL culture medium. Cells were then recovered by centrifugation ( $200 \times \text{gravity}$  ( $g$ ), 5 minutes ( $\text{min}$ )), the supernatant was discarded, and the cell pellet was resuspended in 0.5 – 1 mL DPBS. Cells were initially evaluated by scatter properties (FSC/SSC) to select a region (“nonapoptotic cell” gate) representing single, nonapoptotic cells while disregarding debris and cellular aggregates. In the case of other gating strategies, the respective strategy will be noted in the experiment. The fluorescence intensity of the microparticles was determined in the absence of cells, and this value was assumed to be the fluorescence intensity of one MPP on average. It should be noted that differentiation between particle uptake and mere particle adhesion to the cells is not possible using flow cytometry.

### 2.2. Characterisation of the used particles in this study

Since particle parameters such as size and surface charge are highly important, the used particles were characterised prior to experiments. Particle characterisation is hereby summed up in Table 1. The characterisation was done by Julia Jasinski if not stated otherwise. All relevant characterisation parameters are additionally added in the respective chapters.  $\zeta$ -potential was measured in KCl and the respective growth medium of the cells. Particles used with the primary cells of *E. fetida* were additionally characterised in the *E. fetida* growth medium. Particle size was measured by dynamic light scattering (DLS). Panels without measurements were either not done or not applicable (columns marked with \*) due to restrictions in the Zetasizer used. Fluorescent particles used in this work are shown by their particle name with the addition of the respective fluorescence colour (e.g. PS<sub>0.2 $\mu\text{m}$</sub> , green for green fluorescent 0.2  $\mu\text{m}$  PS particles ). If no other noted, fluorescence wavelengths were Ex/Em: 441/486 nm for green fluorescent particles and Ex/Em: 491/554 nm for red fluorescent particles.

**Table 1 Characterisation of the used particles**

Particle	ζ-potential (mV)			Size [μm]
	KCl	Growth medium	<i>E. fetida</i> Medium	
PS <sub>0.2μm</sub>	- 47.4 ± 0.3	- 26.3 ± 0.1	- 25.3 ± 0.0	0.2 ± 0.006
PS <sub>0.5μm</sub>	- 52.8 ± 0.2	- 26.2 ± 0.1	- 27.6 ± 0.0	0.5 ± 0.008
PS <sub>1μm</sub>	- 66.1 ± 0.1	- 29.2 ± 0.5	- 28.8 ± 0.0	
PS <sub>2μm</sub>	- 76.7 ± 0.3	- 30.7 ± 0.1		2.25 ± 0.15
PS <sub>3μm</sub> / PS <sub>polyscience</sub>	- 78.4 ± 0.4	- 28.6 ± 0.1	- 29.3 ± 0.2	3.1 ± 0.08
PS <sub>6μm</sub>	- 85.4 ± 1.4	- 11.7 ± 0.2		
PS <sub>43h</sub>	- 67.1 ± 0.7	- 33.9 ± 0.2		1.88 ± 0.05
PS <sub>86h</sub>	- 67.8 ± 0.4	- 29.5 ± 0.1		1.49 ± 0.10
PS <sub>130h</sub>	- 64.6 ± 1.6	- 26.4 ± 0.2		1.63 ± 0.22
PS <sub>micromod</sub>	- 1.6 ± 0.1	- 1.5 ± 0.0		
PS <sub>0.5μm</sub> in Prescott <sub>ref</sub>		- 53.4 ± 0.2		
PS <sub>0.5μm</sub> in Prescott <sub>NaCl</sub>		- 30.7 ± 0.2		
PS <sub>0.5μm</sub> in BSA		- 24.8 ± 0.4		
PS <sub>0.5μm</sub> in FCS		- 49.8 ± 0.3		
PS <sub>0.5μm</sub> in Prescott <sub>ref</sub>		- 44.7 ± 0.5		
PS <sub>0.5μm</sub> in Prescott <sub>NaCl</sub>		- 12.2 ± 1.2		
PS <sub>0.5μm</sub> in BSA		- 14.2 ± 1.1		
PS <sub>0.5μm</sub> in FCS		- 49.3 ± 5.7		
PE <sub>1-4μm</sub>	- 48.2 ± 0.6	- 27.7 ± 0.6		1.80 ± 0.35
PVC <sub>1.4μm</sub>	- 41.1 ± 2.3	- 26.1 ± 0.2		1.40 ± 0.15
PLA <sub>0.5μm</sub>	- 1.1 ± 0.0		- 1.3 ± 0.4	
PLA <sub>2μm</sub>	- 3.0 ± 0.4	- 21.9 ± 1.3	- 11.2 ± 1.1	1.75 ± 0.85
CA <sub>1.5μm</sub>	- 9.8 ± 0.5	- 6.9 ± 0.2		1.50 ± 0.40
PS <sub>&lt;20μm</sub>	*	*		16.1 ± 4.7
PS <sub>20-40μm</sub>	*	*		33.0 ± 9.8
PS <sub>40-75μm</sub>	*	*		49.9 ± 12.5
PS <sub>0.2μm</sub> , lysozyme	+ 8.0	- 27.2		
PS <sub>0.2μm</sub> , fibrinogen	- 0.6	- 18.2		
PS <sub>0.2μm</sub> , myoglobin	- 13	- 25.2		
PS <sub>3μm</sub> , fibrinogen	- 2.5	- 36.3		
PS <sub>3μm</sub> , lysozyme	+ 17.4	- 36.4		
PS <sub>3μm</sub> , myoglobin	- 16.1	- 37.1		
PS <sub>SHPA</sub> #	- 26 mV			0.515 ± 0.017
PS <sub>MIPA</sub> #	- 26 mV			0.507 ± 0.007
Paint 1 Supernatant ##	*	*		0.242 ± 0.059
Paint 2 Supernatant ##	*	*		Dissolved co-polymer
Paint 1 Solid Phase ##	- 37 mV			6.8 ± 1.1
Paint 2 Solid Phase ##	- 30 mV			150 nm to 10 μm

# Characterisation was done by Zhang and is published in the submitted paper Zhang et al. (2022)

## Characterisation was done by Müller and is published in Müller et al. (2022)

### 2.3. Cell lines used in this work

Cell culture shows the above-explained advantages of an established, quick and relatively straightforward approach to generating data. This is highly interesting in the not yet extensively analysed MP field. Overview experiments in this work were, therefore, mainly restricted to cell lines to identify critical parameters and possible biological effects. For the experiments in this work, five cell lines were used (Table 2)

*Table 2 Cell lines used in the cell cultivation experiments*

Cell line	Lot Number	Strain	Tissue	Cell phenotype	Growth properties	Doubling time [h] *
ImKC	SCC119	H-2Kb-tsA58	Liver	resident macrophages	adherent	24
BNL CL.2	ATCC® TIB-73™	BALB/c	Liver	epithelial	adherent	40
J774A.1	ATCC® TIB-67™	BALB/cN	ascites	macrophage	mostly adherent	17
STC-1	ATCC® CRL-3254™	C57B1/6J	intestine	epithelial-like	adherent	54
NCTC L - 929	ATCC® CCL1™	C3H/An	subcutaneous connective tissue; areolar and adipose	fibroblast	adherent	21 – 24

\*according to supplier information

These cell lines were chosen for various reasons. Different tissues and phenotypes were used to cover a broad spectrum of tissue or phenotype-specific behaviour. A nearby conclusion is selecting cells (ImKC, BNL CL.2) from the liver as the central detoxification organ. The epithelial layer from the intestine (STC-1) is another likely interaction tissue due to the predominant uptake of MP via food consumption. J774A.1 as macrophage from the ascites was chosen due to high comparability to other literature as a widely used cell line. Furthermore, J774A.1 was derived from wandering macrophages, while ImKC cells are immortalised Kupffer cells, the resident liver macrophages, again covering different specifications. L-929 was additionally used in some experiments as a commonly used reference cell line. Different cell phenotypes are also expected to show different behaviour and analysis methods. While macrophages are more likely to interact and ingest particles as natural killer cells, penetration experiments are more reasonable with the epithelial cells.

ImKC cells were cultivated in RPMI1640 supplemented with 2 mM glutamine. STC-1, BNL CL.2, and J774A.1 cells were cultivated in DMEM (DMEM<sub>ATCC</sub> for STC-1 and BNL CL.2; DMEM<sub>Lonza</sub> for J774A.1 and L929). For J774A.1 cells, the medium was supplemented with 4 mM glutamine, 24 mM HEPES, and 0.1

mM sodium pyruvate. For L929 cells, the medium was supplemented with 2 mM glutamine. All media compositions were supplemented with 10% (v/v) FCS and 100 Units (U)/mL penicillin/streptomycin and are referred to as “growth media” throughout the manuscript. Adjustments to the media are specifically mentioned for the respective experiment. All cells were cultivated in a standard cell culture incubator (5% CO<sub>2</sub>/ 95% humidity) at 37°C. For cell maintenance, all cell lines were passaged three times a week at a starting concentration of about 100,000 cells/mL in a 10 cm cell culture dish. For detaching, cells were washed twice with Dulbecco’s Phosphate Buffered Saline (DPBS) and either 1 mL/dish at 37°C pre-warmed citric saline buffer (135 mM potassium chloride + 15 mM sodium citrate, 5 and 10 min incubation at 37°C for J774A.1 and ImKC, respectively) or 1 × Trypsin/ Ethylenediaminetetraacetic acid (EDTA) (for STC-1, BNL CL.2 and L929) was used. Cells were regularly observed by an inverse light microscope. This cultivation process is referred to as “standard cultivation” throughout the manuscript, and changes are specifically named for the respective experiment.

For all seeding processes, cells were incubated for at least one week after thawing. Afterwards, the whole cultivation dish was washed twice with DPBS, detached and harvested in fresh growth media. The cell number was then determined by trypan blue exclusion (2.5), the needed cell concentration was adjusted and the cells were seeded according to the respective experimental setup. All seeding processes in this manuscript were done accordingly, if not else stated.

#### **2.4. Cryopreservation and thawing of cells**

For cryopreservation, cells were washed twice with DPBS, harvested as previously described, and a cell concentration of 3 – 5 x 10<sup>6</sup> cells/mL was adjusted. Cells were then centrifuged (200 x *g*, 5 min), the supernatant was aspirated, and the cells were resuspended in the same volume of cryomedium (for ImKC and STC-1: 90 % growth medium, 10 % DMSO; For BNL CL.2, L929 and J774A.1: 95 % growth medium, 5 % DMSO). 1 mL of this suspension was transferred to special cryopreservation tubes. Subsequently, the cells were placed in a Mr. Frosty™ and pre-cooled in a freezer at - 80°C for 24 hours (h). The cryovials were transferred to a cryogenic storage tank and stored at - 195°C in liquid nitrogen for long-term storage.

For thawing, a single cryovial was put in a water bath at 37°C to defrost slowly until only a little ice drop was left. The vial was then transferred into 9 mL of the growth medium, and cells were centrifuged (200 x *g*, 5 min). The supernatant was discarded, and cells were resuspended in 10 mL of fresh growth medium. The whole suspension was then transferred to a cell culture dish, and standard cell cultivation was performed for at least 7 days before using freshly thawed cells in an experiment.

## 2.5. Estimation of the cell count and viability

A trypan blue staining was performed to determine the cell count and viability. Trypanblue is non-membrane permeable for healthy cells, resulting in dark blue staining of dead cells with a damaged membrane. The cell count was analysed using a hemocytometer. Therefore, 10 µL of the cell suspension was mixed with 10 µL trypan blue. 10 µL of this suspension was transferred to one chamber of a hemocytometer, and the cell count of live and dead cells in the four large chambers was counted by light microscopy. Cell count was afterwards calculated by Equation 1.

*Equation 1 Living cell count calculation when using a hemocytometer*

$$\text{Living cell count } \left[ \frac{\text{cells}}{\text{mL}} \right] = \text{cell count living cells} \times \text{dilution factor} \times \frac{10^4}{\text{mL}}$$

Where: dilution factor in most cases was 2 due to the 1:1 dilution of trypan blue to cell suspension.

Cell viability was afterwards calculated by the ratio of living cells to the total cell count multiplied by 100 for the percentage.

## 2.6. Polarisation of macrophages

Macrophages were polarised to analyse whether MP uptake depends on the respective polarisation. In this work, common stimuli (LPS for M1 and IL-4 for M2) from the literature [216–220] were used to polarise macrophages to their respective state. The used concentrations were adapted from literature sources, where concentrations between 10 – 1000 ng/mL LPS and 1 – 100 ng/mL IL-4 were used [216–220]. The overproduction of ROS and the development of specific surface markers were analysed to verify the polarisation.

For the ROS approach, 150,00 cells (ImKC and J774A.1) were seeded in a 12-well plate and incubated for 24 h at standard cell culture conditions. Afterwards, the respective amount of polarisation agent (10, 20, 50, 100 ng/mL LPS and 10, 20, 50 ng/mL IL-4) was added for the given experimental time (3, 6, 24 h). For J774A.1, the incubation with the polarisation agent was prolonged to 48 h, since this cell line did not react as quickly as the ImKC cells. After the respective polarisation time, 37.5 µm DCFDA was added and incubated for 1 h. The ROS amount was then measured as described in 2.12.3. In the case of the polarisation kinetic, the respective polarisation agent was added for 24 h. Afterwards, the supernatant was aspirated, each well was washed twice with DPBS, and 1 mL growth medium was added per well. After 3, 6 or 24 h, 37.5 µm DCFDA was added and incubated for 1 h, and the ROS amount was measured as described in 2.12.3.

Analysis by antibody staining of the surface markers was performed as follows. 150,000 cells/well (J774A.1, ImKC) were seeded in a 12-well plate and incubated for 24 h. Afterwards, the respective

polarisation agent was added for 24 h in the respective concentration (20 and 100 ng/mL LPS and 20 ng/mL IL-4). M1 cell polarisation was analysed by antibody staining of the CD68, CD80 and CD86 surface markers. M2 polarisation was analysed by the CD206 surface marker. Cells were collected after 24 or 48 h incubation with the polarising substance, centrifuged (200 x g, 5 min), washed with DPBS, resuspended in 100 µL DPBS and afterwards counted. For every 10<sup>6</sup> cells, the respective amount of antibody (CD68: 0,25 µg/100 µL; CD80: 0,5 µg/100 µL; CD86: 1 µg/100 µL; CD163: 0,125 µg/100 µL) was added and incubated for 20 min in the dark at room temperature. Afterwards, 900 µL DPBS was added, and cells were centrifuged (200 x g, 5 min), washed with DPBS and resuspended in 750 µL DPBS. The staining was measured by FC (Ex/Em: CD68 488/690 nm; CD80 488/578 nm, CD86 488/520 nm; CD163 488/785 nm).

To analyse the PCI of polarised macrophages, cells were polarised with the respective stimuli (24 h for ImKC, 48 for J774A.1), 15 µg/mL PS<sub>2µm, red</sub> were added per well and incubated for 6 h with the polarised cells. Afterwards, cells were detached, washed twice with DPBS, and the PCI was analysed by flow cytometry with the established method (2.1).

## **2.7. Isolation and cultivation of primary *E.fetida* cells**

The isolation and cultivation of primary intestinal cells from *E.fetida* was done according to Riedl et al. (2022) <sup>[118]</sup>. Briefly, the intestine was freshly extracted from an organism and treated with 10 µg/mL Collagenase II at 37°C in 500 µL M-HBSS supplemented with 100 U/mL penicillin, 100 µg/mL streptomycin, 60 µg/mL tetracyclin, 50 µg/mL gentamicin and 2,5 µg/mL amphotericin B (PSTGA) under agitation in an Eppendorf Thermomixer (500 rpm) to start digesting the intestine. After 90 min of incubation, the supernatant with the isolated cells was centrifuged (200 x g, 5 min), washed in M-HBSS/PSTGA and filtered with a 20 µm cell strainer. Cells were again centrifuged, and the pelleted cells were transferred in a specialised media (60% (v/v) L-15 medium, 20% (v/v) ddH<sub>2</sub>O, 10% (v/v) FCS and 10% (v/v) worm filtrate, 4 mM L-glutamine, 25 mM HEPES and PSTGA), to ensure high viability for six days. Cells were seeded in 48 well plates (0.1 – 0.15 x 10<sup>6</sup> cells/well) and incubated in an airtight box containing a reservoir of sterile ultrapure water at room temperature (20 to 22°C).

## **2.8. Transwell seeding**

For the initial seeding, 100,000 cells (BNL CL.2 and L929) per transwell insert were seeded in 200 µL of growth medium in the upper well. 800 µL growth medium was added subsequently in the lower well. The cells were cultivated at standard cell culture conditions. Every 48 h, the medium was changed. Therefore, the medium was carefully aspirated, with special care not to touch the membrane of the insert. Afterwards, fresh medium was carefully added, again with particular care not to damage the membrane. Particles were added freshly according to the respective experiments.

## 2.9. Spheroid formation

For spheroid formation in Petri dishes, BNL CL.2 cells were washed twice with DPBS and collected by trypsinisation. 50  $\mu$ L drops of media containing 10,000 cells were placed on the lid of a Petri dish, the bottom of the dish was filled with 5 mL PBS to prevent drying out, and the lid was carefully placed back (Scheme 19). Medium change was conducted every 48 h by carefully removing 20  $\mu$ L of depleted medium with the pipette and adding the same amount of fresh medium. Spheroid formation was checked by tracking the growth microscopically.

For spheroid establishment in the GravityPLUS™ plate, BNL CL.2 cells were washed twice with DPBS and collected by trypsinisation. 10,000 cells per well of the hanging drop plate were seeded in 40  $\mu$ L of growth medium. As recommended by the manufacturer, a gauze wetted with sterile DPBS was placed at the bottom plate to ensure high humidity and prevent the drops from drying out. The seeded plates were incubated at standard cell culture conditions. Medium change was conducted every 48 h by carefully removing 10  $\mu$ L of depleted medium and adding the same amount of fresh medium. Spheroid formation was checked by tracking the growth microscopically.

The spheroids were captured by placing the cultivation plate on top of the Gravity Trap™ plate, and 70  $\mu$ L fresh media was added to the respective well. Due to the increased volume, the spheroid drop falls into one of the Gravity Trap™ well, where it could be further processed (see 4.2.1).

A personalised plate for capturing the spheroids was designed by 3D printing (Table 3).

*Table 3 3D printing parameters for the personalised capture plate*

Factor	Value
Printer	Creality Ender-3
Material	Pima Value™ PLA (1.75 mm diameter – grey colour)
CAD software	Solidworks 2021
Slicing software	Cura Ultimaker 4.8.0.
Nozzle temperature	220°C
Bed temperature	60°C
Printing speed	40 mm/sec
Layer height	0.2 mm
Infill density	100 %
Infill pattern	Lines

When using the personalised plate, 200  $\mu$ L Eppendorf reaction tubes were placed in the respective well. Each reaction tube was filled with 40  $\mu$ L of the growth medium to prevent a bubble formation in the tube. Afterwards, 70  $\mu$ L fresh media was added to the respective well of the cultivation plate, and the spheroids were transferred into one reaction tube for further processing.



For fixation, spheroids were harvested as described. The media was then carefully aspirated from the Eppendorf tube, and the spheroid was washed with 80  $\mu$ L DPBS. Afterwards, the DPBS was removed, and 100  $\mu$ L 3.7 % (w/v) paraformaldehyde (PFA) was added. The spheroid was incubated for 30 min at 37°C and, for further processing, washed thrice in 100  $\mu$ L DPBS. For longer preservation, the fixed spheroids were kept in PFA and stored at 4°C for further analysis.

For the penetration analysis of the particles into the spheroids, spheroids were seeded as described above for 5 days to ensure a full formation. Afterwards, freshly prepared particle suspension was added by pipetting  $1 \times 10^5$  particles/well in 10  $\mu$ L per well and carefully resuspending the droplet. Particles were afterwards incubated for 24 h, and spheroids were subsequently analysed.

To establish a suitable co-cultivation medium, 150,000 cells per well were seeded in 12-well plates. The respective media composition was added for 48 h. Afterwards, cells were harvested, and the cell count and viability were determined via trypan blue exclusion.

In the case of co-cultivation, spheroids were grown, and particles were added on day 5, as described above. ImKC cells were detached and stained with CTV for better determination in the following analysis. The macrophages were added by pipetting 10  $\mu$ L with 500 macrophages per spheroid in the hanging drop 24 h after particle incubation and incubated for further 24 h. Spheroids were afterwards harvested, fixed, stained and analysed by confocal microscopy.

## 2.10. Agarose micro-array embedding

The agarose microarray embedding was performed as proposed by Ivanov and Grabowska (2018) <sup>[221]</sup>. First, the microarray compartments (bottom and top) were 3D printed by using an SLA printer (Table 4). Once printed, both moulds were washed in isopropanol, cured under UV light, and polished to improve geometrical accuracy.

*Table 4 3D printing parameters for the microarray compartments*

Factor	Value
Printer	Formlabs Form 2
Material	Formlabs clear resin FLGPCL04
CAD software	Solidworks 2021
Slicing software	Cura Ultimaker 4.8.0.
Cleaning agent	Isopropanol
Curing temperature	60°C
Curing time	60 min

To create the agarose mould, the bottom of the microarray was filled with 1.9 mL liquidised, warm agarose (2 %, 5 %, 10 % in deionised water, low melting and high melting agarose). Immediately after, the top of the microarray was placed in the agarose, and the compartment was placed in the freezer

for 3 min to enable a hardening of the agarose. Afterwards, the mould with wells was formed by carefully removing the top. The moulds were kept at 4°C for further processing.

For embedding spheroids, one fixed spheroid was carefully pipetted into a well of the prepared moulds. The mould was carefully sealed by pipetting 1.2 mL of the same agarose as used for the mould on top. The gel was afterwards frozen at - 20°C. Finally, the spheroid containing agarose block was removed from the mould by gently applying pressure with a laboratory spatula, transferred into a histological cassette, and stored in the fridge until slicing (at 3°C).

### **2.11. Gelatine Capsules Embedding**

Gelatine capsules were placed in a 48-well plate used as a holder. The bottom of each capsule was filled with 200 µL of Tissue Tek optimum cutting temperature (O.C.T.) compound. To prevent the capsules from melting, they were immediately placed in dry ice to harden the bottom half, as the capsules had a melting temperature of around 30°C. To facilitate the localisation of the spheroid, a small aluminium foil ball (approximately 1 mm diameter) was added as a tracer. Fixed or unfixed spheroids were transferred directly from the medium to the capsule using a pipette. The spheroids were slowly and carefully covered with O.C.T. compound to fill half the capsule while remaining on dry ice. The prepared capsule was stored at - 80°C until further processing.

### **2.12. Cell Assays**

#### **2.12.1. MTT Assay**

For the procedure, 10.000 cells/well (J774A.1, ImKC, BNL CL2) were seeded per well in 100 µL of their respective growth medium (25.000 cells per well for STC-1 to accommodate for their slower growth rate). In the case of the experiments with 72 h particle incubation time, the seeding density was reduced, i.e. adapted to the different cellular growth rates, and a “conditioned medium” was used. The seeding densities, in this case, were 2000 cells/ well (ImKC and BNL CL.2), 4000 cells/well (J774A.1), and 6000 cells/well (STC-1). Conditioned media was fully growth media, which was already used for incubation with cells to enrich growth factors. Therefore, media was aspirated after 24 h of incubation with cells, collected, sterile-filtrated and 2mM L-glutamine was added. Conditioned media was used to ensure optimal growth conditions despite the relatively low cell densities. Cells were then incubated for 24 h at standard cell culture conditions (95 % humidity, 5 % CO<sub>2</sub>, 37°C). The particle solution was freshly prepared by diluting the particle stock solution in full growth media to the desired concentration. Afterwards, the medium was aspirated, and 100 µL of the freshly prepared particle solution in the respective concentration was added. Cells were again incubated for 24 h (other incubation times are added in the text). After the respective particle incubation time, the medium was aspirated, and cells were washed twice with DPBS and 50 µL freshly prepared MTT solution (1 mg/mL

MTT in phenol-red free minimum essential media (MEM), sterile-filtrated with 0.2 µm cellulose acetate filters) was added per well. MTT solution was incubated for 2 h to allow a sufficient conversion of MTT but not surpass the plate reader's linear dependency, which might occur after a longer incubation. In the case of primary intestinal cells from *E. fetida*, the incubation time was prolonged to 24 h <sup>[118]</sup> due to a lower baseline metabolic activity for these cells. After the respective incubation time, the supernatant was aspirated, and 100 µL Isopropanol was added per well to dissolve the formazan crystals. Again, the procedure had to be adjusted for *E. fetida* cells since these cells were not adherent. The entire well was collected and transferred to reaction tubes, then centrifuged at 400 × *g* for 5 min. After centrifugation, the supernatant was carefully removed and discarded. The cells containing the formazan crystals were then mixed with 250 µL isopropanol. This cell suspension was then divided equally and transferred to two wells of a 96-well plate. After 5 min of shaking to homogenise the suspension, the absorbance at 570 nm (reference wavelength 650 nm) was measured using a TECAN GENios Pro plate reader. For all assays, cells incubated without particles or with 0.3% Triton X - 100 in the respective cell culture medium, under otherwise identical conditions, were used as negative and positive controls, respectively. The metabolic activity was calculated according to Equation 2.

**Equation 2 Calculation of the metabolic activity**

$$\text{metabolic activity [\%]} = \frac{\text{Abs570}_{\text{sample}}}{\text{Abs570}_{\text{blank}}} \times 100$$

where: Abs570<sub>sample</sub> is the mean value of the measured absorption of the test sample; Abs570<sub>blank</sub> is the mean value of the measured absorption of the negative control.

### 2.12.2. Proliferation assay by cell count

100,000 cells (J774A.1, ImKC, BNL, CL.2 STC-1) were seeded in 1 mL growth medium per well in a 12-well plate and left to settle for 3 h at standard cell culture conditions. Afterwards, the cells were treated with 37.5, 150 and 1500 µg/mL of PS<sub>polyscience</sub> and PS<sub>micromod</sub>. Cells were collected after the respective incubation time (0, 24, 48 and 72 h) and resuspended in 1 mL cell growth medium. Special care was taken with the voluminal used for this experiment to estimate the cell number precisely. Cell number was evaluated using an automated fluorescence cell counter. Therefore, a 2 µL cell suspension sample was mixed with 18 µL Staining-Mix (Acridine Orange and Propidium iodide, proprietary concentrations from Logos Biosystems) and loaded into the chamber of a PhotonSlide. Every sample was determined threefold, and the mean value was taken. Cells incubated without particles at otherwise identical conditions were used as references.

### 2.12.3. ROS Assay

For all experiments, 150,000 cells/well (J774A.1, ImKC, BNL CL.2, STC-1) were seeded in 12-well plates in 1 mL of growth medium. Cells were incubated for 24 h at standard cell culture conditions.

Afterwards, the respective, freshly prepared particle suspension was added. As control wells, cells incubated without particles or in the presence of 50  $\mu\text{M}$  (5  $\mu\text{M}$  for STC-1) antimycin A, a ROS-promoting antibiotic, were used as negative and positive controls under otherwise identical conditions. After 60 min incubation, 37.5  $\mu\text{M}$  DCFDA was added per well (5  $\mu\text{M}$  for STC-1), followed by another 24 h incubation in the cell incubator. For STC-1 cells, the DCFDA concentration was reduced because of concerns regarding the cytotoxicity of the dye, which had manifested itself during the establishment of the assay. Afterwards, cells were detached, and the DCF fluorescence intensity was measured using FC. ROS amount was calculated according to Equation 3.

*Equation 3 Calculation of ROS amount by FC*

$$ROS \text{ amount } [\%] = \frac{MFI_{\text{sample}}}{MFI_{\text{NC}}} \times 100$$

where:  $MFI_{\text{sample}}$  is the mean fluorescence intensity of the green fluorescence of the test sample;  $MFI_{\text{NC}}$  is the mean fluorescence intensity of the green fluorescence of the negative control (i.e., cells incubated without MP).

#### 2.12.4. CFSE staining

For staining, cells (J774A.1, ImKC, BNL CL.2, STC-1) were detached, counted, and adjusted to  $5 \times 10^6$  cells/mL. Cells were centrifuged (200 x g, 5 min), washed twice with DPBS, and resuspended in 1 mL DPBS. 1 mL of freshly prepared CFSE solution (10  $\mu\text{M}$  in DPBS) was added for a working concentration of 5  $\mu\text{M}$ /5 x 10<sup>6</sup> cells. Cells were then incubated for 5 min at room temperature and protected from light. Afterwards, 12 mL of the respective growth medium was added to bind free staining dye. Cells were centrifuged (200 x g, 5 min), the supernatant was discarded, and another 10 mL of growth medium was added. After 5 min of incubation, cells were again centrifuged (200 x g, 5 min), resuspended in 5 mL growth medium and seeded in the respective volume or well plate, depending on the experiment.

For analysing the size-dependent influence of MPP on proliferation (3.3.2), 150,000 CFSE-stained cells were seeded per well in 12-well plates (cultivation volume 1 mL). After 24 h of incubation, a freshly prepared particle suspension was added, and the cells were incubated for another 72 h. Cells incubated without particles under otherwise identical conditions were used as the negative control. After incubation, cells were harvested, washed with DPBS and measured by FC (Ex/Em CFSE: 492/517 nm).

#### 2.12.5. CTV staining

Cells were stained using a CTV Proliferation Kit (Ex/Em CTV: 405/450 nm) according to the manufacturer's instructions. Briefly, cells (J774A.1, ImKC) were detached, counted, and adjusted to  $10^6$  cells/mL. Cells were centrifuged (200 x g, 5 min), washed twice with DPBS, and resuspended in

1 mL DPBS. Afterwards, 1 µL of CTV stock solution per 1 mL cell suspension was added for a working concentration of 5 µM CTV. Cells were then incubated for 20 minutes at room temperature and protected from light. Afterwards, cells were centrifuged (200 x g, 5 min), the supernatant was discarded, and the pellet was resuspended in a volume of complete growth medium corresponding to five times the original staining volume to remove free staining dye. After 5 min incubation, cells were centrifuged (200 x g, 5 min), resuspended in growth medium and seeded in the respective volume or well plate, depending on the experiment.

#### 2.12.6. LDH assay

The CyQUANT™ LDH Cytotoxicity Assay was performed according to the manufacturer's instructions. Initially, 10,000 cells (ImKC) were seeded in 100 µL of complete growth medium in a 96-well plate and incubated for 24 h under standard cell culture conditions. Then, the medium was aspirated, and freshly prepared particle suspension was added at the respective concentration. Cells incubated under identical conditions but without particles served as a negative control to determine the spontaneous release of LDH. Subsequently, the cells were incubated for an additional 24 h in the cell culture incubator. To determine the maximum LDH release, 10 µL of diluted lysis buffer (proprietary mixture, incubation time 45 min) was added to cells without MPP. Following this, 50 µL of supernatant from each well was transferred to a fresh 96-well plate, after which 50 µL of a freshly prepared reaction mixture was added and incubated for another 30 min in the cell culture incubator. Lastly, 50 µL of stop solution was added to each well, and the absorbance was measured at 490 nm (reference wavelength 680 nm). The LDH release was calculated according to Equation 4.

##### *Equation 4 Calculation of the LDH release*

$$LDH \text{ release } [\%] = \frac{Abs_{sample} - Abs_{spontaneous}}{Abs_{max} - Abs_{spontaneous}} \times 100$$

Where:  $Abs_{sample}$  is the mean value of the measured absorption of the test sample;  $Abs_{spontaneous}$  is the mean value of the measured absorption of the negative control;  $Abs_{max}$  is the mean value of the measured absorption of the positive control.

#### 2.12.7. COMET Assay

The here used experimental setup is described in the following. 150,000 cells (ImKC) were seeded on a 12-well plate and incubated for 24 h at standard cell culture conditions. Afterwards, the freshly prepared particles at the respective concentration were added in the respective concentration, followed by another 24 h incubation. For the embedding process, microscope slides were pre-coated with electrophoresis agarose. The slides were cleaned with Milli-Q water and rinsed with absolute ethanol and air-drying. The slides were then dipped in a container filled with melted 1 %

electrophoresis agarose in H<sub>2</sub>O. After removing any excess agarose, the back of the slides was wiped off to ensure cleanliness. Finally, the coated slides were dried on a heating plate at 55°C.

Cells were then harvested, the cell density was set at 60,000 cells in 1 mL ice-cold DPBS, and the cell suspension was centrifuged (200 x *g*, 5 min). The supernatant was discarded, and the cell pellet was resuspended in melted 0.1 mL of 1 % low melting point agarose in DPBS heated to 40°C in a water bath. The suspension was carefully pipetted onto an agarose pre-coated slide, and a cover glass (24 x 50 mm) was placed on top of the agarose to spread the suspension evenly. The slide was then placed for 5 min on ice to harden the agarose, and the cover glass was carefully removed afterwards. The slides were stored in a wet chamber at 4°C overnight. After that, 2 mL of lysis buffer (1 % v/v Triton-X-100, 2 M NaCl, 0.1 M EDTA at 8.0 pH, 10 mM Tris-HCl at pH 9.0) was pipetted on top of the slide and the slide incubated for 1 h at 4°C in the dark. The lysis buffer was removed carefully, and 2 mL of electrophoresis solution (0.3 M NaOH, 1 mM EDTA at pH 8.0) were added for a 20 min incubation. This step was repeated twice. Slides were then placed in an electrophoresis tank filled with electrophoresis solution and incubated for 40 min at 4°C. Then, the electrophoresis was conducted at 20 V (0.6 V/cm) and 200 mA for 30 min, conditions which had been determined in pre-experiments. Slides were washed thrice (5 min each) in neutralisation buffer (0.4 M Tris, pH 7.5). The DNA on the slides was stained using 1 mL of a 2 µg/mL DAPI suspension, which was incubated for 20 min in the dark. Slides were rinsed with 5 mL of DPBS and then analysed using a fluorescence microscope. Pictures were subsequently analysed with the COMETSCORE™ software (version 2.0.0.38). As a positive control, non-treated cells were incubated in 170 µM H<sub>2</sub>O<sub>2</sub> for 5 min before the agarose-adding step. As a negative control, the procedure was identical except for the treatment with particles.

#### 2.12.8. Enzyme-Linked Immunosorbent-Assay

The TNF-α ELISA MAX™ Deluxe Set was performed according to the manufacturer's instructions. First, 10,000 cells/well (ImKC) were seeded in 100 µL of growth medium in a 96-well plate and incubated for 24 h in the cell culture incubator. Particles in their respective concentration were added and incubated for another 24 h (5 % CO<sub>2</sub>, 95 % humidity, 37°C). To estimate the baseline TNF-α secretion (negative control), cells were incubated without MPP, while cells in the positive control were stimulated with 2.5 µg LPS. Regarding the TNF-α release in spheroids, spheroids were grown for 5 days, challenged with particles for 24 h and co-cultivated with 500 macrophages for further 24 h. Positive and negative control were comparable to the previous analysis. 16 – 18 h prior to running the ELISA, the plate was coated with 100 µL of the capture antibody solution. The plate was washed (4 x with 300 µL wash buffer, same for consecutive washing steps), and non-specific antibody binding was blocked by 1 h incubation with a coating agent. For both methods, samples were extracted from the supernatant, and the sample was diluted (1:10; 1:100; 1:1000; 1:10000) to cover the detection range of the ELISA kit. A

TNF- $\alpha$  standard curve dilution was prepared according to the provided kit. All samples were used for at least two times repeated determination. After washing, 100  $\mu$ L of the appropriate sample dilutions and standards were added and incubated for 2 h. The plate was washed, and 100  $\mu$ L of the detection antibody was added (incubation time 1 h). After further washing, 100  $\mu$ L of diluted Avidin-HRP solution was added to each well for 30 min. After the final washing step, 100  $\mu$ L of freshly mixed TMB Substrate Solution was added for 15 min, and the reaction was stopped by adding 100  $\mu$ L of the stop solution. The absorbance was measured within 15 min at 450 nm (reference wavelength 570nm). With the help of the standard curve, calculated by the added standard, the TNF- $\alpha$  concentration in the supernatant could be calculated, considering the dilution factors.

#### 2.12.9. Lucifer Yellow Assay

BNL CL.2 cells were seeded as described in (2.8). After 4 days of incubation (standard cell cultivation), particles were added in the respective concentration and incubated for 24 h. Afterwards, the medium in the upper and lower well was aspirated, and 200  $\mu$ L of 1 mM LY in DPBS was added to the upper well, while the lower well was filled with 800  $\mu$ L DPBS. As a negative control, a transwell with no cells seeded was used to estimate the blocking of the membrane itself. After 2 h of incubation, the bottom well was thoroughly mixed by pipetting, and 100  $\mu$ L of the bottom well was pipetted in a 96-well plate (5-fold determination, the mean of the five technical replicates was used). Afterwards, the fluorescence of the wells was measured by using the plate reader (Ex: 485 nm, Em: 530 nm). The fluorescence intensity of the negative control was treated as 100 % permeable, and the permeability of the wells was calculated according to Equation 5.

*Equation 5 Calculation of the relative LY fluorescence*

$$\text{relative LY fluorescence [\%]} = \frac{MFI_{\text{sample}}}{MFI_{\text{NC}}} \times 100$$

where:  $MFI_{\text{sample}}$  is the mean fluorescence intensity of the fivefold determination of the test sample in the lower well;  $MFI_{\text{NC}}$  is the mean fluorescence intensity of the fivefold determination of the negative control (i.e., well seeded without cells).

### 2.13. Ribonucleic acid Sequencing

Ribonucleic acid (RNA) sequencing (RNAseq) can gain information about gene expression by analysing the up and down-regulation of specific genes. Usually, the ratio of a treated sample (in this case, with MPP) is set to an untreated sample to compare the reaction of the cell on the transcriptional level to an active substance. Here, RNAseq was used to unravel the different reactions to pristine and weather MPP.

Samples for the RNAseq were prepared as follows: 300,000 cells/well (ImKC) were seeded in 2 mL growth medium in a 6-well plate and incubated for 24 h at standard cell culture conditions. Afterwards, 150 µg/mL PS<sub>2µm</sub> and PS<sub>130</sub> were added and incubated for another 24 h. The supernatant was discarded, and the cells were washed twice with DPBS. 350 µL lysis buffer RLT<sup>®</sup> was added to each well and incubated for 1 min. The lysate was immediately transferred to an RNase-free Eppendorf tube and frozen at - 20°C. After that, the preparation and data processing of the RNAseq samples was done by AG Weig, according to Völkl et al. (2022).

#### **2.14. Particle distribution during cell division**

To track a possible, specific distribution of engulfed MP during cell division, cells were initially stained with CTV, and 150,000 stained cells/ well were seeded in 1 mL in a 12-well plate and incubated for 24 h at standard cell culture condition. Afterwards, cells were loaded with particles ( $1.68 \times 10^6$  PS<sub>2µm, red</sub> particles/well) for 24 h to ensure enough ingestion time. All wells were washed thoroughly several times with DPBS to remove unbound particles, and fresh growth medium was added. Then, cells in one well were detached, and the particle distribution in the cells was analysed by FC with the established method 3.1.1 (data corresponding to day 0). With this data set, the approximation of a perfect homogeneous distribution was calculated (see Equation 6). Cells were subsequently analysed on day 1 and day 2 by FC to track the distribution of the PCI and to compare the approximation with the measured data ( $\Delta$ ).

#### **2.15. Analysis of particle excretion after ingestion**

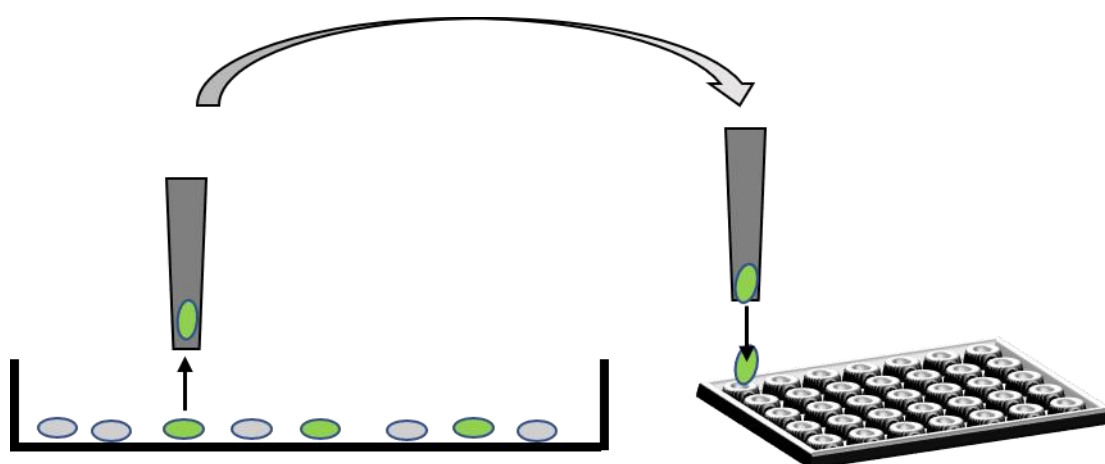
A possible particle excreting and re-ingesting of MPP was analysed with the following experimental procedure. 150,000 cells/well (J774A.1, ImKC) were seeded in a 12-well and incubated for 24 h at standard cell culture conditions. Afterwards, cells were incubated with  $1.68 \times 10^6$  particles/well PS<sub>2µm, green</sub> or PS<sub>2µm, red</sub> for 24 h. All wells were washed thoroughly several times with DPBS to remove unbound particles, and fresh growth medium was added. Cells were detached, and the cell count was determined. A mixture containing 75,000 PS<sub>2µm, green</sub> loaded cells with 75,000 PS<sub>2µm, red</sub> loaded cells was seeded in 12 well plates. Control wells only contained cells pre-loaded with either PS<sub>2µm, green</sub> or PS<sub>2µm, red</sub> (150,000 cells/well each). Cells were washed, detached, and analysed every other day by FC (Ex/Em: PS<sub>2µm, green</sub>: 441/486 nm; PS<sub>2µm, red</sub>: 512/565 nm).

#### **2.16. Single-cell sorting**

The single-cell sorting of cells was conducted for the COMET assays to sort cells with a high PCI. Briefly, 300,000 ImKC cells were seeded in 2 cm cell culture dishes and incubated for 24 h at standard cell culture conditions. Afterwards, 150 µg/mL particles were added, and cells were incubated for further 24 h at standard cell culture conditions. The plate was then washed with DPBS twice and detached by



treatment with citric buffer. Cells were collected and centrifuged (200 x g, 5 min), the supernatant was removed, and the cells were reseeded in a 2 cm cell culture dish. After 15 min incubation, to allow low attachment for the cells, the plate was placed in the SingleCell sorter at the AG Weig. It has to be noted that a longer attachment time would result in difficult harvesting of the cells since the SingleCell sorter sucks up cells via a capillary, while a too-short incubation would result in floating cells, making them hard to catch. Cells with a specific fluorescence threshold (133) were picked up as individuals with a high PCI. 100 cells were sorted and transferred into an Eppendorf reaction tube, and the COMET assay was conducted as described in 2.12.7.



*Scheme 14 Principle of the SingleCell sorter*

## 2.17. Protist cultivation

### *Cultivation of T. pyriformis and Amoeba proteus*

*T. pyriformis* was cultivated in 20 mL of a 2 % (w/w) protease-peptone broth at room temperature (20 – 25°C) in a 10 cm petri dish. Thrice a week, 1 mL of the culture was transferred into a fresh medium for maintenance, and the rest of the suspension was discarded.

*A. proteus* was cultivated as proposed by Prescott and James <sup>[222]</sup>, in the following referred to as Prescott<sub>Ref</sub> (KCl 12.4 mM, CaHPO<sub>4</sub> 2.9 mM, MgSO<sub>4</sub> 1.7 mM, pH 6.4). Briefly, amoebae were cultured in a 10 cm glass Petri dish at room temperature in Prescott<sub>ref</sub> medium and were fed twice a week with approximately 10 – 20 *T. pyriformis* per amoeba. The amount of tetrahymena added was high enough to ensure a close vicinity between prey and predator. For passaging amoebae from dish to dish or seeding in case of experiments, individuals were pipetted with an 1 mL Eppendorf pipette while observing them under the microscope. Amoeba seeded for experiments were kept for 24 h without prey organisms to ensure a high uptake demand.

### *Induction of pinocytosis*

Induction of pinocytosis was conducted to analyse the uptake mechanism of MP particles. Pinocytosis was induced by adjusting the pH of the Prescottt<sub>Ref</sub> medium to pH 4.3 with HCl. Additionally, 125 mM NaCl was added to the medium (Prescottt<sub>NaCl</sub> medium). For the uptake experiments, the amoebae were incubated for 45 min in the Prescottt<sub>NaCl</sub> medium. Afterwards, organisms were transferred back to the standard Prescottt<sub>Ref</sub> medium for longer incubation or analysis.

### *Uptake of MP in amoeba and ciliates*

To analyse the uptake of different-sized MPP or fragments, 50 – 100 amoebae were first starved for 24 h by transferring them to 35 mm glass dishes containing 2 mL Prescottt<sub>Ref</sub> medium without any prey organisms provided to stimulate the need for food uptake. 10 – 15 amoeba were afterwards transferred to one well of a 12-well glass plate. 1  $\mu$ L of the respective MP suspension was added to the starved amoeba in Prescottt<sub>Ref</sub> corresponding to the following MP end concentrations: PS<sub>0.5 $\mu$ m</sub>:  $3.6 \times 10^7$  beads/mL; PS<sub>6 $\mu$ m</sub>:  $2.1 \times 10^4$  beads/mL; PS<sub><20 $\mu$ m</sub>, PS<sub>20-40 $\mu$ m</sub> and PS<sub>40-75 $\mu$ m</sub>:  $5 \times 10^3$  fragments/mL. After the respective incubation time specific to the experiment, amoebae were washed by transferring them twice to fresh wells in 1 mL Prescottt<sub>Ref</sub> medium to remove leftover MPP. Afterwards, several amoebae were transferred to a microscopic glass slide. To not squash the amoeba, the cover glass was placed on fragments of a second cover glass to slightly increase the space between the slide and the cover glass. Subsequently, amoeba were analysed under the fluorescent microscope, and particles were counted manually (magnification x400 for PS<sub>0.5 $\mu$ m</sub> beads and x100 for  $\geq 6 \mu$ m beads/ fragments).

To investigate if phagocytosis induction increases the uptake of MPP, *A. proteus* was seeded as described above. The organisms were additionally incubated with a mixture of *T. pyriformis* ( $5 \times 10^4$  cells/mL) and PS<sub>20-40 $\mu$ m</sub> or PS<sub>40-75 $\mu$ m</sub> ( $5 \times 10^2$  fragments/mL) simultaneously, and uptake analysis was done as described above.

To assess the uptake of particles in *T. pyriformis*, 10  $\mu$ L of a densely grown culture were exposed to PS<sub>0.5 $\mu$ m, red</sub> (end concentration:  $3.6 \times 10^7$  beads/mL) for 24 h in a 35 mm glass dish containing 2 mL Prescottt<sub>Ref</sub> medium. For observations, 10  $\mu$ L of MPP-exposed individuals were transferred onto a microscopy slide and analysed by a fluorescence microscope.

### *Particle coating with proteins*

For protein coating, MPP (1  $\mu$ L of the 2.5 % (w/v) aqueous suspension) were incubated overnight at 37°C in 1 mL of a 2 % (w/v) bovine serum albumin (BSA) solution or 1 mL of a 10 % (v/v) fetal calf serum (FCS) solution in Prescottt<sub>ref</sub> medium. Afterwards, the particles were centrifuged (13,000  $\times g$ , 5 min). The supernatant was carefully discarded, the resulting pellet was once resuspended in bi-distilled

water to wash leftover protein solution, again centrifuged (13,000 x g, 5 min), resuspended in Prescott<sub>ref</sub> and used immediately for the experiments as described above.

#### *Trophic transfer of MP particles*

*T. pyriformis* was incubated with the respective amount of MPP (PS<sub>0.5µm</sub>: 3.6 x 10<sup>7</sup> beads/mL; PS<sub>6µm</sub>: 2.1 x 10<sup>4</sup> beads/mL; PS<sub><20µm</sub>: 5 x 10<sup>3</sup> fragments/mL) for 24 h as described above. Afterwards, the individuals were washed to remove leftover MP and resuspended in Prescott<sub>ref</sub> medium. The organisms were then offered to starved amoebae in a prey : predator ratio of approximately 10 : 1. After the indicated incubation time, several amoebae were washed and observed under the microscope for uptake experiments (as described above). The remaining amoebae were incubated for the respective time for retention experiments.

#### *Fixation and staining of amoeba*

Amoebae were stained to visualise ingested prey organisms inside the food vacuole. Therefore, individuals were transferred on a glass slide and fixed by incubation in 1 mL 3.7 % (v/v) PFA in DPBS for 15 min at room temperature. Afterwards, the PFA was aspirated, the slide was carefully washed with DPBS, and 1 mL of 25 µg/mL Hoechst 33342 dye in DPBS was added to the fixed amoeba for 15 min in the dark to stain genomic DNA in prey and predator. The stained amoebae were washed with DPBS and observed by fluorescence microscopy.

### **2.18. Statistics**

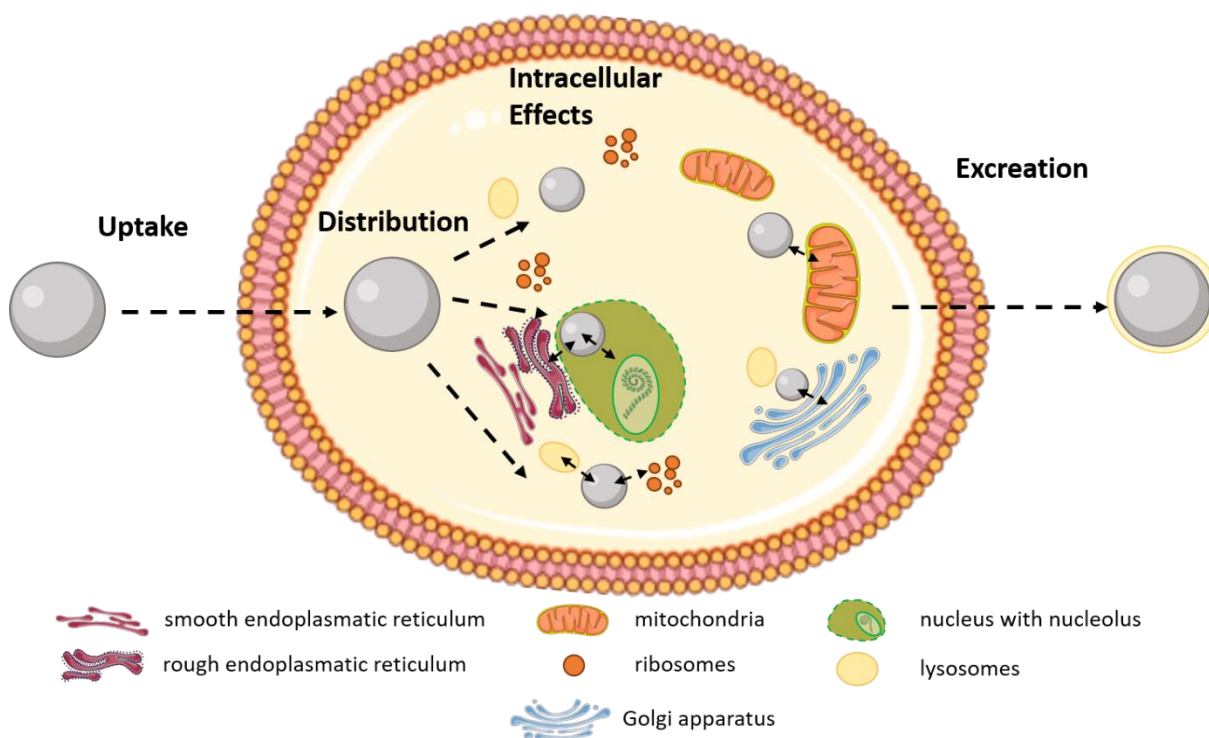
If not otherwise stated, data are reported as mean ± standard deviation. n represents the number of biological replicates. OriginPro software was used for ANOVA with Holm-Bonferroni multiple comparison test and Tukey-Post-hoc-analysis to determine whether data groups differed significantly. The p-value indicates the significance of the analysis

### **2.19. Licence agreements**

Parts of the schemes and figures were drawn by using pictures from Servier Medical Art. Servier Medical Art by Servier is licensed under a Creative Commons Attribution 3.0 Unported License (<https://creativecommons.org/licenses/by/3.0/>).

### 3. Biological interactions and effects of microplastic on a cellular level

Potential damage due to MP on the cellular level can occur at different stages in the pathway of a particle through a cell (Scheme 15). The first encounter of the MP and the cell is probably of high relevance. Without interaction between the particle and the cell or an intracellular uptake, it is unlikely that effects will occur. Following this, the intracellular distribution of the particles and the subsequent intracellular effects need to be addressed. These effects likely vary on various particle parameters and can arise on different biological levels, making the analysis highly complex and multi-parametrical. Lastly, a possible excretion of the particles needs to be analysed to estimate the fate of ingested particles. In the following, these fundamental questions are addressed to explore the complexity of microplastic toxicity on a cellular level.



*Scheme 15 Possible pathway and interaction sites of a MPP with a mammalian cells*

#### 3.1. Quantitative PCI analysis and the dependency of macrophages' polarisation state

As mentioned in the introduction, PCI is highly important when assessing microplastic toxicity. The fundamentals and more in-depth analysis was there mainly done in cooperation (see 1.2). Nevertheless, for this work, methods were established to quickly and quantitatively analyse PCI. The influence of the polarisation state on the PCI as a further factor was complementary analysed.

### 3.1.1. Quantification of PCI with the flow cytometry

A method for measuring the PCI via FC was established since a high amount of cells can be measured in a relatively short amount of time. Furthermore, this method has the advantage that the PCI can be put in relation to parallel analysis methods in the FC and interpret data on a more complex level, e.g. relate measured effects with the number of particles that interacted with an individual cell. This method was established in cooperation with Julia Jasinski and was published in “Noxic effects of polystyrene microparticles on murine macrophages and epithelial cells” by Rudolph, Völkl et al. (2021). As the first approach, green fluorescent particles (PS<sub>0.2µm</sub>, PS<sub>0.5µm</sub>, PS<sub>1µm</sub>, PS<sub>2µm</sub>, PS<sub>3µm</sub> and PS<sub>6µm</sub>) were used. For particles > 1 µm, the fluorescence of the particles attached or ingested to the cells could be measured well, and a quantitative PCI could be determined (Figure 1).

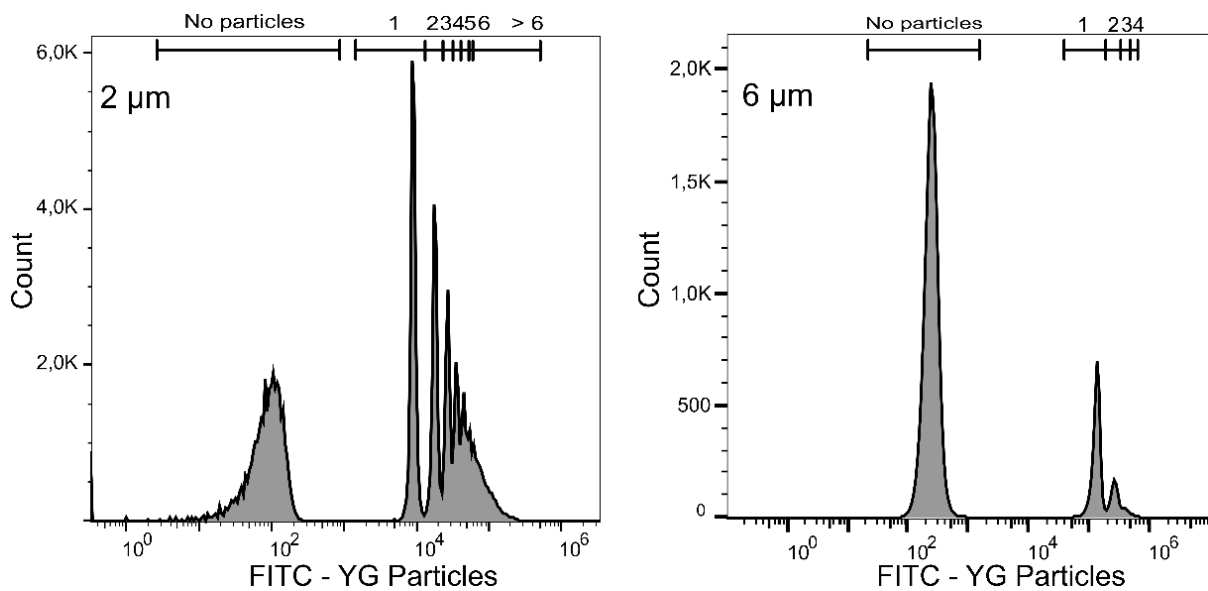


**Figure 1 Representative PCI analysis via FC using ImKC cells**

Shown is the fluorescence of ImKC cells interacting with PS<sub>2µm</sub> and PS<sub>6µm</sub>. Gates represent fluorescence for the respective PCI. Particle fluorescence (Ex/Em: 441/486 nm) was measured with the FITC filter. 25 µg/mL particles were added per 150,000 cells in a 12-well plate and incubated for 24 h.

While a distinct fluorescence signal could be measured for the smaller particles (PS<sub>0.2µm</sub> and PS<sub>0.5µm</sub>), the difference between single PCI was too small to differentiate (Figure S5).

A highly linear dependency could be measured when gating the respective populations and applying the median fluorescence intensity to the gates (Figure 2). This, on the one hand, verifies the gating strategy. On the other hand, it also opens the possibility to discriminate higher particle counts (> 6) by placing the gates according to Figure 2. This way, despite the difficulty of visual discrimination between populations with more than 6 particles per cell, higher PCI can be calculated and accordingly gated.

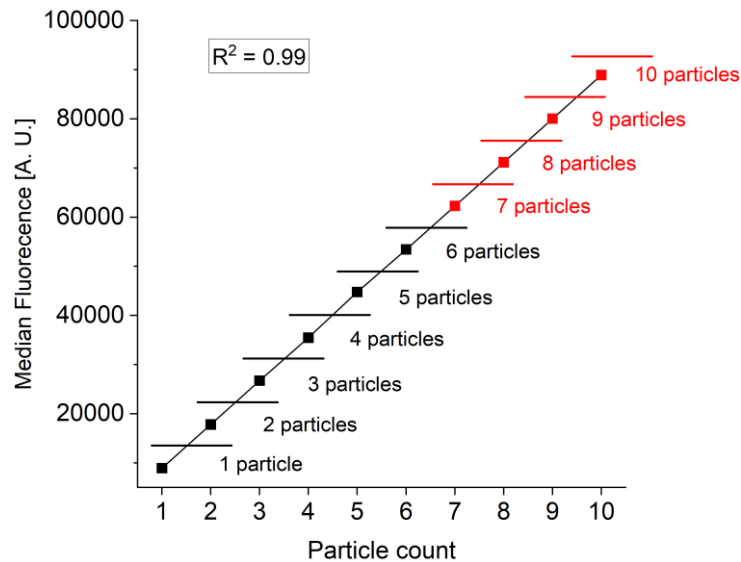


**Figure 2** Linearity of PCI and the respective median fluorescence measured by FC

Data are extracted from the respective cell populations from Figure 1 and show the representative method for 2  $\mu\text{m}$ . Black colour represents measured data points, red colour exemplarily calculated gate borders.

The analysis by FC could be expanded further. A linear relationship between the side scatter and the number of interacting particles was additionally observed (Figure 3).

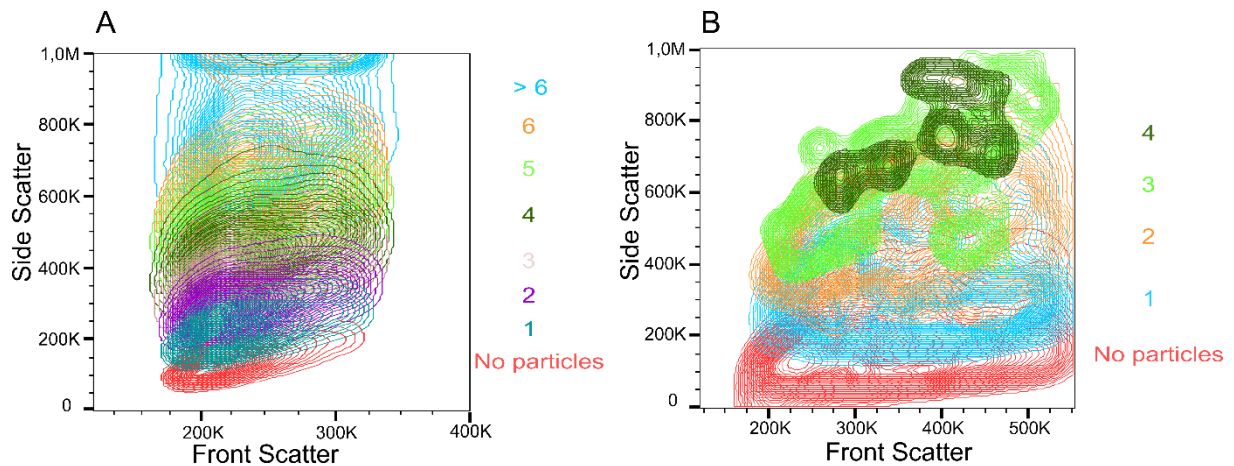


**Figure 3** Relationship of the side scatter measurement and the PCI

Shown are ImKC cells, gated after the respective amount of PCI after the established strategy in Figure 1 for A: PS<sub>2μm</sub> and B: PS<sub>6μm</sub>.

Although the selectivity between the respective populations decreased, a differentiation between cell populations was still possible. This method of analysis furthermore opens the possibility to work with non-fluorescent particles, enabling the usage of staining and analysis methods which otherwise might overlap with the fluorescence of the particles. It has to be noted, though, that this method only detects PCI and can not discriminate between interaction or full particle ingestion.

### 3.1.2. Influence of polarisation state of macrophages on the PCI

In addition to the previously mentioned particle parameters, cell-specific states, e.g. different polarisation states of the macrophages, can influence the PCI. Therefore, the influence of M1 and M2 polarisation on PCI in both macrophage cell lines (J774A.1, ImKC) was investigated. To preliminarily verify a successful polarisation, two approaches were used. First, the ROS amount was measured via FC.

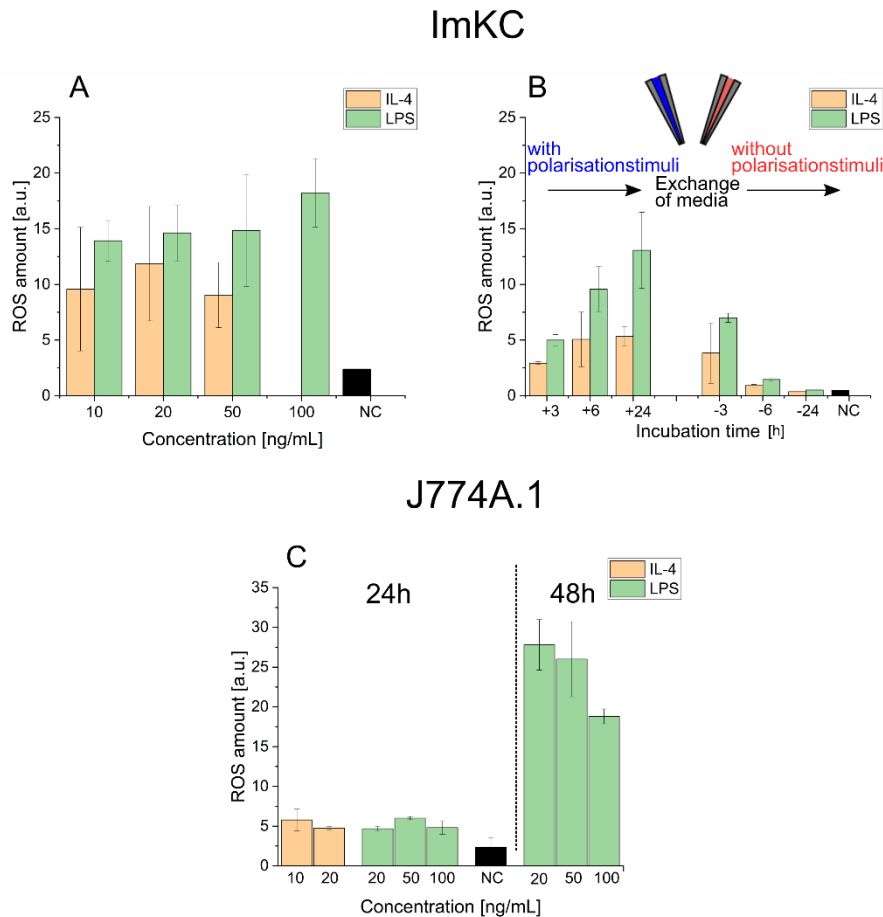


**Figure 4 Determination of the polarisation by measuring the ROS amount**

*A: Different concentrations of the respective polarisationstimuli were tested in ImKC with an incubation time of 24 h. B: Polarisationkinetic was analysed by testing the time-dependent polarisation (with polarisationstimuli) as well as the recovery afterwards (without polarisationstimuli) for 100 ng/mL LPS and 20 ng/mL IL-4. C: Different concentrations and incubation times with respective polarisationstimuli were tested in J774A.1 by measuring the ROS amount by FC.*

In the case of ImKC cells, the ROS amount increased significantly after polarising for 24 h, with a slight concentration-dependent trend for LPS (Figure 4A). For IL-4, an increase in ROS could be observed as well. The trend showed a lower ROS production compared to LPS, and no concentration dependency was observed. A kinetic was furthermore recorded to analyse how quickly the polarisation is assembled (Figure 4B). Here, an explicit time dependency could be observed for LPS. The ROS amount started to increase after 3 h, with a significant increase up to 24 h. In the case of IL-4, a maximum of ROS was already reached after 6 h. For both polarisation states, when incubating the polarised cells

with fresh growth medium, the ROS amount quickly decreased and, after 6 h, was almost comparable to the negative control.

For J774A.1, the ROS amount did not increase significantly after 24 h incubation with LPS or IL-4 (Figure 4C). Incubation time with the polarisation stimuli was therefore increased to 48 h, where a significant ROS increase could be measured, indicating a slower reaction of the J774A.1 cells compared to ImKC. This could also be observed in the literature, where incubation times between 12 – 72 h of the polarisation stimuli were used by different groups for J774A.1 cells [223–225].

Additionally, an antibody staining of polarisation-specific surface markers was used. Commonly used markers in the literature are, e.g. CD68, CD80 and CD86 for M1 polarisation, while CD163 is predominantly utilised for M2 analysis (see 1.5). For ImKC, the used antibody stains did not significantly increase to any treatments except for CD80 and the highest used LPS concentration (Figure 5A). For J774A.1, in contrast, CD80 and CD86 showed the expected significant increase when treated with LPS (Figure 5B). CD68 showed, comparable to ImKC cells, no increase at any treatment. Surprisingly, CD163 showed a significant increase when treated with LPS but only a slight increase for IL-4 after 24 h.

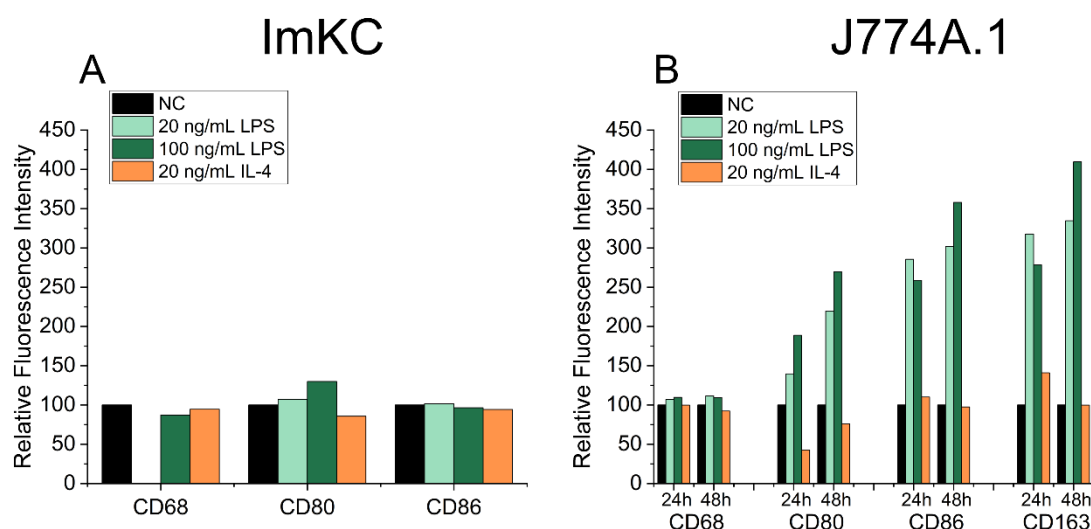


**Figure 5 Determination of the polarisation state by antibody staining of polarisation-specific surface markers**

Fluorescence was measured in the flow cytometer and is given in relation to the non-polarised cells (100). NC represent non-polarised cells as mock control. A: ImKC cells were incubated for 24h with the respective stimuli, harvested and stained with the antibodies. B: J774A.1 cells were seeded in a 12-well plate, incubated for 24h or 48h with the respective stimuli, harvested and stained with the antibodies.

The low reaction of both cell lines regarding CD68 production could be explained by the structure of the surface marker, where most of the protein is located intracellularly. Despite being one of the primary markers for hepatic macrophages, it can therefore be complicated to use as a surface marker [226]. The high increase in CD163 for J774A.1 can be related to an unspecific expression that is



a side effect of the LPS treatment <sup>[219]</sup>. However, the only moderate increase in CD163 and the following M2 verification needs to be analysed further. On the one hand, another polarisation stimulus, e.g. IL-10, might induce a higher marker expression. On the other hand, CD204 or CD206, as other surface markers, might as well be beneficial to analyse. However, the M2 polarisation is a complex mechanism with various pathways. Due to the complementary results of ROS measurement and antibody staining, the polarisation of the macrophages can be regarded as successful for the following interaction experiments.

Subsequently, the PCI's dependency on the respective polarisation state was analysed. Therefore, cells were first polarised (24 h for ImKC, 48 h for J774A.1) and afterwards challenged with PS<sub>2µm, red</sub>. Since the polarisation state was already diminishing after 6 h without stimuli, the particles were added to the medium with the polarisation agent and then incubated for 6 h with the cells. PCI was afterwards measured by the established method in 3.1.1 (Figure 6). Cell populations were divided into no particle uptake (0 particles), low PCI (1 – 4 particles) and high PCI (> 4 particles).

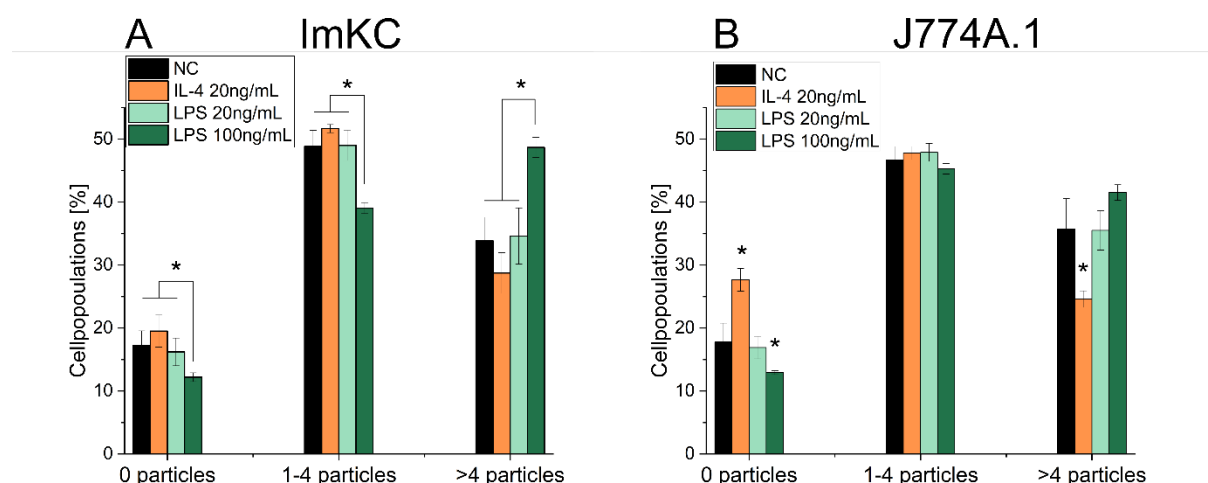


**Figure 6** PCI dependency of polarised macrophages

The polarisation stimuli was added for 24 h (ImKC) and 48 h (J774A.1). NC represent non-polarised cells as mock control. Afterwards, 15 µg/mL PS<sub>2µm, red</sub> particles were added for 6 h to the medium with the respective polarisation stimuli. Cells were detached, and PCI was measured in the FC with the established method (3.1.1). significance level: \* = p ≤ 0.05

In the case of ImKC cells, a significant dependency of the polarisation state to the PCI could be observed. For treatment with 100 ng/mL LPS, fewer cells with no or low PCI were observed, while the cell population with > 4 particles was significantly increased. When polarised with IL-4, the distribution shifted contrastively. The distribution shift was similar in the case of the J774A.1 cells, but LPS treatment showed a non-significant change to more PCI, while the treatment with IL-4 resulted in a more significant change, especially for cells without PCI. This points out the cell-specific reactions of cells to MPP. The purpose of the M1 polarisation can explain the increase in the PCI for this state. Next to the high excretion of cytokines, M1 polarisation is characterised by a high phagocytic activity due to

its role in microbial defence <sup>[139,142]</sup>. Activated macrophages wander around more actively on the plate and can therefore interact with particles more efficiently. M2 polarisation, on the other hand, is a complex process with subtypes that all have different functions *in vivo*. IL-4 mainly recruits M2a and M2d polarisation, primarily responsible for wound-healing and angiogenesis, translating into less effective phagocytosis activity. M2c polarisation, on the other hand, mostly induced by IL-10, is responsible for the phagocytosis of necrotic cells. This shows that the stimulus might already be responsible for the interaction with cells and that these cells react differently. This establishes a more complex mechanism, which could also explain the contradictory literature results. While Stock et al. found no polarisation effect in the PCI for THP-1 cells polarised with LPS and IFN- $\gamma$  (M1) or IL-4 and IL-13 (M2) <sup>[80]</sup>, other studies found increased uptake of nanoparticles in M1 polarised (by LPS) J774A.1 cells <sup>[225]</sup>, while others showed an increase in uptake for M2 macrophages (IL-4 and IL-10 stimulated) <sup>[218,227]</sup>. Binnemars-Postma et al. furthermore showed an influence of the protein corona on the particle interaction of polarised cells <sup>[220]</sup>. M1 macrophages ingested more particles when incubated without serum, while M2 macrophages had the upper hand for particles preincubated in serum. Finally, Akilbekova et al. investigated the influence of the polarisation (LPS and IL-4 stimulated) on the uptake of various particles (e.g. polystyrene, PMMA, various functional groups like Sulfonate, Amino, Amidine and more) and found different results for all particles <sup>[228]</sup>. Overall, it can be concluded that the polarisation state and the PCI are indeed connected, though various parameters like cells, particle properties and polarisationstimuli affect the uptake probability.

### 3.1.3. Summary and conclusion

The established method for the quantitative interaction rate with particles via FC proved reliable and quick. It opens the analysis of PCI via FC, which in return helps for analysis methods using the FC to dedicate effects to particular cell populations with a specific PCI amount.

Macrophage polarisation proved to have a significant influence on the PCI in the here-used experimental setup. The classically activated M1 macrophages showed an increased uptake attendance, while alternatively activated M2 macrophages rather decreased the interaction.

As shown in Scheme 15, the first encounter of the cell with the particle should be a crucial moment for the later fate and effect on the cells. This investigation, especially in cooperation with the expertise of others (see 1.2), therefore, was an important setup for later experiments about understanding the possible effects of MP on the cells. It is likely that without interaction, no measurable impact will be observed. Therefore, establishing analysis via FC and polarisation dependency of the PCI mainly served to understand and interpret later data with the here-used cells and particles.

### 3.2. Particle distribution after ingestion of MPP

A further important factor for effect triggering concerns the particle distribution inside the cell (Scheme 15). Two main questions were hereby asked: Do particles accumulate at specific organelles? How are particles distributed during cell division? These findings are summarised in the submitted manuscript “Polystyrene microparticle distribution after ingestion by murine macrophages” by Jasinski, Völkl et al.

A possible accumulation or co-localisation of the particles at specific organelles was hereby analysed by Julia Jasinski <sup>[229]</sup>. By antibody staining of specific organelles (mitochondria, ER, Golgi apparatus, and lysosomes, nuclei, cytoplasm, early and late endosome), co-localisation of particles was analysed with PS<sub>0.2µm</sub>, PS<sub>0.5µm</sub> and PS<sub>3µm</sub>. Experiments were conducted with both macrophage cell lines (ImKC and J774A.1) since these specialised scavenger cells were more likely to ingest particles. After an incubation of 24 h with the particles, the respective organelles were stained, and the localisation of particles was analysed. Ingested particles were mainly located in the cytoplasm, no matter the size. Only the smaller particles (PS<sub>0.2µm</sub> and PS<sub>0.5µm</sub>) were additionally found in the ER, but no co-localisation was seen with the nuclei, mitochondria, Golgi apparatus, or the lysosome. A co-localisation in the endosome could only be observed in the case of PS<sub>0.5µm</sub>.

The next step was to analyse the distribution of the particles during cell division. Various publications about the distribution of nanoparticles during cell division exist <sup>[230–233]</sup>, and it has been established that these particles are randomly distributed. However, for the magnitudes larger microparticles, no data exist. Particles might either be distributed randomly to the respective daughter cells or split symmetrically. To analyse this, the particle count was related to the number of cell divisions for one cell. Therefore, cells were initially stained with CTV. After staining the cells, 25 µg/mL PS<sub>2µm, green</sub> were added, and the number of particles per cell was traced for various days. Using the FC, the fluorescence intensity of the CTV and the respective particle number could be brought in proportion due to the parallel measurement (Figure 7).

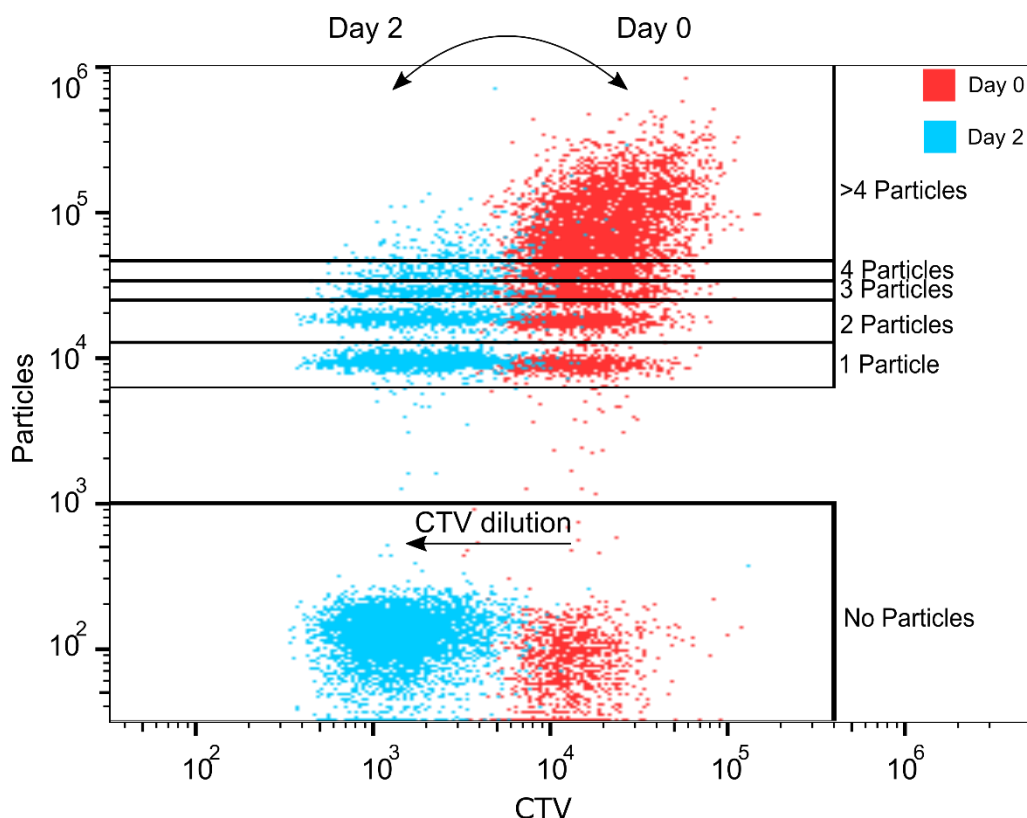


**Figure 7 Particle distribution during the cell division measured by FC**

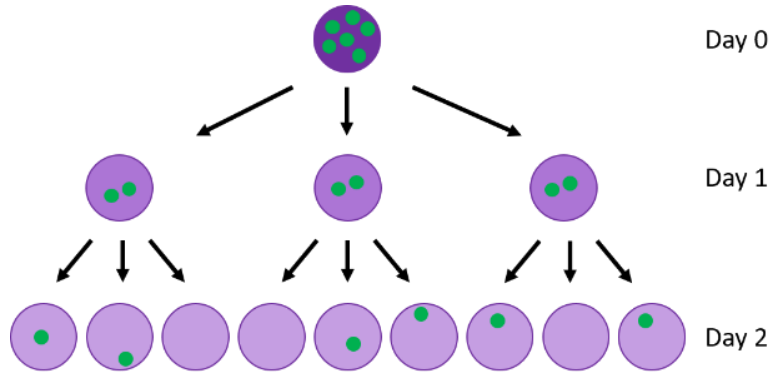
*Shown is a representative dot plot of the time-dependent distribution of 25  $\mu\text{g/mL}$   $\text{PS}_{2\mu\text{m}}$ , green in 150,000 ImKC on the y-axis and the corresponding dilution of the CTV dye on the x-axis for ImKC cells after 2 days*

PCI were counted up to 15 PCI/cell, using the established method in 3.1.1. For the following calculation, populations of up to 15 PCI were used. The figures and tables combine these populations in  $> 4$  PCI for a more straightforward representation. By measuring the number of particles on the first day and tracking the CTV intensity, an approximation of how the particle number per cell should look in case of a symmetrical distribution was calculated.

This approximation was calculated as follows (see also Scheme 16 and Equation 6):

- The number of particles per cell at day 0 ( $P_{n,t_0}$ ) was measured for the respective cell populations
- Cell division was calculated by measuring the CTV fluorescence every other day
- In the case of ImKC, the CTV intensity was only 1/3 on day 1 compared to day 0, indicating three times the amount of cells or approximately 3 cells out of 1 (for J774A.1. 1/2 CTV intensity was measured, indicating twice the amount of cells or approximately 2 cells out of 1)
- A symmetrical distribution was assumed
- Particles per cell on the assumed Day 1 were calculated, counted, summarised ( $P_{all,t_1}$ ) and normalised to 100% ( $P_{n,t_1}$ )
- Same procedure for the following days ( $P_{n,t_m}$ )

- The calculated numbers were used as an approximation for a symmetrical distribution and compared to the measured data



**Scheme 16 Exemplary process scheme for the calculation of the approximation considering a symmetrical distribution for ImKC cells**

**Equation 6 Mathematical equation for the calculation of the approximation**

$$\begin{aligned}
 P_{all,t_0} &= P_{0,t_0} + P_{1,t_0} + P_{2,t_0} + \dots + P_{n,t_0} \\
 P_{all,t_1} &= (3 * P_{0,t_0} + 2 * P_{1,t_0} + 1 * P_{2,t_0}) + (1 * P_{1,t_0} + 2 * P_{2,t_0} + 3 * P_{3,t_0}) + \dots \\
 &\quad + (1 * P_{n,t_0} + 2 * P_{n+1,t_0} + 3 * P_{n+2,t_0}) \\
 P_{0,t_1} &= \frac{(3 * P_{0,t_0} + 2 * P_{1,t_0} + 1 * P_{2,t_0}) * 100\%}{P_{all,t_1}} \\
 P_{1,t_1} &= \frac{(1 * P_{1,t_0} + 2 * P_{2,t_0} + 3 * P_{3,t_0}) * 100\%}{P_{all,t_1}} \\
 P_{2,t_1} &= \frac{(1 * P_{4,t_0} + 2 * P_{5,t_0} + 3 * P_{6,t_0}) * 100\%}{P_{all,t_1}} \\
 P_{m,t_1} &= \frac{(1 * P_{n,t_0} + 2 * P_{n+1,t_0} + 3 * P_{n+2,t_0}) * 100\%}{P_{all,t_1}} \\
 P_{all,t_2} &= (3 * P_{0,t_1} + 2 * P_{1,t_1} + 1 * P_{2,t_1}) + (1 * P_{1,t_1} + 2 * P_{2,t_1} + 3 * P_{3,t_1}) + \dots \\
 &\quad + (1 * P_{n,t_1} + 2 * P_{n+1,t_1} + 3 * P_{n+2,t_1}) \\
 P_{all,t_m} &= (3 * P_{0,t_m} + 2 * P_{1,t_m} + 1 * P_{2,t_m}) + (1 * P_{1,t_m} + 2 * P_{2,t_m} + 3 * P_{3,t_m}) + \dots \\
 &\quad + (1 * P_{n,t_m} + 2 * P_{n+1,t_m} + 3 * P_{n+2,t_m}) \\
 P_{all,t_0} &= \text{Combined cell population at } t_0 \text{ [\%]} \\
 P_{all,t_1} &= \text{Combined cell population at } t_1 \text{ [\%]} \\
 P_{0,t_0} &= \text{cell population with 0 PCI at } t_0 \text{ [\%]} \\
 P_{1,t_0} &= \text{cell population with 1 PCI at } t_0 \text{ [\%]} \\
 P_{2,t_0} &= \text{cell population with 2 PCI at } t_0 \text{ [\%]} \\
 P_{n,t_0} &= \text{cell population with } n \text{ PCI at } t_0 \text{ [\%]} \\
 m &\in \mathbb{N} \\
 n &= 1 + (3 * m)
 \end{aligned}$$

The measured cell populations and the calculated approximation are shown in Table 5. These results were then compared to the calculated approximation, and the difference ( $\Delta$ ) was calculated.

*Table 5 Measured cell populations for particle distribution and the respective value of the calculated approximation*

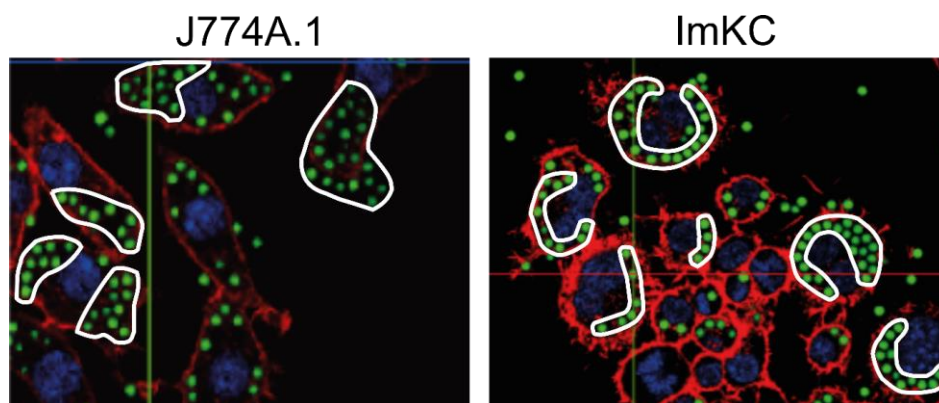
<b>J774A.1</b>							
<b>Day 0</b>		<b>Day 1</b>			<b>Day2</b>		
<b>Particles per cell</b>	Measured [%]	Measured [%]	Approximation [%]	$\Delta$ [%]	Measured [%]	Approximation [%]	$\Delta$ [%]
<b>0</b>	47.70	73.69	65.68	8.01	79.21	84.89	- 5.69
<b>1</b>	22.62	16.43	26.20	- 9.78	14.62	14.42	0.20
<b>2</b>	12.19	5.44	5.23	0.21	3.39	0.69	2.70
<b>3</b>	6.595	1.92	1.39	0.53	0.91	-	0.91
<b>4</b>	3.625	0.78	0.93	- 0.15	0.31	-	0.31
<b>&gt; 4</b>	6.77	0.91	0.57	0.34	0.16	-	0.16

<b>ImKC</b>							
<b>Day 0</b>		<b>Day 1</b>			<b>Day2</b>		
<b>Particles per cell</b>	Measured [%]	Measured [%]	Approximation [%]	$\Delta$ [%]	Measured [%]	Approximation [%]	$\Delta$ [%]
<b>0</b>	15.86	37.29	29.79	7.50	59.20	56.52	2.67
<b>1</b>	13.78	19.60	31.08	- 11.49	18.54	38.26	- 19.72
<b>2</b>	11.81	12.82	18.04	- 5.23	9.055	5.21	3.84
<b>3</b>	9.91	8.68	9.58	- 0.91	4.91	-	4.91
<b>4</b>	8.06	5.74	7.37	7.50	2.635	-	2.64
<b>&gt; 4</b>	37.86	16.77	4.14	10.99	5.01	-	5.97

Results indicated that the distribution was more similar to the approximation for J774A.1 cells, while a more random distribution for the ImKC cells was observed. For cells with low PCI, the difference between approximation and the measured distribution proved to be the highest for both cell lines. Furthermore, a fraction of cells (10 %) with > 4 particles per cell remained after 2 days for ImKC cells, which should not be the case when considering the approximation. It can be excluded that these cells are loaded with more particles due to less cell division since the CTV dye showed no specific dependence for fewer cell divisions with higher particle numbers in this range of particle numbers (see Figure 7).

The distribution of intracellular material can be symmetrical, ordered or random during cell division. Organelles are hereby often distributed symmetrically, and the distribution of cellular material is often carefully choreographed to ensure viable cells after cell division <sup>[234,235]</sup>. On the other hand, the distribution of cell-foreign material is a more complex problem. Zhao et al. showed that particular proteins trigger the distribution of ingested bacteria from random to symmetrical distribution or even a one-sided distribution of all bacteria to one daughter cell with the other cell remaining without bacteria <sup>[236]</sup>. The bacteria can manipulate this distribution by expressing proteins to either increase bacterial spreading by a more symmetrical distribution or direct the distribution to an unbalanced distribution. The distribution is controlled by the formation of intercellular tubules, which connect the bacterial-loaded phagolysosomes during cell division. Without the formation of these tubules, no directed distribution is possible, and a more or less symmetrical distribution is more likely <sup>[236]</sup>. Interestingly, when comparing the uptake behaviour of the two cell lines, particles seem aligned in a distinct, round-shaped, tube-like pattern for the ImKC cells, while J774A.1 seems to distribute the particles more randomly over the whole cells (Figure 8).



**Figure 8 Particle distribution of PS<sub>2µm, green</sub> in ImKC and J774A.1 cells**

*White circles illustrate the clumped distribution of PS<sub>2µm, green</sub> in the J774A.1 and the tube-like formation for ImKC cells. Confocal microscopy pictures were done by Julia Jasinski.*

This might indicate a formation of tubules for ImKC while J774A.1 spread the particles mostly in the cytoplasm. ImKC cells seem to interact with the particles more, treating them as some intruding foreign matter that needs to be deposited. This fits with the distribution data, where J774A.1 seemed to distribute the particles more symmetrically, while ImKC showed a higher deviation to the approximation, arguing for specific storage of particles. Naturally, possible staining of the tubules and more experiments regarding the formation of these tubules are necessary for a more precise statement.

To summarise, co-localisation with specific organelles was only found in the cytoplasm and, in the case of smaller particles in the ER or endosome. This, and especially the not-observed co-localisation in the lysosomes, argues for unspecific ingestion by macrophages or at least no misrecognition as bacteria.

On the other hand, the distribution pattern of the particles during the cell division argues for a, at least cell-specific, handling of the particles after ingestion. Significant differences between J774A.1 and ImKC were observed, and for the distribution in ImKC cells, one can assume a bacteria-like handling of the particles. A cell-specific reaction was observable despite no clear conclusion for a systematical distribution of the particles.

*In vivo*, some cells might handle the particles as a stowaway, while others misrecognize them as bacterial intruders, alerting an immune response. Both options affect the organism since either accumulation or a debilitated organism might be the consequence, showing the high relevance of the fate of particles after a cellular uptake.



### 3.3. Cellular effects induced by MPP

The previous paragraphs analysed relevant fundamentals for possible effects on the cells. The critical parameters for the PCI and ingestion were identified, and the intracellular distribution to specific organelles as well as the distribution during the cellular division was determined. Results indicated that the particles might be ingested by specific cells and remain intracellular for at least various days. This allows numerous reactions between the cells and the MP, possibly resulting in different biological impacts and outcomes (Scheme 15). The following passage addresses the central part of this work, the cellular responses to different MPP parameters.

According to the literature, various critical particle parameters were identified which might induce toxic effects (see Scheme 3). As summarised in four recent reviews <sup>[90,93,94,96]</sup>, size, concentration, surface charge, leachables or additives, adsorbed pollutants or microorganisms, and the ageing status of MP were identified to affect the following toxicity. Cytotoxicity, oxidative stress, immune response, genotoxicity, viability, membrane integrity, proliferation and polarisation were named as possible biological effects. Carcinogenicity and mutagenicity due to additives or leachables were further added. Despite efforts being put into microplastic research in the last years, these reviews stressed the importance of multi-parametrical, comparable studies using well-characterised particles with environmental relevance and concentrations closer to environmental ones. Therefore, in this work, a systematical approach was chosen. First, the biological response in dependency on the PCI or ingestion using particles with different surface charges was investigated. Afterwards, the influence of narrow size differences on the toxicity was determined. For both parameters, solely pristine PS beads were used due to their availability in narrow, monodisperse size ranges and easy surface chemistry. Specially prepared particles were subsequently used to assess the influence of monomer residues on toxicity. Afterwards, experiments were expanded to other petroleum-based polymer types like PE or PVC, as well as biological-based polymers PLA and cellulose acetate (CA). Particles with a pre-defined protein-corona were subsequently used to transfer observed effects to the particles' surface layer. Finally, environmentally more relevant particle compositions were used. Artificial weathering was applied to the particles, comparing the effects to pristine ones. Lastly, particles extracted from commercially available wall paints were used in a final attempt to converge to realistic models. Complementary assays were used to analyse the distinct cellular effects to determine which particle properties implicate which biological outcome.

#### 3.3.1. Influence of the PCI

As described previously, the surface charge of MPP influences the PCI and ingestion strongly. In return, interactions between particles and cells are probably highly important for cellular effects. This was

investigated and published in the cooperational paper “Supposedly identical microplastic particles substantially differ in their material properties influencing particle-cell interactions and cellular responses” by Ramsperger, Jasinski, Völkl et al. (2022). Well-characterised particles from this study (PS<sub>polyscience</sub>: high PCI; PS<sub>micromod</sub>: low PCI; both 3 µm in size; surface charge PS<sub>polyscience</sub>: - 28.6 ± 0.1 mV PS<sub>micromod</sub>: - 1.5 ± 0.0 mV) with known PCI were applied to analyse subsequent effects on the macrophage cell lines ImKC and J774A.1. First, an MTT assay was used to determine the metabolic activity of the cells and, in return, conclude the overall viability of the cells (Figure 9).

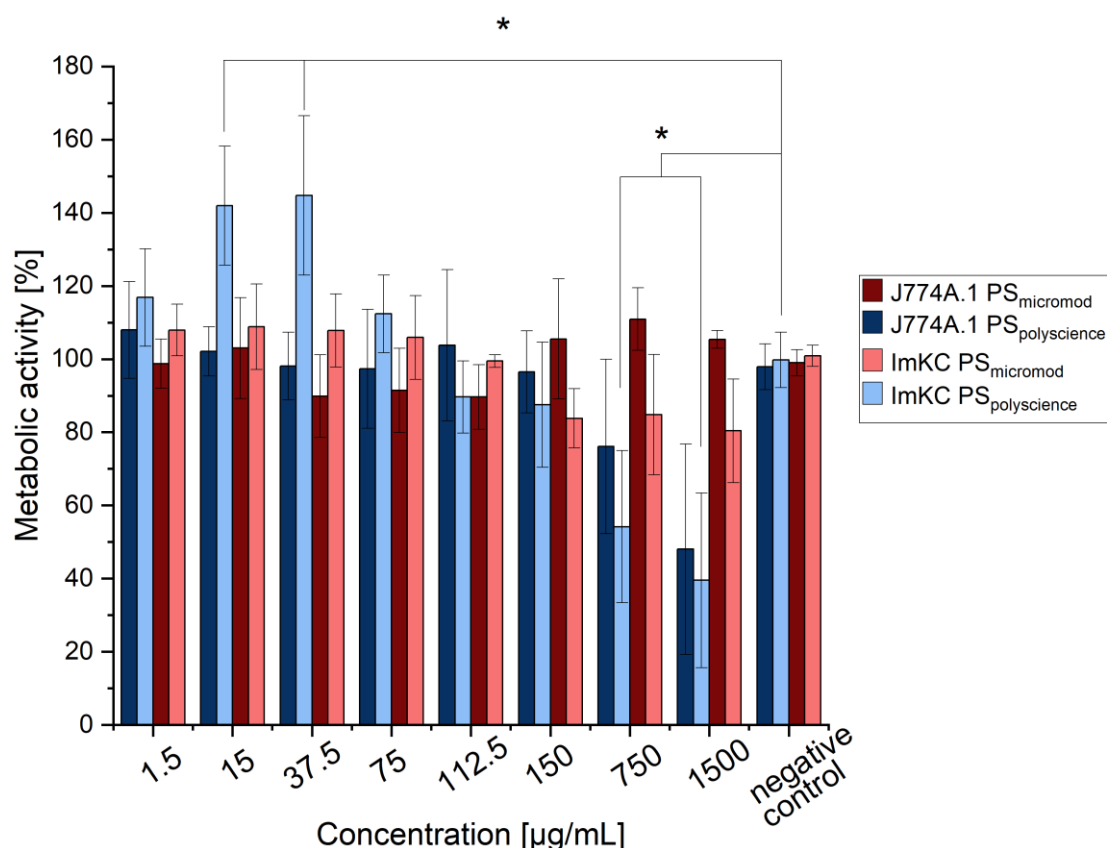


**Figure 9 MTT analysis of ImKC and J774A.1 macrophage cell lines in dependency of the surface charge of the particles**

Data represent the percentage of the respective experiment to the metabolic activity of the negative control (cells without particles). Blue colour represents PS<sub>polyscience</sub>, red colour PS<sub>micromod</sub>. Dark shaded codes for J774A.1, lightly shaded for ImKC. significance level: \* =  $p \leq 0.05$ . Data points represent mean + SD,  $n = 3 - 6$ . Figure is adapted from Ramsperger, Jasinski, Völkl et al. (2022) and modified

Significant differences could be observed between PS<sub>polyscience</sub> and PS<sub>micromod</sub>, as well as between both cell lines. For PS<sub>micromod</sub>, no effect could be observed, no matter the concentration or the cell line. Cells treated with PS<sub>polyscience</sub> showed decreased metabolic activity for concentrations > 150 µg/mL. As shown in Ramsperger, Jasinski and Völkl (2022), PS<sub>polyscience</sub> showed significantly higher PCI and ingestion rates for both cell lines, while cells seemed to ignore PS<sub>micromod</sub>. Since other particle parameters are supposed to be identical, the PCI results, combined with the results of the MTT assay, indicate an interaction-dependent cytotoxicity. It was further shown that an increase in particle internalisation leads to induced oxidative stress<sup>[73,99]</sup>, which in turn might damage the DNA<sup>[237]</sup> or lead

to bioenergetic failure <sup>[238]</sup>. Since the MTT assay, as described above, represents an overview of the metabolic activity, these side effects might also influence the results. Furthermore, phagocytic ingestion of particles is energy-dependent <sup>[42]</sup>. Due to the high amount of ingested particles in the case of PS<sub>polyscience</sub>, and subsequently a higher energy consumption, less energy could be available for cell proliferation or cellular metabolism resulting in the lower measured MTT.

When comparing both cell lines, for ImKC, the decrease in metabolic activity was more distinct and significant, while a similar trend, but no significance for J774A.1, was found. This higher sensitivity of ImKC can be associated with the different origins of the macrophages. It was shown that Kupffer cells react more sensitively to stress factors compared to other macrophage cell lines (RAW 264.7 cells) <sup>[239]</sup>. J774A.1, on the other hand, are generally described as more robust. When, e.g. treated with 2  $\mu\text{m}$  <sup>[240]</sup> or 1  $\mu\text{m}$  <sup>[72]</sup> carboxylated-PS particles, no acute influence on the viability could be measured with comparable assays for J774A.1.

Interestingly, ImKC cells showed increased metabolic activity for concentrations of 15 and 37.5  $\mu\text{g/mL}$  for PS<sub>polyscience</sub>. This can be correlated with the hormesis effect. This effect describes the phenomena of a positive influence on organisms when challenged with low concentrations of otherwise toxic components. It has been shown that an increase in metabolic activity at low concentrations was measured for some contaminants, with a continuous drop at higher concentrations <sup>[241,242]</sup>. This unique appearance for ImKC, in combination with PS<sub>polyscience</sub>, again argues for cell specificity and a dependency on PCI to trigger reactions.

To support the finding from the MTT assay, the cell proliferation in response to both particles was measured for a low, medium and high particle concentration (37.5, 150 and 1500  $\mu\text{g/mL}$ ) and compared to control cells (Figure 10).

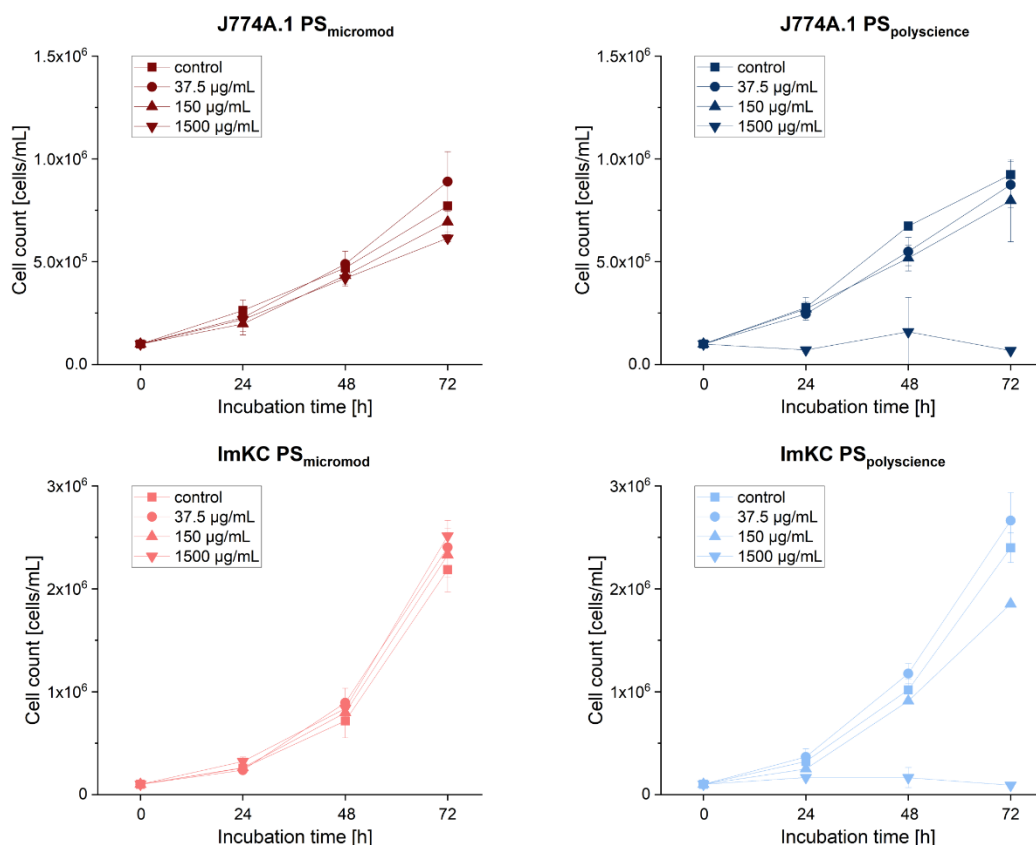


**Figure 10 Cell proliferation of J774A.1 and ImKC in response to PS<sub>polyscience</sub> and PS<sub>micromod</sub>**

Experiments were performed in 12-well plates with an initial seeding density of 100,000 cells per well in 1 mL growth medium. Data represent mean  $\pm$  SD,  $n = 3$ . Figure is adapted from Ramsperger, Jasinski, Völkl et al. (2022) and modified

Results from the MTT assay could be confirmed. While PS<sub>micromod</sub> showed no significant influence, no matter the concentration or cell line, PS<sub>polyscience</sub> significantly impacted the proliferation. For the highest concentration (1500 µg/mL), proliferation was almost completely depleted for both cell lines. In the case of ImKC, 150 µg/mL already showed a small impact after 72 h.

This concludes, at least in *in vitro* 2D cell culture and the here tested particle properties, that the presence of MPP alone is not critical, but effects mainly develop when a PCI occurs. In return, it shows a high relevance of the surface charge to the possible measured effects and other parameters that impact the PCI. Therefore, in the following chapters, the surface charge of the used particles was always analysed (carried out by Julia Jasinski).

### 3.3.2. Influence of the particle size

As the following particle parameter, particle size-dependent effects on the cells were analysed. Various considerations were taken into account to decide which particle sizes should be used. Particles in the environment are highly polydisperse, and the size range of MP is defined between 1 µm to 5 mm. To assess the influence of the size, though, it is beneficial to work with monodisperse particles to assign effects to specific sizes. Naturally, particle sizes over 10 µm are unrealistic to react with cells *in vitro*

since they are only around 20  $\mu\text{m}$ . In Rudolph, Völkl et al. (2021), it was shown that for a particle size of 6  $\mu\text{m}$ , the PCI with macrophages already drastically reduces, while epithelial cells only react with even smaller sizes. The previous chapter furthermore showed that particles which do not interact with the cells do not trigger toxic effects. Combining these findings to analyse the influence of the size, monodisperse PS particles with narrow size ranges were used (PS<sub>0.2 $\mu\text{m}$</sub> , PS<sub>0.5 $\mu\text{m}$</sub> , PS<sub>1 $\mu\text{m}$</sub> , PS<sub>2 $\mu\text{m}$</sub> , PS<sub>3 $\mu\text{m}$</sub> , PS<sub>6 $\mu\text{m}$</sub> , coefficient of variation < 10 % according to the supplier). Their surface charge did not vary significantly when incubated in a growth medium except for PS<sub>6 $\mu\text{m}$</sub>  (Table 6). This allows a reduction to the sole influence parameter “particle size”. Both epithelial cell lines (BNL CL.2, STC-1) and macrophages (ImKC, J774A.1) were used. These data are published in the paper “Noxic effects of polystyrene microparticles on murine macrophages and epithelial cells” by Rudolph, Völkl et al. (2021).

**Table 6**  $\zeta$ -potential of the particles used in 3.3.2

Particle	KCl	Growth medium
PS <sub>0.2<math>\mu\text{m}</math></sub>	- 47.4 $\pm$ 0.3	- 26.3 $\pm$ 0.1
PS <sub>0.5<math>\mu\text{m}</math></sub>	- 52.8 $\pm$ 0.2	- 26.2 $\pm$ 0.1
PS <sub>1<math>\mu\text{m}</math></sub>	- 66.1 $\pm$ 0.1	- 29.2 $\pm$ 0.5
PS <sub>2<math>\mu\text{m}</math></sub>	- 76.7 $\pm$ 0.3	- 30.7 $\pm$ 0.1
PS <sub>3<math>\mu\text{m}</math></sub>	- 78.4 $\pm$ 0.4	- 28.6 $\pm$ 0.1
PS <sub>6<math>\mu\text{m}</math></sub>	- 85.4 $\pm$ 1.4	- 11.7 $\pm$ 0.2

Data represent mean  $\pm$  SD, n = 3. Data was measured by Julia Jasinski and is published in Rudolph, Völkl et al. (2021)

First, an MTT assay with MPP incubation times of 24 h and 72 h was carried out (Figure 11). No reduced metabolic activity could be measured in epithelial cells (BNL CL.2 and STC-1), regardless of concentration, particle size or incubation time. When taking previous results into account, this finding seems fitting. Both epithelial cell lines showed low PCI with the used particles <sup>[71]</sup>, while in 3.3.1, it could be demonstrated that PCI are crucial for triggering effects. The finding of no significant effects was, therefore, comprehensible.

For macrophage cell lines, concentrations above 250  $\mu\text{g/mL}$  showed a decrease in metabolic activity for incubation times of 24 h. An extension of the incubation time to 72 h decreased the critical concentration to 10 – 100  $\mu\text{g/mL}$ , with ImKC cells once more seeming to be more sensitive (40 % metabolic activity compared to 60 % for J774A.1 for the same treatment).

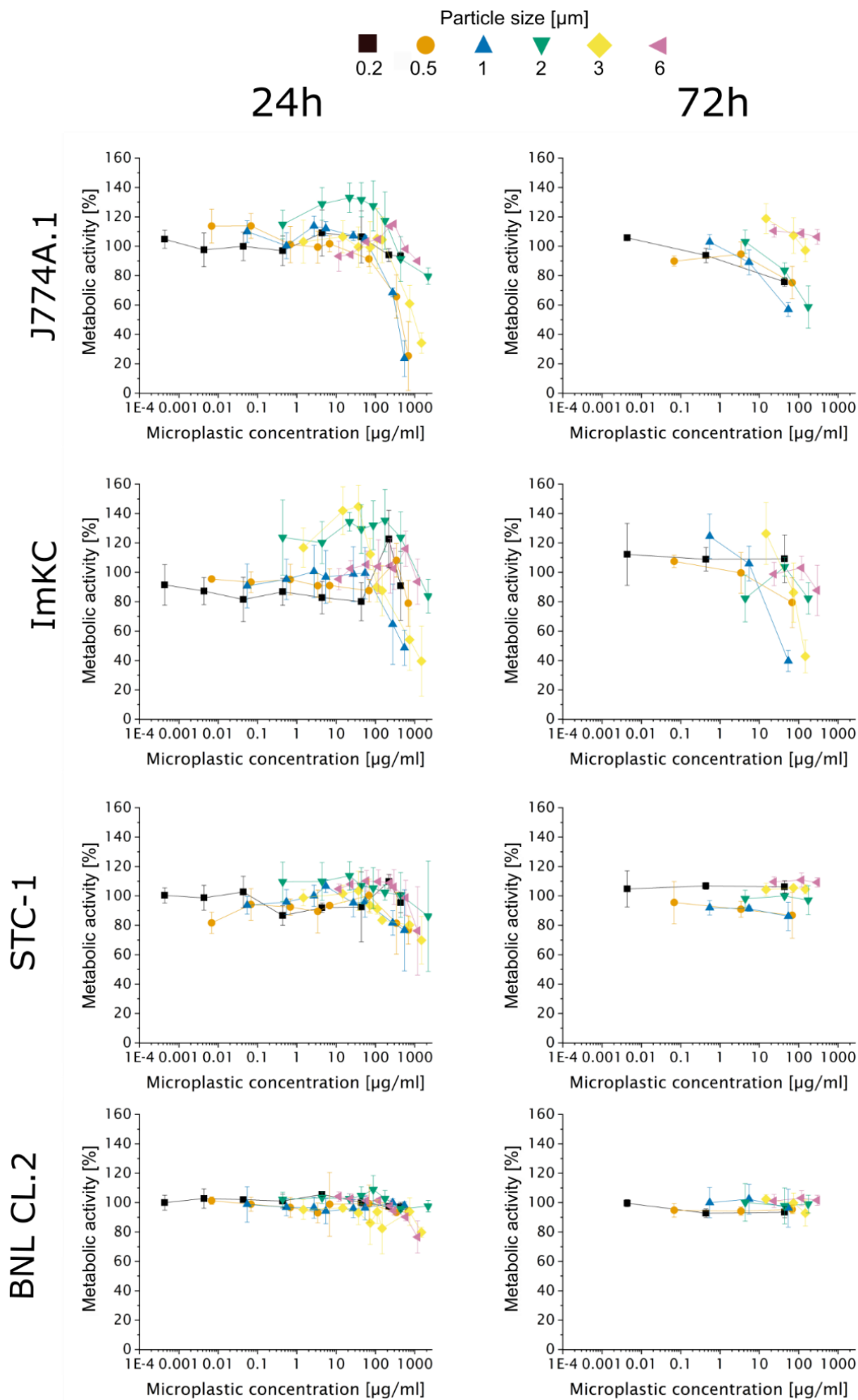


**Figure 11 Metabolic activity of cells after 24 h and 72 h incubation with differently sized MPP**

MTT assay was used to determine the metabolic activity. Data represents a correlation of the metabolic activity to cells without particles acting as negative control (100 % metabolic activity). Data represent mean  $\pm$  SD,  $n = 3$ . Figure is adapted from Rudolph, Völkl et al. (2021) and modified

The observed effects were size-dependent. The highest reduction in metabolic activity could be measured for particle sizes between 0.5 – 3  $\mu\text{m}$ , while  $\text{PS}_{0.2\mu\text{m}}$  and  $\text{PS}_{6\mu\text{m}}$  showed little response to the MPP burden, no matter the concentration. This can be associated with the uptake mechanism of the particles. The energy-dependent phagocytosis is mainly used for particulate matter in the size range of 0.5 – 5  $\mu\text{m}$ . For the smaller  $\text{PS}_{0.2\mu\text{m}}$ , pinocytosis might be responsible for the uptake, which is less energy intensive. Furthermore, in the case of  $\text{PS}_{6\mu\text{m}}$  particles, only a few PCI were measured [71]. The neglectable effects for  $\text{PS}_{0.2\mu\text{m}}$  and  $\text{PS}_{6\mu\text{m}}$  can thereby be explained. Comparable to 3.3.1, a slight but significant increase in the metabolic activity was measured for  $\text{PS}_{2\mu\text{m}}$  and  $\text{PS}_{3\mu\text{m}}$  in a concentration range of 10 – 37.5  $\mu\text{g/mL}$  for ImKC cells, with J774A.1 showing a similar trend. This might again be a sign of a hermetic response, leading to a stimulation of the cellular metabolism in response to the mild stress.

To additionally analyse other biological effects of MPP at not acute cytotoxic concentrations (low concentration = 5  $\mu\text{g/mL}$ , medium concentration = 50  $\mu\text{g/mL}$ , high concentration = 150  $\mu\text{g/mL}$ ), the oxidative stress caused by MPP after 24 h was evaluated. Therefore, the intracellular ROS amount of the cells was measured (Figure 12).

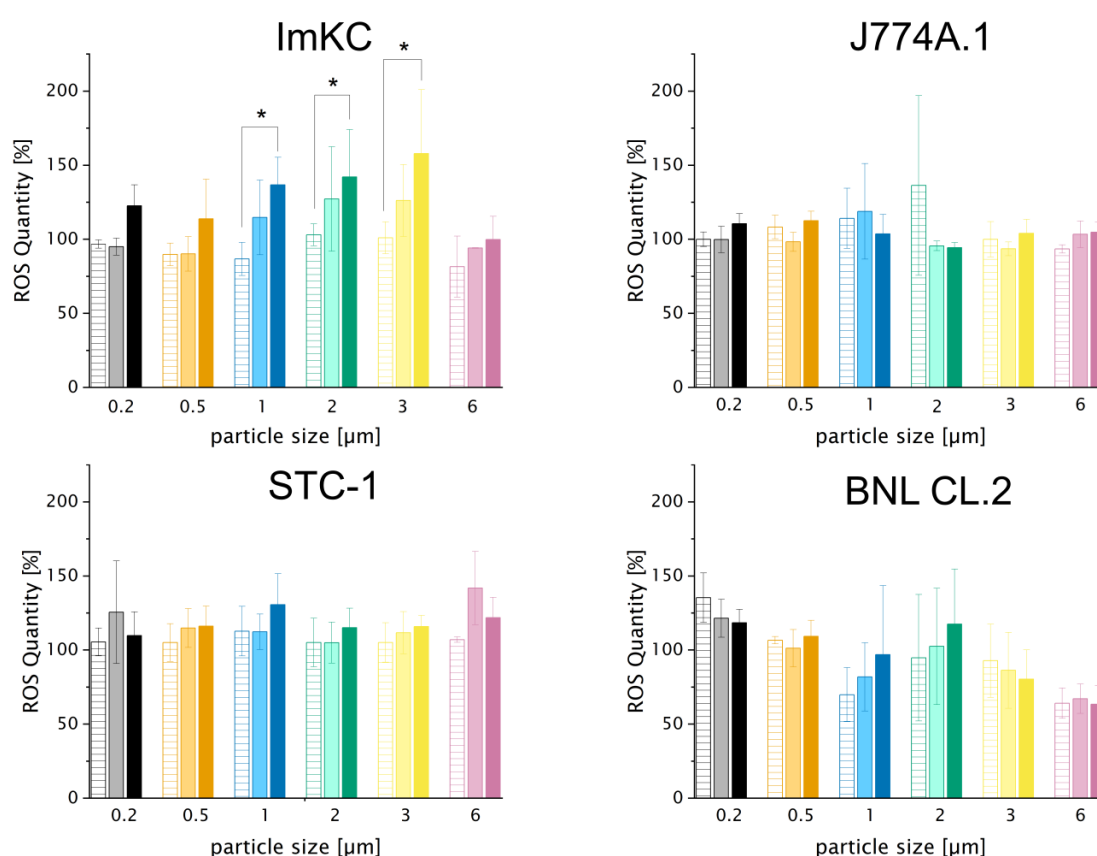


**Figure 12 Intracellular ROS concentration in dependence of size and concentration**

The medium ROS quantity of the whole cell population was measured by flow cytometry. Quantity is represented in relation to a negative control without particles (100 %). Stripped bar represents low, light bar medium and full bar high concentration. low = 5  $\mu\text{g/mL}$ , medium = 50  $\mu\text{g/mL}$ , high = 150  $\mu\text{g/mL}$ . Data represent mean  $\pm$  SD,  $n = 3$ . significance level: \* =  $p \leq 0.05$ . Figure is adapted from Rudolph, Völkl et al. (2021) and modified

For three out of four cell lines (J774A.1, STC-1, BNL CL.2), no significant ROS increase could be observed, regardless of size or concentration. Only in the case of ImKC a concentration-dependent significance could be observed for 1 – 3  $\mu\text{m}$  particles. A similar but insignificant trend could be observed for  $\text{PS}_{0.2\mu\text{m}}$  and  $\text{PS}_{0.5\mu\text{m}}$ . While Kupffer cells are known to react quickly and non-specifically with an increase in ROS to phagocytosis of particular matter, peritoneal (J774A.1 are ascites derived) macrophages respond less intensively [243,244]. This cell-specific reaction, furthermore, might explain the different findings in the literature. While some studies found a significant increase in ROS after treatment with MPP [35,87], others did not see changes in the ROS levels [78,99].

Regarding the size, the highest impact was, comparable to the findings in the MTT assay, found for particles between 1 – 3  $\mu\text{m}$ . The higher uptake for this particle size can be the reason for the increased ROS compared to other particle sizes. To take a deeper look into this assumption, a gating strategy according to Figure 3 was applied (Figure 13A and B) to split the flow cytometry data into subpopulations with an increasing amount of PCI (NC = comparable to the negative control, I - V show increasing PCI). With the help of this gating strategy, ROS production could be directly related to the PCI (Figure 13C). Furthermore, this method could consider the number of cells in the respective population to determine the impact of the subpopulation on the entire population. The higher the number of cells per subpopulation, the higher the effect on the whole population.

When looking at the subpopulations separately, a strong correlation between the PCI and the amount of ROS could be drawn. This analysis further explains the low response when looking at the whole cell population. Only for ImKC, a significant increase combined with a big cell population for high PCI could be found. E.g. for STC-1, the ROS amount increased significantly (200 – 400 % compared to the negative control) for higher PCI, but the respective populations were too small (<5%) to impact the results for the entire population. Furthermore, for populations with low PCI, the amount of ROS even decreased below 100 % of ROS, especially among the macrophages. Defence mechanisms induced by cells with high PCI, e.g., the excretion of inflammatory factors or ROS antioxidants, could have affected cells with lower PCI, impacting their natural ROS equilibrium. Interestingly, the highest detected ROS responses were seen in the case of small ( $\text{PS}_{0.2\mu\text{m}}$  and  $\text{PS}_{0.5\mu\text{m}}$ ) and large ( $\text{PS}_{6\mu\text{m}}$ ) MPP for all cell lines, except for BNL CL.2. Smaller particles have a higher surface-to-volume area, providing more possible spots for reactive groups, which could lead to a higher ROS production. For the  $\text{PS}_{6\mu\text{m}}$  sized particles, a possibly low baseline defence due to the few PCI measured could be the reason for the high response in case of high PCI.



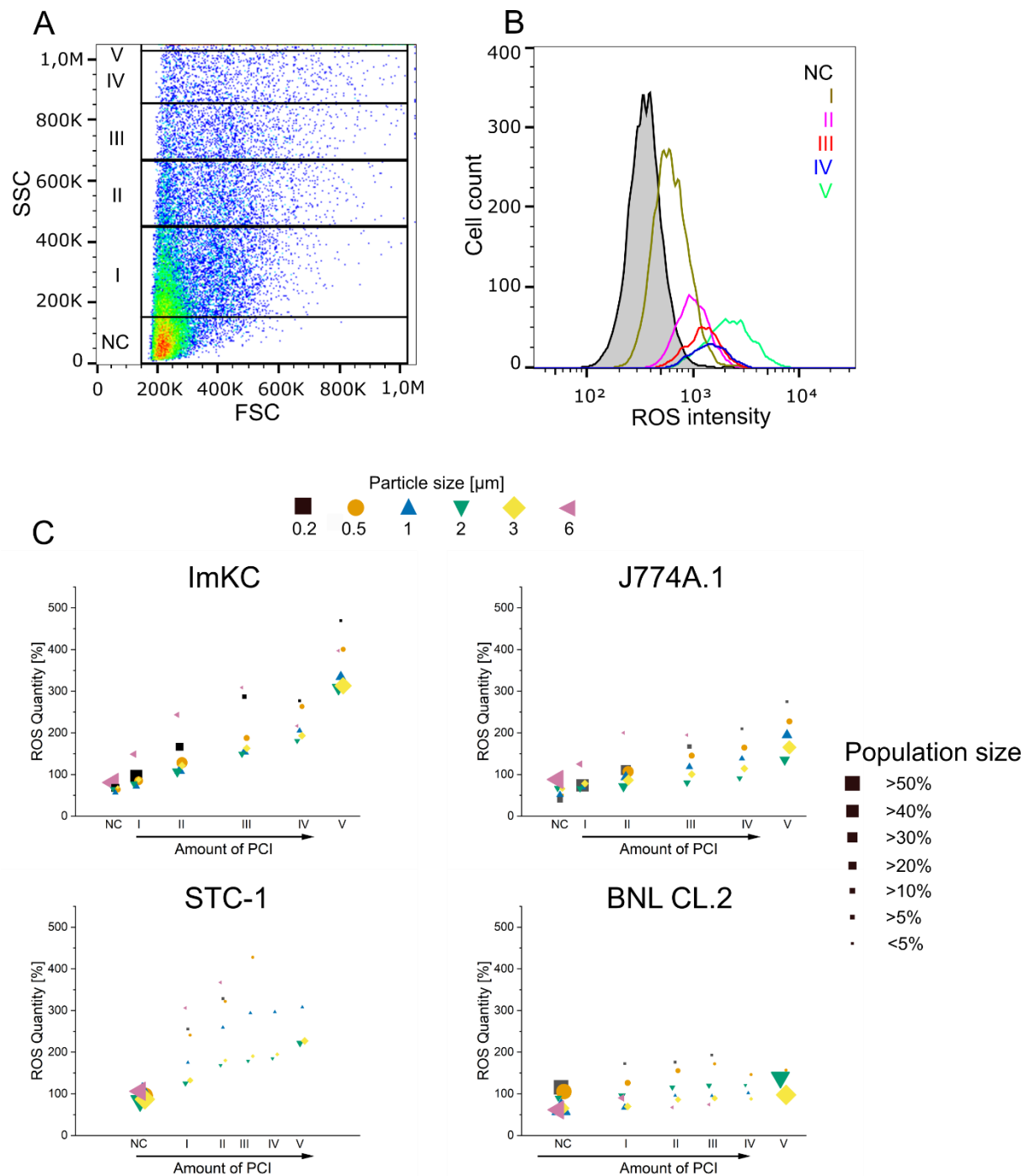


**Figure 13 Correlation between ROS generation and PCI**

*A: Representative gating strategy as established in 3.1.1. Gate NC represents cells with no particle interactions, I – V show increasing PCI (SSC = side scatter, FSC = forward scatter). B: The increasing ROS intensity in relation to the gated PCI shown in A. C: Correlation between PCI, normalised ROS quantity, and gated cell count. ROS quantity was normalised (100%) to control cells incubated without particles. Size of the data points represents the % of the respective cell population. Cell population analysis was done for the high concentration from Figure 12 (150  $\mu\text{g}/\text{mL}$ ). Figure is adapted from Rudolph, Völkl et al. (2021) and modified*

To gain more insight into the effects of the subpopulation, the cell proliferation was tracked via FC using CFSE staining with the same gating strategy as in Figure 13. Results of the CFSE are shown for the whole population (Figure 14A) and their respectively gated subpopulations (Figure 14B).

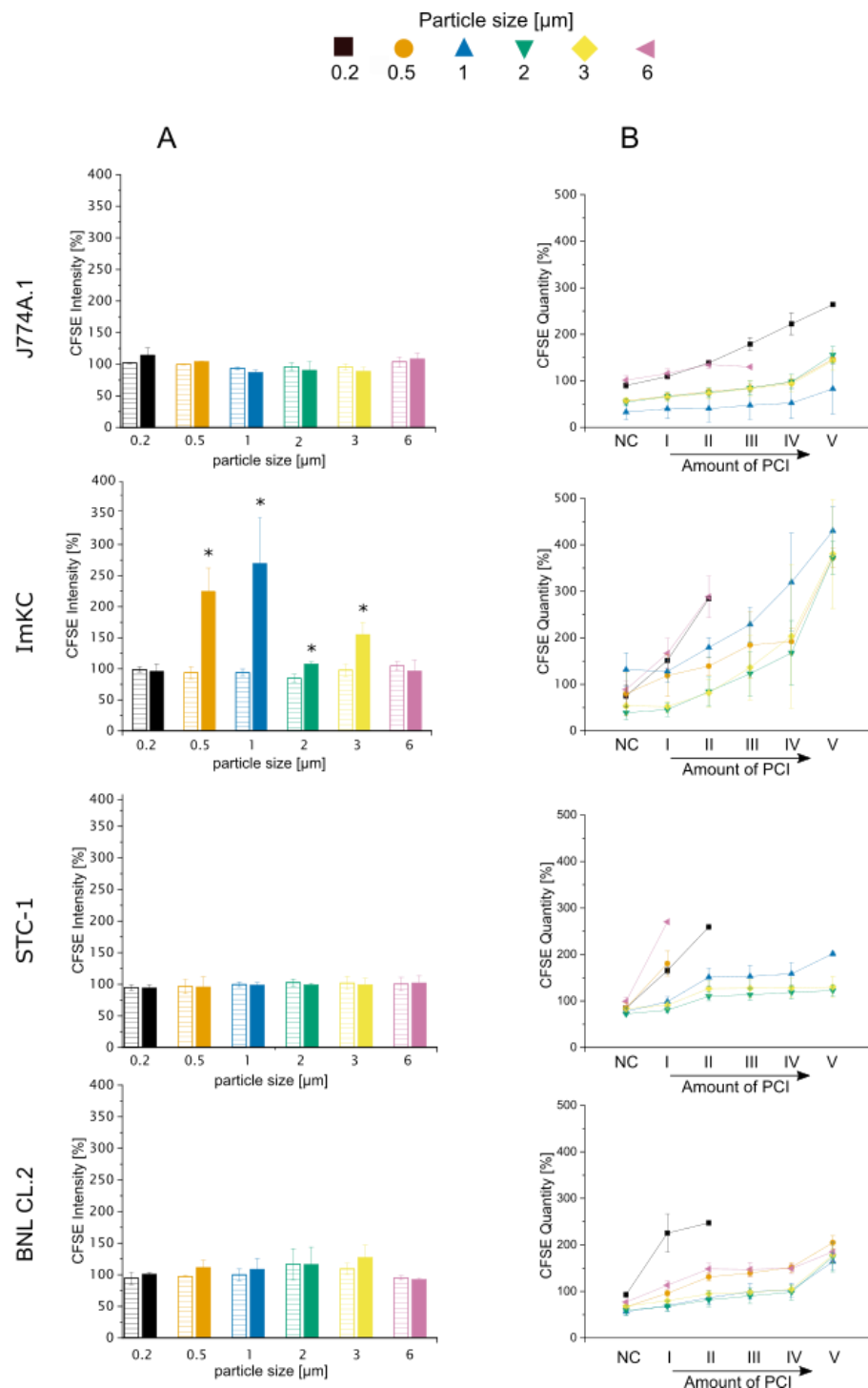


**Figure 14 CFSE dilution assay after 72 h of incubation with differently sized MPP**

The CFSE intensity for the respective cell lines is shown after 72 h of incubation with MPP. Data is normalised to the negative control (cells incubated without particles). As the CFSE intensity per cell decreases with every division, higher values for “CFSE intensity” indicate a reduced number of cell divisions. (A) Analysis of the entire population for low (striped bars, 5 μg/mL) and high concentration (filled bars 150 μg/mL) (B) CFSE amount of the subpopulations (as in Figure 13). Data represent mean  $\pm$  SD,  $n = 3$  biological replicates, significance level against the negative control: \* =  $p \leq 0.05$ . Figure is adapted from Rudolph, Völkl et al. (2021) and modified

Again, only ImKC cells showed a significant reaction with a decelerated proliferation for particles between 0.5 and 3  $\mu\text{m}$  for the higher concentration. The other three cell lines showed no significant response to no concentration or size. A similar dependency of high PCI, comparable to the ROS analysis, was detected when analysing the subpopulations. These two findings are probably connected. It is known that increased levels of ROS affect cell proliferation <sup>[124–126]</sup>. This has been shown for the treatment with nanoparticles as well <sup>[237]</sup>. Furthermore, microplastic-induced oxidative stress leads to DNA damage <sup>[245]</sup>, which in turn affects cell proliferation.

Once more, the importance of the cell phenotype has to be noted. Epithelial cell lines seemed to react to a lesser extent compared with the macrophages. This is most likely connected with the amount of PCI, which is significantly lower for epithelial cells but highly relevant for toxic effects. In addition, between both macrophage cell lines, significant differences were observed, with ImKC again reacting more sensitively compared to J774A.1. These differences were even more apparent when looking at subpopulations for increasing PCI, demonstrating that considering the whole cellular population for analysis of MPP effects might bias the final results, as correlations involving only small cellular subpopulations may be masked.

Combining these results, the importance of the particle size could be shown. Already narrow size distributions might affect the cells differently, as seen for, e.g. PS<sub>0.2 $\mu\text{m}$</sub>  and PS<sub>0.5 $\mu\text{m}$</sub> . Furthermore, the size is one of the main properties influencing the PCI and uptake mechanism, which in turn is highly important for the cytotoxicity, as can be seen for the low observed cytotoxicity for PS<sub>0.2 $\mu\text{m}$</sub>  and PS<sub>6 $\mu\text{m}$</sub> , and the observed dependency when analysing the subpopulations.

### 3.3.3. Influence of the protein corona design

Another possible influencing factor to cellular effects might be the protein corona of the particles. Just recently, Jasinski et al. found a significant influence of a tailor-made protein corona on the PCI for STC-1 and BNL CL.2 cells (1.2) <sup>[246]</sup>. Therefore, the same pre-coated particles (PS<sub>0.2 $\mu\text{m}$</sub>  and PS<sub>3 $\mu\text{m}$</sub> ; lysozyme, myoglobin, fibrinogen pre-coating, Table 7) were used to evaluate the metabolic activity via MTT assay for all four cell lines (Figure 15).

**Table 7**  $\zeta$ -potential of the particles used in 3.3.3

Particle	$\zeta$ -potential [mV] in KCl	$\zeta$ -potential [mV] in Growth medium
PS <sub>0.2<math>\mu\text{m}</math></sub> , lysozyme	+ 8.0 $\pm$ 0.1	- 27.2 $\pm$ 0.1
PS <sub>0.2<math>\mu\text{m}</math></sub> , fibrinogen	- 8.6 $\pm$ 0.1	- 18.2 $\pm$ 0.4
PS <sub>0.2<math>\mu\text{m}</math></sub> , myoglobin	- 13 $\pm$ 0.2	- 25.2 $\pm$ 0.2
PS <sub>3<math>\mu\text{m}</math></sub> , fibrinogen	- 2.5 $\pm$ 0.1	- 36.3 $\pm$ 0.1
PS <sub>3<math>\mu\text{m}</math></sub> , lysozyme	+ 17.4 $\pm$ 0.3	- 36.4 $\pm$ 0.3
PS <sub>3<math>\mu\text{m}</math></sub> , myoglobin	- 16.1 $\pm$ 0.2	- 37.1 $\pm$ 0.1

Data represent mean + SD, n = 3. Data was measured by Julia Jasinski and is published in Jasinski et al. (2022)

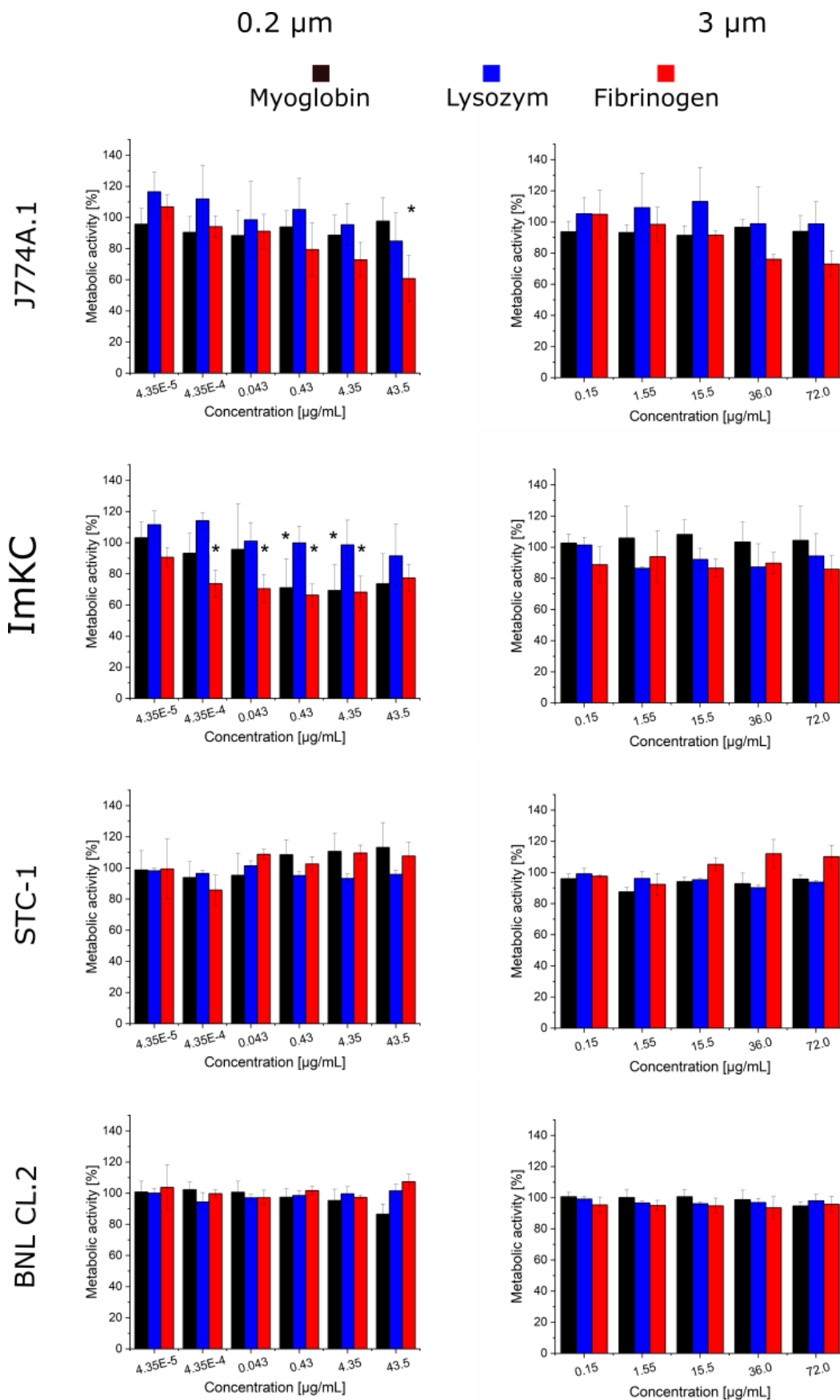


**Figure 15 MTT assay with protein-coated particles**

Data represent the percentage of the particular experiment to the metabolic activity of the negative control (cells without particles). Data represent mean  $\pm$  SD,  $n = 3$  biological replicates, significance level against the negative control: \* =  $p \leq 0.05$

No reduction in metabolic activity could be measured for both epithelial cell lines, regardless of size or concentration. The observed changes in PCI did not seem to affect the epithelial cells' viability. For J774A.1 and ImKC, a reduction in metabolic activity could be measured for PS<sub>0.2µm, fibrinogen</sub>. While a significant reduction could be measured for J774A.1, only for the highest concentration (43.5 µg/mL), ImKC cells showed a significant reduction already for 0.043 µg/mL. This reduction, though, was only low (80 % metabolic activity) and did not seem to be concentration-dependent. ImKC cells showed further a reduction for PS<sub>0.2µm, myoglobin</sub> (concentrations > 0.43 µg/mL). These results seem counter-intuitive compared to 3.3.1 and 3.3.2 since PS<sub>0.2µm, fibrinogen</sub> induced the highest cytotoxicity despite their reduced PCI with cells. For 3 µm particles, a trend of a concentration-dependent reduction for fibrinogen coating could also be observed for J774A.1 and ImKC.

Controversially, fibrinogen-coating is used to reduce the cytotoxicity of nanomaterials <sup>[247,248]</sup>, and despite the reduced PCI, these particles showed the highest cytotoxicity. The here-found results, therefore, need to be treated carefully. However, it must be noted that while Jasinski et al. found traces of the pre-coating, the topmost coating layer formed changed during the incubation in the growth medium <sup>[246]</sup>. This change in composition could have also affected the particles' cytotoxicity. Further analysis is therefore needed to determine the effect of protein corona.

#### 3.3.4. Influence of monomer residues

As yet, especially the surface of the particles was analysed. Another possible parameter might be residual monomers. Styrene monomers, e.g. are known to be toxic <sup>[249]</sup> when leaching from packing materials. To verify if this finding is true for PS-MPP as well, the influence of the residual monomer on the cytotoxicity was analysed. These results are processed in the submitted paper "The role of residual monomers in the manifestation of (cyto)toxicity by polystyrene microplastic model particles" by Zhang et al. 2023. To assess the influence of the residual monomer, particles were synthesised in-house by emulsifier-free emulsion polymerisation and characterised (PS<sub>SHPA</sub>; number average molar mass (Mn) = 25370, diameter 515 ± 17 nm, ζ-potential = - 26 mV) by the group of Prof. Greiner from Yuanhu Zhang. The cytotoxic effect of these particles was then compared to commercially available particles (PS<sub>MIPA</sub>; Mn = 33090, diameter 507 ± 7 nm, ζ-potential = - 26 mV) in this work. The in-house synthesised particles were additionally purified by autoclaving and rapidly dialysed against methanol/water (50/50) mixed solvents to reduce the monomer residues to a minimum. Compared to the 99.26% purity of the PS<sub>MIPA</sub>, a 99.96% purity could be achieved for PS<sub>SHPA</sub>, resulting in a 20 x higher monomer burden for PS<sub>MIPA</sub> compared to PS<sub>SHPA</sub>. L929 cells, a known standard fibroblast cell line in toxicity testing, were subsequently used to assess the cytotoxicity of these different particles (concentration range: 0.1 µg/mL – 1900 µg/mL) via the MTT assay (Figure S6). A significantly higher cytotoxicity for PS<sub>MIPA</sub> was found compared to PS<sub>SHPA</sub> for all particle concentrations except the highest.

Since all other tested parameters were comparable, the observed cytotoxicity was ascribed to the styrene monomer residues. However, other potentially cytotoxic surfactants can be present on the PS<sub>MIPA</sub>. While PS<sub>SHPA</sub> were synthesised by emulsifier-free emulsion polymerisation, residual proprietary surfactant might be present on PS<sub>MIPA</sub>. These surfactants often bear cytotoxic potential as well. However, as a conclusion from this study, it could be shown that monomer residue adds a further cytotoxic potential to MPP.

### 3.3.5. Influence of the polymer type

So far, experiments have been solely conducted with PS particles. Since the main focus in the first experiments did not depend on the polymer type but on other particle parameters, which are easy to control for PS particles (size and surface chemistry), using PS particles was sufficient. This pattern of using PS beads can be followed in the field of microplastic research as well, where over 50 % of studies worked with PS microspheres and “only a few studies compared the effects of different polymer types (...) [for particles of similar size and shape] on organisms” <sup>[94]</sup>. Nevertheless, MPP pollution in the environment is highly polydisperse, with PP and PE as the main pollutant (combining about 70 % of total pollution), and PET, PVC or PS only combining about 20 % with about 10 % left for more specialised polymers <sup>[250,251]</sup>. The following section, therefore, uses PE and PVC beads as well as biological-based polymers (PLA and CA). These polymers were selected since beads in a similar size range, and  $\zeta$ -potential (Table 8) were applicable, proving critical in the previous experiments. All four cell lines (J774A.1, ImKC, STC-1, BNL CL.2) were used for the experiments. These data are processed in the finished manuscript “Cellular effects of different polymer microparticles on murine cells” by Jasinski, Völkl et al.

**Table 8** Size and  $\zeta$ -potential of the particles used in 3.3.5

Particle	Size [ $\mu\text{m}$ ]	$\zeta$ -potential [mV]
PS <sub>2<math>\mu\text{m}</math></sub>	2.25 $\pm$ 0.15	- 30.7 $\pm$ 0.1
PE <sub>1-4<math>\mu\text{m}</math></sub>	1.80 $\pm$ 0.35	- 27.7 $\pm$ 0.6
PVC <sub>1.4<math>\mu\text{m}</math></sub>	1.40 $\pm$ 0.15	- 26.1 $\pm$ 0.2
PLA <sub>2<math>\mu\text{m}</math></sub>	1.75 $\pm$ 0.85	- 21.9 $\pm$ 1.3
CA <sub>1.5<math>\mu\text{m}</math></sub>	1.50 $\pm$ 0.40	- 6.9 $\pm$ 0.2

Data represent mean  $\pm$  SD, n = 3. Data was measured by Julia Jasinski

To compare the data of these used particles and reduce the parameter to the used polymer, Julia Jasinski compared the PCI and ingestion of the particles by confocal microscopy. There were no significant differences in macrophage uptake rate for all particles except CA<sub>1.5 $\mu\text{m}$</sub> . This reduced ingestion rate might be related to the lesser  $|\zeta\text{-potential}|$  for CA<sub>1.5 $\mu\text{m}$</sub>  compared to the other used particles. For the BNL CL.2 cell line, uptake was only observed for PS<sub>2 $\mu\text{m}$</sub>  particles and, interestingly, low uptake for

CA<sub>1.5</sub> $\mu$ m. In the case of STC-1, no uptake was observed. However, PCI interactions were found for all used polymer particles.

After verifying the PCI and uptake, which proved to be critical when estimating possible toxic effects (see 3.3.1), MTT and ROS assay were used to assess the effect of the chosen polymer. In the case of MTT, no distinct toxic effects could be measured in the applied concentrations, no matter the polymer type or the cell line (Figure 16). For PLA<sub>2</sub> $\mu$ m, a trend towards a higher cytotoxicity (< 80 % metabolic activity) above concentrations of 150  $\mu$ g/mL could be followed for macrophages. These data are comparable to the previous result, where only high concentrations above 150  $\mu$ g/mL showed cytotoxicity. This indicates that the polymer does not significantly determine cytotoxic effects, but other parameters might be responsible for cytotoxicity.

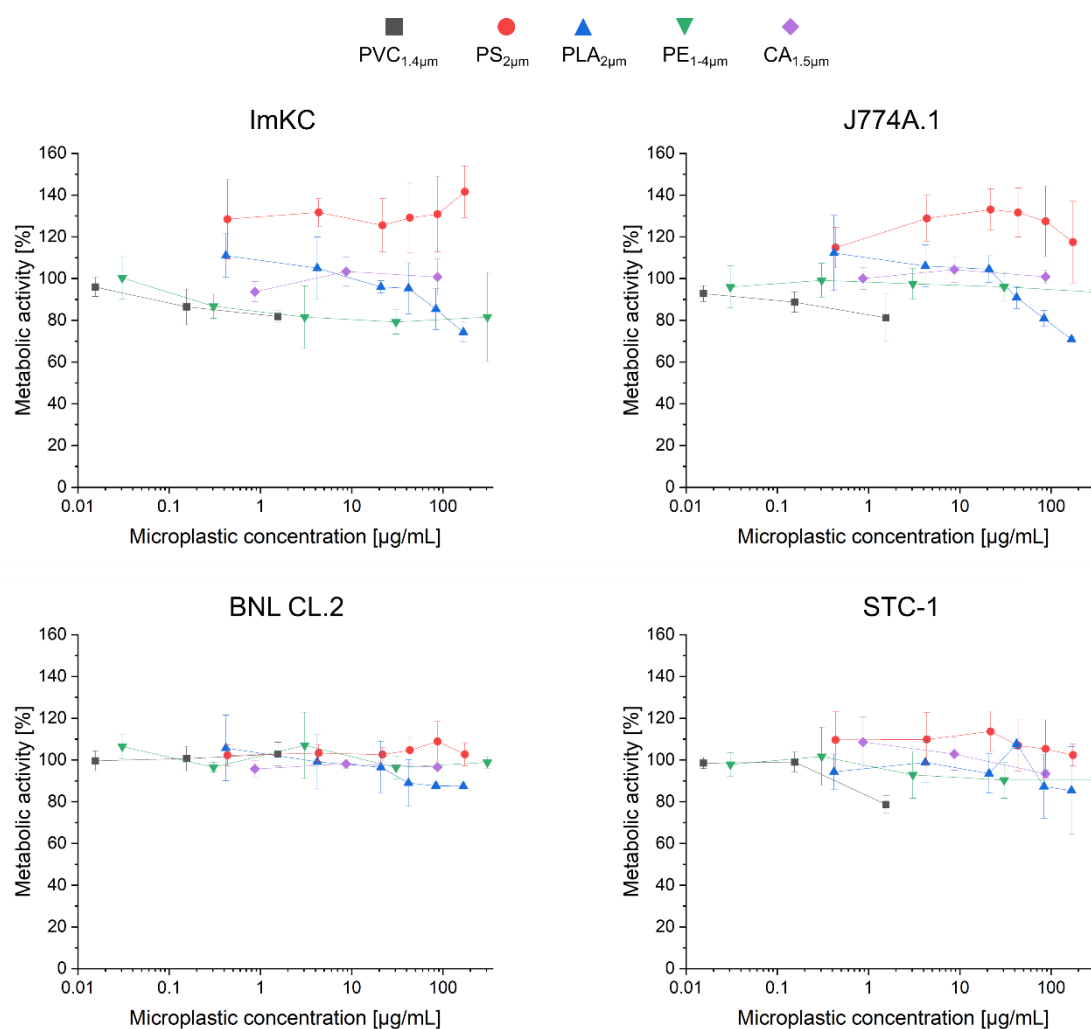


**Figure 16** Metabolic activity after 24 h incubation with the different MPP polymers

Data represent the percentage of the particular experiment to the metabolic activity of the negative control (cells without particles). Data represent mean  $\pm$  SD, n = 3 biological replicates

Additionally, a ROS assay was conducted to complement the data for a high and a low concentration (Table 9, Figure 17).

**Table 9 Particle concentrations of the used polymer beads for the ROS assay in Figure 17**

Particle	Low concentration [ $\mu\text{g/mL}$ ]	High concentration [ $\mu\text{g/mL}$ ]
PS <sub>2<math>\mu\text{m}</math></sub>	0.44	43.54
PE <sub>1-4<math>\mu\text{m}</math></sub>	0.31	30.60
PVC <sub>1.4<math>\mu\text{m}</math></sub>	0.15	1.55
PLA <sub>2<math>\mu\text{m}</math></sub>	0.42	41.87
CA <sub>1.5<math>\mu\text{m}</math></sub>	0.87	87.04

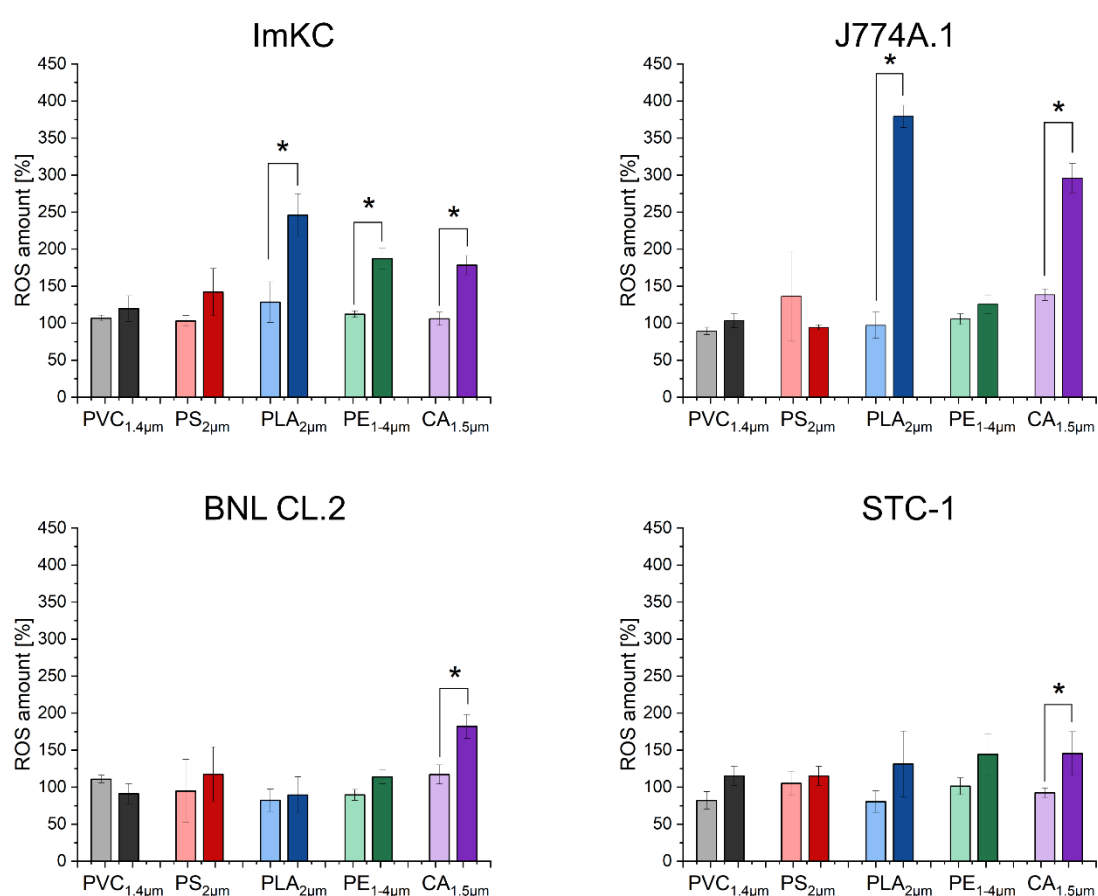


**Figure 17 Intracellular ROS concentration in dependence of polymers**

Medium ROS of the whole cell population was measured by flow cytometry. Quantity is represented in relation to a negative control without particles (100 %). Light bars represent low, full bars high concentration (concentration used, see Table 9). Data represent mean  $\pm$  SD,  $n = 3$ . significance level against the negative control: \* =  $p < 0.05$

Especially PLA<sub>2 $\mu\text{m}$</sub>  and CA<sub>1.5 $\mu\text{m}$</sub>  particles showed a significant increase in ROS for both macrophage cell lines. CA<sub>1.5 $\mu\text{m}$</sub>  showed a small but significant increase in ROS for both epithelial cell lines as well. ImKC cells showed a significant increase in ROS after treatment with PE<sub>1-4 $\mu\text{m}$</sub> . All increases, though, were only seen for the higher concentration used. Interestingly, the highest ROS increase was conducted by both



biological-based particles (CA<sub>1.5µm</sub>, PLA<sub>2µm</sub>). Contradictory biopolymers are often used as antioxidant coating agents in, e.g. food packing or medical implants <sup>[252]</sup>. However, the biopolymers in these applications are mainly used as coating agents and not in particulate shape. Furthermore, biological and intracellular degradation might be an affecting point when using biopolymers, albeit the incubation time (24h) in the used setup was quite short <sup>[253]</sup>. Either way, the effects of biodegradable particles need to be analysed more to understand possible mechanisms behind the observed ROS increase. The observed significant increase in ROS for PE particles was again only observed for the ImKC cell line, which was also the most sensitive in previous experiments. Once more, the phenotype of the cells is also highly important, as macrophages were more affected in MTT and ROS assay compared to epithelial cells.

Comparable studies analysing the effect of particles other than PS beads on cells are rare. Some studies indeed used particles like PE, PVC, PP or PET <sup>[73,79,91,99]</sup>, but particles were quite large (> 10 µm) and polydisperse. A direct comparison to other studies is therefore difficult since the particle size highly affects the uptake, and cytotoxic effects depend highly on the cellular interaction and uptake (3.3.1). Here, no matter the polymer, significant effects on the cytotoxicity could not be found either. Effects occurred only for high concentrations (> 150 µg/mL), comparable to results in 3.3.2. This indicates that effects are more induced by the particles themselves than the polymer used. However, this statement can only be made for inert polymer beads in laboratory conditions. Environmental conditions might alter particle properties differently for diverse polymers, which can affect the particles' cytotoxicity.

### 3.3.6. Influence of artificial ageing of particles

As previously mentioned, commonly used pristine PS particles do not necessarily replicate MPP found in the environment <sup>[100]</sup> due to the expected environmental degradation by mechanical stress or photo- and biotic-degradation <sup>[6,101,102]</sup>, leading to a change in size and surface characteristics (physical and chemical) <sup>[83,94,103]</sup>. Therefore, in converging to more realistic particles, artificial weathering of PS<sub>2µm</sub> and PS<sub>2µm, green</sub> via UV irradiation and mechanical stress was conducted to simulate environmental degradation and compare effects of these aged particles to pristine ones. These data are published in the paper "Pristine and artificially-aged polystyrene microplastic particles differ in regard to cellular response" by Völkl et al. (2022). Artificially aged PS<sub>2µm</sub> were prepared by and with the method of Meides et al. (2021), with irradiation times of 200, 400 and 600 h. These ageing times were used since their study also showed that mainly surface abrasion is happening in this period, but the particle size is not changing significantly. A low size change was necessary since particle size affects the uptake and cytotoxicity (see 3.3.2), which would be a change in more parameters (ageing and size), complicating the interpretation of the data. Due to the accelerated laboratory weathering (factor 5.2), these ageing times approximately correspond to 43, 86 and 130 days in the environment. Aged particles are

therefore called PS<sub>43</sub>, PS<sub>86</sub> and PS<sub>130</sub>, respectively. ImKC cells were used since they proved the most sensitive in previous experiments.

Before evaluating the cytotoxicity, the size and surface charge of the particles were analysed as important influencing factors by Julia Jasinski (Table 10).

**Table 10** Size and  $\zeta$ -potential of the particles used in 3.3.6

	MP size [ $\mu\text{m}$ ]	$\zeta$ -potential [mV]
PS <sub>2<math>\mu\text{m}</math></sub>	$1.5 \pm 0.04$	$-30.7 \pm 0.1$
PS <sub>43</sub>	$1.88 \pm 0.05$	$-33.9 \pm 0.2$
PS <sub>86</sub>	$1.49 \pm 0.10$	$-29.5 \pm 0.1$
PS <sub>130</sub>	$1.63 \pm 0.22$	$-26.4 \pm 0.2$

Data represent mean  $\pm$  SD, n = 3. Data was measured by Julia Jasinski and is published in Völkl et al. (2022)

The size analysis by DLS revealed that the size did not change significantly, but the deviation increased with longer ageing times. The  $\zeta$ -potential did not differ highly for the different treatments, with a slightly lower absolute value for PS<sub>130</sub>. Since the ageing of the particles should influence especially the surface, further characterisation was conducted. Using SEM, Julia Jasinski analysed the particles' morphology (Figure 18). While there was no difference in the morphology for PS<sub>2 $\mu\text{m}$</sub> , PS<sub>43</sub> and PS<sub>86</sub>, the longest ageing period seemed to influence the particles. A high frequency of cracks and a caving-in of the particles was observable, explaining the higher size deviation of the particles.

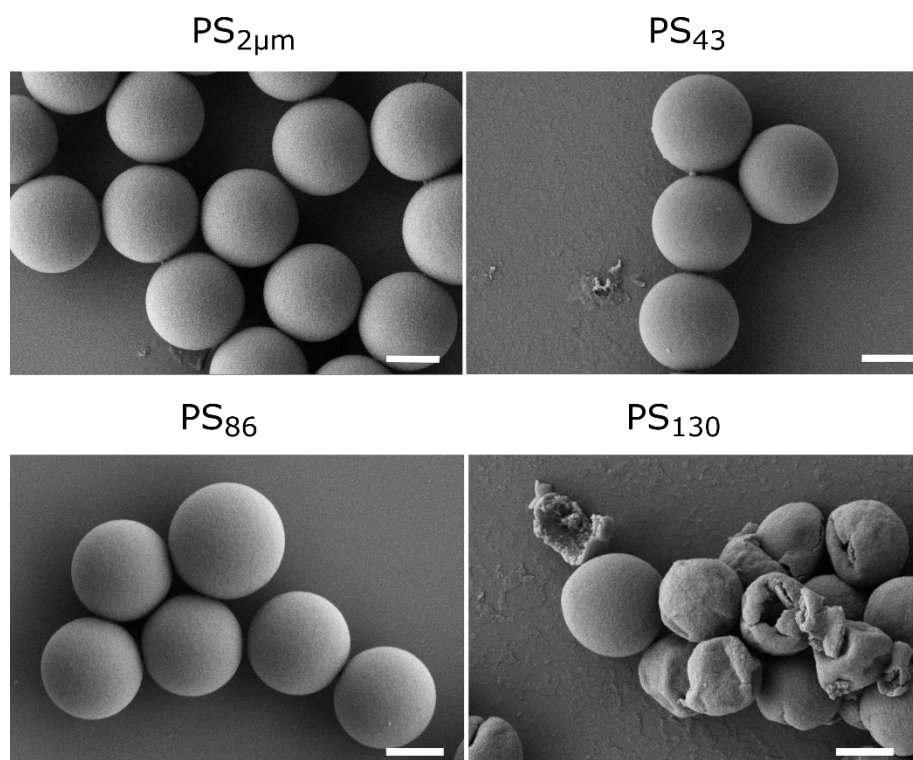


**Figure 18** Representative SEM pictures of the used particles at the respective ageing times

Scale bar = 1  $\mu\text{m}$ , samples were prepared and pictures were taken by Julia Jasinski.

In addition to the visual morphological analysis, the surface chemistry of aged particles was analysed by Nora Meides in Meides et al. (2021) since especially reactive groups on the surface are supposed to interfere with the cell's homeostasis. Due to UV irradiation, these reactive groups are promoted <sup>[107,108]</sup>, which needs to be verified. Indeed, the measured O/C ratio increased exponentially at the surface, arguing for increasing amounts of carboxyl, peroxide, and keto groups <sup>[6]</sup>. As the final characterisation, the fluorescence intensity of the aged particles was measured since some of the assays depended on fluorescence analysis (Figure 19).

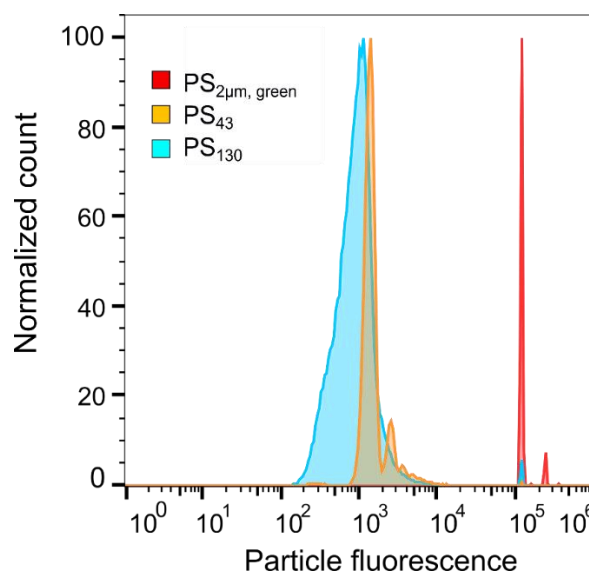


**Figure 19 Particle fluorescence measured using flow cytometry**

*Shown is the green fluorescence of the particles for the respective weathering time using FC. At least 100,000 particles were measured for the quantification of the fluorescence. Figure is adapted from Völkl et al. (2022) and modified*

The fluorescence intensity and deviation of the particles decreased with increasing ageing time. Since fluorescence could be measured, though, FC and confocal microscopy were used to quantitatively and qualitatively analyse the uptake and interaction rate. First, the PCI measured by flow cytometry was compared between PS<sub>2µm, green</sub>, PS<sub>43</sub> and PS<sub>130</sub> (Figure 20). Here, no significant differences in the PCI between the used particles could be observed using the FSC/SSC method developed in 3.1.1. The differentiation between the amount of ingested particles via fluorescence proved more problematic. Due to the decreased fluorescence intensity, no distinct particle populations could be observed.

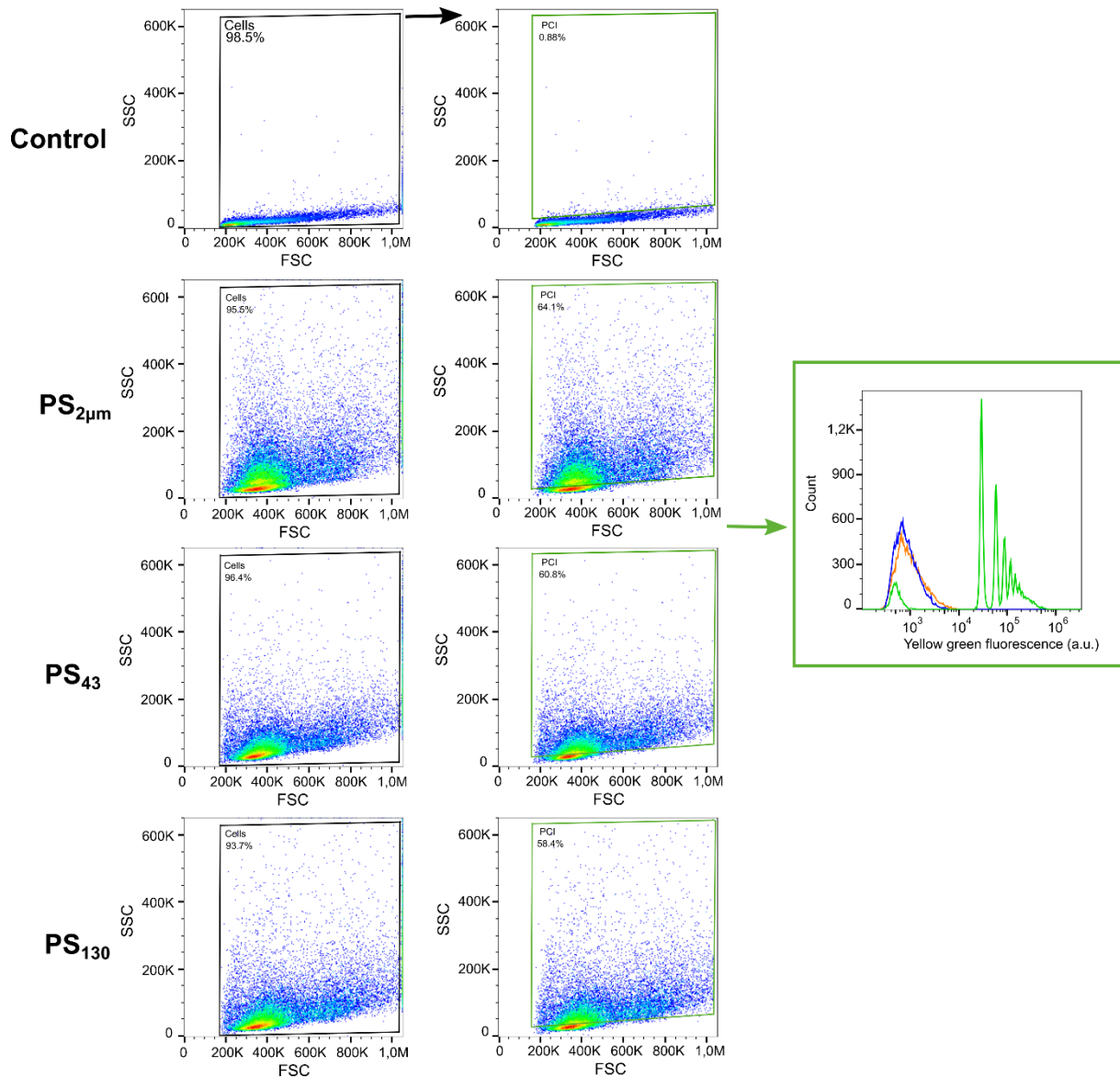


**Figure 20** Representative gating strategy for the quantitative uptake of  $PS_{2\mu m}$ ,  $PS_{43}$  and  $PS_{130}$

150,000 cells per well were seeded and treated with 150  $\mu g/mL$  fluorescent particles ( $PS_{2\mu m}$ ,  $PS_{43}$  and  $PS_{130}$ ) for 24 h. Shown is the gating strategy for investigating particle-cell interactions (PCI). Cells were initially evaluated by scatter properties (FSC/SSC) to select a region ("cells" gate, black line) representing single, nonapoptotic cells while disregarding debris and cellular aggregates. Upon uptake or cellular interactions of MP, the SSC fluorescence increased, allowing to define an additional sub-gate containing cells with particle interactions (PCI, red line). The gate PCI was set with the non-treated cells (i.e., control population without PCI (control) and then transferred to  $PS_{2\mu m}$ ,  $PS_{43}$  and  $PS_{130}$ . The intensity of fluorescence of the cells in the PCI gate is depicted in the histogram representation ( $PS_{2\mu m}$  (green line),  $PS_{43}$  (orange line) and  $PS_{130}$  (blue line)). Figure is adapted from Völkl et al. (2022) and modified

A qualitative confirmation of the ingestion was done by Julia Jasinski by confocal microscopy<sup>[116]</sup>. Aged particles, no matter the ageing status, were similarly ingested as pristine ones.

Since no significant differences in PCI or ingestion were observed, and other particle properties like size and  $\zeta$ -potential were similar as well, a comparison between PS<sub>2 $\mu$ m</sub> and PS<sub>aged</sub> was applicable. For a first estimation of the cytotoxicity, the MTT assay was used (Figure 21).

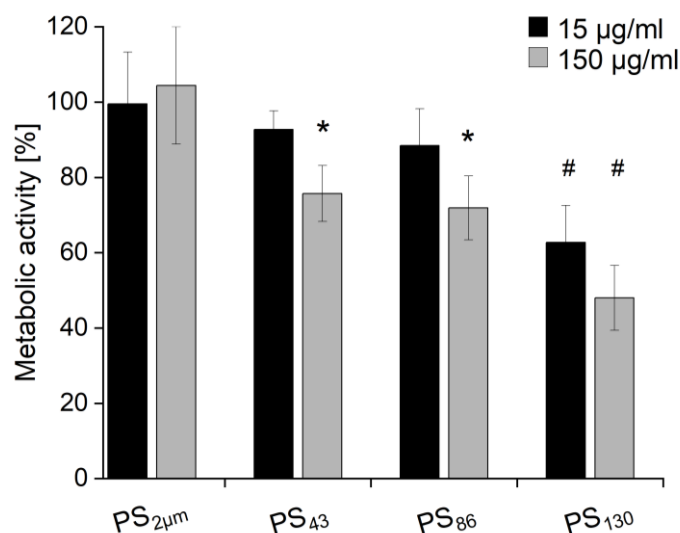


**Figure 21** MTT assay determines the metabolic activity of PS<sub>aged</sub>

Data represent the percentage of the particular experiment to the metabolic activity of the negative control (cells without particles). Data represent mean  $\pm$  SD,  $n = 3$  biological replicates. Significance level: \* = significantly lower compared to PS<sub>pristine</sub> within a concentration group, # = significantly lower than all previous data points within a concentration group,  $p < 0.05$ . Figure is adapted from Völkl et al. (2022) and modified

Interestingly, when using concentrations (15 and 150  $\mu$ g/mL) unharmed for the cell with PS<sub>2 $\mu$ m</sub> (see 3.3.2), the artificial weathering of the particles induced an ageing-dependent cytotoxic effect. While for PS<sub>43</sub> and PS<sub>86</sub>, the cytotoxicity was only increased for the higher concentration (150  $\mu$ g/mL). In the case of PS<sub>130</sub>, which was the most affected by ageing according to the characterisation, effects were visible already for 15  $\mu$ g/mL (63 % metabolic activity) and even higher for 150  $\mu$ g/mL (48 % metabolic activity). However, while the MTT assay might be a useful tool for the first evaluation of toxic effects, it is affected by various biological aspects<sup>[113]</sup>. Therefore, further analysis of the mechanisms of toxicity on different biological levels were conducted. Membrane integrity, genotoxicity, oxidative stress and the immune response were analysed, identified as key parameters by various reviews<sup>[93,94,96]</sup>. First, to study the membrane integrity, an LDH assay was applied (Figure 22).

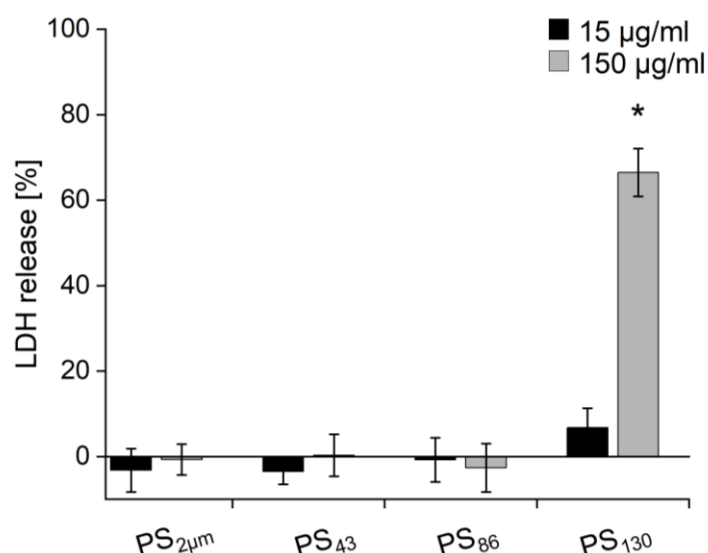


**Figure 22 LDH assay used to determine the membrane integrity**

Data represents a correlation to lysed cells acting as control group (100 % LDH release). Data represent mean  $\pm$  SD,  $n = 3$ .  
 \* significantly higher compared to all other samples,  $p < 0.05$ . Figure is adapted from Völkl et al. (2022) and modified

No significant LDH release was observed for PS<sub>2µm</sub>, PS<sub>43</sub> and PS<sub>86</sub>, for neither low nor high concentration. Treatment with PS<sub>130</sub>, on the other hand, induced a concentration-dependent increase in LDH release. This release is likely associated with the morphological change of the PS<sub>130</sub> compared to the other particles. Sharp edges and fragments presumably damaged the plasma membrane, resulting in a release of LDH and reduced metabolic activity, probably due to the reduced viability of the cells. MTT and LDH assays can be used as indicators of apoptosis (programmed process of autonomous cellular dismantling) and necrosis (passive, accidental cell death resulting from environmental perturbations), respectively <sup>[254]</sup>, suggesting a hypothesis regarding the mechanism of action of the investigated MP. Whereas PS<sub>2µm</sub> neither induces apoptosis nor necrosis, the observed cytotoxic effects of PS<sub>aged</sub> could mainly be attributed to necrosis due to the highly significant effect in the LDH assay. However, some apoptotic processes cannot be ruled out. The MTT assay was conducted 24 h post-treatment, at which the apoptosis process was assumably completed. Yet, the observed decrease in metabolic activity could also reflect a post-apoptotic secondary necrosis process <sup>[255]</sup>.

Other studies affirm the observed membrane damage. Studies found increased effects triggered by irregular microplastic fragments for human cell lines and primary blood cells <sup>[256,257]</sup>, while preserved smooth spherical morphologies showed no effect on the plasma membrane integrity. This concludes, that the morphology of the particles seems to be a toxicity mechanism.

Subsequently, genotoxicity triggered by the treatment with the microparticles was analysed by the COMET assay (Figure 23).

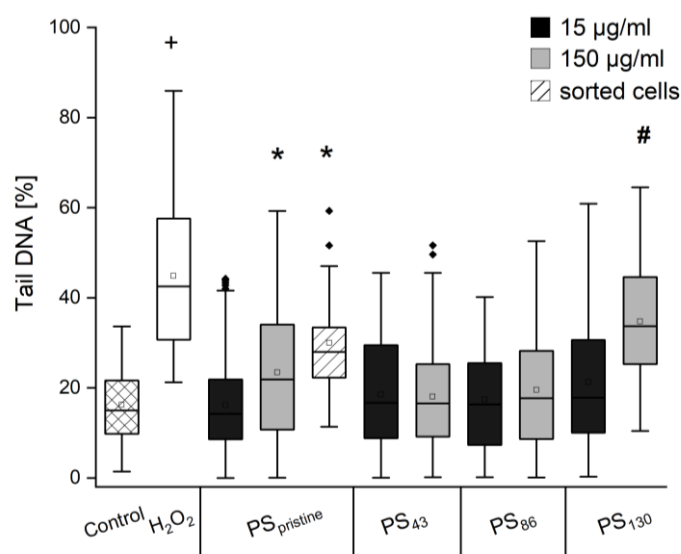


**Figure 23 COMET assay to estimate the genotoxicity**

Pictured is the percentage of Tail DNA for the respectively treated cells. Data are represented with whisker boxplots showing the 25% and 75% quartile, with the whiskers representing the maximal and minimal values. Outliers are defined as 1.5 times the 25% and 75% quartile threshold values and are represented as diamonds outside the box plot. The median is indicated as a black line and the mean value as a black square. Sorted particles by single-cell sorting were used to determine the influence of the PCI on genotoxicity. Control ( $n = 314$ ),  $H_2O_2$  ( $n = 59$ ),  $PS_{2\mu m}$  15  $\mu g/mL$  ( $n = 418$ ),  $PS_{2\mu m}$  150  $\mu g/mL$  ( $n = 324$ ),  $PS_{2\mu m}$  sorted particles 150  $\mu g/mL$  ( $n = 20$ ),  $PS_{43}$  15  $\mu g/mL$  ( $n = 103$ ),  $PS_{43}$  150  $\mu g/mL$  ( $n = 107$ ),  $PS_{86}$  15  $\mu g/mL$  ( $n = 71$ ),  $PS_{86}$  150  $\mu g/mL$  ( $n = 71$ ),  $PS_{130}$  15  $\mu g/mL$  ( $n = 72$ ),  $PS_{130}$  150  $\mu g/mL$  ( $n = 102$ ). \* significantly higher compared to control, # significantly higher within MP-treated groups, + significantly higher than all other groups,  $p < 0.05$ . Figure is adapted from Völkl et al. (2022) and modified

No significant influence for 15  $\mu g/mL$  treatments was found. Slight and comparable increases in tail DNA percentage compared to the negative control (14.98 %) for the higher treatment concentration (150  $\mu g/mL$ ) could be observed for  $PS_{2\mu m}$ ,  $PS_{43}$  and  $PS_{86}$  (21.84 %, 18.05 %, 19.55 %).  $PS_{130}$  treated cells showed a significant increase in tail DNA percentage with 33.69 % for the higher concentration. Noticeably, a relatively high deviation was measured. This could be associated with the different amounts of PCI for the respective cells. Cells with a higher PCI rate might show an increased tail DNA compared to cells with few particles, comparable to the findings in 3.3.2 and the PCI-dependent ROS increase. To verify this, cells with a high PCI were sorted via fluorescence single-cell sorting. Only  $PS_{2\mu m, green}$  could be used since the fluorescence of the aged particles was too low for sorting. Indeed, the measurement deviation could be narrowed to the expected upper sector for high PCI, arguing again for a PCI dependency.

Studies regarding the genotoxicity of MP *in vivo* in comparable size ranges are rare. However, when considering nanoplastic, more predictions might be made. Shi et al. (2022) compared the genotoxicity of 80 nm and 2  $\mu m$  PS particles with COOH and  $NH_2$  surface functionalisation [258]. Here, the smaller particles with  $NH_2$  functionalisation showed the highest genotoxicity on A549 (human cancerogenic

lung tissue cells). Paget et al. (2015) compared genotoxic effects for non-functionalised, carboxylated and aminated 50 nm particles [259]. Interestingly, NH<sub>2</sub> functionalisation showed the highest impact as well. Furthermore, the same study showed increased effects for macrophages (THP-1) compared to epithelial cells (Calu-3). Other studies showed increased genotoxicity for fragmented PP and PET particles (100 – 600 nm) on Caco-2 cells (human cancerogenic intestinal epithelial cells) [260] and 50 nm PS particles on human primary lymphocytes [261]. However, other studies showed no increased genotoxicity on Caco-2 cells for 50 – 500 nm PS particles [119,262]. Overall, it can be concluded that smaller particles and specific surface modifications (e.g. NH<sub>2</sub>) induce higher genotoxicity. Again, macrophages seem to be affected more than epithelial cells. These findings are comparable to the results of this work. The particle fraction of PS<sub>130</sub> includes significantly smaller fragments than the other fractions, which can contribute to the observed genotoxicity. Furthermore, the surface chemistry of PS<sub>130</sub> is the most affected, adding to the genotoxic potential.

The level of oxidative stress of the aged particles was evaluated subsequently. A similar analysis strategy as in 3.3.2 was applied using the ROS amount of an entire cell population (Figure 24A) and a gated fraction with high PCI (Figure 24B). Here, the gated PCI fraction was compared to a fraction with no PCI in the same sample, corresponding to the ROS intracellular background in the same sample.

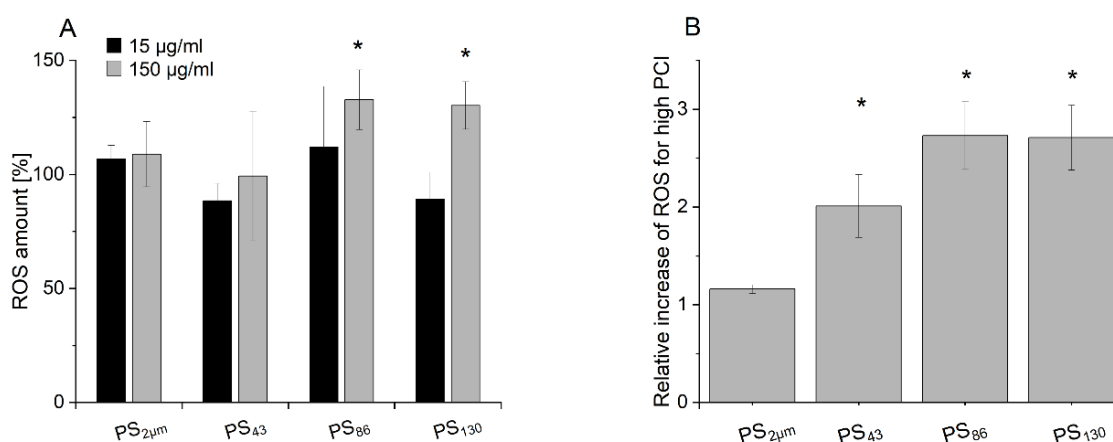


**Figure 24 Level of oxidative stress for ImKC treated with aged particles**

A: Shown is the ROS amount of the whole cell population. Quantity was normalised to a negative control without MP. \* significantly higher within concentration and treatment groups,  $p < 0.05$ . B: Shown is the fold increase of ROS amount in the subpopulation of cells with high PCI (see Figure 13) compared to cells without PCI in the same sample for the high microplastic concentration. \* significantly higher compared to PS<sub>2µm</sub>,  $p < 0.05$ ,  $n = 3$ . Figure is adapted from Völkl et al. (2022) and modified

While no significant increase in ROS could be observed for PS<sub>2µm</sub> and PS<sub>43</sub>, in the case of PS<sub>86</sub> and PS<sub>130</sub>, a significant 1.3 - fold increase could be observed for the high-concentration treatment. Similar to 3.3.2, the ROS amount proved to be dependent on the PCI, with an additional ageing-dependent ROS increase. When gating only cells with high PCI, PS<sub>43</sub> already showed a 2 - fold increase in ROS. PS<sub>86</sub> and PS<sub>130</sub> induced even higher oxidative stress with a 2.7 - fold increase compared to cells without PCI. This is comparable with the literature as well. E.g., Zhu et al. showed an increased ROS amount for phenol-



formaldehyde particles with a translated ageing time of 18 and 37 days in lung epithelial cells (A549) <sup>[111]</sup>. As mentioned above, especially reactive groups on the surface of microparticles might induce ROS accumulation. During the ageing process, photooxidation reactions occur at the surface due to the UV-irradiation. In this process, polymers undergo chemical chain scission or O<sub>2</sub>/H<sub>2</sub>O addition, forming radicals on the surface <sup>[110,263]</sup>. This time-dependent formation of groups like carboxylic acids, peroxides or ketones was previously shown for weathered particles in the same ageing model <sup>[6]</sup>. This can explain the linear increase of ROS from PS<sub>2µm</sub> to PS<sub>86</sub>. The observed plateau for PS<sub>130</sub> weathered MP can be associated with other mechanisms inside the cell. First, only the intracellular ROS content of cells was measured by the method used (i.e., displaying an intact cell membrane). In the case of PS<sub>130</sub>, a loss in membrane integrity was already shown by the LDH assay. ROS loss during the experiment can, therefore, not be excluded. In return, high ROS amounts can also influence the integrity of the cellular membrane <sup>[264,265]</sup>. Both factors interact, resulting in the observed result. Furthermore, an increased amount of ROS influences other biological pathways, e.g. cross-reactions with mitochondria, nucleophilic reactions with biomacromolecules, biomembranes or the cytoskeleton and toxic reactions towards the DNA <sup>[265–267]</sup>. ROS can lead to mitochondrial dysfunction <sup>[190,245,268]</sup>, which is contributing to reduced metabolic activity. Oxidative stress is finally known to contribute to DNA damage <sup>[87,269]</sup>. The observed increased genotoxic damage can therefore be associated with increased ROS. These findings conclude that the increased amount of ROS is also highly contributing to the observed effects of other assays and another highly important cytotoxicity mechanism.

Finally, the inflammatory response was measured. Inflammation in macrophages is usually triggered by the uptake of a foreign matter <sup>[137]</sup> or cell-cell communication by the secretion of cytokines <sup>[270]</sup>, like, e.g. TNF-α as one of the main cytokines involved in the inflammatory response <sup>[138]</sup>. Therefore, an ELISA was conducted to measure the amount of released TNF-α (Figure 25).

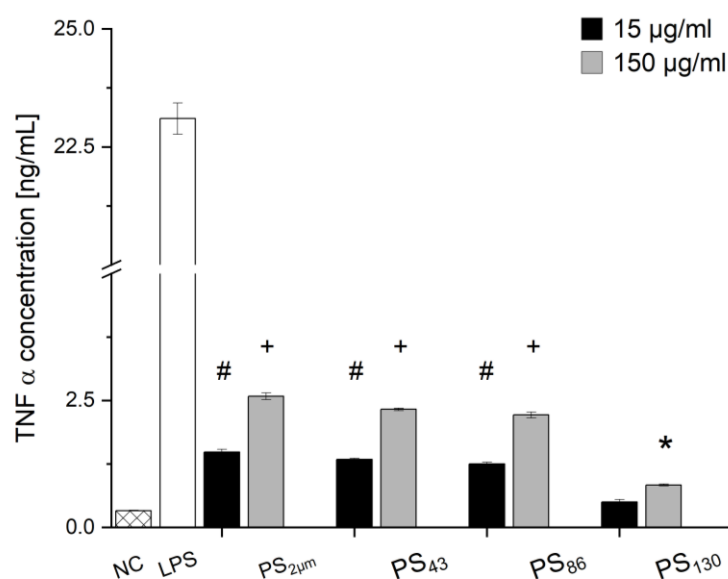


**Figure 25 TNF-α concentration measured by ELISA after treatment with aged particles**

Data represents the TNFα concentration in the supernatant. Cells without any treatment acted as negative control (NC). LPS (2.5 µg/mL) was used as positive control. Data represent mean ± SD, n = 3 biological replicates. \* significantly higher compared to control, # significantly higher than PS<sub>130</sub>, + significantly higher within a treatment group, p < 0.05. n = 3. Figure is adapted from Völkl et al. (2022) and modified

Control cells showed the expected amount of secreted TNF-α (0.35 ng/mL) from the literature (≈ 0.25 ng/mL) [53]. Cells treated with MPP showed a significantly increased TNF-α level. In contrast to the previous assays, though, the level of secreted TNF-α was the highest for PS<sub>2µm</sub> (2.58 ng/mL). Both PS<sub>43</sub> and PS<sub>86</sub> showed comparable but slightly lower TNF-α levels (2.33 and 2.2 ng/mL, respectively). Treatment with PS<sub>130</sub> showed the lowest induction of TNF-α (0.84 ng/mL). At first glimpse, these data seem contradictory to the previous assays, all demonstrating induced cytotoxicity for a longer ageing time. However, various assumptions can be made to explain this finding. First, cells with damaged cell membranes or otherwise weakened biological mechanisms up to the extent of necrosis or apoptosis due to the treatment with PS<sub>130</sub> might not be able to produce TNF-α anymore, hence reducing the accumulation of TNF-α. Additionally, phagocytosis is an important factor in the TNF-α cascade [271,272]. Due to the differing morphology, the uptake mechanism probably differs for the longer-aged particles. The smaller and more reactive fragments from PS<sub>130</sub> might enter the cells via non-biological pathways like piercing the plasma membrane due to their sharp edges, resulting in a lower secretion of TNF-α compared to the morphologically similar PS<sub>2µm</sub>, PS<sub>43</sub> and PS<sub>86</sub>. Choi et al. found a similar explanation for increased TNF-α levels in human mast cells after the treatment with pristine PE particles compared to mechanically fragmented and rougher particles, supporting the hypothesis from this study [257].

In order to interpret the results of the preceding assays on a higher level, a transcriptome analysis was performed. The analysis was limited to PS<sub>2µm</sub> and PS<sub>130</sub> with 150 µg/mL since the most significant effects were measured for these parameters. Compared to an untreated control population, PS<sub>2µm</sub>, as

well as PS<sub>130</sub>, showed significant differences when comparing the transcriptome analysis for differently-expressed (DE) genes, which is represented by a multidimensional scaling (MDS) plot (Figure 26).

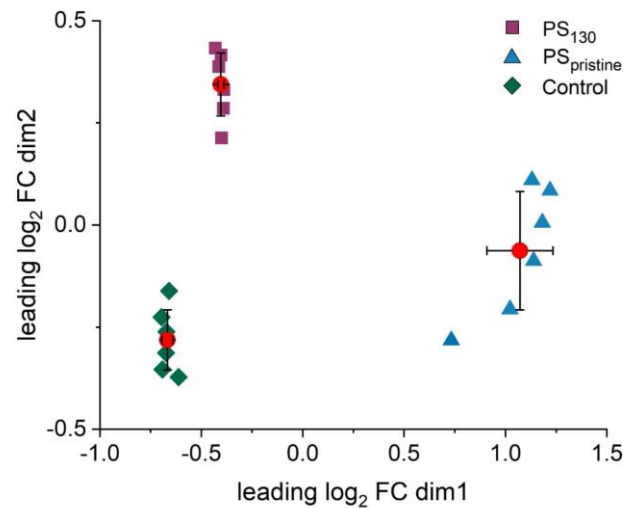


**Figure 26 Different transcriptomic impacts of PS130 and PSpristine**

A: Multidimensional scaling plot based on the log<sub>2</sub> fold changes (FoC) between control, PS<sub>2μm</sub> and PS<sub>130</sub> samples. The axes of the MDS plot represent dimensional reductions of gene expression, visualising the variability of the transcriptional changes for a given treatment. Figure is adapted from Völkl et al. (2022) and modified

The axes of the MDS plot hereby visualise the variability of the transcriptional changes for a given treatment. While replicates show only slight deviation, ensuring a high significance, the significant difference between the treatment groups argues for a different transcriptomic response to the particles. This can also be seen when comparing the number of induced (Up) and repressed (Down) genes (full data set see 8.1). Comparing PS<sub>2μm</sub> to the control cells, 251 upregulated and 126 downregulated ones were found (log<sub>2</sub>fold change > ± 1, false discovery rate (FDR) < 0.05). A treatment with PS<sub>130</sub> only induced 39 genes and repressed 15 (log<sub>2</sub>fold change > ± 1, FDR < 0.05). Of these regulated genes, only 20 upregulated and eight repressed ones were found for both treatments (≈ 50 %), again arguing for a different cellular response to both particle types. Table 11 and Table 12 show the ten most up- and downregulated genes for the respective treatments. Here, for both treatments, an immune-related response can be found. PS<sub>2μm</sub> notates five up- and five downregulated genes associated with the immune response, indicating a bi-directional regulation. PS<sub>130</sub>, on the other hand, showed exclusively downregulated genes (4) linked with the immune response. Furthermore, the fold change value indicates a higher reaction to PS<sub>2μm</sub>, with about four times higher up- and two times higher downregulation.

**Table 11 Top 10 up and downregulated differentially expressed genes for  $PS_{2\mu m}$  vs control**

	Gene Name	Gene Annotation	Function	Log fold change
<b><math>PS_{2\mu m}</math> vs Control - Top 10 UP</b>	Dok7	docking protein 7	formation of neuromuscular synapses	8.676
	Csf3	colony-stimulating factor 3	Cytokine factor	7.611
	Nos2	nitric oxide synthase 2	Immunity reaction against viruses, bacteria, fungi and parasites	7.598
	Il7r	interleukin 7 receptor	Development of immune cells	7.544
	Serpib9b	serine (or cysteine) peptidase inhibitor	coagulation, fibrinolysis, complement fixation, matrix remodelling, and apoptosis	7.528
	Sstr5	somatostatin receptor 5	inhibits the release of many hormones and other secretory proteins	7.505
	Pgf	placental growth factor	Placental growth factor	7.416
	Efcab6	EF-hand calcium-binding domain 6	recruits histone-deacetylase complexes to repress transcription activity of androgen receptor	7.340
	Ccl22	chemokine (C-C motif) ligand 22	Inflammatory ligand	6.809
	PDPN	podoplanin	Antigen receptor	6.573
<b><math>PS_{2\mu m}</math> vs. Control - Top 10 DOWN</b>	Bmf	BCL2 modifying factor	Apoptotic regulator	- 2.070
	Cib2	calcium and integrin-binding family member 2	Important in intracellular calcium homeostasis by decreasing ATP-induced calcium release	- 2.079
	Asb10	ankyrin repeat and SOCS box-containing 10	suppressor of cytokine signalling (SOCS) proteins	- 2.124
	Hp	haptoglobin	Haptoglobin functions to bind the free plasma haemoglobin, allowing degradative enzymes to gain access to the haemoglobin	- 2.179
	BTLA	B and T lymphocyte-associated	inhibition and activation capacities of the immune system	- 2.217
	Slco2b1	Solute carrier organic anion transporter family, member 2b1	Registered in a group of membrane transport proteins	- 2.223
	Vsig4	V-set and immunoglobulin domain containing 4	inhibits proinflammatory macrophage activation	- 2.478
	Clec4b1	C-type lectin domain family 4, member b1	recognition receptor (PRR) of the innate immune system	- 3.134
	Cd24a	CD24a antigen	wide range of downstream signalling networks and crucial for neural development	- 3.332
	Ccl24	Chemokine (C-C motif) ligand 24	Inflammatory ligand	- 3.504

Table is adapted from Völkl et al. (2022) and modified

**Table 12 Top 10 up and downregulated differentially expressed genes for PS<sub>130</sub> vs control**

	Gene Name	Gene Annotation	Function	Log fold change
<b>PS<sub>130</sub> vs Control - Top 10 UP</b>	5_8S_rRNA	5.8S ribosomal RNA	Protein translation	2.288
	Mmp12	Matrix metalloproteinase 12	breakdown of extracellular matrix; tissue remodelling	2.171
	PDE6B	Phosphodiesterase 6B, cGMP, rod receptor, beta polypeptide	transmission and amplification of visual signals	1.737
	Fabp4	Fatty acid-binding protein 4,	fatty acid uptake, transport, and metabolism	1.698
	Tlcd4	TLC domain containing 4	lipid trafficking, metabolism	1.580
	Chst11	Carbohydrate sulfotransferase 11	transfer of sulphate to position 4 of the N-acetyl-galactosamine	1.513
	Cdk8	Cyclin-dependent kinase 8	regulate transcription	1.495
	H1f4	H1.4 linker histone, cluster member	nucleosome structure of the chromosomal fibre	1.453
	Mir6236	MicroRNA 6236	affecting both the stability and translation of mRNAs	1.434
	Gm48099	Predicted gene, 48099	-	1.410
<b>PS<sub>130</sub> vs Control - Top 10 DOWN</b>	Rtp4	Receptor transporter protein 4	chaperone protein which facilitates trafficking and functional cell surface expression	- 1.300
	BMF	BCL2 modifying factor	anti- or pro-apoptotic regulators	- 1.365
	Slco2b1	Solute carrier organic anion transporter family, member 2b1	group of membrane transport proteins	- 1.370
	Serpinf1	Serine (or cysteine) peptidase inhibitor, clade F, member 1	antiangiogenic, antitumorigenic, apoptosis of endothelial cells	- 1.385
	Tm4sf5	Transmembrane 4 superfamily member 5	cell-surface protein	- 1.431
	IFI44L	Interferon-induced protein 44 like	decreasing IFI44L expression impairs virus production, IFI44L expression negatively modulates the antiviral state	- 1.450
	Apol9a	Apolipoprotein L 9a	interferon-stimulated gene (ISG) that has antiviral activity	- 1.455
	Tgfb1	Transforming growth factor, beta-induced	extracellular matrix proteins modulating cell adhesion	- 1.460
	Apol9b	Apolipoprotein L 9b	interferon-stimulated gene (ISG) that has antiviral activity	- 1.496
	Ccl24	Chemokine (C-C motif) ligand 24	Inflammatory ligand	- 1.890

Table is adapted from Völkl et al. (2022) and modified

A gene set enrichment analysis (GSEA) was performed using the gene ontology (GO) annotations of the mouse genome to get a better correlation to biological effects. The GSEA identifies classes of genes, clusters them and annotates them to the respective GO to identify superordinate groups of genes. This analysis allows to point out the effects of the cells toward a specific biological reaction more effectively. To stress this focus even more, the analysis was restricted to the most specific GOs

(FDR < 0.01). When comparing PS<sub>2μm</sub> and PS<sub>130</sub> against each other, most GO annotations were treatment-specific again, as shown in a Venn diagram (Figure 27). Only 6.1% (for up-regulated) and 7.8% for (down-regulated) of the GOs were overlapping.

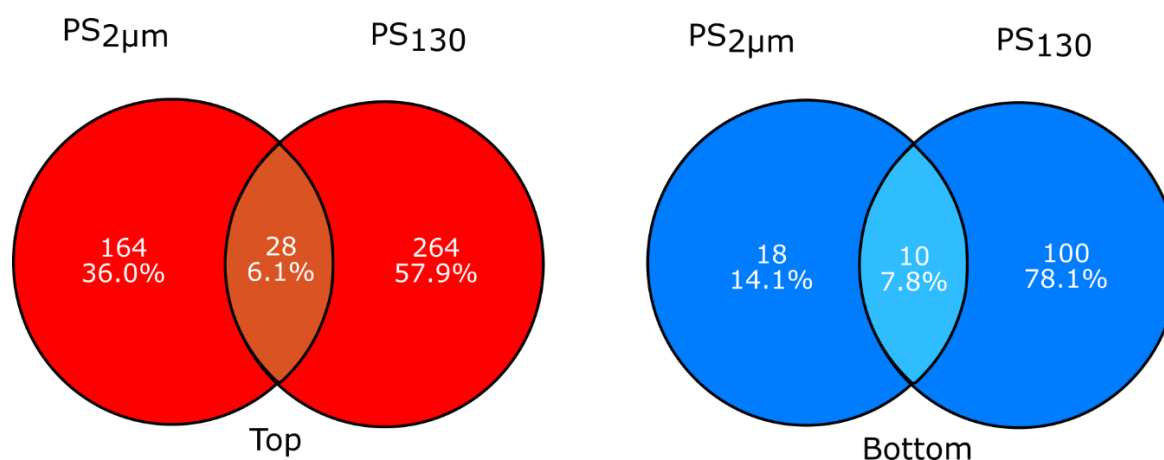


**Figure 27 Venn diagram comparing the most specific GOs**

GOs were identified by GSEA for PS<sub>pristine</sub> and PS<sub>130</sub>, respectively, against the control. Red: upregulated genes; blue: downregulated genes. Figure is adapted from Völkl et al. (2022) and modified

By using the hierarchical structure of the GO database, the top 50 upregulated and top 50 downregulated GO terms for PS<sub>2μm</sub> and PS<sub>130</sub> were reduced to the most specific terms. Therefore, the normalised enrichment score (NES) was used. The higher the value of the NES, the more significant the specific GO. The 36 remaining GOs with an NES > 2.000 were sorted manually to superordinate, unifying terms (Table 13). The pattern of a distinct response can again be followed. 20 out of the 36 terms were unique for the respective treatment group. Furthermore, parental GO terms like “Uptake” and “Immune response” were more pronounced for PS<sub>2μm</sub>, while PS<sub>130</sub> affected “Cellular respiration” more significantly. Overall, the terms “Cellular respiration” (eleven annotations), “Immune response” (seven annotations) and “Membrane related” (six annotations) were the most affected.

**Table 13 Direct comparison of appearing GOs**

reduced to the most specific ones for PS<sub>2μm</sub> and PS<sub>130</sub> treatment. Boxes highlight upregulated GOs

Parental GO term	Gene Ontology	GO ID [GO-xx]	NES	
			PS <sub>2μm</sub> vs. Control	PS <sub>130</sub> vs. Control
<b>Uptake</b>	early endosome	0005769	2.904	
	vacuole organisation	0007033	2.714	
	nucleotide transport	0006862	- 2.248	
<b>Ribosomes</b>	cytosolic small ribosomal subunit	0022627	- 3.388	- 3.540
	cytosolic large ribosomal subunit	0022625	- 2.963	- 3.764
	structural constituent of ribosome	0003735	- 2.913	- 6.619
<b>Immune response</b>	positive regulation of response to external stimulus	0032103	3.152	
	cellular response to interleukin-1	0071347	2.799	
	regulation of inflammatory response	0050727	- 2.482	- 2.460
	transforming growth factor-beta binding	0050431	- 2.242	
	interleukin-1 production	0032612	- 2.238	
	cellular response to interferon-beta	0035458		- 3.348
	defence response to virus	0051607		- 3.307
<b>Oxygen Level</b>	cellular response to hypoxia	0071456	2.858	2.068
	positive regulation of reactive oxygen species	2000379	- 2.402	
	metabolic process			
<b>Cellular Respiration</b>	mitochondrial respiratory chain complex I	0005747	- 3.174	- 3.658
	proton-transporting V-type ATPase complex	0033176	3.114	2.353
	fatty acid beta-oxidation	0006635	- 2.884	- 2.107
	mitochondrial respiratory chain complex I assembly	0032981	- 2.830	- 3.644
	proton-transporting ATPase activity, rotational mechanism	0046961	2.779	2.017
	glycolytic process	0006096	2.660	
	NADH dehydrogenase (ubiquinone) activity	0008137	- 2.449	- 2.348
	mitochondrial electron transport, NADH to ubiquinone	0006120	- 2.240	- 2.848
	small GTPase binding	0031267	2.030	3.856
	mitochondrial large ribosomal subunit	0005762		- 3.447
	GTPase activator activity	0005096		2.890
<b>Membrane- related</b>	nucleotide transmembrane transporter activity	0015215	- 2.366	
	basement membrane	0005604	- 2.363	
	cell projection membrane	0031253	2.123	2.788
	apical plasma membrane	0016324	2.095	2.878
	focal adhesion	0005925		3.294
	phosphatidylinositol binding	0035091		2.988
<b>Other</b>	positive regulation of peptidyl-serine phosphorylation	0033138	2.671	
	DNA repair	0006281	- 2.230	
	cholesterol biosynthetic process	0006695	2.228	3.123
	ALTERNATE of GO:0140658	0070615		3.054

Table is adapted from Völkl et al. (2022) and modified

The expression of biological effects is often not only regulated by the activation or suppression of individual genes but by complex gene networks or cascades that influence gene regulation. These clusters can be analysed using the Cytoscape plugin ClueGO. Here, involved upregulated GOs were analysed (Figure 28A). Clusters were again specifically found for the respective treatment (Figure 28B). Clusters for PS<sub>2μm</sub> showed increased frequency for inflammatory responses, while PS<sub>130</sub> mainly induced differentiation and a new arrangement of the cell and the cell membrane.

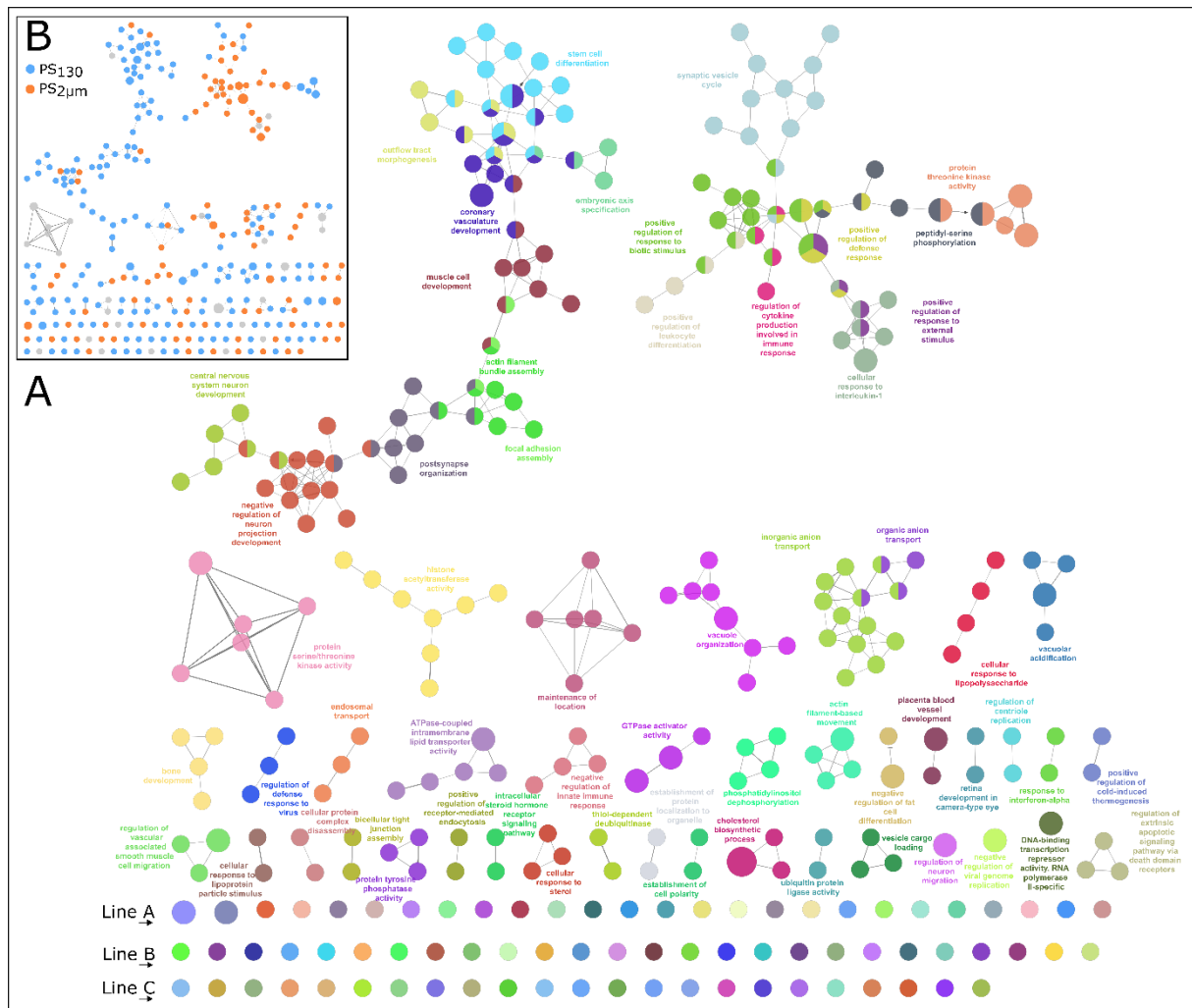


**Figure 28 GO networks visualised by ClueGO**

The display is based on GO by the positive NES (corresponding to induced genes), reduced to most specific GO terms. Network connectivity is based on  $\kappa$ -value  $\geq 0.2$  and shown for GOs with FDR  $\leq 0.05$ . (A) GO group names (same colour) were inferred from connected GO terms by ClueGO. GOs belonging to multiple groups are displayed as circles filled with the respective colours. (B) The respective affiliation of clusters to PS<sub>130</sub> (blue) and PS<sub>2μm</sub> (orange) or unspecific (grey) is shown in the insert. Notations for “Line A, B and C” are shown in Table 14. Figure is adapted from Völkl et al. (2022) and modified



**Table 14 Group annotations for Line A, B and C from Figure 28**

<b>Line A</b>	<b>Line B</b>	<b>Line C</b>
glycolytic process	hematopoietic progenitor cell differentiation	regulation of embryonic development
post-embryonic development	embryonic digit morphogenesis	regulation of shape
negative regulation of protein maturation	positive regulation of leukocyte apoptotic process	G1/S transition of mitotic cell cycle
heterotypic cell-cell adhesion	developmental pigmentation	spleen development
structural constituent of synapse	exopeptidase activity	hair follicle development
Wnt signalling pathway	negative regulation of neuron death	protein folding
positive regulation of protein kinase B signalling	blastocyst formation	cholesterol homeostasis
cellular zinc ion homeostasis	positive regulation of peptidyl-tyrosine phosphorylation	regulation of chromosome aggregation
intestinal absorption	phosphatidic acid biosynthetic process	liver morphogenesis
negative regulation of intrinsic apoptotic signalling pathway	establishment of endothelial barrier	positive regulation of protein localisation to plasma membrane
nuclear import signal receptor activity	positive regulation of organelle assembly	stress granule assembly
phosphatidylinositol phosphate biosynthetic process	cilium assembly	neuroblast proliferation
positive regulation of phospholipase activity	negative regulation of protein localisation	N-terminal protein amino acid modification
cortical actin cytoskeleton organisation	ubiquitin-dependent ERAD pathway	negative regulation I-kappa/NFkB signalling
vascular process in circulatory system	positive regulation of ERBB signalling pathway	negative regulation of Ras protein signal transduction
regulation of smoothened signalling pathway	regulation of multicellular organism growth	negative regulation of cysteine-type endopeptidase activity
response to radiation	developmental maturation	cellular response to hypoxia
response to cAMP	rRNA processing	response to temperature stimulus
intermediate filament cytoskeleton organisation	cerebellar cortex formation	fatty acid biosynthetic process
wound healing, spreading of cells	regulation of cell division	response to temperature stimulus
glucose transmembrane transport	tolerance induction	response to ischemia
positive regulation of DNA-binding transcription factor activity	cytoplasmic microtubule organisation	regulation of early endosome to late endosome transport
gene silencing by miRNA	neuronal stem cell population maintenance	exopeptidase activity
nuclear receptor coactivator activity	adult walking behaviour	binding of sperm to zona pellucida
cellular carbohydrate metabolic process	endoplasmic reticulum organisation	
regulation of binding	iron ion homeostasis	

The annotations in Figure 28 for lines “A”, “B” and “C”, read from left to right, are shown in this table top-down. Table is adapted from Völkl et al. (2022) and modified

Finally, the Kyoto Encyclopedia of Genes and Genomes (KEGG) pathway database (mouse-specific version of ClueGO) was used to analyse to stress the connection of the genes with biological effects even more. Biomacromolecules are often induced by pathways, e.g. TNF- $\alpha$ . If various genes in a pathway are enriched, the likeliness of this pathway being affected is naturally higher. Therefore, induced genes were used to identify enriched KEGG pathways. 35 KEGG significant affected pathways could be identified from 251 PS<sub>2 $\mu$ m</sub> induced genes. The ten most significant (based on FDR) pathways are shown in Figure 29.

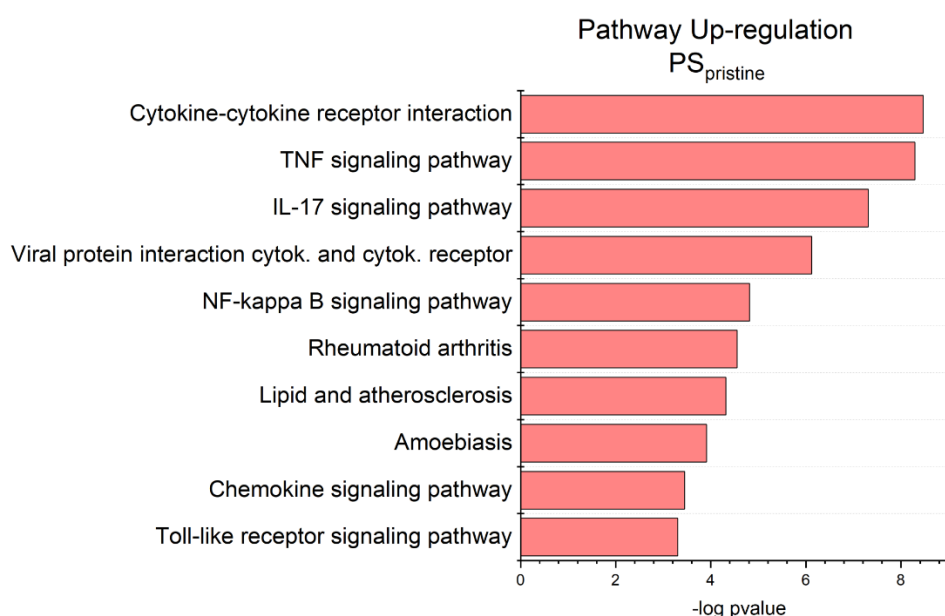


**Figure 29** Pathway analysis by KEGG for the upregulated genes of PS<sub>2 $\mu$ m</sub>

Shown are the ten most significantly upregulated pathways predicted by KEGG analysis with Cytoscape ClueGO. Figure is adapted from Völkl et al. (2022) and modified

Seven out of ten, among them the five most significant pathways, are allocated to known inflammation-related pathways (e.g., “cytokine-cytokine receptor, TNF signalling, IL-17 signalling, Viral protein interaction cytokine and cytokine receptor and NF- $\kappa$ B signalling”) [85,273–275]. Interestingly, no pathways were significantly affected when using the same parameters, neither for downregulated genes of PS<sub>2 $\mu$ m</sub> treatments nor for up- and downregulated genes in PS<sub>130</sub> experiments. This is probably associated with the considerably smaller number of identified genes in these cases (see 8.1).

The transcriptome analysis allows a cautious linking of the observed biological and cellular responses with potential molecular pathways. A specific response to the respective particle treatment could also be found on the transcriptomic level. Different GOs, clusters and pathways are assigned to detected effects measured by the assays. GOs associated with “Cellular respiration” and “ribosome”, i.e., genes relevant for cellular metabolism and translation, are significantly more affected by PS<sub>130</sub>. This could be

connected with the finding in the MTT assay, which is an image of the metabolic activity and, eventually, the cellular respiration. Cluster analysis further revealed mainly differentiation and arrangement of the cell and the cell membrane mechanism. The LDH assay showed reduced membrane integrity when treated with PS<sub>130</sub>. The reaction on the transcriptomic level might be associated with repair- or restructuring attempts of a damaged membrane. PS<sub>2μm</sub> showed a lower reaction in the mentioned GOs or clusters, comparable to the assay results. On the other hand, especially genes associated with “*uptake*” are increased for PS<sub>2μm</sub>, supporting the hypothesis that more pristine MP enter the cells via phagocytosis compared to aged ones. The uptake and phagocytosis of MPP by cells is greatly impacted by the nature of the protein corona surrounding it [64,246]. It can therefore be theorised that the weathering process, in addition to altering the morphological characteristics, also alters the particles' surface topology, which results in modifications to the protein corona composition [276]. Furthermore, PS<sub>2μm</sub> treatment revealed a dominant, pathogen-driven response, which would indicate that the cells confuse PS<sub>2μm</sub> as some form of a biological system. The pathway analysis using the KEGG database identified various signalling pathways associated with inflammatory responses in cells exposed to PS<sub>2μm</sub>. Especially the TNF-α signalling pathway must be noted, which was consistent with the observed accumulation of this cytokine in the cell culture medium analysed by ELISA. Literature has also reported similar inflammatory pathways following exposure to 5 μm PS-MPP and < 2.5 μm environmental particulate matter [85,274].

To conclude, a coherent, ageing-time-dependent cytotoxic effect of PS<sub>aged</sub> on ImKC cells could be observed, indicating an increased toxic potential for PS<sub>aged</sub> compared to PS<sub>2μm</sub>. Especially, the physical aspect (i.e., morphology) of PS<sub>aged</sub> and the formation of intracellular ROS due to the more reactive, weathered particles are hereby assumed to contribute to the high toxicity. Pristine particles, on the other hand, bear a higher inflammatory potential. Furthermore, pristine spherical particles are more likely to recruit the endocytic and phagocytic pathways, whereas irregular-shaped structures use a non-biological pathway (i.e., destabilisation of the plasma membrane). When comparing the transcriptomic data, major differences between PS<sub>aged</sub> and PS<sub>2μm</sub> were observed, giving first insights at a molecular level. The transcriptomic data could be associated well with results from the cell-based assays. The work demonstrated for the first time that the effects of pristine laboratory particles and weathered MPP induce different cellular responses on different biological levels. The usage of aged particles is therefore not only necessary to converge to more realistic experiments, but different results for different ageing methods or the ageing of various polymers are expected, which must be considered when interpreting data sets.

### 3.3.7. Influence of paint microparticle fractions

The final convergence to environmentally relevant particles is the actual usage of environmental particles. Therefore, two standard wall and ceiling paints (Paint 1 and Paint 2) have been used since primary micro- and nanoplastic is introduced at high rates into these materials, proving them responsible for a high amount of microplastic pollution worldwide<sup>[277,278]</sup>. Particle extraction from both paints was prepared and characterised by Ann-Kathrin Müller, according to Müller et al.<sup>[117]</sup>. Briefly, paint dispersions were centrifuged, washed and partitioned into a solid particle fraction and a supernatant. While the supernatant of Paint 1 consists of polyacrylate with hydroxyl functionalities and particle leftovers with a size of  $242 \pm 59$  nm, *Paint 2* supernatant only consisted of an added copolymer in dissolved form. The solid phase of *Paint 1* was a mixture of TiO<sub>2</sub> and silicon dioxide particles with a size of  $6.8 \pm 1.1$  µm. *Paint 2* showed CaCO<sub>3</sub> composition in a highly heterogeneous size distribution between 150 nm to 10 µm. The ζ-potential of the solid phase particles was measured to be - 37 mV and - 30 mV, respectively, for *Paint 1* and *Paint 2*.

The cytotoxicity of these particles was subsequently tested with L929 cells, a known standard cell line in toxicity testing, by conducting an MTT assay with the supernatant and the solid phase of *Paint 1* and *Paint 2* (Figure 30).

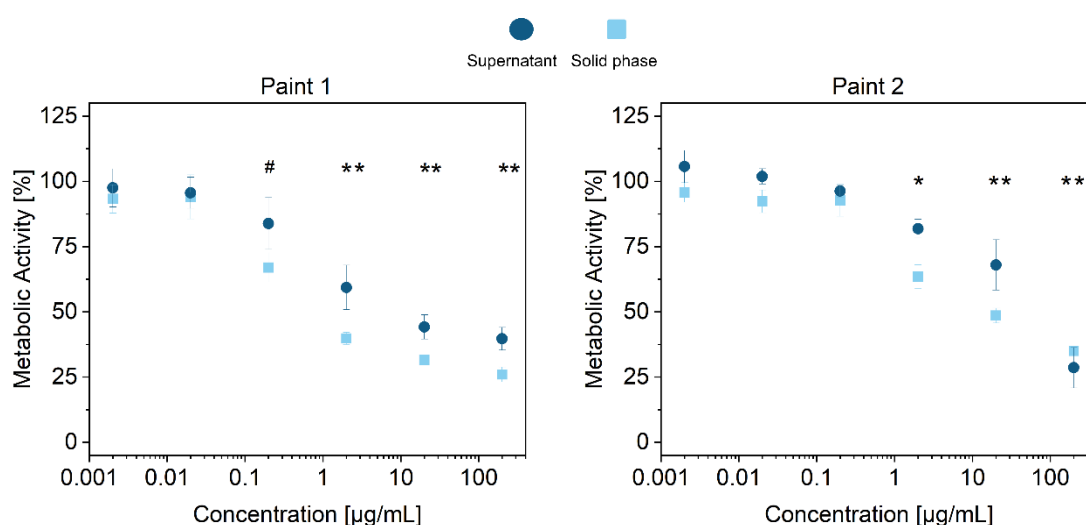


**Figure 30 MTT Assay of L929 cell line and the respective paint fractions**

Cells were exposed for 24 h to Paint 1 and Paint 2. Data points represent mean  $\pm$  SD,  $n = 3$  biological replicates. Significance level: # only the solid phase is significant,  $p < 0.05$ ; \* solid phase and supernatant is significantly higher than the negative control  $* = p < 0.05$ ,  $** = p < 0.01$ . Figure is adapted from Müller et al. (2022) and modified

A significant metabolic activity reduction could be observed for all analysed fractions. A reduction below 50 % metabolic activity appeared at lower concentrations for *Paint 1* (2 µg/mL for the solid phase, 20 µg/mL for supernatant) compared to *Paint 2* (20 µg/mL for the solid phase, 200 µg/mL for the supernatant). Interestingly, these concentrations were lower compared to analysed pristine PS beads (3.3.2). Various reasons can be named for this finding. Examining the SEM images of the different

fractions (Figure S7) <sup>[117]</sup>, the particulate matter was highly polydisperse compared to the bead-shaped PS particles. Morphology proved an important factor (3.3.6), with irregularly shaped particles being more toxic than spherical ones. Further, the polydispersity of the fractions might contribute to the increased cytotoxicity <sup>[35]</sup>. Additives added to the paints can accumulate on the particles' surface and contribute to cytotoxicity (3.3.4). Finally, it must be noted that the here used cell line (L929) is another compared to previously used ones, which might also affect the results.

The differences between *Paint 1* and *Paint 2* can be ascribed to their different composition. CaCO<sub>3</sub>, often used as a component in drug-delivery systems <sup>[279]</sup>, is known to possess low cytotoxicity. For TiO<sub>2</sub> nanoparticles and polyacrylate, concentrations of 100 µg/mL <sup>[280]</sup> and 60 µg/mL <sup>[281]</sup> showed toxic effects on L929 cells. The more pronounced cytotoxicity here might be ascribed to the previously mentioned morphologic aspect, the high polydispersity or possible additives. As a further comparison in Müller et al. (2022), the influence of the paint-derived particles was tested on *Daphnia magna* by AG Laforsch. This organism was mainly affected by the dissolved polymer fraction (*Paint 2* supernatant), with only a lower decreased cell vitality induced by the other fractions. Furthermore, most particles were found to accumulate in the gut of the individuals, which might develop long-term effects. Interestingly, the most harmful fraction for *D. magna* was the least harmful for the cells. This shows that the cell phenotype and the model organism are highly important for risk assessment, and results can be even counterintuitive.

To conclude, higher cytotoxicity for environmentally exposed particles could be shown compared to pristine PS particles. It could further be shown that different dispersion paints induced varying responses to different organisms, fortifying the multi-parametrical risk of MP. It is therefore highly recommended to increase the effort in studying environmentally relevant particles.

### 3.3.8. Summary and conclusion

In summary, the hypothesis of the multiparametric problem of MP on mammalian cells (see Scheme 3) can be confirmed. The cell phenotype proved to be of high relevance. Both used epithelial cell lines did not show high interaction rates with MPP. As a consequence, the effects of MPP on these cells were only small. Macrophages, on the other hand, interacted strongly with specific MPP. For all tested parameters, macrophages showed more distinct cellular effects. Especially the uptake probability could be expected due to the natural purpose of the different phenotypes (barrier vs scavenger cells). Further, it has to be noted that within the same phenotype (ImKC vs J774A.1), significant differences occurred. ImKC proved here to be more sensitive against MPP compared to J774A.1.

Not less important than the cell phenotype are the particle properties. As noted above, effects are highly correlated with the interaction of MPP. Particle characteristics influencing the interaction were, therefore, of specific interest. These interaction or uptake rates proved to be size-, surface charge- and protein-corona-dependent. The highest effects could be observed for parameters promoting the PCI or uptake. Furthermore, monomer residues could be identified as contributing factor to cytotoxicity. The selection of the polymer did not seem to influence the effects of the microparticles highly, indicating that effects are more induced by the particles themselves than the polymer used. However, this statement can only be made for inert polymer beads used in the laboratory since no artificially aged particles other than PS were available.

This ageing of the particles proved to be the most affecting factor analysed. While effects on cytotoxicity, genotoxicity and oxidative stress were significantly increased for aged particles, the immune response compared to pristine particles was lower. This difference in biological reaction could be shown on various assays (MTT, LDH, ROS, COMET, ELISA) and confirmed by RNA sequencing. As influencing factors, the morphology of the aged particles (e.g. sharper edges) and an increased reactivity on the particle's surface due to the UV-irradiation during the artificial weathering could be identified. Environmentally relevant paint particle fractions also showed higher cytotoxicity than comparable pristine beads.

Concluding the data, pristine MPP only provokes toxic effects in comparably high concentrations. Significant effects were not found for concentrations below 250 µg/mL, which lies above environmental concentrations. This might implicate from the laboratory data that microplastic is not as harmful as suspected. However, some studies estimating the environmental pollution report difficulties detecting particles < 5 µm<sup>[199]</sup>. Especially this particle size proved to be of greater concern than larger ones in this study. Furthermore, accumulation and a lack of excretion might lead to higher concentrations in organisms than in the environment. This could be shown by Lee et al., who estimated

a microplastic concentration in human blood of 99.4 µg/mL/day <sup>[282]</sup> or Leslie et al., who measured a concentration of 1.6 µg/mL microplastics in human blood samples <sup>[29]</sup>. Furthermore, mostly pristine, spherical particles were used in most comparable studies in the literature. This work, though, could show that environmental ageing can significantly increase the toxicity of particles. 15 µg/mL of the aged particles already showed acute toxicity, decreasing a critical concentration of pristine particles tenfold. This concentration range is already found in environmental or organismic concentrations, stressing the importance of further expanding methods and particles used for the risk assessment of microplastic particles.

### 3.4. Excretion behaviour of ingested particles

Finally, after ingestion, distribution and effect activation, the disposition or excretion of the particles might be the final step in their journey through the cell (Scheme 15). Especially for the accumulation or distribution *in vivo*, it might be an important consideration if particles remain inside the cells or are actively excreted.

To establish an analysis method for a possible accumulation, ImKC cells were first treated for 24 h with PS<sub>3μm, red</sub>. Subsequently, they were additionally challenged with PS<sub>3μm, green</sub> (Figure 31). The differently used fluorescence wavelength (green Ex/Em: 441/486 nm, red Ex/Em 491/554 nm) were used since they were easy to discriminate by FC.

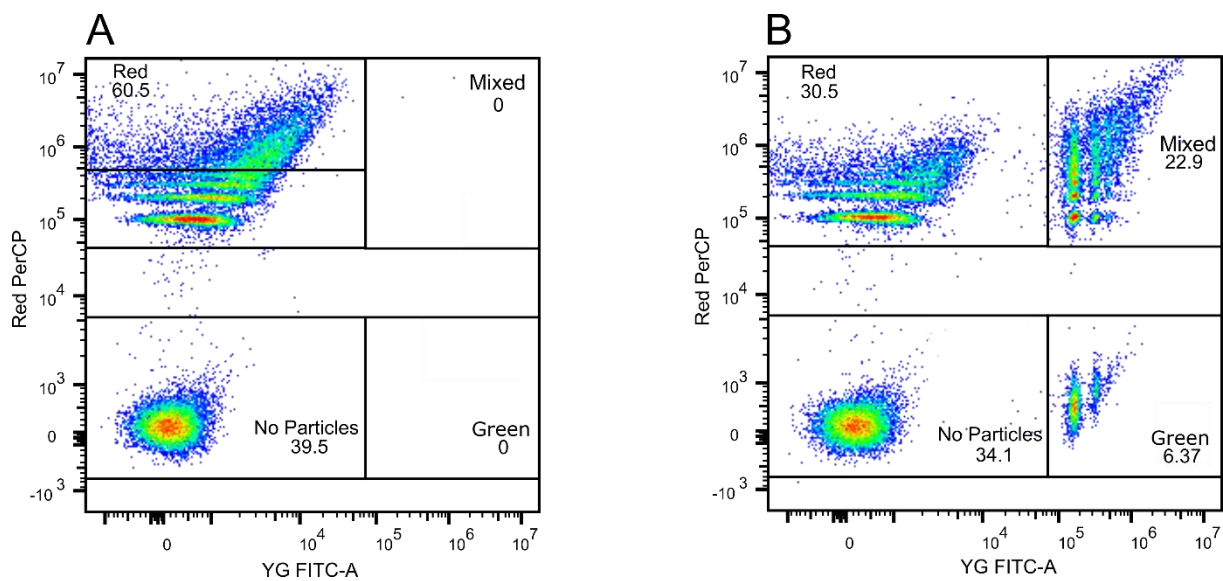


**Figure 31 Uptake of particles from cells already challenged with particles**

A: Shown are ImKC cells treated with 150 μg/mL PS<sub>3μm, red</sub> for 24 h. B: Shown are the cells from A, challenged additionally with 15 μg/mL PS<sub>3μm, green</sub> for 24 h. Measurement was performed by FC, according to 3.1.1.

Within 24 h, both particles could be detected via FC for a high amount of cells, proving that cells challenged with particles are able to further ingest new particles, enabling an accumulation of particles. This raises the question if particles are stored inside the cells or are actively excreted over time.

Two batches of cells were therefore prepared simultaneously. One batch was incubated with PS<sub>3μm, green</sub>, while another batch was incubated with PS<sub>3μm, red</sub>. Particles were incubated for 24 h, followed by extensive washing with DPBS to remove unbound particles from the batch. Afterwards, both batches were pooled and incubated for a further 72 h. In case of excretion of the particles, an increasing cell population with both colours should arise since excreted particles are likely to be re-ingested by the macrophages (Figure 32 and Figure 33).



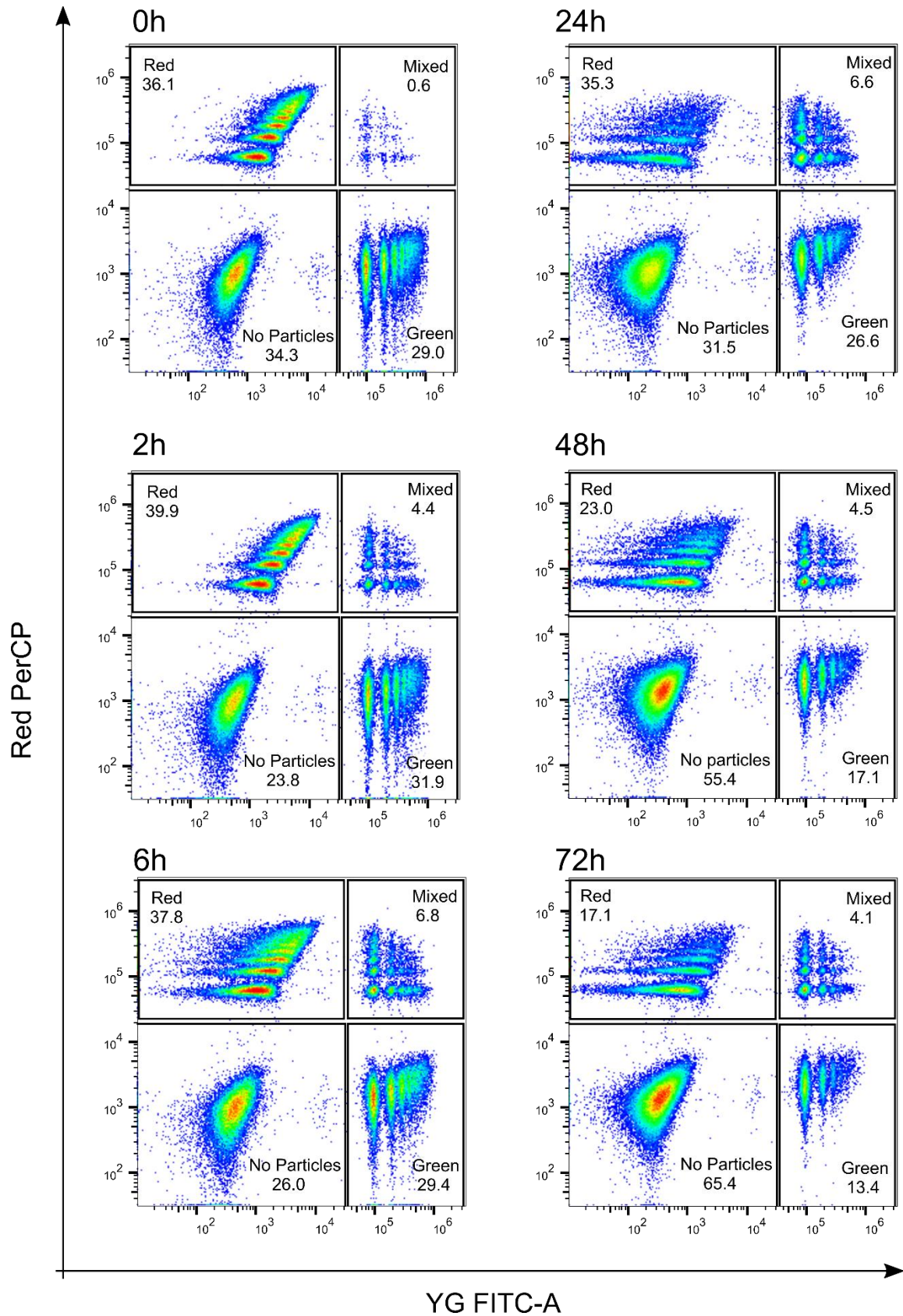


**Figure 32** Detection of particle release over time for J774A.1 cells

One batch of cells was incubated with  $PS_{3\mu m, green}$ ; another batch was incubated with  $PS_{3\mu m, red}$  for 24 h incubation. 150,000 cells were seeded per well, and 25  $\mu g/mL$  particles/well were added. Cells were then pooled (0 h), and the particle distribution was measured for 72 h via flow cytometry. "Red" gate = only  $PS_{3\mu m, red}$ , "Green" gate = only  $PS_{3\mu m, green}$ , "Mixed" gate = at least one particle of  $PS_{3\mu m, red}$  and  $PS_{3\mu m, green}$ .

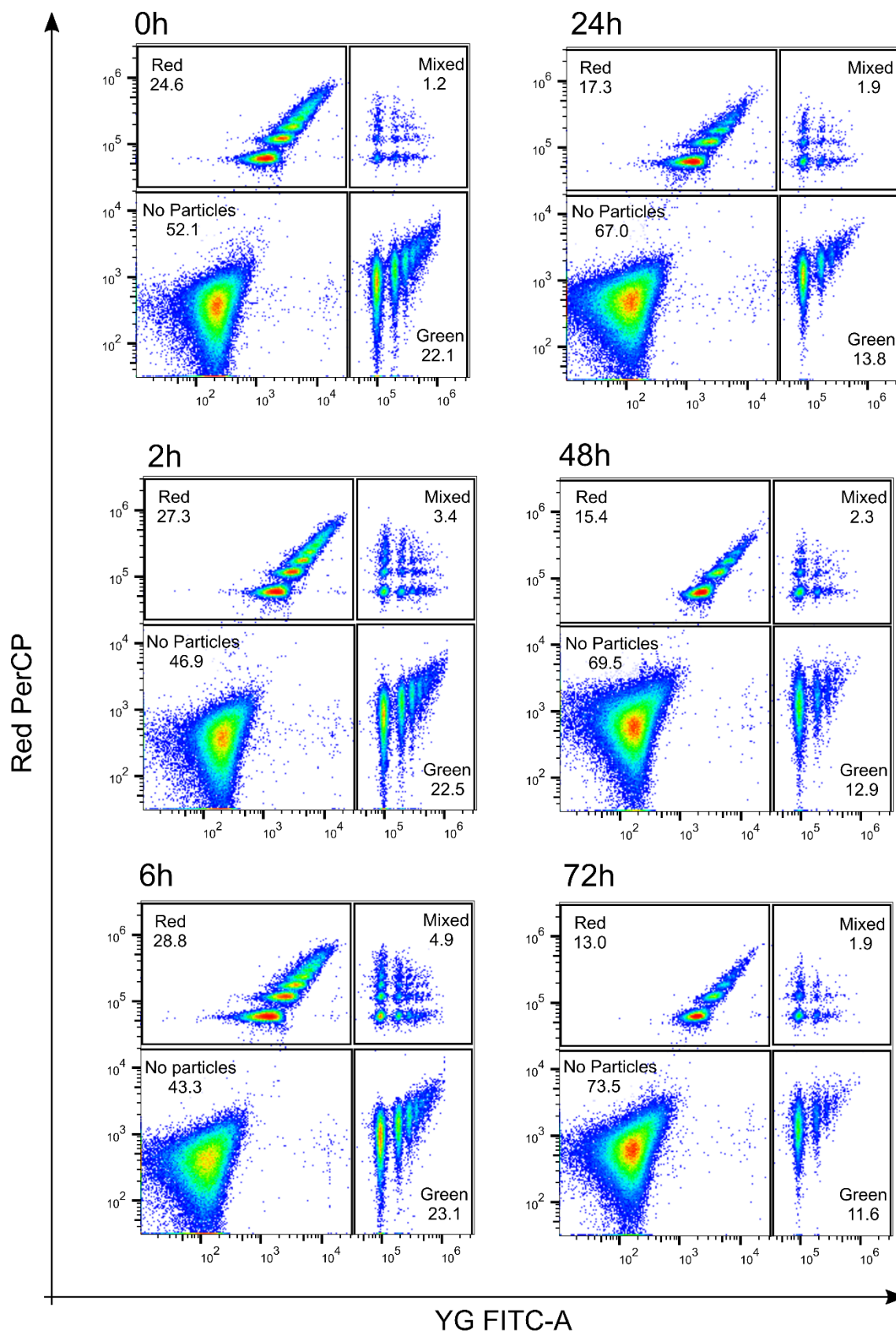


**Figure 33** Detection of particle release over time for ImKC cells

One batch of cells was incubated with  $PS_{3\mu m, green}$ ; another batch was incubated with  $PS_{3\mu m, red}$  for 24 h incubation. 150,000 cells were seeded per well, and 25  $\mu g/mL$  particles/well were added. Cells were then pooled (0 h), and the particle distribution was measured for 72 h via flow cytometry. "Red" gate = only  $PS_{3\mu m, red}$ , "Green" gate = only  $PS_{3\mu m, green}$ , "Mixed" gate = at least one particle of  $PS_{3\mu m, red}$  and  $PS_{3\mu m, green}$ .

A small population of mixed cells could be observed for both cell lines. This population increased for the first 6 h (< 6.8 % for J774.1, < 4.9 % for ImKC) but did not expand further. It could be assumed that despite the intensive washing, some particles were not washed off or that some particle-cell interactions were only weak and separated during seeding. Since the “mixed” population did not grow but remained and even decreased over time, an active excretion after the initial mixture can be disregarded. The cell population with no particles increased over time while particle gates (“green”, “red”, “mixed”) decreased for both cell lines. This can be associated with a dilution of the particles by cell division. However, the relative decrease for “mixed” was slightly lower compared to the “red” and “green”. This slight dilution might derive from some dead cells, which lose their particles after apoptosis. These particles might be re-ingested on purpose or randomly by other macrophages. Especially in the liver, one of the main macrophage functions is the removal of apoptotic cells via efferocytosis <sup>[283]</sup>. Particles might as well be ingested together with cell debris. Kupffer cells are further known to remove, e.g. gold nanoparticles from the liver *in vivo* <sup>[52]</sup>. However, since this only considers a low representation of cells in this experiment, it can be assumed that the re-ingestion of released particles seldom occurs.

The lack of excretion can be associated with the lack of localisation of particles this size with, e.g. endosomes, phagosomes or lysosomes, the most popular excretion pathways. For nanoparticles, it is known that particles incorporated in lysosomes are actively excreted, while sharp-edge nanoparticles, which already escape the endosomes to the cytoplasm throughout the endocytic processes, remain significantly longer in the cells <sup>[284]</sup>. The high co-localisation within the cytoplasm of the here-used particles argues for a similar finding here.

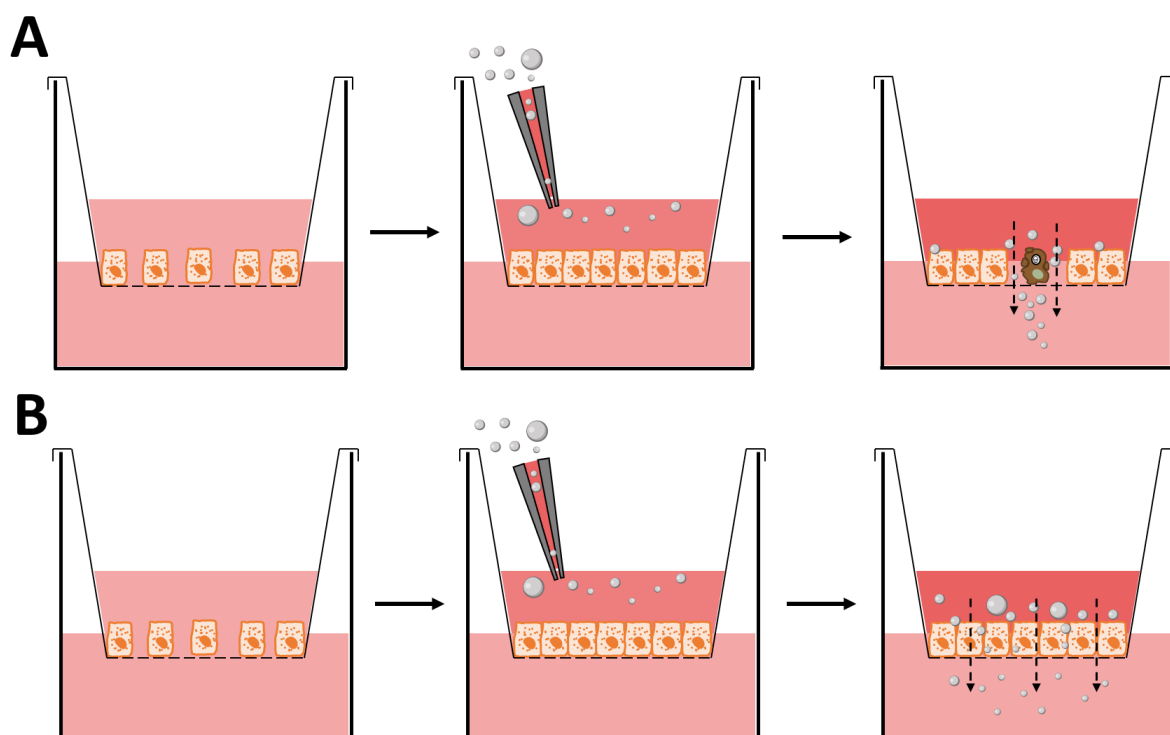
In summary, particles are released by cell death, but no active exocytosis was observed in this experiment. Neighbouring cells could re-ingested released particles together with cell debris. Contrary to ingested cell debris, microplastic particles are probably indigestible, which can result in an accumulation or at least a prolonged remaining of the particles inside the tissue/organ. This finding might as well help in explaining distribution or accumulation mechanisms *in vivo*, where particle interactions could last for a much longer period compared to *in vitro* experiments.

## 4. Effects of MP on microtissue

After the end of the particles' journey on a single cell level, an attempt is now being made to transfer the collected data to 3D microtissue cultivation systems for a more realistic approach. Therefore, in this work, the so-called transwell method, as well as the establishment and implementation of spheroids, were carried out. The transwell method is a suitable assay for cell migration, piercing of particles, and permeability studies, mimicking the epithelial barrier *in vivo*. Spheroids, on the other hand, are considered more representative of the *in vivo* microenvironment than two-dimensional (2D) cell cultures and are often used in invasion and distribution experiments as well as the estimation of toxicity on microtissues. Both methods might provide additional insights into the behaviour of microplastic *in vivo* and will be evaluated in the following paragraph. These data are summarised in the finished manuscript "Analysis of Microplastic in 3D Cell Spheroids" by Völkl, Ritschar et al.

### 4.1. Effects of microplastic in the transwell assay

Two main ideas were tackled in this work by using the transwell assay. The first question was if the particles affect the integrity of the epithelial layer (Scheme 17A). Second, a possible piercing through a fully developed epithelial membrane was analysed (Scheme 17B). BNL CL.2 cells were used as cell lines due to their phenotype as epithelial cell line and their non-cancerogenic origin, supporting the formulation of an epithelial monolayer.



**Scheme 17** Conducted transwell experiments

A: Possible effects of particles on the membrane integrity B: Piercing of particles through an closed barrier

#### 4.1.1. Influence of microplastic on the epithelial monolayer integrity

To evaluate the integrity of the epithelial monolayer with and without particle treatment, the lucifer yellow (LY) assay was conducted. Therefore, transwell inserts with 3  $\mu\text{m}$  pores were seeded according to the methods section (2.8). This pore size was chosen since 3  $\mu\text{m}$  should be big enough for the used particles to pass but still small enough for the cells as a suitable base foundation. After four days of cell incubation, which was determined to form a closed epithelial layer, 25  $\mu\text{g/mL}$  particles ( $\text{PS}_{0.5\mu\text{m}}$  and  $\text{PS}_{2\mu\text{m}}$ , in pristine and aged versions) were added for 24 h. Afterwards, the lucifer yellow assay was conducted (Figure 34).

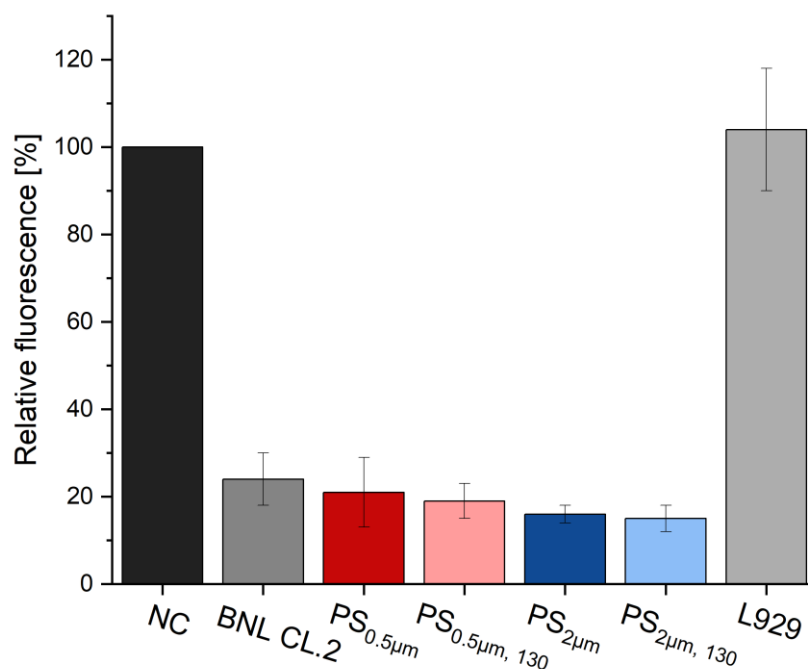


**Figure 34 Transwell permeability assay**

*Shown is the relative fluorescence of the LY in relation to the NC. 100,000 cells were seeded initially and incubated for 4 days on the transwell insert. 25  $\mu\text{g/mL}$  particles were afterwards added for 24 h, LY was added on day 5 for 2 h and subsequently measured. NC = only transwell insert without cells; BNL CL.2 / L929 = cells were seeded, with no additional particle challenge*

As an additional control, L929 cells were used. Fibroblast cell lines are known to grow very dense but assemble no tight junctions <sup>[285,286]</sup>, which are highly important in forming the cell-cell connection and barrier in tissues. No barrier properties could be measured for the L929 cells compared to the control well (no cells at all). BNL CL.2 cells, on the other hand, proved a significant development of epithelial connection (only 25 % fluorescence compared to NC). The observed fluorescence by the LY assay for BNL CL.2 treated transwell shows that the epithelial layer is distinct but not completely closed. A particle challenge did not significantly change the fluorescence intensity of LY, no matter the size or ageing status. A reduction or disruption in the barrier property due to the particles could therefore be

ruled out. This finding is coherent with the results from 3.3, where BNL CL.2 cells showed little to no biological effects due to the particles.

#### 4.1.2. Migration of particles through an epithelial layer

Still, a piercing through the epithelial layer can not be ruled out. Especially smaller particles might cleave between cells, or cells might ingest particles with a following release. To analyse this, a method to detect the particles in the lower well had to be established. Two different approaches were used. For both methods, a transwell insert without cells was placed inside the well,  $10^5$  PS<sub>0.5µm</sub> and PS<sub>2µm</sub> particles per well were incubated for 24 h, and the whole bottom well (0.5 mL) was collected in an Eppendorf tube. The first approach used a vacuum centrifuge to concentrate the particle suspension up to 10 µL. This sample was collected and transferred to a fluorescence microscope to count the particles manually. However, only a few particles with a high sample variance could be detected. This, combined with the high effort for a single sample, made this approach impracticable. Therefore, the second approach used the FC (Figure 35 and Figure 36). Due to the small size of the particles, and the, therefore, very low cut-off filters for front and side scatter, a high amount of background noise was measured (Figure 35A/B and Figure 36A). While for PS<sub>2µm</sub>, the measurement was still practicable, in the case of PS<sub>0.5µm</sub>, the overlap was too high for a measurement using the front or side scatter. Therefore, the fluorescence of the particles was used to quantify the number of particles (Figure 35C/D and Figure 36B/C).

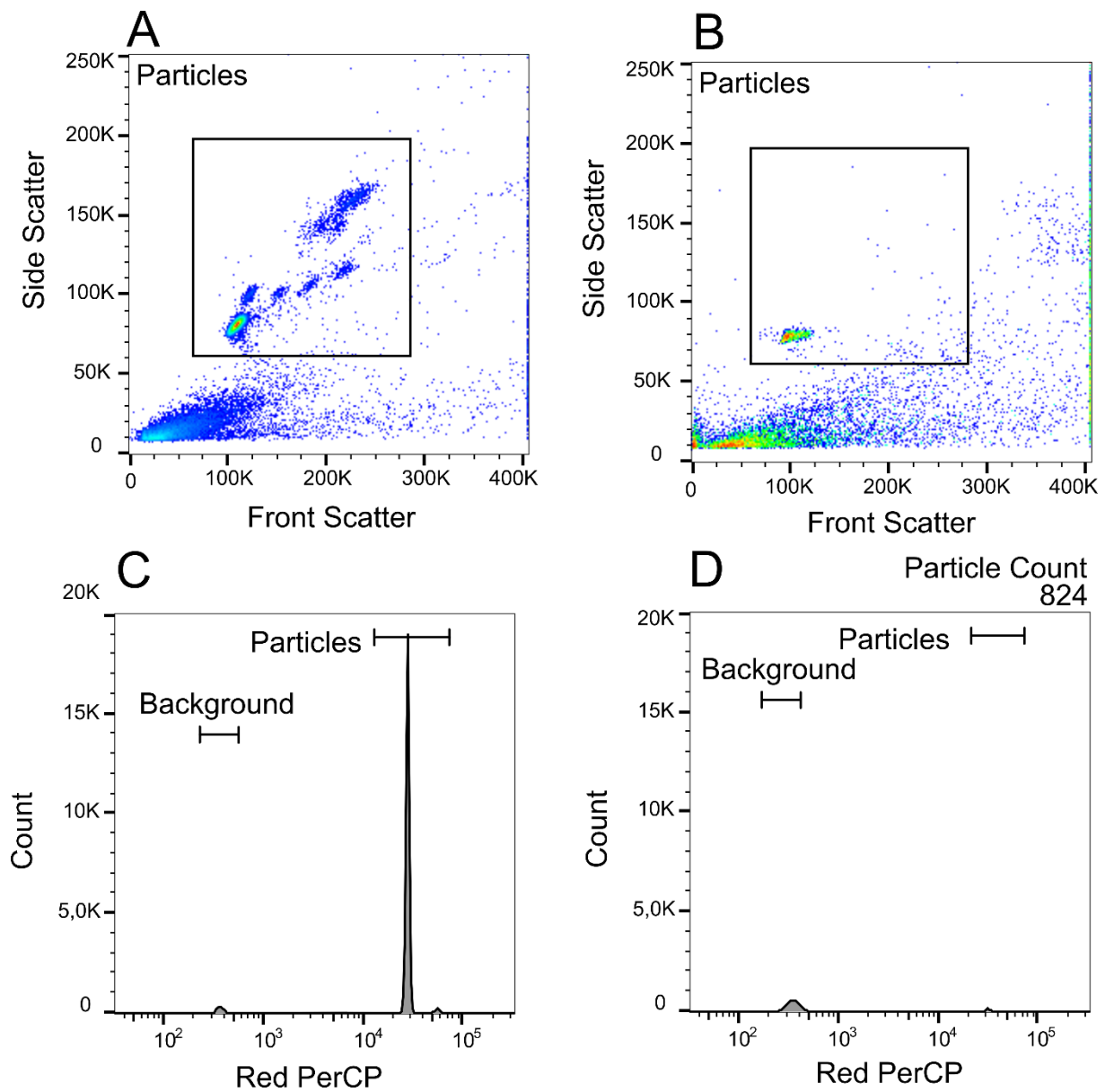


**Figure 35** Establishment of the particle detection method for transwell assays for  $PS_{2\mu m}$

A: Front scatter and side scatter representation of a control sample of  $PS_{2\mu m}$  in DPBS. B: Front scatter and side scatter representation of  $10^5$   $PS_{2\mu m}$  particles after incubation of 24 h on a transwell insert. C: Histogram representation of A with the fluorescence intensity of the particles as x-axis D: Histogram representation of B with the fluorescence intensity of the particles as x-axis B



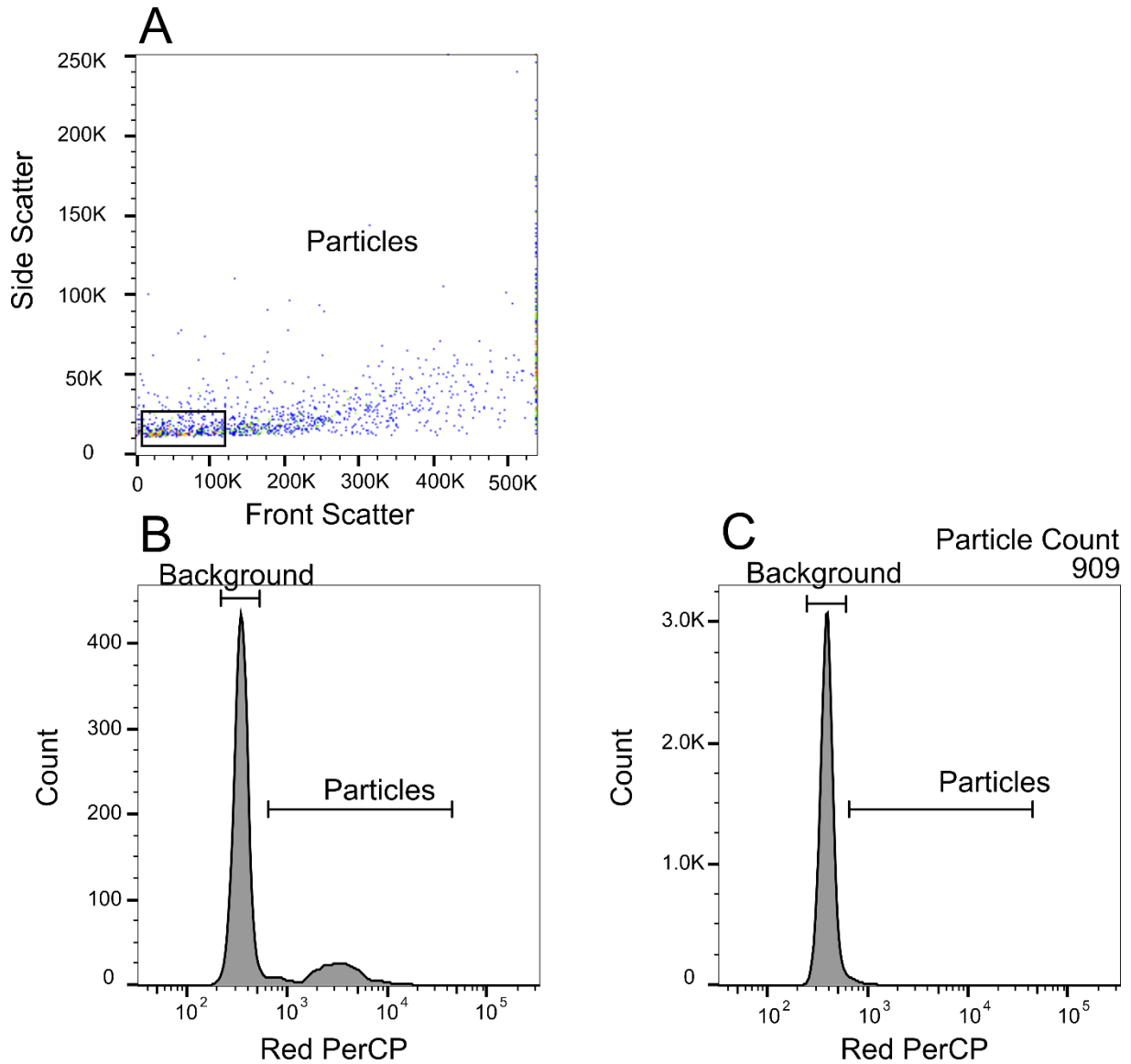


**Figure 36 Establishment of the particle detection method for transwell assays for  $PS_{0.5\mu m}$**

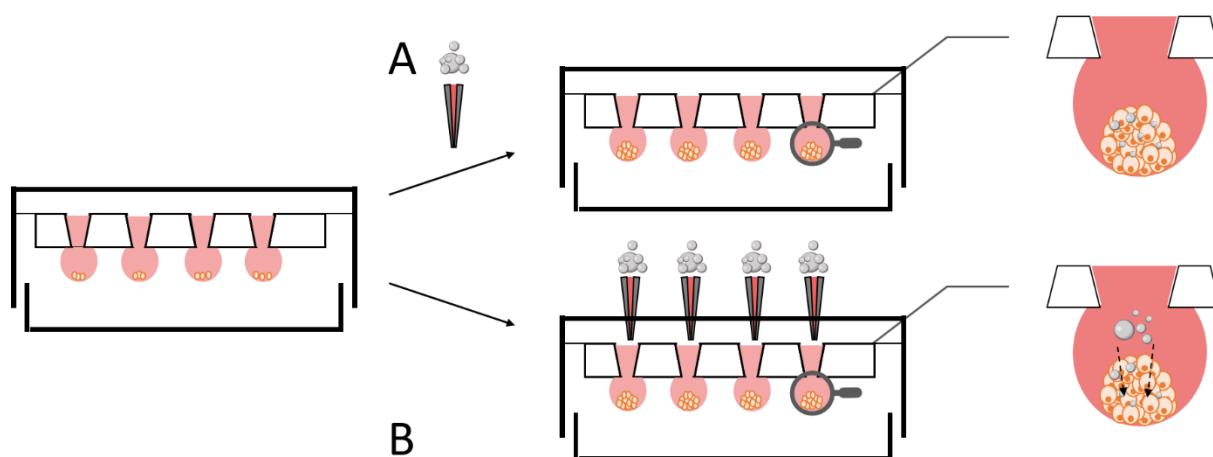
*A: Front Scatter and side scatter representation of a control sample of  $PS_{0.5\mu m}$ . B: Histogram representation of a A with the fluorescence intensity of the particles as x-axis C: Histogram representation of  $10^5$   $PS_{0.5\mu m}$  particles after incubation of 24 h on a transwell insert*

However, out of the  $10^5$  seeded particles, only 824 for  $PS_{2\mu m}$  and 909 for  $PS_{0.5\mu m}$  were detected. The vast amount of particles was probably stuck in the membrane or could not pass the  $3\mu m$  pores. Since only about 1 % of the particles could be detected, even without any cells, the penetration analysis with cells was neglected. A bigger pore size would probably be needed to ensure a passage of particles through the inserts for practicable penetration assays. Predictions about the penetration of the epithelial barrier with the performed experiments must therefore be vacated or shifted to the spheroid analysis.



## 4.2. Interactions of microplastic with spheroid microtissue

Two main ideas considering the spheroids were carried out (Scheme 18). The effect of MPP on the initial formation of the spheroid and the penetration of particles inside fully formed spheroids.

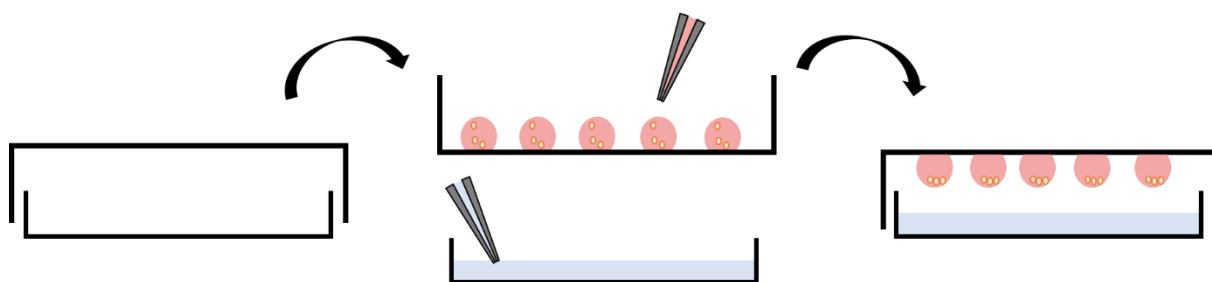


**Scheme 18** Conducted spheroid experiments

A: Formation of spheroids challenged initially with MPP B: Penetration of particles inside a fully formed spheroid

### 4.2.1. Establishment of spheroid cultivation

To tackle these questions, the spheroids' formation had to be established primarily. BNL CL.2 and STC-1 cells were identified as suitable cell lines. When growing in Petri dishes, these cell lines showed a high interaction and connection, making them likely to form a connected tissue. Furthermore, their nature as epithelial cells from the liver and gut, respectively, proves them highly interesting in penetration assays. As an initial attempt, 50  $\mu$ L drops of media containing 10,000 cells were placed on the lid of a Petri dish, the bottom of the dish was filled with PBS to prevent drying out, and the lid was carefully placed back, producing a cheap and quick hanging drop cultivation system (Scheme 19).

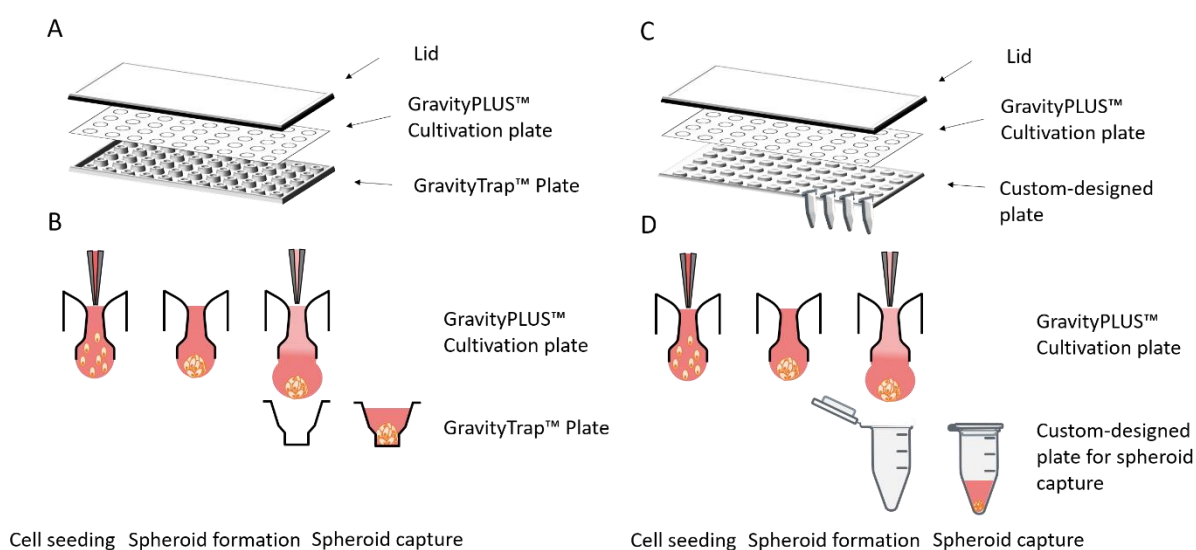


**Scheme 19** Spheroid formation inside a Petri dish by hanging drop method

While this method was quite useful for a first estimation of the cell formation, the risk of losing drops due to the turning of the lid, e.g. for media change or microscopical observation, was quite high. Furthermore, the droplet shape was quite irregular due to the turning, resulting in a relatively high deviation in the spheroid shape. However, in this system, BNL CL.2 cells formed spheroids in several

days, while STC-1 cells did not form a uniform spheroid. BNL CL.2 cells were, therefore, solely used in the following experiments.

To optimise spheroid cultivation, a specialised hanging drop cultivation plate (GravityPLUS™) was applied (Scheme 20A/B). This system is similarly built like a 96-well plate, with a hanging drop cultivation plate and a specific bottom plate (GravityTrap™) for collecting the formed spheroids. The inlet shape of the cultivation plate aids in forming a robust droplet. Furthermore, a media change or, e.g. the addition of particles is easily applicable.



**Scheme 20 Principal of the GravityPLUS™ hanging drop spheroid cultivation system**

*A: Overview with the commercial GravityTrap™ System B: Microtissue formation in the GravityPLUS™ Cultivation Plate and subsequent transfer to the Gravity Trap™ system C: Overview with the custom-designed capture plate D: B: Microtissue formation in the GravityPLUS™ Cultivation Plate and subsequent transfer to individual Eppendorf tubes*

While the formation of the spheroids proved as a straightforward process, one big constraint of GravityTrap™ plates was the difficulty of isolating fully-formed spheroids individually. Independently from the number of transferred microtissues, the whole plate was required. For further processing or transfer, removing the spheroids from the reservoir wells proved difficult as well. Therefore, a custom-designed plate was designed and 3D printed to improve the spheroid transfer protocol (Scheme 20C/D). This device acted as a 96-hole rack for 200 µl Eppendorf tubes aligned vertically below the spheroids. This way, each spheroid could be transferred into a single 200 µl Eppendorf tube by applying the established transfer technique. For subsequent analysis, the transfer in the Eppendorf tube had further benefits, like rinsing with DPBS, transferring PFA and storing the fixed spheroid proved easier for the personalised plate.

Besides the diameter of the spheroids, circularity and roundness (i.e., morphological scores) were calculated as second parameters, indicating the quality of the spheroids. The analysis of circularity and

roundness was done according to Zdilla et al. using ImageJ <sup>[287]</sup>. Circularity (C) is defined as a degree of similarity to a perfect circle (Equation 7).

**Equation 7 Calculation of circularity**

$$C = 4 * \frac{[Area]}{[Perimeter]^2}$$

Roundness (R) is considered similar to circularity but has a reduced sensitivity to irregular borders. It also considers the major axis of the best-fit ellipse to calculate its value with Equation 8.

**Equation 8 Calculation of Roundness**

$$R = 4 * \frac{[Area]}{\pi * [Major Axis]^2}$$

Spherical structures (i.e. roundness/circularity > 0.8), in particular, are a sign of a stable aggregation and are less likely to develop structural changes or necrotic regions during the cultivation <sup>[288]</sup>. They are an important but quick and easily applicable parameter for characterising spheroids <sup>[175]</sup>. The morphology indicates further compactness, cell-cell adhesion and the formation of an extracellular matrix (ECM) <sup>[289,290]</sup>. Before day 5, the spheroid formation was not fully completed, characterised by a looser structure in the microscopic images (Figure 37). Therefore, no calculation of the respective parameters could be done before day 5.

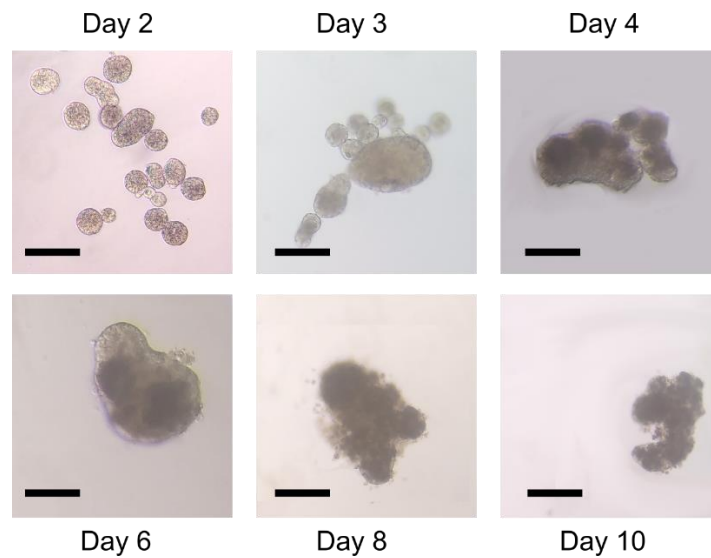


**Figure 37 Microscopical analysis of the spheroid growth**

10,000 BNL CL.2 cells were initially seeded. Pictures were taken microscopically, scale bar = 100 µm

Subsequently, spheroid growth and both morphological parameters in the GravityPLUS™ for BNL CL.2 cells were analysed for 14 days (Figure 38).

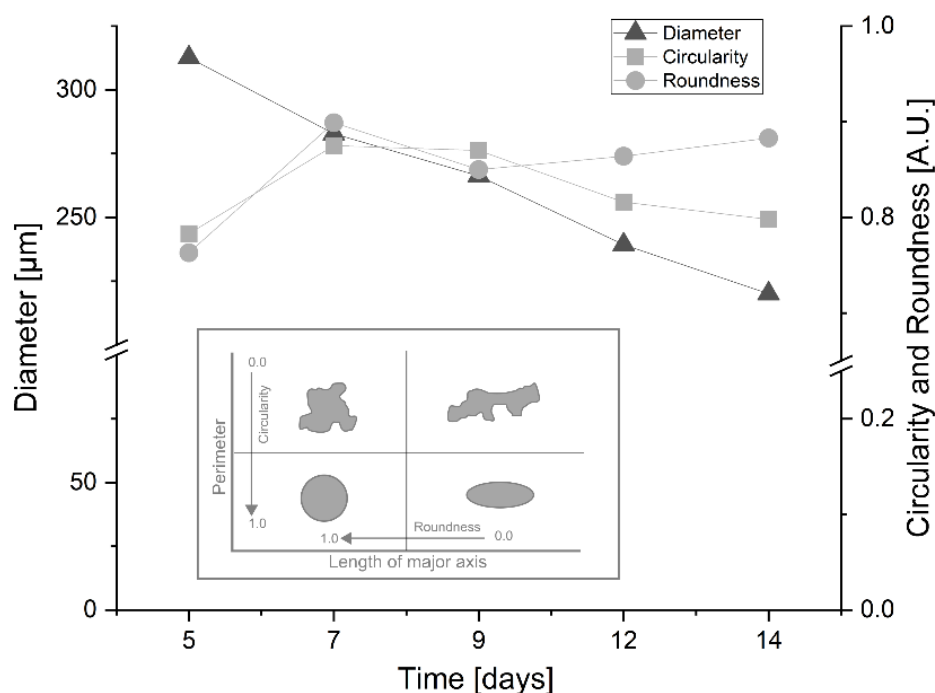


**Figure 38 Diameter, roundness and circularity for the assessment of the spheroids**

10,000 BNL CL.2 cells per well were seeded in the GravityPLUS™ plate. Pictures were taken microscopically and analysed using Fiji ImageJ. Values of 1.0 for circularity or roundness would indicate a perfect sphere. Insert graphic is adapted from Ahmad et al. [291]

5 – 7 days of incubation resulted in spheroids of a size of about 300  $\mu\text{m}$  in diameter with a roundness and circularity > 0.8. Prolonged incubation times decreased spheroid size and circularity/roundness, possibly due to over-cultivation leading to cell overgrowth and hypoxic regions within the spheroid, which can lead to cell death and, consequently, a decrease in the diameter [292]. The measured morphological scores further indicated that a cultivation time of 5 – 7 days was beneficial for generating spheroids with stable aggregation, compactness, and cell-cell adhesion. After day 7, both values started to decrease slightly. Since all measured factors supported the 5 – 7 days incubation, further experiments avoided longer incubation times due to the observed decrease in all parameters, For further analysis (e.g. confocal microscopy), a fluorescence staining method was established. Therefore, the spheroids were harvested (see Scheme 20D), fixed in paraformaldehyde, three times rinsed in DPBS and stained with rhodamine-phalloidin for the actin-filament and DAPI for the nuclei (Figure 39).

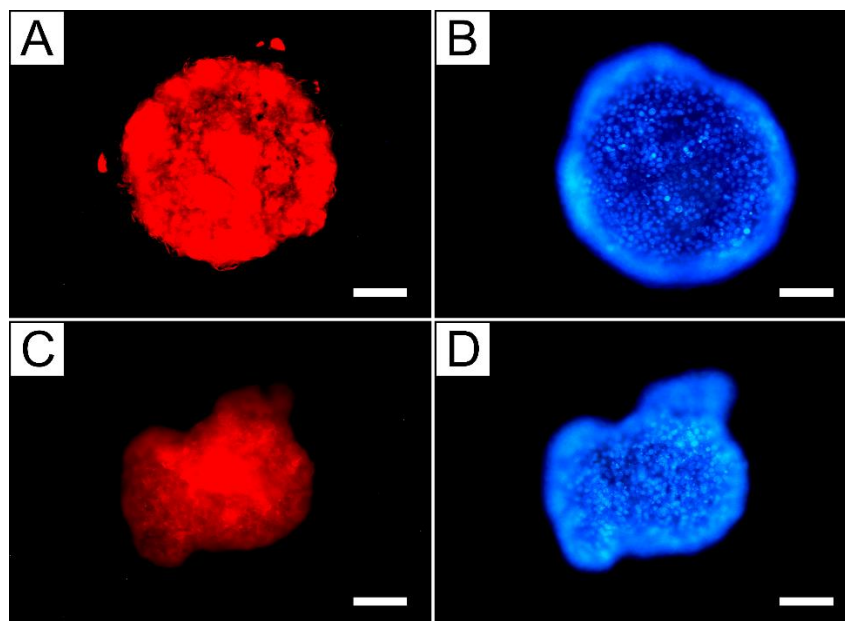


**Figure 39 Stained spheroids analysed with fluorescence microscopy**

Spheroids were harvested after 7 days of incubation and stained with 100 nM rhodamine-phalloidin (actin-filament, red, A/C) and 100 nM DAPI (nucleus, blue, B/D), incubation time 1 h. Scale bar = 50  $\mu$ m

The stained epifluorescence pictures showed a highly connected actin filament with homogenous staining. It has to be noted, though, that these fluorescence pictures can show no 3D information. However, the growth of the spheroids could be reproducibly managed and harvesting as well as treatment of the spheroids proved applicable with the custom-designed plate.

#### 4.2.2. Interaction of spheroids with MPP

After establishing the growth of spheroids, the interaction between MPP and spheroids was investigated. First, the formation of spheroids in dependence on the presence of MPP was analysed. Therefore, PS<sub>2 $\mu$ m</sub> and PS<sub>130</sub> were added from the start of the spheroid formation. Spheroids challenged with MPP did not form one spheroid but smaller, loose aggregations (Figure 40).

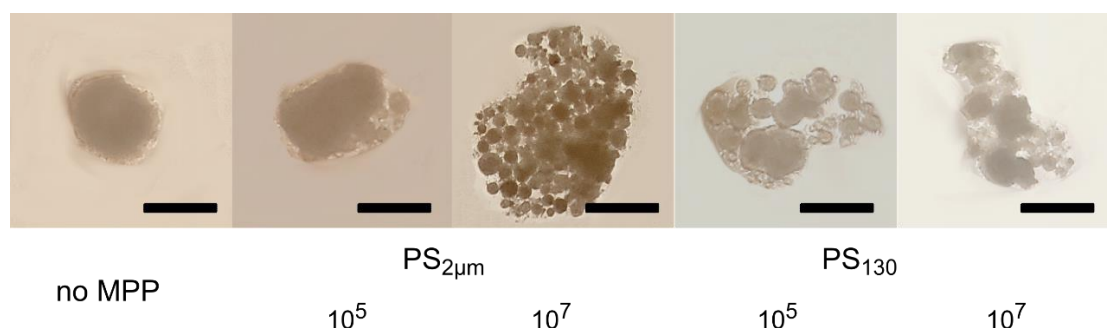


**Figure 40 Representative microscopic pictures of spheroids challenged with MPP during the formation**

10,000 BNL CL.2 cells were initially seeded per well. No MPP represent a spheroid formation without additional particle burden. 10<sup>5</sup> and 10<sup>7</sup> represent the particle count added. Pictures are taken on day 7 of the cultivation, scale bar = 200  $\mu$ m

The possibility of tracking the morphological parameters diameter, circularity and roundness was not given due to the highly irregular spheroids. Especially for the artificially weathered particles and the high concentration of PS<sub>2μm</sub>, this could be observed. Most likely, this is coherent with a looser formation of the spheroids and an integration of the particles between the cells in the initial formation process. This could result in a weaker cell-cell interaction due to the presence of the particles. One explanation can simply be a physical disruption between the cells due to particles sticking on the surface. Furthermore, the membrane integrity was decreased when treated with PS<sub>130</sub> (3.3.6) in ImKC cells, which could also contribute to reduced cell-cell interaction. Currently, little comparable data regarding MP exists in the literature for spheroids. Sambale et al. found a similar behaviour of a looser structure of NIH-3T3 and A549 spheroids in response to ZnO and TiO<sub>2</sub> nanoparticle treatment <sup>[293]</sup>.

After evaluating the influence of MPP on the formation of the spheroids, an interaction and possible penetration with an already-formed microtissue was analysed in the next step.  $1 \times 10^5$  PS<sub>2μm</sub> were added for 24 h to hanging drops containing fully-formed spheroids at day 5 after the initial cell seeding. Afterwards, the spheroids were harvested, fixed, stained and subsequently analysed by confocal microscopy by Julia Jasinski. Figure 41 shows a spheroid crosssection of a spheroid challenged with PS<sub>2μm</sub>.

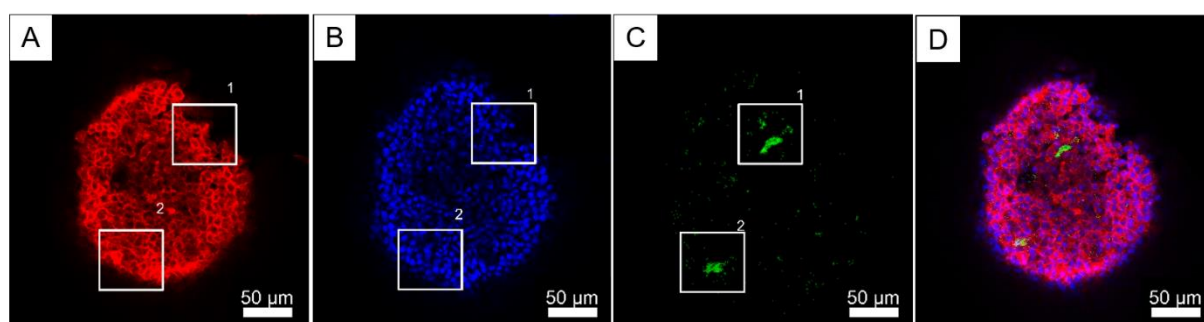


**Figure 41 Confocal microscopy of a spheroid after incubation with MPP**

*1 × 10<sup>5</sup> PS<sub>2μm</sub> particles were added to preformed spheroids (day 5 of cultivation) in the hanging drop and incubated for 24 h. Spheroids were harvested, fixed and stained with 100 nM rhodamine-phalloidin (actin-filament, red, A) and 100 nM DAPI (nucleus, blue, B) for 1 h. MPP showed green fluorescence (C). D represents a merged picture. Insert 1 and 2 represent significant accumulations of particles inside the spheroid. Confocal pictures were taken by Julia Jasinski.*

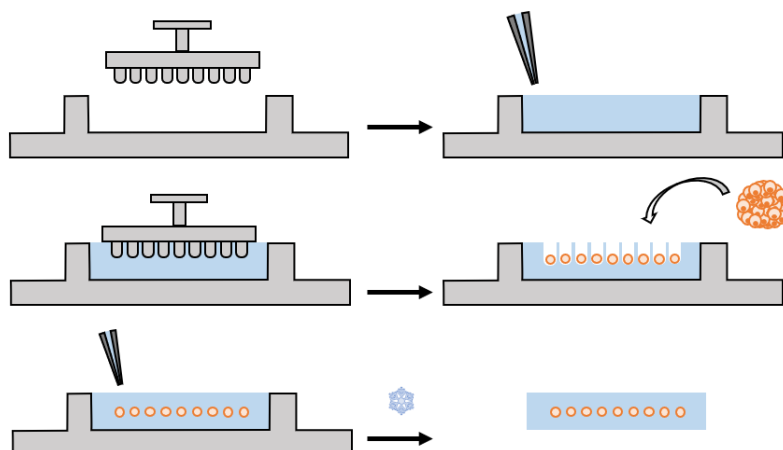
The analysis by confocal microscopy bears the advantage of 3D information, which could not be taken by epifluorescence microscopy. While the actin filament of the cells appears to be highly connected, comparable to the epifluorescence microscopy, staining the spheroid's core proved difficult, represented by a slighter staining intensity of the core area. Even though the dye molecules are fairly small (DAPI ≈ 300 Da and rhodamine-phalloidin ≈ 1300 DA), there seems to be a transfer limitation into the core of the spheroids. While this supports the assumption of a tight cellular 3D structure, analysing the spheroid close to the core is harder. Despite these limitations, MPP could be detected inside the spheroids. Hence they were able to penetrate the microtissue, either transcellular or paracellular.

While scattered PS<sub>2μm</sub> particles were found in the whole spheroid, two specific areas with a high particle accumulation could be detected (Figure 41C). Different transport mechanisms might influence the distribution of the particles and the difference compared to the staining. While the staining dye is mainly transported by diffusion, particles might be transported actively by the cells <sup>[294]</sup>. It was previously shown that the used particles interact and get ingested by BNL CL.2 cells <sup>[71]</sup>. Further, Liang et al. suspect a preferentially entering of MPP into human liver organoids consisting of hepatocytes, endothelial cells, and hepatic stellate cells via the endothelial cells <sup>[84]</sup>, supporting the hypothesis of active transport. The accumulation spots of particles might stem from clumped particles or cells with high PCI. However, it can not be excluded that less connected spots in the spheroid serve as a paracellular pathway for the particles. Additional information, particularly about the situation in the core of the spheroids, is therefore needed.

#### 4.2.3. Establishment of spheroid analysis using thin sectioning

To enlarge the analysis methods and gain more information about the core of the spheroid, a method for producing thin sections of the spheroids as a complementary analytical method was established in cooperation with Sven Ritschar (AG Laforsch). While the embedding process and establishment were done in this work, the following work at the cryotome and the histological staining was done by Sven Ritschar. Thin sections can be used for histological examination, increasing the analysis spectrum (e.g., more staining possibilities, better resolution inside the spheroid core) <sup>[295,296]</sup>. To prepare these thin sections, the microtissue needs to be embedded and sliced using a microtome. These thin slices ( $\approx 10 \mu\text{m}$ ) can then be transferred on a microscopy slide, stained and analysed.

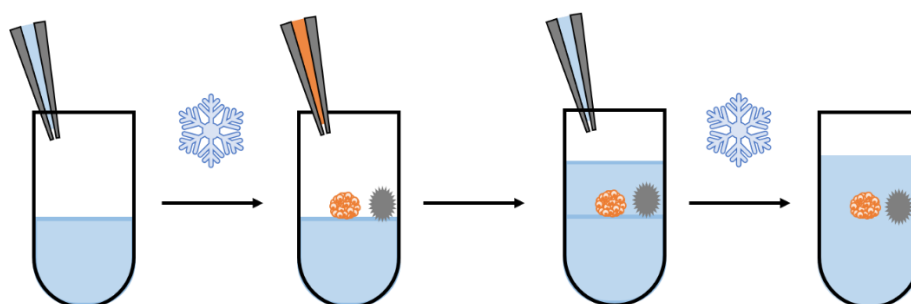
As the first embedding approach, an agarose micro-array embedding, according to Ivanov and Grabowska, was established (Scheme 21) <sup>[221]</sup>. The used parts of the micro-array were 3D printed based on Ivanov and Grabowska and manually adapted if necessary.



*Scheme 21 Embedding procedure for the agarose micro-array*

Briefly, the hot agarose layer was pipetted in the bottom of the microarray. The top of the micro-array was placed in the agarose, and the solution was left to harden in the freezer shortly. By removing the top, a mould with slots was formed. Into each slot, one fixed spheroid was carefully pipetted, the top of the slots was sealed with agarose, and the gel was frozen at -20°C. This way, a rapid, high throughput method for the subsequent cryosectioning might be produced. However, when applying the recommended embedding procedure (one bath of 50 %, 70 %, and 90 %, and four baths of 100 % methanol, 1 h each, cleared in xylene (three baths, 1 h each), and infiltration with molten paraffin (two baths, 2 h each, under vacuum)), the agarose mould started to degrade, resulting in a loss of the embedded spheroids<sup>[297]</sup>. An adaption of the agarose concentration (2 %, 5 %, 10 %) and the usage of low-melting and high-melting temperature agarose did not result in a better outcome. Either during the hydration step or during the paraffin embedding step, the agarose mould collapsed. As an additional problem, using xylene proved to be disadvantageous since this organic compound is known to dissolve plastic, making it not applicable for usage with MPP.

Therefore, an alternative method was developed, which did not depend on paraffin embedding or the agarose mould. The new procedure was based on gelatine capsules as a vessel and an embedding compound compatible with MPP<sup>[298,299]</sup> (Scheme 22).



**Scheme 22 Encapsulation of spheroids in O.C.T. compound**

This Optimal Cutting Temperature (O.C.T.) compound is a commonly used embedding chemical for cryosectioning and should not interfere with MP detection. Briefly, a bottom layer of the O.C.T. compound was pipetted in the capsules. After the first cooling step on dry ice, the spheroid was carefully added on top of the frozen base layer. A small aluminium ball was added at the same level as the spheroid as an additional visual tracer. The capsule was carefully sealed with O.C.T. compound while remaining on dry ice. The prepared capsules were then ready for cryosectioning and subsequent analysis.

Based on these embedded spheroids, Ritschar could produce thin sections ( $\approx 10 \mu\text{m}$ ) and subsequently histologically stain them with Hematoxylin/ eosin (H&E) or analyse them by fluorescence microscopy (Figure S8). In these thin sections,  $2 \mu\text{m}$  particles could be identified and quantified (average particle number of  $145.5 \pm 42$  / section<sup>[300]</sup>), translating to approximately 1 % of the added particles/spheroid.



The successful establishment of these thin sections opens the possibility of complementary staining methods (e.g. antibody staining), and further analysis methods are applicable to the frozen thin sections (e.g. mass spectrometry and infrared-sed imaging) <sup>[301,302]</sup>. This greatly enlarges the analysis possibilities regarding the interaction between MPP and microtissues.

#### 4.2.4. Co-cultivation of spheroids with macrophages

To further improve the experimental possibilities, a co-cultivation system of spheroids with ImKC cells was established. A selected targeting of particles from the macrophages inside the spheroid could be analysed, as well as cytotoxic and inflammatory reactions of the macrophages in a microtissue environment. Before the analysis of these parameters, the co-cultivation had to be established. As media composition, a 75 % DMEM and 25 % RPMI1640 ratio with 10% v/v FCS was chosen to achieve high viability for both cell lines (ImKC 86.8 %, BNL CL.2 94 %) after 4 days of incubation (compared to ImKC 91.7 %, BNL CL.2 97.5 % in their respective growth medium). Afterwards, cells were seeded on a 1:10 ratio (ImKC to BNL CL.2), and their respective growth was tracked using FC (Figure 42). The different side scatter value for the respective cell line was used to differentiate between the cell lines (Figure 42A), and the cell growth ratio was analysed for 6 days (Figure 42B).

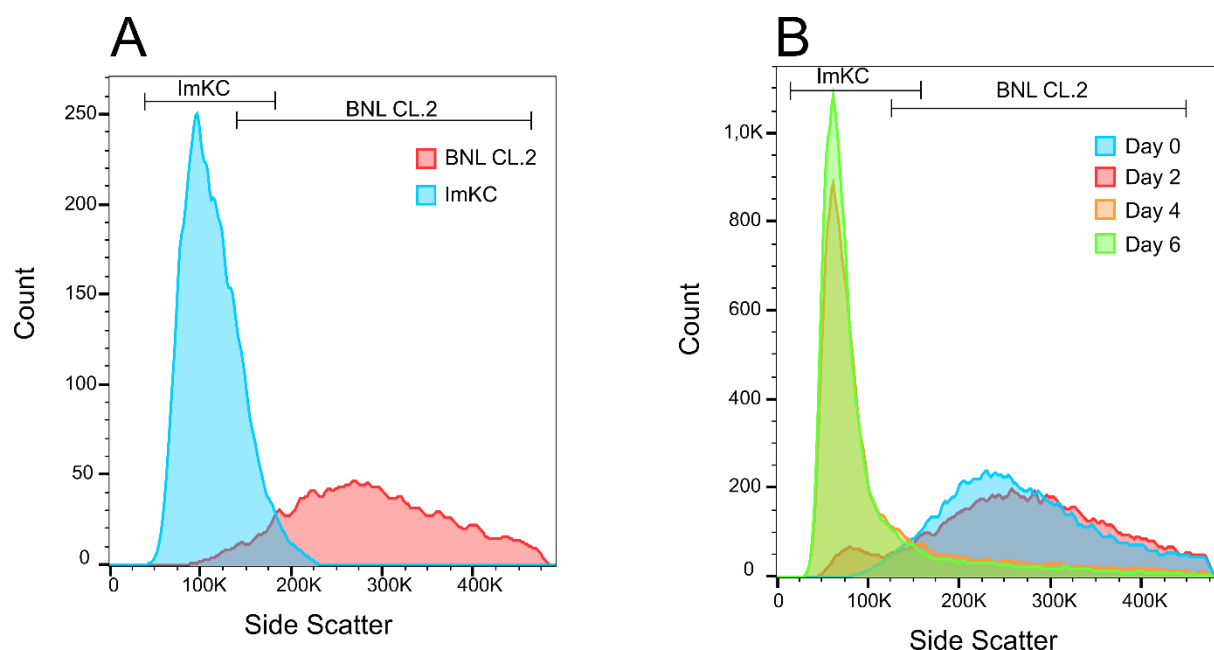


**Figure 42 Ratio of cell count for a co-cultivation of ImKC and BNL-CL2 cells**

*A: Display of the different values in the Side scatter for single populations of ImKC and BNL. CL2 B: Development of both cell populations over 4 days when cultivated together. The initial seeding ratio on day 0 was 1:20 ImKC to BNL CL.2*

While the ratio of ImKC cells increased for the first two days, BNL CL.2 remained the majority. A significant shift in the population between day 2 and day 4 could be observed. ImKC cells seemed to overgrow the BNL CL.2 cells highly. This proved problematic for co-cultivation with spheroids since the stability of the spheroids could not be ensured in this cell ratio. Co-cultivation experiments, therefore,

were restricted to 24 h of co-cultivation. After 5 days of the initial formation of the spheroids, particles were added for 24 h. After a washing step to remove unbound particles, 500 macrophages were added to a single spheroid. To further allow tracking of the macrophages via fluorescence or confocal microscopy, macrophages were stained with 5  $\mu$ M CTV before adding to the unstained spheroid. Only rhodamin-phalloidin was used when staining the spheroid afterwards. While BNL CL.2 cells were only stained red, macrophages showed additional blue fluorescence to differentiate both cell types. Combined with the green fluorescence of the used particles, specific targeting of particles by macrophages could be tracked.

Indeed, Julia Jasinski could show by confocal microscopy (Figure S9) that macrophages take up particles next to and inside the spheroid <sup>[303]</sup>. The observed pattern of the macrophages hints at a migration of macrophages towards MPP inside the microtissue.

This interaction between particles and macrophages can increase oxidative stress or inflammation reactions (3.3) on a single-cell level, which might be translated to the microtissue level. Interestingly, these effects are among the most observed for the liver in mammalian *in vivo* studies as well <sup>[304]</sup>. To further investigate this, an ELISA was conducted to measure the TNF $\alpha$  amount in the media of the hanging drop cultivation system after treatment of PS<sub>2 $\mu$ m</sub> and PS<sub>130</sub> and the subsequent addition of macrophages (Figure 43).

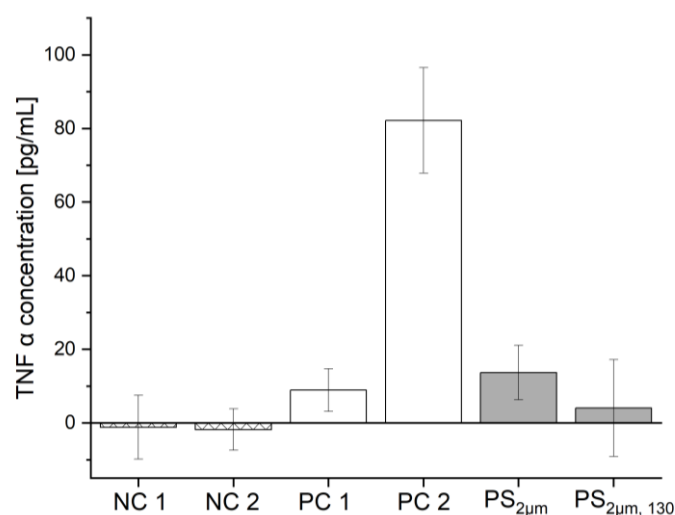


**Figure 43 ELISA assay to determine the TNF  $\alpha$  amount in the hanging drop cultivation system**

Spheroids were grown for 5 days.  $1 \times 10^5$  particles were added for 24 h. Afterwards, 500 macrophages were added for 24 h. TNF $\alpha$  amount was subsequently determined in the hanging drop supernatant. NC 1 = negative control consisting only of BNL CL.2 cells with no further treatment. NC 2 = negative control consisting of BNL CL.2 cells with the addition of ImKC cells but no particles. PC 1 = positive control consisting only of BNL CL.2 cells with an addition of 2.5  $\mu$ g/mL LPS instead of particles. PC 2 = positive control consisting of BNL CL.2 cells with the addition of ImKC cells and an addition of 2.5  $\mu$ g/mL LPS instead of particles. PS<sub>2 $\mu$ m</sub> / PS<sub>2 $\mu$ m</sub>, 130 = consisting of BNL CL.2 cells with the addition of ImKC cells and addition of the respective particles.  $n = 3$

No significant increase for no treatment could be measured, though. It has to be noted that the overall measured concentrations, e.g. the positive control, were 250 x lower compared to Figure 25. This most

likely was connected with the low number of macrophages added. BNL CL.2 cells alone produced no significant amount of TNF  $\alpha$ , no matter the treatment. The slight increase for PS<sub>2 $\mu$ m</sub> and PS<sub>130</sub> argues for an interaction of the macrophages with the MPP. However, due to the low concentration measured, no clear conclusions about the role of the macrophages in microtissue cytotoxicity could be made with this experiment.

#### **4.3. Summary and conclusion**

Analysis by the transwell assay did not show the expected surplus in results. The penetration of particles could not be measured, probably due to a too-small membrane pore size. Particles could not pass through the pores without cells, making further analysis with the available experimental setup redundant.

On the other hand, spheroid cultivation proved a valuable benefit. Establishing the formation, microscopical analysis and thin sectioning provided various options for analysing the effects of MPP on a microtissue. The formation of spheroids under the presence of MPP was disturbed, resulting in a lower connection between the cells and the incorporation of the particles inside the spheroid. When challenged with MPP after the formation, particles penetrated the spheroid either way, which could be analysed by the established workflow. Finally, the co-cultivation of macrophages with the spheroids gave the first insights into the behaviour of more complex model systems, converging to more realistic environments.

It is commendable that the presented workflow provides an alternative to *in vivo* experiments to analyse the effects of MPP on liver microtissues. The approach can also offer insights into the accumulation and distribution of particles within the microtissues, which could aid in understanding the mechanisms involved in particle transport and tissue response. Moreover, the ability to apply 2D and 3D microscopic analysis can provide a better understanding of the cellular response to MPP exposure in the microtissue models. This information can be crucial in designing targeted therapies or interventions to prevent or minimise the negative effects of MPP. The flexibility of the approach also allows for the use of other staining methods depending on the research question. This opens up the possibility of studying different cell types and their response to MPP exposure in the microtissues, which could provide a more comprehensive understanding of the effects of MPP on liver tissue.

## 5. The effect of MP on primary intestinal cells from *E. fetida*

Using the 3D cell model proved useful in estimating MPP's effects *in vitro* and simplifying the transfer to *in vivo* data. Still, only immortalised cell lines were used, which significantly deviate from the cellular situation *in vivo*. In the next step, the isolation of primary cells of environmentally relevant organisms was approached to close this gap. As described in the introduction, one common model organism is the earthworm *E. fetida*. While studies exist analysing the effect of MPP on endpoint fitness markers like survival, increase in body weight, reproductive fitness, or changes in oxidative stress markers <sup>[209]</sup>, little knowledge about effects or mechanisms on the cellular level exists. Just recently, Riedl, Völkl et al. established an isolation protocol of primary intestinal epithelial cells from *E. fetida* for the analysis of environmental pollutants <sup>[118]</sup>. The suitability of the cells for cytotoxicity analysis was shown by known ecotoxins ( $\text{Cu}^{2+}$ ,  $\text{Cd}^{2+}$ ), assuming that the cells were also competent for other toxicological analyses. Therefore, these cells were used to analyse the effect of PS and PLA particles ( $\text{PS}_{0.2\mu\text{m}}$ ,  $\text{PS}_{0.5\mu\text{m}}$ ,  $\text{PS}_{2\mu\text{m}}$ ,  $\text{PS}_{3\mu\text{m}}$ ,  $\text{PLA}_{0.5\mu\text{m}}$ ,  $\text{PLA}_{2\mu\text{m}}$ ). Both polymers were chosen as representatives of non-biodegradable commodity plastics and biodegradable polymers. Furthermore, studies analysing the whole organism used PS and PLA <sup>[209]</sup>, which might help compare or link cellular effects with the ones on an organismic level. Before the analysis, the surface charge of the particles in the specialised growth medium was characterised by Julia Jasinski (Table 15).

**Table 15 Measured  $\zeta$ -potential of the used MPP**

Measurement in KCl represents the measured  $\zeta$ -potential of the MPP stock solution in KCl buffer without proteins. In the case of "Growth medium", MPP were incubated overnight in full growth medium for the primary intestinal cells.

MPP	$\zeta$ -potential (mV)	
	KCl	Growth medium
$\text{PS}_{0.2\mu\text{m}}$	- 47.4 $\pm$ 0.3	- 25.3 $\pm$ 0.0
$\text{PS}_{0.5\mu\text{m}}$	- 52.8 $\pm$ 0.2	- 27.6 $\pm$ 0.0
$\text{PS}_{2\mu\text{m}}$	- 76.7 $\pm$ 0.3	- 28.8 $\pm$ 0.0
$\text{PS}_{3\mu\text{m}}$	- 78.4 $\pm$ 0.4	- 29.3 $\pm$ 0.2
$\text{PLA}_{0.5\mu\text{m}}$	- 1.1 $\pm$ 0.0	- 1.3 $\pm$ 0.4
$\text{PLA}_{2\mu\text{m}}$	- 3.9 $\pm$ 0.3	- 11.2 $\pm$ 1.1

Data represent mean  $\pm$  SD, n = 3. Data was measured by Julia Jasinski and is published in Riedl, Völkl et al. (2022)

No significant differences in the surface charge of the particles could be found when comparing incubation in the *E. fetida* medium with the cell culture media. Only for  $\text{PLA}_{0.5\mu\text{m}}$ , a very low  $\zeta$ -potential was observed, which could influence their interaction with the cells. Jasinski verified this interaction via confocal microscopy <sup>[118]</sup>. No apparent uptake of particles of any type or size by the cells could be found. In the case of the smaller particles (0.2 and 0.5  $\mu\text{m}$ ), some interactions with the cell membrane could be assumed (Figure S10). Despite the lack of interaction between particles and cells, an MTT assay was conducted to analyse the metabolic activity of the cells (Figure 44).

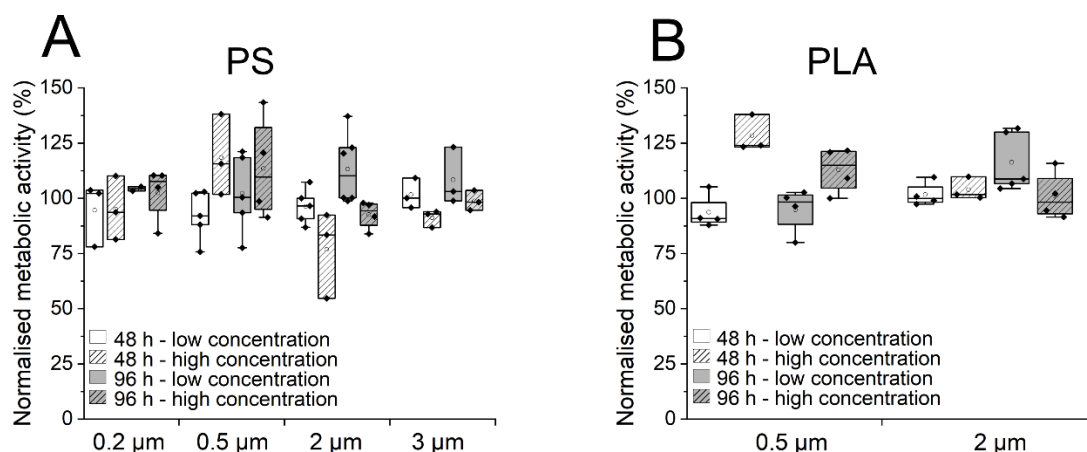


**Figure 44** MTT assay with primary intestinal cells from *E. fetida*

Data represent the percentage of the particular experiment to the metabolic activity of the negative control (cells without particles). A: influence of PS particles B: Influence of PLA particles. Low concentration:  $2.5 \mu\text{g MPP}/0.1 \times 10^6$  cells, high concentration:  $250 \mu\text{g MPP}/0.1 \times 10^6$  cells.  $n \geq 3$ . significance level against the negative control: \* =  $p < 0.05$  Figure is adapted from Riedl, Völkl et al. (2022) and modified

However, only PS<sub>2µm</sub> particles incubated at high concentrations for 48 h showed significantly reduced metabolic activity. For PLA<sub>0.5µm</sub>, even a significantly higher metabolic activity for the high treatment after 48 h of incubation could be measured. This discovery appears counterintuitive, but the correlation between the amount of exposure and the corresponding reaction may not always follow a straight line. This has already been demonstrated in previous research on the organismic level for *E. fetida* [208,305] and with coelomocytes [306]. The lack of uptake and effects might as well be associated with the cell phenotype. Murine epithelial cells did not show any effects on the same particles as well (see 3.3.2 and 3.3.5). Since the effect was significantly dependent on the PCI, it can be assumed that the neglectable influence here might stem thereof. Nevertheless, the smallest particles seem to attach to cells. Possible secondary or cumulative effects can, therefore, not be excluded. As shown in 4.2.2, particles can penetrate tissue and persist in extracellular spaces, where long-term or cumulative effects might arise.

The usage of primary intestinal cells confirmed some findings of the cell line approach. The size of the particles proved to be an important factor in the PCI, and epithelial cells did not show acute cytotoxicity to MPP as well. Long-term effects or accumulation on a tissue level can not be excluded since in it could be shown that particles might penetrate microtissue, despite not showing effects on cells on a 2D cell culture approach (see paragraph 4). However, from the data in this work, a connection between the cellular and the organismic level could not be made.

## 6. Effects of MP on unicellular organisms

A final convergence to an environmentally realistic approach, unicellular organisms were used. Their behaviour in the presence of MPP was tracked, uptake and distribution analysed, and the bioaccumulation and biomagnification of MPP along a simplified food web was tracked. *A. proteus* as test organism was chosen based on its ecological relevance and ease of maintenance under laboratory conditions. In the approach to simulate a simplified food web, *Tetrahymena pyriformis* was used as a prey organism for the amoeba. *Paramecium caudatum* as second prey organism, was analysed by Simona Mondellini and Michael Schwarzer (AG Laforch), and results considering this organism were generated mainly by them and are added as a comparison. These data are presented in the finished manuscript “Trophic transfer between unicellular protists: Microplastic accumulation in *Amoeba proteus* through *Tetrahymena pyriformis* and *Paramecium caudatum*” from Völkl, Mondellini et al. All organisms were cultivated as described in 2.17. In the case of using a specialised medium, the respective media composition will be described individually. As particles, PS<sub>0.5µm</sub> and PS<sub>6µm</sub> were used. Furthermore, larger fractions of particles were obtained from the department Macromolecular Chemistry I, University of Bayreuth, produced within the CRC 1357 cohort. Sieved red fluorescent PS particles in a size fraction of < 20 µm (PS<sub><20µm</sub>), 20 – 40 µm (PS<sub>20-40µm</sub>) and 40 – 75 µm (PS<sub>40-75µm</sub>) were used. The ζ-potential of the particles in the used amoeba medium and the precise size range was measured as characterisation by Julia Jasinski (Table 16).

**Table 16 Measured ζ-potential and size of the used MPP in the respective medium**

Particles were incubated overnight in the respective medium before measurement.

	ζ-potential [mV]				Size [µm]
	Prescott <sub>ref</sub>	Prescott <sub>NaCl</sub>	BSA	FCS	
PS <sub>0.5µm</sub>	- 53.4 ± 0.2	- 30.7 ± 0.2	- 24.8 ± 0.4	- 49.8 ± 0.3	0.5 ± 0.02
PS <sub>6µm</sub>	- 44.7 ± 0.5	- 12.2 ± 1.2	- 14.2 ± 1.1	- 49.3 ± 5.7	6.0 ± 0.6
PS <sub>&lt;20µm</sub>	n.a.	n.a.	n.a.	n.a.	16.1 ± 4.7
PS <sub>20-40µm</sub>	n.a.	n.a.	n.a.	n.a.	33.0 ± 9.8
PS <sub>40-75µm</sub>	n.a.	n.a.	n.a.	n.a.	49.9 ± 12.5

n.a.: not applicable due to size restrictions in the analyser. Prescott<sub>ref</sub>: standard Prescott medium, pH 6.4. Prescott<sub>NaCl</sub>: standard Prescott medium supplemented with 125 mM NaCl, pH 4.3. BSA: 2 % (w/v) bovine serum albumin in Prescott<sub>ref</sub>. FCS: 10% (v/v) Fetal calf serum in Prescott<sub>ref</sub>. Data represent mean ± SD, n = 3. Data was measured by Julia Jasinski

The ζ-potential of the particles varied for the respective media, with Prescott<sub>NaCl</sub> and BSA showing significantly lower surface charge values than Prescott<sub>ref</sub> and FCS. The ζ-potential could not be measured for larger particles due to limitations in the method, though a similar trend for these fractions can be assumed. The size ranges were located in the expected values.

### 6.1. Ingestion of particles in protists

At first, the possible ingestion of particles inside the test organisms was analysed. Both *T. pyriformis* and *P. caudatum* are filter feeders, unspecifically channel surroundings into their oral grooves [307]. The uptake of particles was therefore expected. In the case of *T. pyriformis*, though, only the smallest particles,  $PS_{0.5\mu m}$ , were ingested (Figure 45).

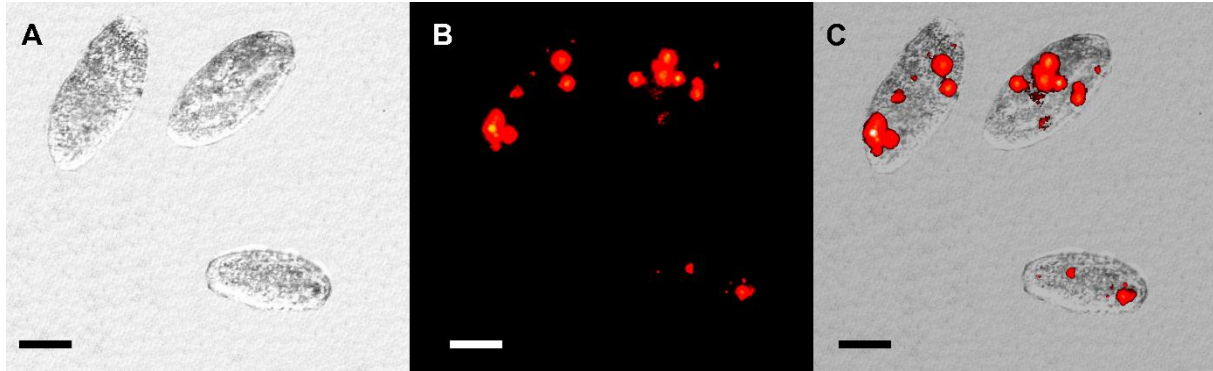


**Figure 45** Ingestion of  $PS_{0.5\mu m}$  by *T. pyriformis*

$PS_{0.5\mu m}$  engulfed after 1 h of incubation. A: bright field picture B: fluorescence microscopy C: merged overlay of A and B Scale bar = 50  $\mu m$ .

*P. caudatum*, on the other hand, engulfed particles up to the  $PS_{<20\mu m}$  fraction [308]. This observed difference in particle uptake between *T. pyriformis* and *P. caudatum* was most likely determined by the different sizes of the organisms (*T. pyriformis*: 60 – 100  $\mu m$ , *P. caudatum*: 180 – 300  $\mu m$ ). The ingested particles seemed to be incorporated into food vacuoles, which can be assumed due to the clumping of the particles in the delimited compartments. Due to this clumping, no exact particle number could be determined.

When analysing *A. proteus*,  $PS_{0.5\mu m}$  and  $PS_{6\mu m}$  were ingested, while the larger fractions could not be observed inside the organisms (Figure 46A-F). For the amoeba, quantification was possible by manually counting the particles inside the respective organism (Figure 46C/G).



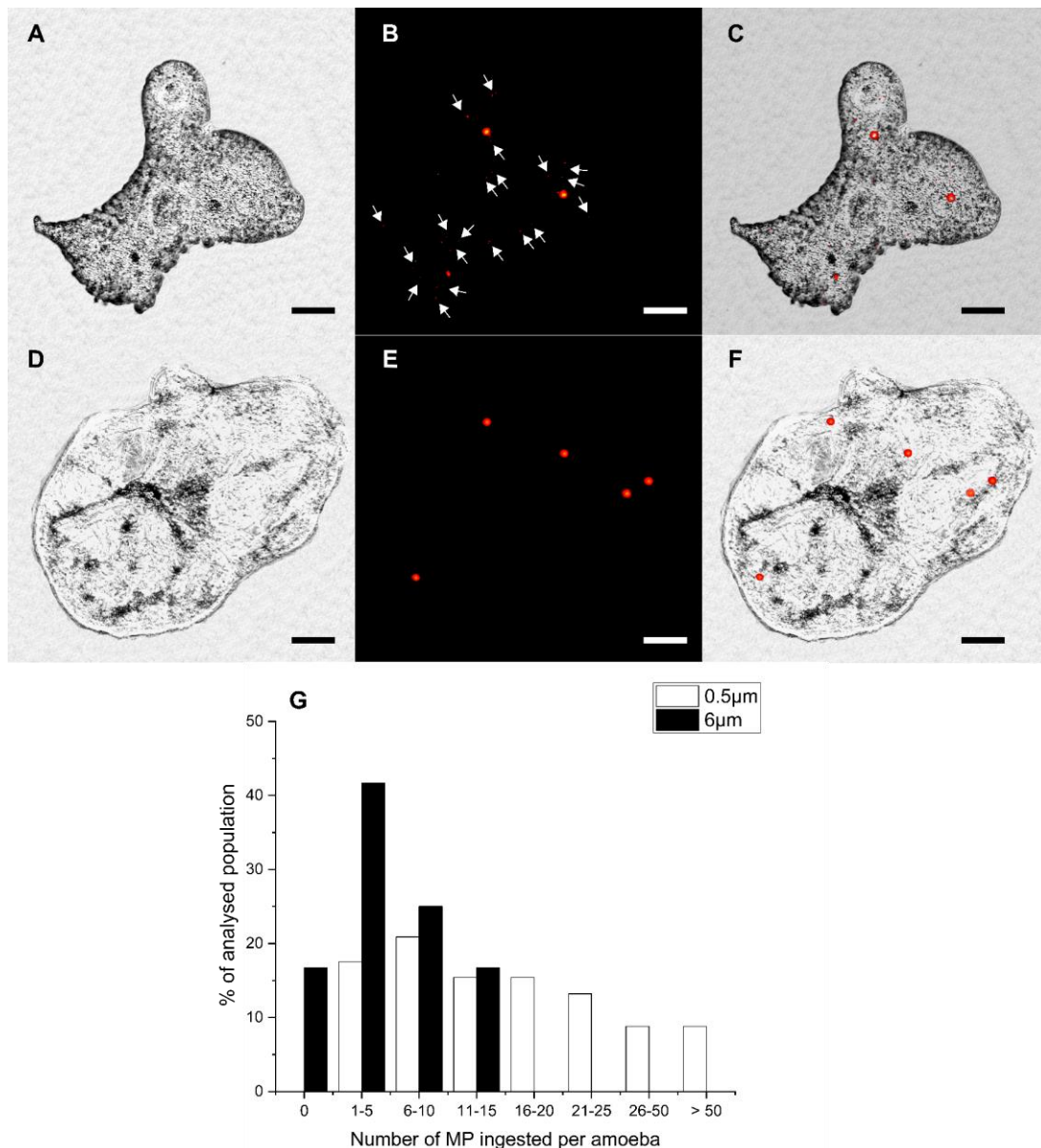


**Figure 46 Ingestion of  $PS_{0.5\mu m}$  and  $PS_{6\mu m}$  in *A. proteus***

A-F: Fluorescently labelled MP beads engulfed by *A. proteus* after 1 h of incubation visualised by fluorescence microscopy. A-C: *A. proteus* with  $PS_{0.5\mu m, red}$ , white arrows are included to indicate single beads better. D-F: *A. proteus* with  $PS_{6\mu m, red}$ . A/D: bright field picture B/E: fluorescence microscopy C/F: merged overlay of A/D and B/E Scale bar = 50  $\mu m$ . G: Quantitative analysis of the MP ingestion as a percentage of the analysed population,  $n = 91$  for  $PS_{0.5\mu m, red}$   $n = 12$  for  $PS_{6\mu m, red}$ .

For  $PS_{0.5\mu m, red}$ , the observed uptake showed a high deviation (average:  $18.8 \pm 18.1$  beads per amoebae, median: 14,  $n = 91$ ), ranging from one to > 50 particles per individuuum.  $PS_{6\mu m, red}$  were taken up at lower numbers, ranging between zero to 15 particles per amoeba (average:  $5.7 \pm 3.4$  beads per amoeba, median = 4,  $n = 12$ ). The observed size-dependent uptake is most likely associated with the uptake mechanism of the MP in the amoeba, which will be investigated in the next paragraph.



## 6.2. Analysis of the uptake mechanism in *A. proteus*

*A. proteus* ingests extracellular matter either via pinocytosis or phagocytosis. While both uptake pathways are initiated by the interaction between a solute/prey with membrane receptors on the surface of amoeba, *A. proteus* generally shows permanent but minor pinocytosis-driven ingestion. Pinocytosis channels in *A. proteus* can reach a diameter of up to 6  $\mu\text{m}$  <sup>[309]</sup>, which could be large enough for the uptake of small MP ( $\leq 6 \mu\text{m}$ ). The restricted uptake of particles  $\leq 6 \mu\text{m}$  is therefore hinting at the uptake of MP via pinocytosis. However, depending on the targeted receptor, channels (pinocytosis) or pseudopods (phagocytosis) can be formed with subsequent uptake of particulates <sup>[310]</sup>. Therefore, phagocytic uptake of particles under certain circumstances can not be excluded. Both uptake mechanisms can be induced (naturally and in the laboratory) to allow an adaptation to environmental conditions <sup>[309]</sup>. This will be utilised to confirm the preferred uptake mechanism of pinocytosis by separately stimulating the respective uptake mechanism. Pinocytosis can be induced artificially by the addition of organic substances (e.g., amino acids or proteins) <sup>[309]</sup>, increased salt concentrations <sup>[311]</sup>, or by lowering the pH value <sup>[312]</sup>. Here, Prescott<sub>ref</sub> was supplemented with 125 mM NaCl, and the pH was shifted to 4.3 by adding HCl as media. This pinocytosis-inducing media is referred to as Prescott<sub>NaCl</sub>. Indeed, an increased formation of pinocytosis channels could be observed when incubating the individuals for 20 min in Prescott<sub>NaCl</sub> (Figure 47)

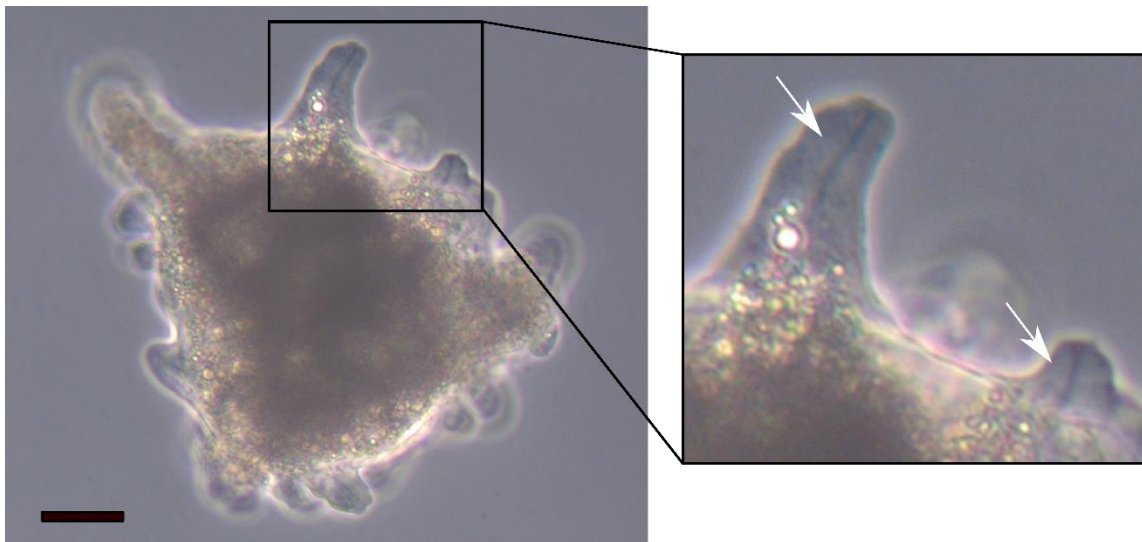


**Figure 47 Induction of pinocytosis channels in *A. proteus***

Pinocytosis channels in *A. proteus* after 20 min incubation in Prescott<sub>NaCl</sub> medium with a zoomed-in section of the pinocytosis channels for better visibility. Scale bar = 50  $\mu\text{m}$

When comparing the uptake of PS<sub>0.5 $\mu\text{m}$ , red</sub> particles in amoeba incubated in Prescott<sub>ref</sub> and Prescott<sub>NaCl</sub>, a significant difference in the uptake rate could be observed (Figure 48).

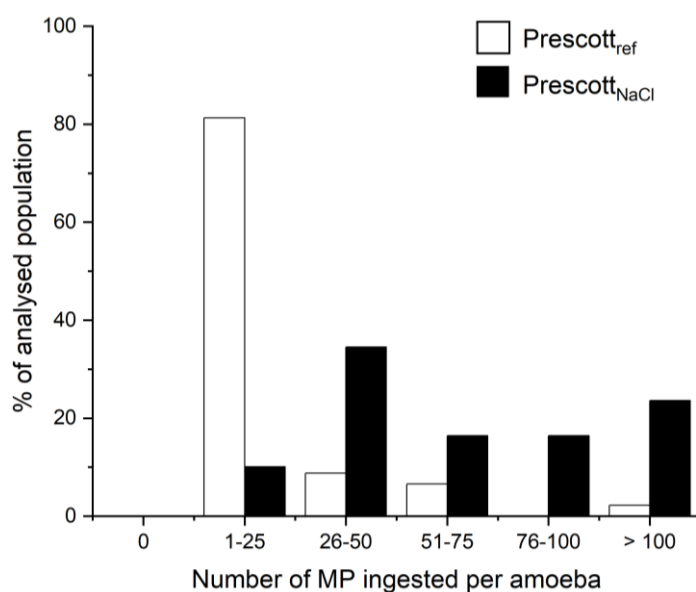


**Figure 48 Number of ingested particles after pinocytosis induction in *A. proteus***

Ingestion of  $PS_{0.5\mu m}$  in amoeba cultivated in Prescott<sub>ref</sub> and Prescott<sub>NaCl</sub> media to induce pinocytosis. Quantitative uptake analysis was done after 60 min incubation with  $PS_{0.5\mu m, red}$  in Prescott<sub>ref</sub> (white bars) and Prescott<sub>NaCl</sub> (black bars) media.  $n = 55$  for Prescott<sub>NaCl</sub>;  $n = 91$  for Prescott<sub>ref</sub>.

Amoebae cultivated in Prescott<sub>NaCl</sub> ingested about 3.8 - fold more  $PS_{0.5\mu m, red}$  (average:  $68.0 \pm 44.0$  beads per amoeba, median = 57,  $n = 55$ ) compared to Prescott<sub>ref</sub> (average:  $18.8 \pm 18.1$  beads per amoeba, median = 14,  $n = 91$ ). Whereas most amoebae ingested 1 to 25  $PS_{0.5\mu m, red}$  beads in Prescott<sub>ref</sub> medium, the number of ingested beads per organism follows a higher and broader distribution after incubation under pinocytic conditions, with some individuals absorbing more than 100 particles.

Phagocytosis, on the other hand, might be triggered chemically through receptor pathways as well as mechanically by the movement of the prey<sup>[310,313,314]</sup>.  $PS_{20-40\mu m}$  and  $PS_{40-75\mu m}$  were coated with BSA (well-characterised, single protein type) or FCS (mixture of non-characterised proteins) to create a protein corona on the particles and subsequently added to the amoeba. Nevertheless, no uptake of these particles could be observed. Either way, the proteins were not adequate to induce a phagocytotic uptake, or the mechanical movement might have been lacking. However, other groups showed the phagocytosis of spherical agarose beads (10 – 40  $\mu m$ ) coated with proteins (e.g.,  $\alpha$ -lactalbumin, RNase A)<sup>[310,315]</sup>. Interestingly though, the uptake efficiency was highly dependent on the protein type. Some coatings increased the ingestion, while others showed no significant difference. In this case, the lack of phagocytosis of the protein-coated MP can only be speculated upon and might be linked to a non-adequate surface charge or the lack of an eco-corona or a biofilm. Both these parameters are described to significantly increase their uptake and biological effects in different organisms<sup>[64,316]</sup>. Surface charge and size of MP were shown to be critical parameters for the ingestion of MP by ciliates as well for the phagocytic ingestion by murine macrophages<sup>[71,115,194]</sup>. The same could be hypothesised for *A. proteus* as well.

In a second attempt to trigger phagocytosis, a mixture of fragments (PS<sub>20-40µm</sub>, PS<sub>40-75µm</sub>), *T. pyriformis* and *A. proteus* was co-incubated to assess whether a known chemical or mechanical trigger (evoked by the prey organisms) could activate phagocytosis. Either way, while prey organisms were engulfed, no uptake of particles could be observed, indicating that *A. proteus* does not ingest MP via phagocytosis under these experimental conditions. This indicates that amoebae can discriminate between prey and MP fragments and that soluble substances released by *T. pyriformis* <sup>[317]</sup>, if any, are insufficient to induce an inadvertent uptake of large MP fragments. Mast and Hahnert (1935) showed that *A. proteus* mainly feeds on living organisms, indicating that the motility of the prey might be an important co-stimulus for ingestion <sup>[318]</sup>, which could explain the absence of phagocytic uptake of inert MP as well.

Combining the results of the experiments, it is plausible to conclude that the pinocytotic pathway is responsible for the internalisation of PS<sub>0.5µm, red</sub> and PS<sub>6µm, red</sub> in *A. proteus*. In the case of phagocytosis, the recognition and ingestion of the prey is a complex process and might be influenced by many parameters. The detailed process varies for not only different prey organisms but also different amoeba strains <sup>[319]</sup>. Therefore, although phagocytosis could not be observed in these experiments, a phagocytic uptake of MP in amoeba in the natural environment cannot be excluded.

### **6.3. Possible transfer of microplastic through trophic levels via a simplified food chain**

Another possibility of particle ingestion inside amoeba might be via a transfer along the food web. Before this experiment, the retention time of ingested particles inside the prey and the predator was analysed (Figure 49).

For *T. pyriformis*, only a few individuals without particles could be observed initially (Figure 49A). Over time, the fraction with no particle uptake increased to 25 % after 24 h. As mentioned above, an exact determination of the number of ingested beads was not possible. Individuals were therefore divided into two groups (“particle uptake” or “no uptake”) by estimating the presence of visible intracellular MP under the microscope. The increase in the “no uptake” group was probably a result of a thinning out of the particles due to cell division.

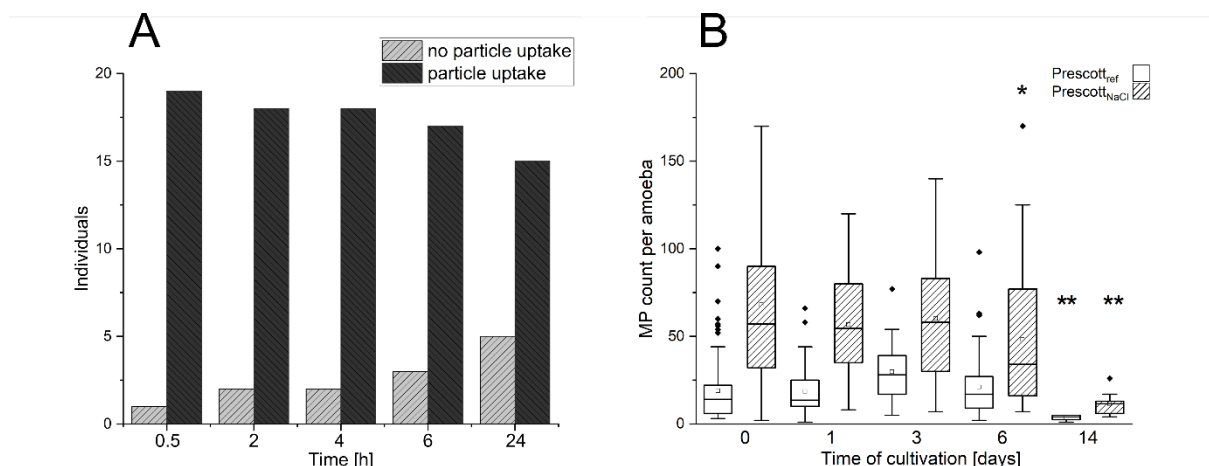


**Figure 49 Retention time of particles after ingestion in *T. pyriformis* (A) and *A. proteus* (B)**

A: *T. pyriformis* were incubated with  $PS_{0.5\mu m, red}$  (end concentration:  $3.6 \times 10^7$ /mL) in Prescott<sub>ref</sub> medium for 60 min and were afterwards placed into fresh Prescott<sub>ref</sub> medium for the remaining time of the incubation. Individuals were analysed at the respective time for particle uptake;  $n = 20$ . B: Amoebae were incubated with  $3.6 \times 10^7$   $PS_{0.5\mu m, red}$ /mL in Prescott<sub>ref</sub> and Prescott<sub>NaCl</sub> media for 60 min and were thereafter placed into Prescott<sub>ref</sub> medium for the remaining time of the incubation. Prescott<sub>NaCl</sub> medium was used to induce pinocytic conditions,  $n$  Prescott<sub>ref</sub> day 0 = 91, day 1 = 62, day 3 = 36, day 6 = 52, day 14 = 8;  $n$  Prescott<sub>NaCl</sub> day 0 = 55, day 1 = 34, day 3 = 39, day 6 = 46, day 14 = 10. Significance level: \* = significantly lower than at day 0, \*\* = significantly lower compared to all other data.

In the case of *P. caudatum* (analysed by Simona Mondellini,  $n = 15$ ),  $PS_{0.5\mu m, red}$  could be found in all observed individuals after 24 h, despite an active excretion could be observed [320]. The released particles were probably re-ingested, and due to the high amount of ingested  $PS_{0.5\mu m, red}$  particles, a complete discharge of particles in one individual was not observed. A higher amount of individuals without MP was observed after 0.5 h (25 %) in the case of  $PS_{<20\mu m}$ . Similar to *T. pyriformis*, the number of individuals without particles increased over time, resulting in 75 % of individuals without ingested MP after 24 h.

For amoeba, individuals were incubated with  $PS_{0.5\mu m, red}$  either in Prescott<sub>ref</sub> or Prescott<sub>NaCl</sub> medium, and the ingested number of MPP per amoeba was recorded for up to 14 days of incubation (Figure 49B). Regardless of the initial amount of  $PS_{0.5\mu m, red}$  ingested on day 0 (Prescott<sub>ref</sub>: average 18.8 beads per amoeba, median 14; Prescott<sub>NaCl</sub>: average 68 beads per amoeba, median 57), a significant decrease in the number of particles per amoeba was not observed within the first three days of incubation. Morphology and locomotion, which are indicators of cellular fitness, did not differ from the corresponding control group during this period. After six days of incubation, a statistically significant 1.7 - fold reduction in MPP count was observed only for amoeba primed in Prescott<sub>NaCl</sub> (median<sub>day 0</sub>: 57; median<sub>day 6</sub>: 34), indicating some degree of egestion of MPP. Egestion is also likely to occur for amoeba primed in Prescott<sub>ref</sub>, but it was not detectable due to the large deviation in MPP counting. After 14 days, the remaining  $PS_{0.5\mu m, red}$  per amoeba was low for both populations (Prescott<sub>ref</sub> median: 4; Prescott<sub>NaCl</sub> median: 11.5). However, the long retention time of particles in all protists possibly enables a transfer along the food web.

To analyse this, prey organisms (*T. pyriformis* and *P. caudatum*) were initially fed with particles ( $PS_{0.5\mu m, red}$  for *T. pyriformis* and  $PS_{<20\mu m}$  for *P. caudatum*). These organisms were afterwards co-cultivated with amoeba to analyse whether particles could be found inside the predator. The ingestion of prey with and without MPP (control group) by amoeba was equal. For both *T. pyriformis* and *P. caudatum*, approximately 70 % of the amoeba population exhibited protists with MPP in their food vacuoles after 3 to 6 h of incubation (Figure 50).

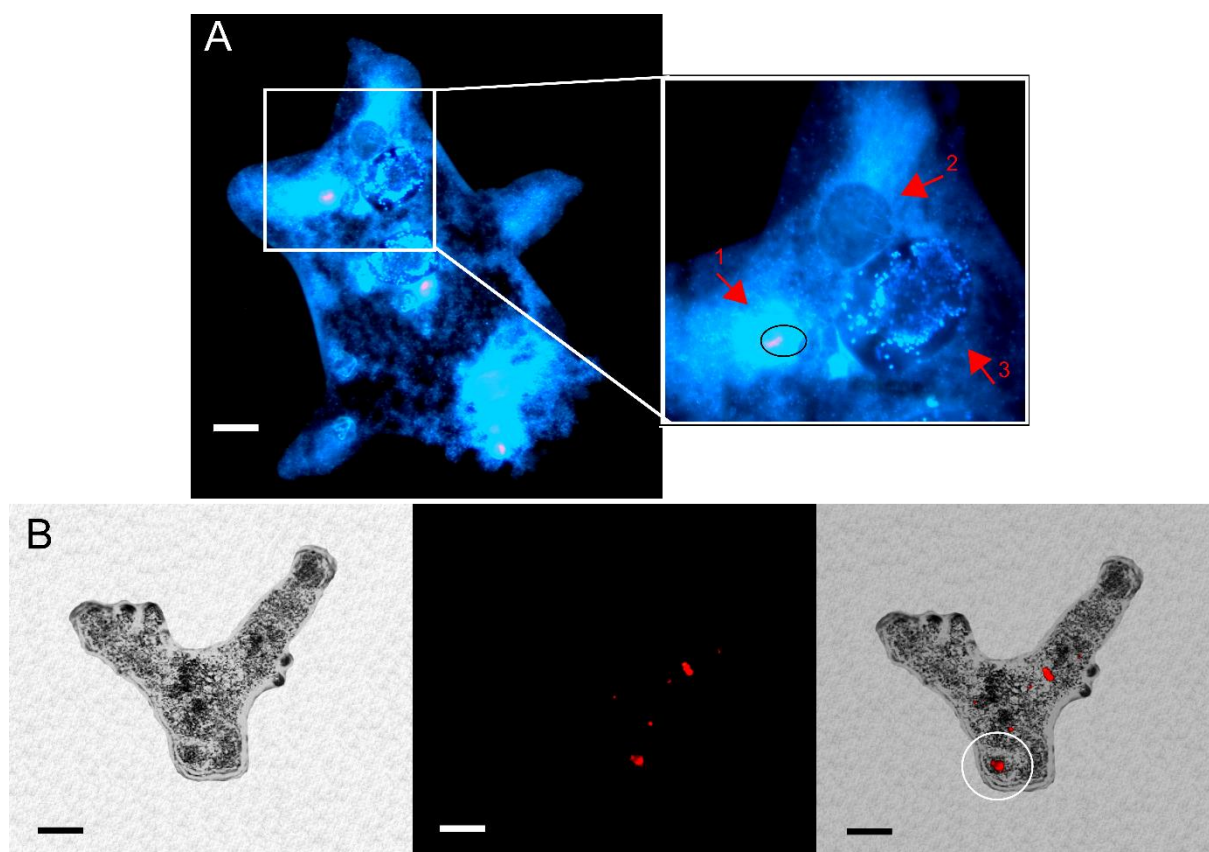


**Figure 50** Ingestion of  $PS_{0.5\mu m}$  loaded *T. pyriformis* by *A. proteus*

A: *T. pyriformis* loaded with  $PS_{0.5\mu m}$ , incubated for 6 h. *A. proteus* stained with 25  $\mu g/mL$  Hoechst 33342 to visualise the ingested *T. pyriformis*. Arrow 1: stained *T. pyriformis* with ingested  $PS_{0.5\mu m}$  (Black circle). Arrow 2: contractile vacuole, Arrow 3: amoeba nucleus. Scale bar = 25  $\mu m$  B: *A. proteus* with clumped  $PS_{0.5\mu m}$  24 h after ingestion of *T. pyriformis*. Beads are clumped in a food vacuole and not as distributed as beads taken up by pinocytosis. Left panel: bright field; middle panel: fluorescence; right panel: merged picture. White circle identifies a food vacuole. Scale bar = 50  $\mu m$ .

Clumped beads were still visible in food vacuoles 24 h after ingestion in cases where the amoeba ingested MP-loaded cells or  $PS_{0.5\mu m}$  beads (Figure 50B). This suggests that the inedible MP remains inside the food vacuoles during the digestion process of the prey. However, after 24 h (for  $PS_{<20\mu m}$  fragments) and 72 h (for  $PS_{0.5\mu m, red}$ ) post-ingestion, less than 10 % of the amoeba contained detectable amounts of MP. Observations revealed that after the digestion of the ciliates, there was an egestion of the MP (Figure 51).

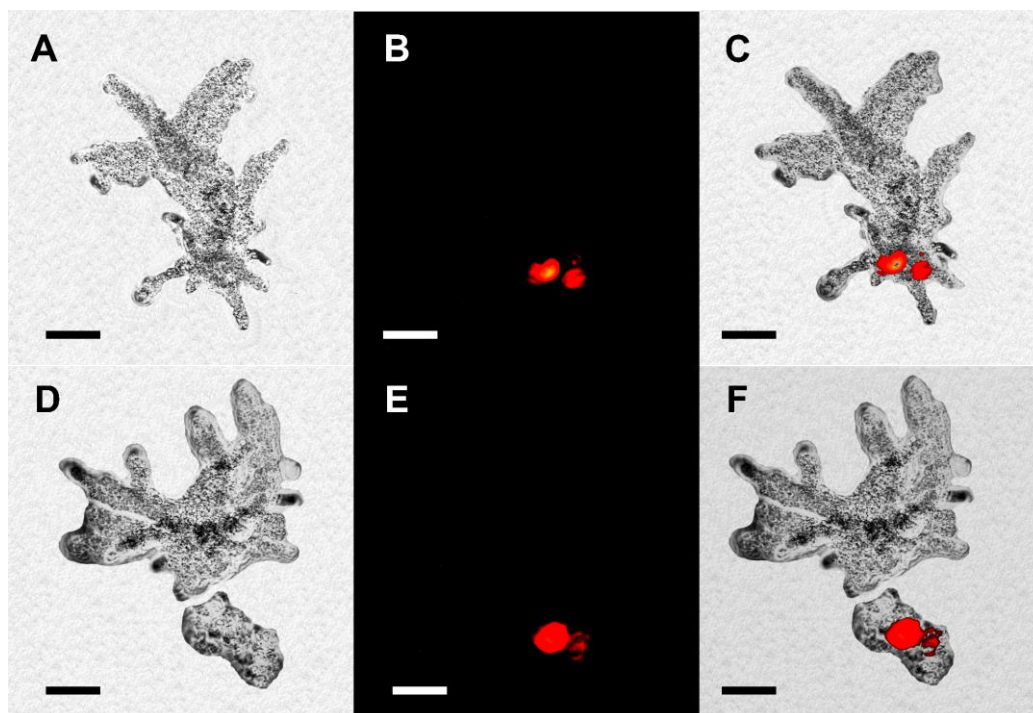


**Figure 51 Excretion of  $PS_{<20\mu m}$  by *A. proteus***

Excretion of  $PS_{<20\mu m}$  and inedible leftovers 24 h after uptake of *P. caudatum*. A-C: Amoeba shortly before the excretion process of two large MP fragments taken up by an individual *P. caudatum*. D-F: Same amoeba 15 min later. Both fragments and inedible leftovers are excreted. Left panel: bright field; middle panel: fluorescence; right panel: merged. Scale bar = 50  $\mu m$ , size of the fragments seems larger, due to their presence in different layers, which resulted in a deformation of the quantum dot. *P. caudatum* was provided by Simona Mondellini and Michael Schwarzer

Interestingly, MPP, small and large alike, that enter via loaded prey were actively excreted by the amoebae after at most 24 h compared to particles ingested by pinocytosis, which remained for at least seven days inside the amoeba. It is known that inedible matter like glass, carbon beads, or indigestible remnants of prey organisms, such as the cuticle of small cladocerans, are excreted shortly after digestion <sup>[318]</sup>. In favourable conditions, though, *A. proteus* is capable of ingesting up to 70 protists per day, which in turn can take up hundreds of MP of various sizes per cell. If the ingestion rate exceeds the excretion rate, possible bioaccumulation of inedible, non-nutritive material at low trophic levels can be proposed, posing a potential hazard to these organisms and their predators.

#### 6.4. Summary and Conclusion

The results showed a fast and size-dependent particle uptake by *T. pyriformis* and *P. caudatum*, while *A. proteus* only took up MPP directly through pinocytosis. Larger fragments could be indirectly ingested by *A. proteus* while feeding burdened prey, which acted as vectors for MP. In amoeba, the uptake pathway (pinocytosis vs phagocytosis of MP-burdened prey) had a significant impact on the fate of the MP. Pinocytic ingested particles remained for up to 14 days, while phagocytic ingested MP through burdened prey was actively excreted, suggesting the presence of selective intracellular mechanisms. The bioaccumulation of MP in freshwater unicellular eukaryotic organisms was therefore found to be



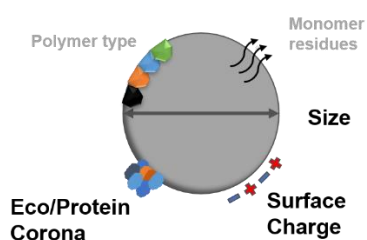
dependent on the particle size and uptake mechanism. Especially smaller MP ( $\leq 6 \mu\text{m}$ ) pose a risk of transfer through trophic levels due to the lack of excretion mechanism in some unicellular organisms and high uptake and availability rates. Overall, this study demonstrated that protists might accumulate MP and highlights the need to consider this risk when assessing MP contamination.

Naturally, a comparison with the mammalian cell culture proves not nearby. However, especially when considering the transfer through the trophic levels, interesting knowledge for the exposure of higher organisms might be observed. The transfer of MPP along the food web is a major factor in the MPP burden of organisms on a higher trophic level. Since this study showed a higher probability for smaller particles to be transferred along the food web, the amount of these particles ultimately ending at the top of the food chain might also be higher. These small particles are furthermore more likely to be ingested by cells, increasing the probability of accumulation and, consequently, the hazardous potential. Certainly, more experiments with, e.g. more complex food webs, higher trophic levels or usage of different particles have to be performed to understand this complex process better.

## 7. Summary and outlook

In summary, this work used advanced culture techniques to create a better understanding of microplastic toxicity. Through the use of pristine, well-characterised microplastic particles, key parameters responsible for inducing toxic effects were identified on a single-cell basis and transferred to more complex microtissue structures and cell cultivation approaches (Scheme 23). Especially the particle-cell interaction, primarily determined by factors such as the surface charge, protein corona and size of the particles, proved highly relevant to trigger effects. However, toxic responses from these pristine particles only arose for relatively high concentrations of  $> 250 \mu\text{g/mL}$ . Interestingly, the artificial ageing of these particles as well as the usage of paint particle fractions, decreased the critical concentration significantly (in order of magnitude) and resulted in distinct cellular reactions towards the different particle types. Next, this study transferred these findings to microtissues using the transwell assay and spheroid cultivation. Penetration studies revealed a piercing of particles into microtissues, as well as a dysfunctional formation of spheroids under the presence of microplastic particles. Results from distribution and excretion studies found no active cellular mechanisms to egest the particles. Finally, previous findings of this work were transferred to more complex primary cells or model organisms. While using primary intestinal cells from *E. fetida* proved to be a promising start, additional methods are needed to transfer results to an organismic level. The usage of *A. proteus* and *T. pyriformis* as model organisms for the lower trophic levels provided insights into bioaccumulation and possible transfer along the food web. Pinocytosis was identified as the main uptake mechanism, resulting in a preferred ingestion of particles  $\leq 6\mu\text{m}$ .

**Parameters increasing Particle-Cell interaction are highly relevant**

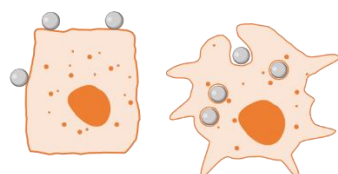


**Artificially weathered particles increase cytotoxicity significant**

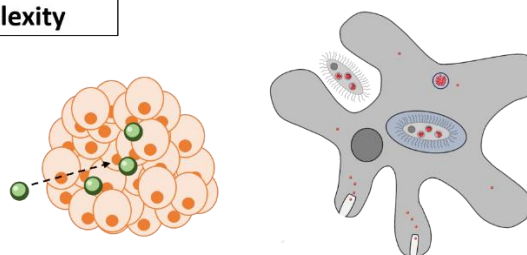


**Complexity**

**Cytotoxicity at high concentrations  
Accumulation in cells**



**Penetration into microtissues  
/ Bioaccumulation**



*Scheme 23 Conclusions of the main findings*



In conclusion, this study highlights the importance of considering the particle-cell interaction in the context of microplastic toxicity. Additionally, it highlights the importance of employing particles more representative of the realistic environmental burden when conducting risk assessments. The findings suggest that the accumulation of microplastics in cells or tissues potentially has detrimental effects. Finally, the study highlights the potential risks associated with the transfer of microplastic particles along the food web.

It is highly recommended that subsequent research is perpetuated in this context. The further usage of weathered MP is hereby of high relevance. Different ageing or weathering methods might induce different outcomes. One possibility is the usage of enzymatically aged particles. The research on enzymes to degrade plastic, e.g. for use in waste management, is increasing <sup>[321,322]</sup>. However, particles aged this way might again trigger different effects than pristine ones. Due to the enzymatic degradation, reactive surface groups can arise, which proved as one main driver for increasing cytotoxic effects. Furthermore, plastic additives contribute to an increase in cytotoxicity <sup>[323]</sup>. It is therefore recommended to extend the analysis to particles with a known amount of additives. Either way, a comprehensive characterisation of the used particles or the self-dependent production of in-house particles can hereby be useful. Furthermore, the ageing mechanism of different polymer types can be an influencing factor. It has already been shown that polystyrene <sup>[6]</sup> and polyethylene <sup>[324]</sup> behave differently during an identical ageing process. Differing effects of these particles on cells or organisms can therefore be as well expected. Finally, the morphological aspect of the analysed fragments can be taken into more consideration. Fibres, e.g., are among the most frequently ingested microplastic fragments <sup>[325]</sup>. Expanding knowledge in these directions bears high potential. To analyse the named parameters, the here established assays and methods are highly promising and cover some of the most frequent stressors of microplastic research.

Furthermore, methods to analyse the chronic effects of MP burden also need to be established. As shown in this work, no active excretion of particles was observed in macrophages, and particles were found to penetrate spheroids. An accumulation of MP over time is, therefore, likely. A cumulative burden over an increasing period or a one-time load and an effect kinetic over several days might reveal further effects. This can be expanded from the 2D cell cultivation level to the 3D microtissue approach.

It is furthermore highly important to understand effects on a mechanistic level. Especially inflammation, which is highly connected with the polarisation of macrophages, is a known *in vivo* effect of MP. The so-called “Plasticosis” was recently proven in seabirds, a fibrosis induced especially by MPP <sup>[21]</sup>. As the first step, the interaction of particles with macrophages in different polarisation states was analysed in this work. Identifying parameters that cause activation or trigger special inflammation

pathways could also help understand effects *in vivo*. It might further explain the different behaviour of cell subpopulations, which could be detected in this work. These subpopulations could be analysed separately by applying the single cell sorter used in this work or establishing new methods like fluorescence-activated cell sorting (FACS). This might improve data sets since effects can be dedicated to cells with a specific particle load.

Increasing the complexity of cell cultivation proved highly beneficial in this work. The proposed workflow from this work can enable a mechanistic understanding of the accumulation and distribution of MPP in microtissue. The range of analytical methods applied to the thin sections needs to be expanded. Various histological analyses, immunohistochemistry, mass spectrometry, and infrared-sed imaging can be used hereby <sup>[301,302]</sup>. These methods can provide a deeper understanding of the role of MPP in tissue. Furthermore, the co-cultivation system of spheroids with macrophages showed promising results. Other analysis methods for the invasion of spheroids, like e.g. the cytofluorimetric analysis of spheroid invasion (CASI), can locate and determine the fate of macrophages in spheroids. The next step in the complexity of cell cultivation would be the dynamic cultivation of microtissues. On the one hand, cultivation duration can be highly expanded in bioreactors. On the other hand, a mechanical force (via e.g. media flow) can be introduced to the MP, which can be seen as more *in vivo* like. Particles travelling through the gastrointestinal tract are likely to be squeezed against the epithelial layer, which could not be mimicked by the assays used this far.

Finally, more information and analysis methods need to be established to transfer results from primary cell cultivation to effects on the organismic level. One approach might be the additional usage of coelomocytes, the immune cells of earthworms. Isolation and cultivation protocols exist in the literature, simplifying the establishment. Other methods to analyse the cells, like, e.g. inflammation, genotoxicity or ROS, could also be approached to understand the possible effects of MPP on a cellular level. Furthermore, the protocol for isolating the intestinal cells can be extended to the formation of microtissue (e.g. spheroids). Possible usage of extracellular matrix might provide the required stability for the cells. This will help by consolidating results from the *in vitro* studies and transferring this knowledge to the organismic level.

## 8. Appendix

### 8.1. Data availability for RNA<sub>seq</sub> raw data

The raw RNA-Sequencing data were deposited at NCBI's Sequence Read Archive (SRA) under Bioproject number PRJNA785767.

### 8.2. Supplementary figures and tables

*Table S1 Overview of MPP concentrations used for Figure S1 and Figure S2*

Particle size [μm]	Low concentration (particles/cell)	High concentration (particles/cell)
0.2	10	100000
0.5	10	10000
1	10	1000
2	10	400
3	10	100
6	2	25

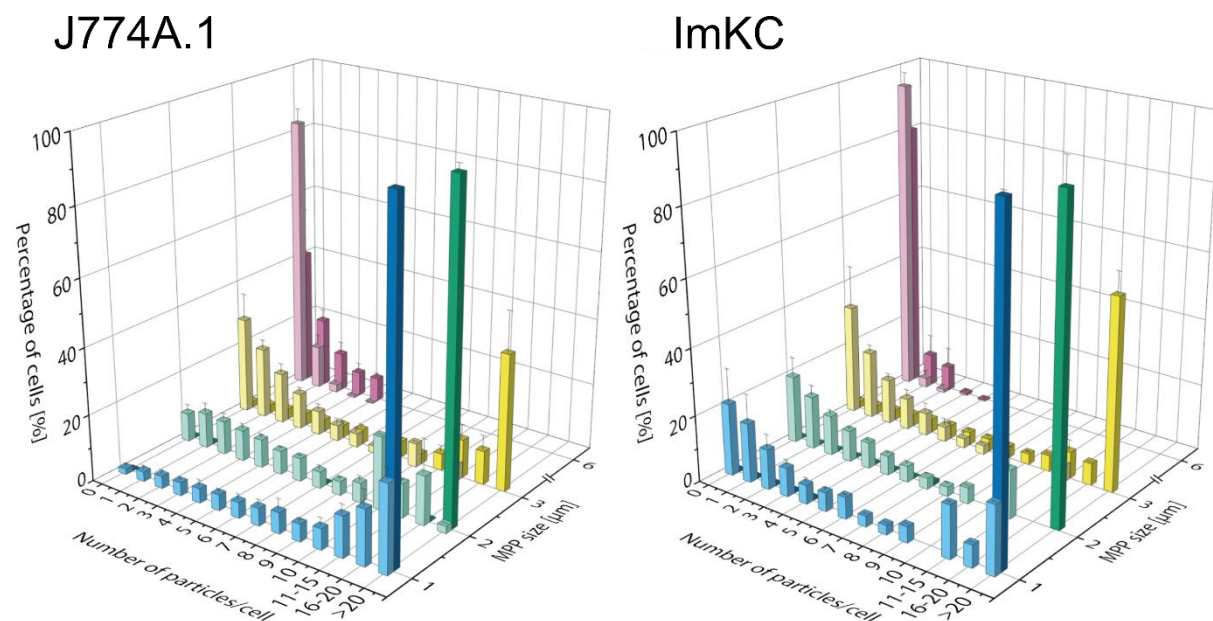
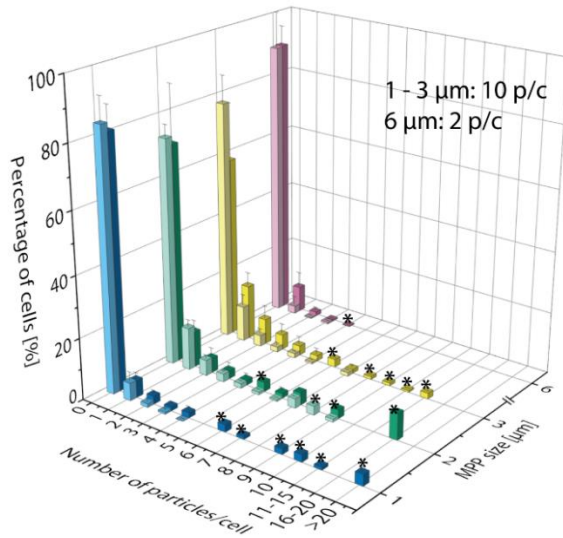


**Figure S1 Analysis of PCI as a function of size, concentration and cell line via flow cytometry using the established method**

Analysis was performed using FC with J774A.1 and ImKC cells. Shown are the percentage of cells in correspondence to the number of interacting particles per cell and the size of the particles. Light colors represent low concentration, dark colors the high concentration of MPP (see Table S1). Note that no data was available for 0.2 and 0.5 μm particles due to lacking resolution of the flow cytometer. The calculation of the number of interacting particles per cell is based on the fluorescence intensity of the particles (3.1.1). Data represent mean ± SD, n = 3. Figure is from Rudolph, Völkl et al. 2021.

## Low concentration



## High concentration

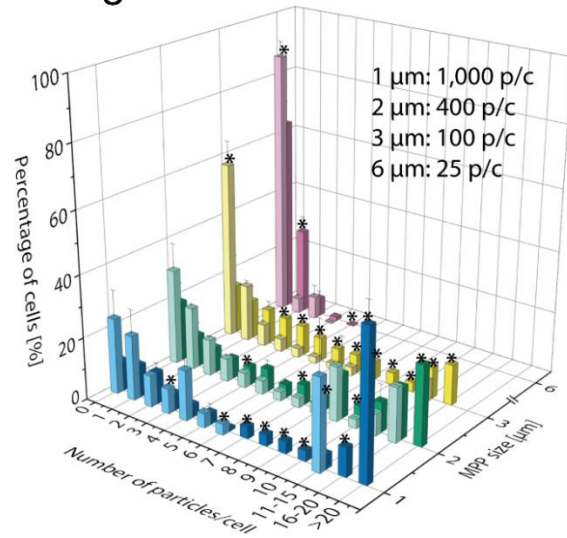


**Figure S2 Analysis of PCI as a function of size, concentration and cell line via flow cytometry using the established method**

Analysis was performed using FC with STC-1 (light colour) and BNL CL.2 (dark colour) cells. Shown are the percentage of cells corresponding to the number of interacting particles per cell and the size of the particles. Note that no data was available for 0.2 and 0.5  $\mu\text{m}$  particles due to lacking resolution of the flow cytometer. The calculation of the number of interacting particles per cell is based on the fluorescence intensity of the particles (3.1.1). Data represent mean  $\pm$  SD,  $n = 3$ . Figure is from Rudolph, Völkl et al. 2021. Figure is from Rudolph, Völkl et al. 2021.

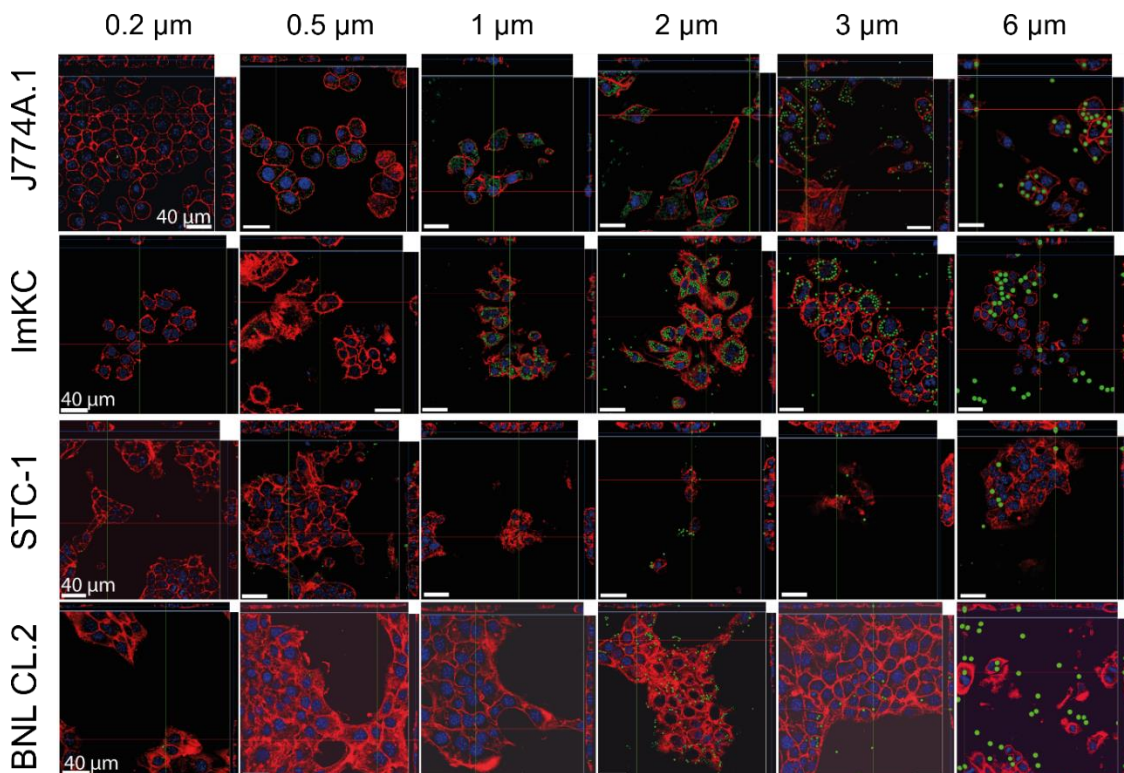


**Figure S3 Verification of particle uptake by CLSM**

Actin filaments were stained with rhodamine-phalloidin (red), nuclei were stained with DAPI (blue), FITC-fluorescent MPP are shown in green. Scale bars: 40  $\mu\text{m}$ . Figure is adapted from Rudolph et al. 2021.

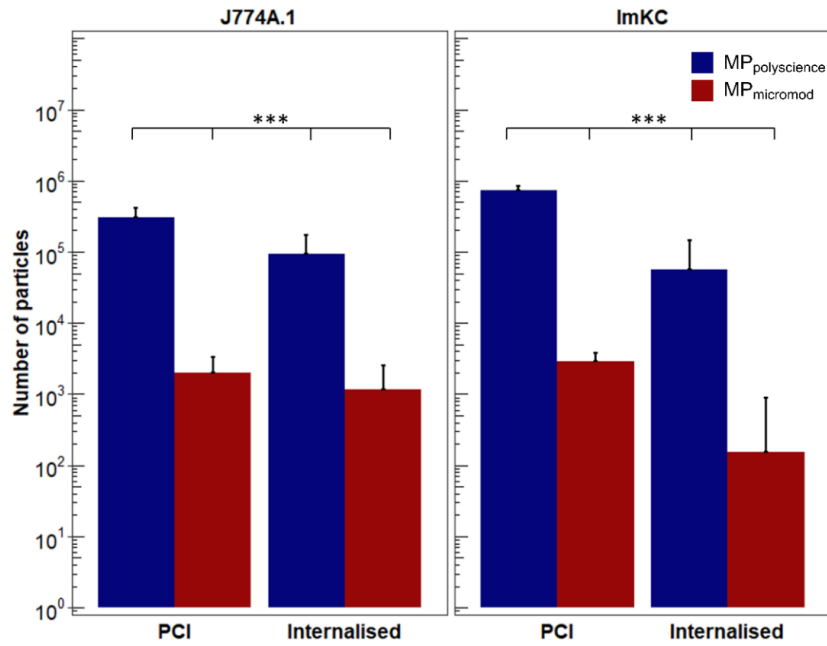


**Figure S4 Comparison of the PCI and internalisation rate of  $MP_{polyscience}$  and  $MP_{micromod}$  for J774A.1 and ImKC cells.**

The numbers of particle-cell interactions and internalised microplastic particles were counted by confocal microscopy and standardised to 20,000 cells for better comparison, as the relative cell area on a coverslip for both cell lines differed. Data points represent mean + SD,  $n = 300$  images ( $MP_{polyscience}$  &  $MP_{micromod}$  J774A.1,  $MP_{polyscience}$  ImKC),  $n = 41$  images ( $MP_{micromod}$  ImKC), significance level: \*\*\*=  $p \leq 0.001$ . Figure is adapted from Rampsberger, Jasinski, Völkl et al. (2022) and modified.

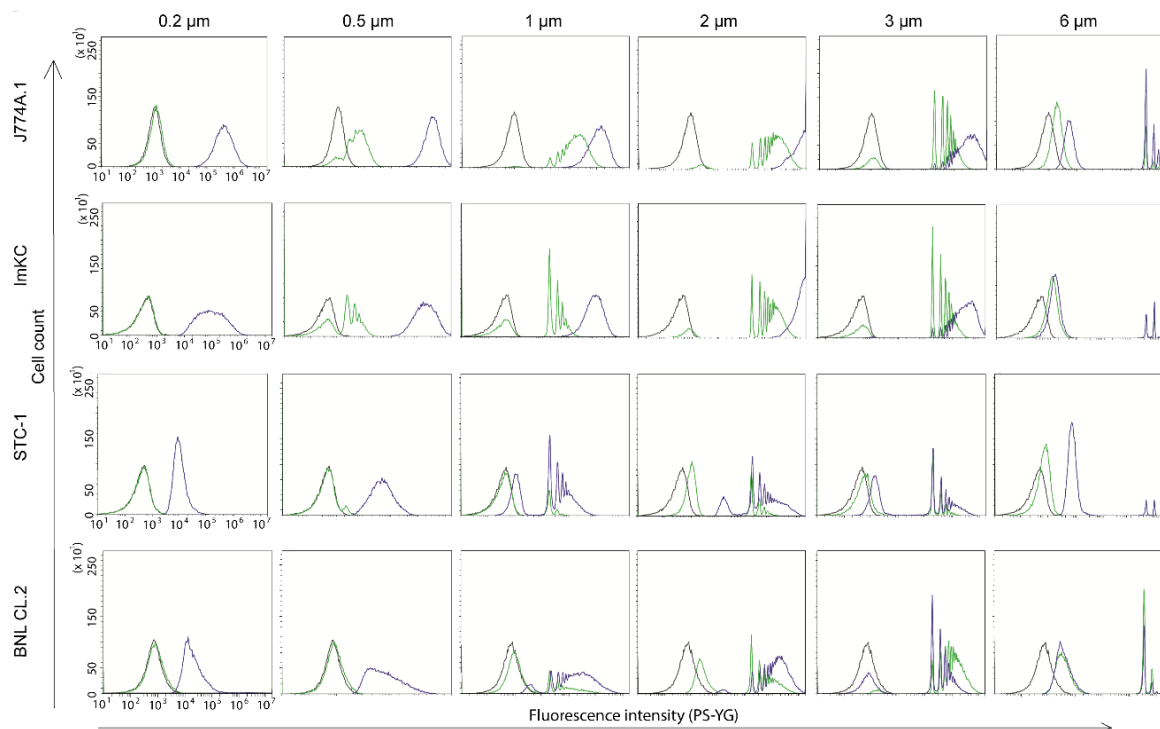


**Figure S5 Calculation of particles per cell based on flow cytometry data.**

Shown is one replicate of each measurement. Grey: control without particles, green: low MPP concentration, blue: high MPP concentration. Figure is adapted from Rudolph et al. 2021.

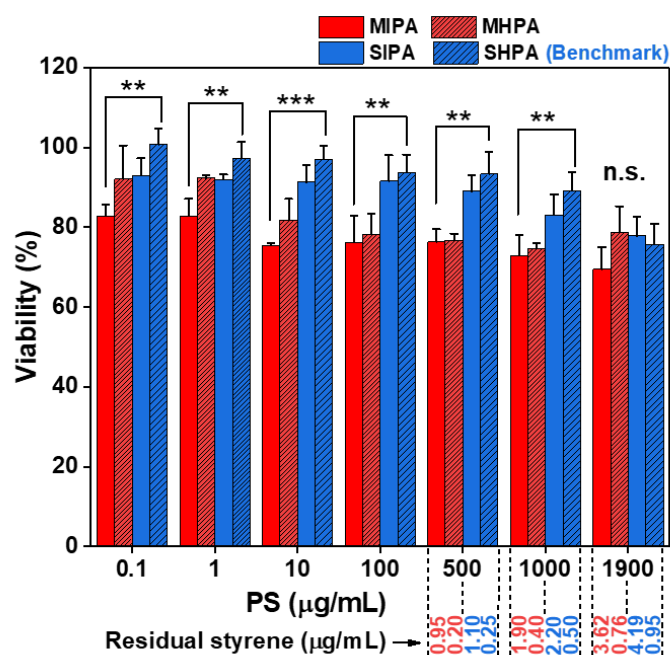


**Figure S6 L929 cell viability for in-house synthesised PS particle dispersion and standard PS model particle dispersion.**

MIP: standard PS model particles dispersion used as received; MIPA: MIP after autoclave; MHP: MIP after rapid dialysis against methanol/water (50/50) mixed solvents; MHPA: MHP after autoclave; SIP: in-house synthesised PS particles dispersion after 40 days dialysis against Milli-Q water; SIPA: SIP after autoclave; SHP: SIP after rapid dialysis against methanol/water (50/50) mixed solvents; SHPA: SHP after autoclave. One-way ANOVA with a Tukey post hoc test was performed to show significant differences between treatments with synthesised and standard PS, \*  $P = 0.05$ , \*\*  $P = 0.01$ , \*\*\* $P = 0.001$ . Figure from Zhang et al. 2023 (accepted paper)



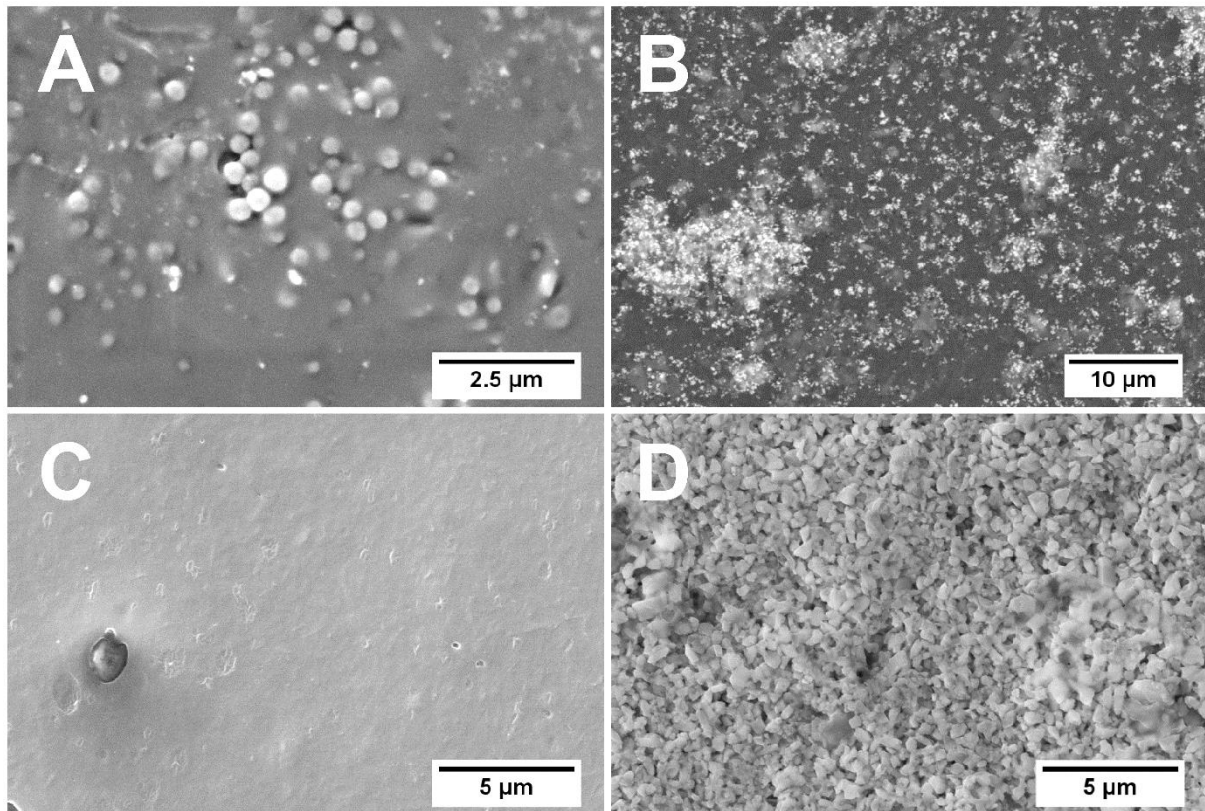


**Figure S7 SEM images of paint fractions at the position of EDX measurement**

Figures show SEM images of A) paint 1 supernatant, B) paint 1 sludge, C) paint 2 supernatant, and D) paint 2 sludge. Figure is from Müller et al. (2022)

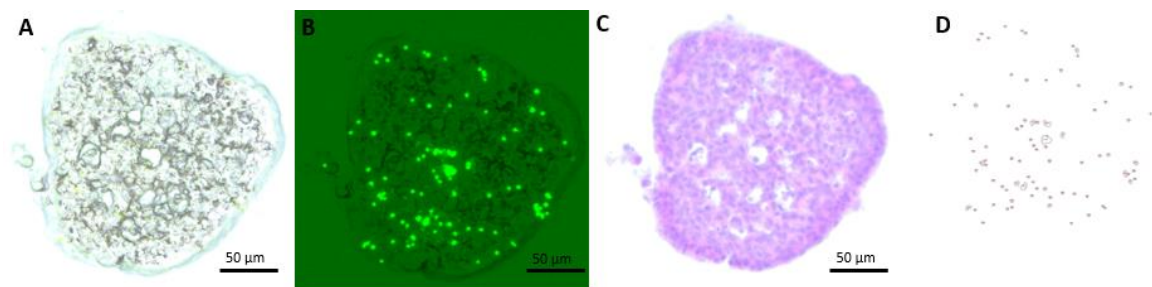


**Figure S8 Exemplary images of stained sections of spheroids challenged for 24 h with 2  $\mu$ m MP particles**

**A:** Brightfield microscopic image of a spheroid section (10  $\mu$ m thickness); **B:** Fluorescence microscopic image of the same section as shown in **A**, particles show green fluorescence; **C:** Section now stained with H&E. **D:** automated particle count of the particles shown in **B** (Fiji ImageJ software). Figure is adapted from the finished manuscript Völkl, Ritschar et al. (2023) and was produced by Sven Ritschar

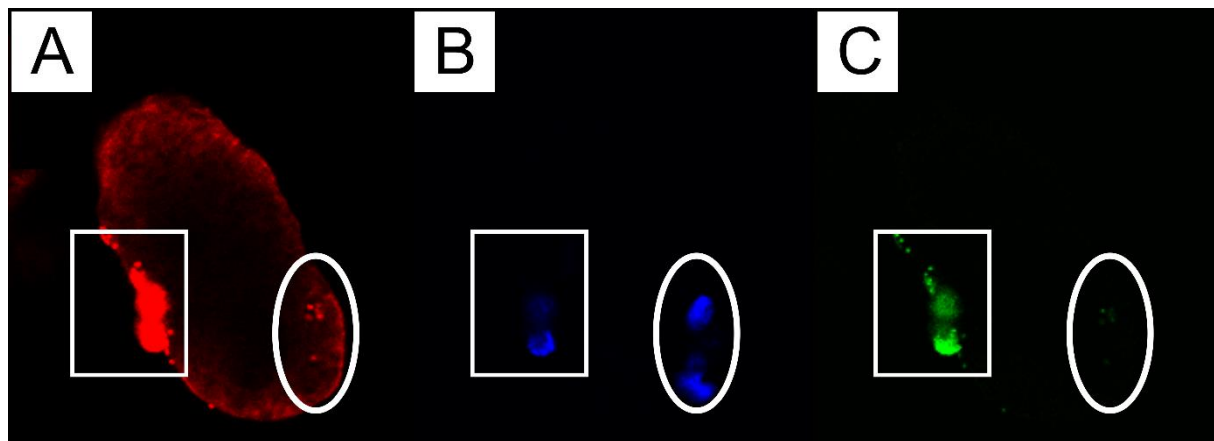


**Figure S9 Confocal microscopy of spheroids with macrophages incubated with MPP**

5 days after the initial formation of the spheroids,  $1 \times 10^5$  particles were added for 24 h. After a washing step to remove unbound particles, 500 macrophages were added to a single spheroid. To further allow tracking of the macrophages via fluorescence or confocal microscopy, macrophages were stained with  $5 \mu\text{M}$  CTV before adding to the unstained spheroid. Only rhodamin-phalloidin was used when staining the spheroid afterwards. While BNL CL.2 cells were only stained red (A), macrophages showed additional blue fluorescence (B) to differentiate both cell types. Combined with the green fluorescence of the used particles (C), specific targeting of particles by macrophages could be tracked. Figure is adapted from the finished manuscript Völkl, Ritschar et al. (2023) and was produced by Julia Jasinski



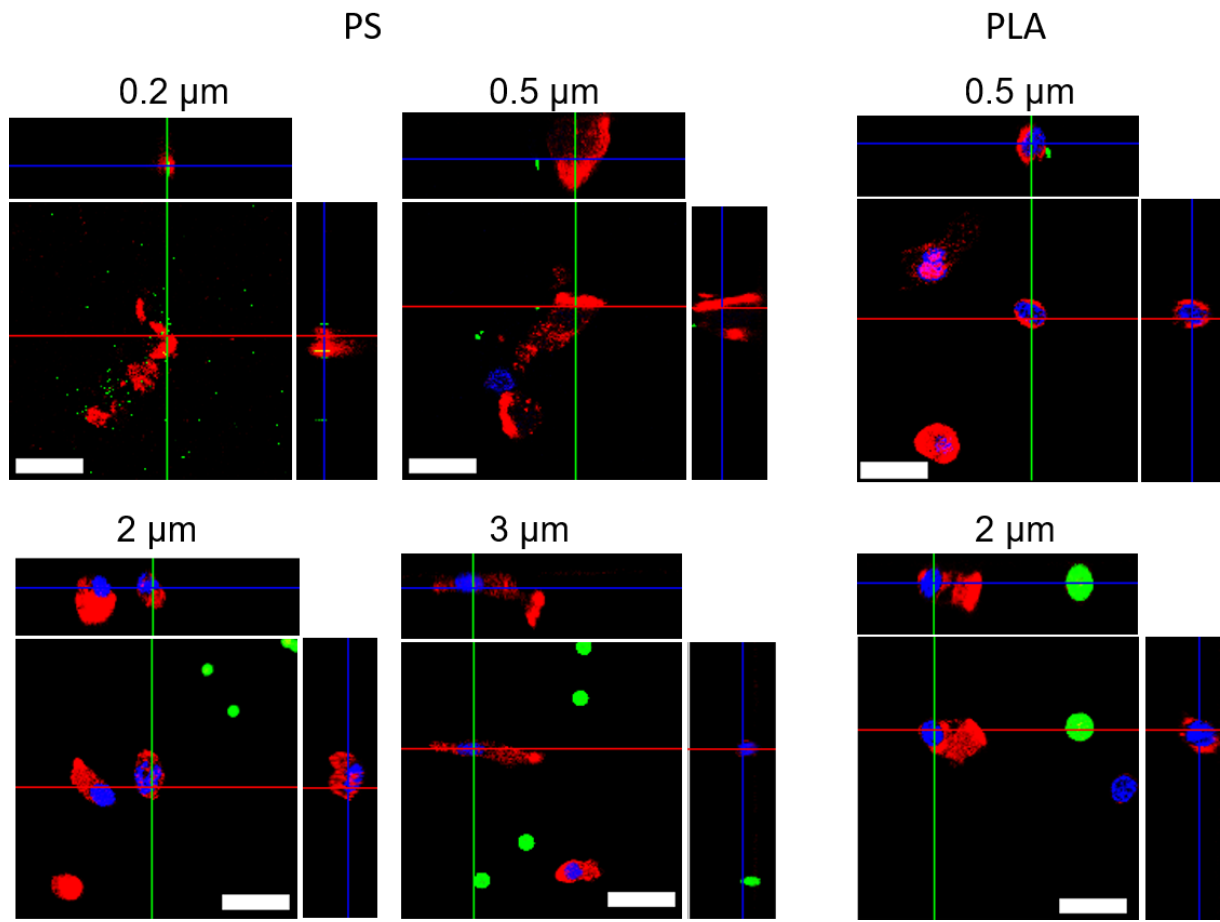


**Figure S10 Confocal laser scanning microscopy images of primary intestinal *E. fetida* cells**

Cells were incubated in presence of 2.5  $\mu\text{g}$  MPP/ $0.1 \times 10^6$  cells for 48 h. The actin filaments were stained with rhodamine-phalloidin (red), nuclei were stained with DAPI (blue) and the FITC-fluorescent MP particles showed a green fluorescence. Scale bar = 20  $\mu\text{m}$  Figure is from Riedl, Völkl et al. (2022) and was produced by Julia Jasinski

## 9. Lists

### 9.1. List of Figures

Figure 1 Representative PCI analysis via FC using ImKC cells.....	45
Figure 2 Linearity of PCI and the respective median fluorescence measured by FC .....	46
Figure 3 Relationship of the side scatter measurement and the PCI.....	46
Figure 4 Determination of the polarisation by measuring the ROS amount.....	47
Figure 5 Determination of the polarisation state by antibody staining of polarisation-specific surface markers .....	48
Figure 6 PCI dependency of polarised macrophages.....	49
Figure 7 Particle distribution during the cell division measured by FC.....	52
Figure 8 Particle distribution of PS <sub>2µm, green</sub> in ImKC and J774A.1 cells .....	55
Figure 9 MTT analysis of ImKC and J774A.1 macrophage cell lines in dependency of the surface charge of the particles .....	58
Figure 10 Cell proliferation of J774A.1 and ImKC in response to PS <sub>polyscience</sub> and PS <sub>micromod</sub> .....	60
Figure 11 Metabolic activity of cells after 24 h and 72 h incubation with MPP .....	62
Figure 12 Intracellular ROS concentration in dependence of size and concentration .....	63
Figure 13 Correlation between ROS generation and PCI .....	65
Figure 14 CFSE dilution assay after 72 h of incubation with MPP.....	66
Figure 15 MTT assay with protein-coated particles .....	68
Figure 16 Metabolic activity after 24 h incubation with the different MPP polymers .....	71
Figure 17 Intracellular ROS concentration in dependence of polymers .....	72
Figure 18 Representative SEM pictures of the used particles at the respective ageing times .....	74
Figure 19 Particle fluorescence measured using flow cytometry .....	75
Figure 20 Representative gating strategy for the quantitative uptake of PS <sub>2µm</sub> , PS <sub>43</sub> and PS <sub>130</sub> .....	76
Figure 21 MTT assay determines the metabolic activity of PS <sub>aged</sub> .....	77
Figure 22 LDH assay used to determine the membrane integrity .....	78
Figure 23 COMET assay to estimate the genotoxicity .....	79
Figure 24 Level of oxidative stress for ImKC treated with aged particles.....	80
Figure 25 TNF-α concentration measured by ELISA after treatment with aged particles.....	82
Figure 26 Different transcriptomic impacts of PS <sub>130</sub> and PS <sub>pristine</sub> .....	83
Figure 27 Venn diagram comparing the most specific GOs .....	86
Figure 28 GO networks visualised by ClueGO .....	88
Figure 29 Pathway analysis by KEGG for the upregulated genes of PS <sub>2µm</sub> .....	90
Figure 30 MTT Assay of L929 cell line and the respective paint fractions .....	92
Figure 31 Uptake of particles from cells already challenged with particles .....	96
Figure 32 Detection of particle release over time for J774A.1 cells .....	97
Figure 33 Detection of particle release over time for ImKC cells .....	98

Figure 34 Transwell permeability assay .....	101
Figure 35 Establishment of the particle detection method for transwell assays for PS <sub>2µm</sub> .....	103
Figure 36 Establishment of the particle detection method for transwell assays for PS <sub>0.5µm</sub> .....	104
Figure 37 Microscopical analysis of the spheroid growth .....	107
Figure 38 Diameter, roundness and circularity for the assessment of the spheroids .....	108
Figure 39 Stained spheroids analysed with fluorescence microscopy .....	109
Figure 40 Representative microscopic pictures of spheroids challenged with MPP during the formation ....	109
Figure 41 Confocal microscopy of a spheroid after incubation with MPP .....	110
Figure 42 Ratio of cell count for a co-cultivation of ImKC and BNL-CL2 cells .....	113
Figure 43 ELISA assay to determine the TNF $\alpha$ amount in the hanging drop cultivation system .....	114
Figure 44 MTT assay with primary intestinal cells from <i>E. fetida</i> .....	117
Figure 45 Ingestion of PS <sub>0.5µm</sub> by <i>T. pyriformis</i> .....	119
Figure 46 Ingestion of PS <sub>0.5µm</sub> and PS <sub>6µm</sub> in <i>A. proteus</i> .....	120
Figure 47 Induction of pinocytosis channels in <i>A. proteus</i> .....	121
Figure 48 Number of ingested particles after pinocytosis induction in <i>A. proteus</i> .....	122
Figure 49 Retention time of particles after ingestion in <i>T. pyriformis</i> (A) and <i>A. proteus</i> (B) .....	124
Figure 50 Ingestion of PS <sub>0.5µm</sub> loaded <i>T. pyriformis</i> by <i>A. proteus</i> .....	125
Figure 51 Excretion of PS <sub>&lt;20µm</sub> by <i>A. proteus</i> .....	126
Figure S1 Analysis of PCI as a function of size, concentration and cell line via flow cytometry using the established method .....	131
Figure S2 Analysis of PCI as a function of size, concentration and cell line via flow cytometry using the established method .....	132
Figure S3 Verification of particle uptake by CLSM .....	132
Figure S4 Comparison of the PCI and internalisation rate of MP <sub>polyscience</sub> and MP <sub>micromod</sub> for J774A.1 and ImKC cells. ....	133
Figure S5 Calculation of particles per cell based on flow cytometry data .....	133
Figure S6 L929 cell viability for in-house synthesised PS particle dispersion and standard PS model particle dispersion. ....	134
Figure S7 SEM images of paint fractions at the position of EDX measurement .....	135
Figure S8 Exemplary images of stained sections of spheroids challenged for 24 h with 2 µm MP particles ..	135
Figure S9 Confocal microscopy of spheroids with macrophages incubated with MPP .....	136
Figure S10 Confocal laser scanning microscopy images of primary intestinal <i>E. fetida</i> cells .....	137

## 9.2. List of Schemes

Scheme 1 Uptake mechanism of particles in mammalian cells .....	8
Scheme 2 Investigated parameters influencing the PCI and ingestion in cooperation projects .....	9
Scheme 3 Multiparametric problem situation of MP on mammalian cells .....	14

<b>Scheme 4 Principle of the MTT assay</b> .....	14
<b>Scheme 5 Principle of the H<sub>2</sub>DCFDA conversion assay</b> .....	15
<b>Scheme 6 Function of the CTV dye for tracking cell proliferation</b> .....	16
<b>Scheme 7 Principle of the LDH assay</b> .....	17
<b>Scheme 8 Principle of the COMET assay</b> .....	17
<b>Scheme 9 Principle of the ELISA sandwich assay</b> .....	18
<b>Scheme 10 Model for the polarisation of macrophages and expression of selected, polarisation-specific surface markers</b> .....	19
<b>Scheme 11 Principle of the transwell system and the lucifer yellow assay</b> .....	21
<b>Scheme 12 Model for the spheroid cultivation in the hanging drop model</b> .....	21
<b>Scheme 13 Objectives of this work</b> .....	24
<b>Scheme 14 Principle of the SingleCell sorter</b> .....	41
<b>Scheme 15 Possible pathway and interaction sites of a MPP with a mammalian cells</b> .....	44
<b>Scheme 16 Exemplary process scheme for the calculation of the approximation considering a symmetrical distribution for ImKC cells</b> .....	53
<b>Scheme 17 Conducted transwell experiments</b> .....	100
<b>Scheme 18 Conducted spheroid experiments</b> .....	105
<b>Scheme 19 Spheroid formation inside a Petri dish by hanging drop method</b> .....	105
<b>Scheme 20 Principle of the GravityPLUS™ hanging drop spheroid cultivation system</b> .....	106
<b>Scheme 21 Embedding procedure for the agarose micro-array</b> .....	111
<b>Scheme 22 Encapsulation of spheroids in O.C.T. compound</b> .....	112
<b>Scheme 23 Conclusions of the main findings</b> .....	128

### 9.3. List of Tables

Table 1 Characterisation of the used particles .....	27
Table 2 Cell lines used in the cell cultivation experiments .....	28
Table 3 3D printing parameters for the personalised capture plate .....	32
Table 4 3D printing parameters for the microarray compartments .....	33
Table 5 Measured cell populations for particle distribution and the respective value of the calculated approximation .....	54
Table 6 $\zeta$ -potential of the particles used in 3.3.2 .....	61
Table 7 $\zeta$ -potential of the particles used in 3.3.3 .....	67
Table 8 Size and $\zeta$ -potential of the particles used in 3.3.5 .....	70
Table 9 Particle concentrations of the used polymer beads for the ROS assay in Figure 17 .....	72
Table 10 Size and $\zeta$ -potential of the particles used in 3.3.6 .....	74
Table 11 Top 10 up and downregulated differentially expressed genes for PS <sub>2<math>\mu</math>m</sub> vs control .....	84
Table 12 Top 10 up and downregulated differentially expressed genes for PS <sub>130</sub> vs control.....	85
Table 13 Direct comparison of appearing GOs .....	87
Table 14 Group annotations for Line A, B and C from Figure 28.....	89
Table 15 Measured $\zeta$ -potential of the used MPP .....	116
Table 16 Measured $\zeta$ -potential and size of the used MPP in the respective medium .....	118
Table S1 Overview of MPP concentrations used for Figure S1 and Figure S2 .....	131

### 9.4. List of Equations

Equation 1 Living cell count calculation when using a hemocytometer.....	30
Equation 2 Calculation of the metabolic activity .....	35
Equation 3 Calculation of ROS amount by FC.....	36
Equation 4 Calculation of the LDH release .....	37
Equation 5 Calculation of the relative LY fluorescence.....	39
Equation 6 Mathematical equation for the calculation of the approximation .....	53
Equation 7 Calculation of circularity.....	107
Equation 8 Calculation of Roundness .....	107

## 10. Materials, Devices and Software

### 10.1. Buffers and Solutions

Buffer/Solution	Constitution
citric saline buffer	135 mM potassium chloride, 15 mM sodium citrate
Cryopreservation media for BNL CL.2, J774A.1 and L929	95 % respective growth medium, 5 % DMSO
Cryopreservation media for ImKC and STC-1	90 % respective growth medium, 10 % DMSO
E. fetida growth medium	60% (v/v) L-15 medium, 20% (v/v) ddH <sub>2</sub> O, 10% (v/v) FCS and 10% (v/v) specialised worm filtrate, 4 mM l-glutamine, 25 mM HEPES and PSTGA
E. fetida isolation buffer	10 µg/mL Collagena, 500 µL M-HBSS supplemented with 100 Units/mL (U/mL) penicillin, 100 µg/mL streptomycin, 60 µg/mL tetracyclin, 50 µg/mL gentamicin and 2,5 µg/mL amphotericin B (PSTGA)
electrophoresis solution	0.3 M NaOH, 1mM EDTA at pH 8.0
ImKC growth media	90% v/v RPMI1640, 10% v/v FCS, 2 mM glutamine
J774A.1 growth media	90% v/v DMEM <sub>LONZA</sub> , 10% v/v FCS, 4 mM glutamine, 24 mM HEPES, 0.1 mM sodium pyruvate
L929 growth media	90% v/v DMEM <sub>LONZA</sub> , 10 % v/v FCS, 2 mM glutamine
lysis buffer	1% v/v Triton-X-100, 2 M NaCl, 0.1 M EDTA at 8.0 pH, 10 mM Tris-HCl at pH 9.0
M-HBSS	5.3 mM KCl, 0.394 mM KH <sub>2</sub> PO <sub>4</sub> , 4.09 mM NaHCO <sub>3</sub> , 0.298 mM Na <sub>2</sub> HPO <sub>4</sub> x 7 H <sub>2</sub> O + 5.5 mM Glucose + 10 mM HEPES + 84.9 mM NaCl in water
neutralisation buffer	0.4 M Tris, pH at 7.5
Prescott <sub>NaCl</sub>	KCl 12.4 mM, CaHPO <sub>4</sub> 2.9 mM, MgSO <sub>4</sub> 1.7 mM, pH 6.4, 125 mM NaCl, pH 4.3
Prescott <sub>Ref</sub>	KCl 12.4 mM, CaHPO <sub>4</sub> 2.9 mM, MgSO <sub>4</sub> 1.7 mM, pH 6.4
STC-1 and BNL CL.2 growth media	90% v/v DMEM <sub>ATCC</sub> , 10 % v/v FCS

## 10.2. Cells and organisms

Cell line	Lot Number	Strain	Tissue	Cell phenotype	Growth properties	Provider
<b>ImKC</b>	SCC119	H-2Kb-tsA58	Liver	resident macrophages	adherent	Merck Darmstadt, Germany
<b>BNL CL.2</b>	ATCC® 73™	TIB-BALB/c	Liver	epithelial	adherent	ATCC Manassas, Vi, US
<b>J774A.1</b>	ATCC® 67™	TIB-BALB/cN	ascites	macrophage	mostly adherent	ATCC Manassas, Vi, US
<b>STC-1</b>	ATCC® 3254™	CRL-C57B1/6J	intestine	epithelial-like	adherent	ATCC Manassas, Vi, US
<b>NCTC L- 929</b>	ATCC® CCL1™	C3H/An	subcutaneous connective tissue; areolar and adipose	fibroblast	adherent	ATCC Manassas, Vi, US
<b>Primary cells</b>						
<b>E. fetida</b>	Isolated from the whole organism – provided by the AG Feldhaar	-	intestine	epithelial	In suspension	-
<b>Microorganisms</b>						
<b>Amoeba proteus</b>	DCS9112	-	-	-	-	Carolina Science
<b>Tetrahymena pyriformis</b>	Tetrahymena Pyriformis	-	-	-	-	Icon Biotech

### 10.3. Particles used in this study

Particle solutions used in this work were prepared directly from the respective stock solutions in the respective growth media.

Particle	Notes	Order number.	Stockconcentration in H <sub>2</sub> O		Manufacturer	Location
			mg/mL	Particles/mL		
PS <sub>0.2μm</sub>		07304-15	25	5.68 x 10 <sup>12</sup>	Polyscience	Hirschberg an der Bergstrasse, Germany
PS <sub>0.2μm</sub> , green		17151-10	25	5.68 x 10 <sup>12</sup>	Polyscience	“
PS <sub>0.5μm</sub>		07307-15	25	3.64 x 10 <sup>11</sup>	Polyscience	“
PS <sub>0.5μm</sub> , green		17152-10	25	3.64 x 10 <sup>11</sup>	Polyscience	“
PS <sub>1μm</sub>		07310-15	25	4.55 x 10 <sup>10</sup>	Polyscience	“
PS <sub>1μm</sub> , green		17154-10	25	4.55 x 10 <sup>10</sup>	Polyscience	“
PS <sub>2μm</sub>		19814-15	25	5.68 x 10 <sup>9</sup>	Polyscience	“
PS <sub>2μm</sub> , green		18338-5	25	5.68 x 10 <sup>9</sup>	Polyscience	“
PS <sub>2μm</sub> , red		19508-2	25	5.68 x 10 <sup>9</sup>	Polyscience	“
PS <sub>3μm</sub> / PS <sub>polyscience</sub>		17134-15	25	1.68 x 10 <sup>9</sup>	Polyscience	“
PS <sub>3μm</sub> , green		17155-2	25	1.68 x 10 <sup>9</sup>	Polyscience	“
PS <sub>6μm</sub>		07312-5	25	2.10 x 10 <sup>8</sup>	Polyscience	“
PS <sub>6μm</sub> , green		17156-2	25	2.10 x 10 <sup>8</sup>	Polyscience	“
PS <sub>43h</sub>	in-house produced by Nora Meides from PS <sub>2μm</sub>		25	≈ 5.68 x 10 <sup>9</sup>	-	-
PS <sub>86h</sub>	in-house produced by Nora Meides from PS <sub>2μm</sub>		25	≈ 5.68 x 10 <sup>9</sup>	-	-
PS <sub>130h</sub>	in-house produced by Nora Meides from PS <sub>2μm</sub>		25	≈ 5.68 x 10 <sup>9</sup>	-	-
PS <sub>micromod</sub>	3 μm	01-00-303	50	3.4 x 10 <sup>9</sup>	Micromod	Rostock, Germany
PE <sub>1-4μm</sub>	Delivered as powder, resuspended 0.1 % (w/v) Tween 20	CPMS- 0.96	2.5	5.4 x 10 <sup>7</sup>	Cospheric LLC, Santa Babara, CA, USA	Cospheric LLC, Santa Babara, CA, USA
PVC <sub>1.4μm</sub>			2.5	8.3 x 10 <sup>7</sup>	Quantum Design	Darmstadt, Germany
PLA <sub>0.5μm</sub>		51-00-502	10	1.5 x 10 <sup>11</sup>	Micromod	Rostock, Germany
PLA <sub>2μm</sub>		11-00-203	10	2.4 x 10 <sup>9</sup>	Micromod	Rostock, Germany
CA <sub>1.5μm</sub>	In-house produced by Julia Jasinski		5	-	-	-



<b>PS<sub>&lt;20µm</sub></b>	In-house produced by cryomilling from AG Strohhriegl; Delivered as powder, resuspended 0.1 % (w/v) Tween 20	2.5	-	-	-
<b>PS<sub>20-40µm</sub></b>	In-house produced by cryomilling from AG Strohhriegl; Delivered as powder, resuspended 0.1 % (w/v) Tween 20	2.5	-	-	-
<b>PS<sub>40-75µm</sub></b>	In-house produced by cryomilling from AG Strohhriegl; Delivered as powder, resuspended 0.1 % (w/v) Tween 20	2.5	-	-	-
<b>PS<sub>SHPA</sub></b>	In-house produced by polymerisation from AG Greiner	2.5	-	-	-
<b>PS<sub>MIPA</sub></b>	In-house produced by polymerisation from AG Greiner	2.5	-	-	-
<b>Paint 1 Supernatant</b>	In-house produced by extraction from AG Greiner	-	-	-	-
<b>Paint 2 Supernatant</b>	In-house produced by extraction from AG Greiner	-	-	-	-
<b>Paint 1 Solid Phase</b>	In-house produced by extraction from AG Greiner	8	-	-	-
<b>Paint 2 Solid Phase</b>	In-house produced by extraction from AG Greiner	8	-	-	-

#### 10.4. Chemicals, Reagents and Kits

Material	Specification	Order number.	Manufacturer	Location
4',6-Diamidino-2-phenylindol (DAPI)	1 mg/mL in DMSO	32670	Sigma Aldrich	Darmstadt, Germany
Acridin Orange/ Propidium Iodide Stain Cell Viability Kit	-	F23001	Logos Biosystems	Gyeonggi-do, Southkorea
Amphotericin B	250 µg/mL Solution	A 2612	Biochrom GmbH	Berlin, Germany
Anti-mouse CD163 - PE Cyanine 7 - Antibody	LOT Nr: B330701	155319	Biolegend	Amsterdam, Netherlands
Anti-mouse CD68 - PE Cyanine 5.5 - Antibody	LOT Nr: B354357	137009	Biolegend	Amsterdam, Netherlands
Anti-mouse CD80 - PE - Antibody	LOT Nr: B358280	104707	Biolegend	Amsterdam, Netherlands
Anti-mouse CD86 - FITC - Antibody	LOT Nr: B354919	105005	Biolegend	Amsterdam, Netherlands
Antimycin A	50mM in H <sub>2</sub> O	A8674-25MG	Sigma Aldrich	Darmstadt, Germany
BSA	≥ 98%, biotin free, Lot Nr. 02892831	0163.2	Carl Roth GmbH + Co. KG	Karlsruhe, Germany
CaHPO <sub>4</sub>	Powder	9490.3	Carl Roth	Karlsruhe, Germany
Carboxyfluorescein succinimidyl ester (CFSE)	5 mM in DMSO	21888-25MG-F	Sigma-Aldrich	Darmstadt, Germany
CellTrace Violet Proliferation Kit	-	Cat#C34557	Invitrogen	Carlsbad, CA, US
CyQUANT™ LDH Cytotoxicity Assay	-	C20301	ThermoFisher	Waltham, MA, USA
DMEM <sub>ATCC</sub>		81282122	ATCC	Manassas, Vi, US
DMEM <sub>LONZA</sub>		12-614F BE12-614F	Lonza Group Ltd	Basel, Swiss
Dichlorofluorescein diacetate (DCFDA)	25 mg/mL in H <sub>2</sub> O	D6883-250MG	Sigma Aldrich	Darmstadt, Germany
Dimethyl sulfoxide (DMSO)	-	D2438-50ML	Sigma-Aldrich	Darmstadt, Germany
DPBS	without Ca <sup>2+</sup> /Mg <sup>2+</sup>	L 1825	Biochrom GmbH	Berlin, Germany
DPBS	without Ca <sup>2+</sup> /Mg <sup>2+</sup>	BE17-512Q	Lonza Group Ltd	Basel, Swiss
EDTA	-	10305	Grüssing GmbH	Filsum, Germany
ELISA MAX™ Deluxe Set	-	430915	Biolegend	San Diego, CA, US

<b>ELISA MAX™ Stop Solution</b>	-	423001	Biolegend	San Diego, CA, US
<b>ELISA MAX™ Wash Buffer</b>	-	421601	Biolegend	San Diego, CA, US
<b>Ethanol</b>	-	20821.310	VWR International GmbH	Darmstadt, Germany
<b>FCS</b>	Not from USA (sterile-filtered)	F7524-500ML	Sigma-Aldrich	Darmstadt, Germany
<b>FCS</b>	South America (sterile-filtered)	S1860-500	Biowest SAS	Nuaillé, France
<b>Gentamicin</b>	50 mg/mL	L0012-100	Biowest SAS	Nuaillé, France
<b>H<sub>2</sub>O<sub>2</sub></b>	-	H175015	ThermoFisher	Waltham, MA, USA
<b>HBSS</b>	without Ca <sup>2+</sup> /Mg <sup>2+</sup> , without Phenolrot	L 2045	Biochrom GmbH	Berlin, Germany
<b>HCl</b>	-	456494P	VWR International GmbH	Darmstadt, Germany
<b>HEPES</b>	1 M, 50 X	L 1613	Biochrom GmbH	Berlin, Germany
<b>HEPES</b>	1 M in 0,85% NaCl Solution	17-737E	Lonza Group Ltd	Basel, Swiss
<b>Hoechst 33342 dye</b>	25 mg/mL in DPBS	62249	ThermoFisher	Waltham, MA, USA
<b>IL-4</b>	LOT Nr: B341863	BLD-574302	BIOZOL	Eching, Germany
<b>Isopropanol</b>	-	33539-1L-M	Sigma-Aldrich	Darmstadt, Germany
<b>KCl</b>	Powder	06157.3600	Bernd Kraft GmbH	Duisburg, Germany
<b>L-15 without Glutamin</b>	-	BE12-700F	Lonza Group Ltd	Basel, Swiss
<b>L-Glutamin</b>	200 mM	K 0283	Biochrom GmbH	Berlin, Germany
<b>Low melting point agarose</b>	Powder	6351.5	Carl Roth	Karlsruhe, Germany
<b>LPS</b>	LOT Nr: 0000112732, 5 mg/mL in H <sub>2</sub> O	L2630-10mg	Sigma Aldrich	Darmstadt, Germany
<b>Lucifer yellow</b>	25 mg/mL in H <sub>2</sub> O	71206-95-6	Biotium	Fremont, CA, US

<b>Lysis buffer RLT®</b>	-	79216	Qiagen	Hilden, Germany
<b>MgSO<sub>4</sub></b>	Powder	106067	Merck	Darmstadt, Germany
<b>3-(4,5-Dimethylthiazol-2-yl)-2,5-diphenyltetrazoliumbromid (MTT)</b>	-	L11939.06	Alfa Aesar	Ward Hill, MA, USA
<b>NaCl</b>	-	27810.295	VWR International GmbH	Darmstadt, Germany
<b>NaOH</b>	-	CN30.3	Carl Roth	Karlsruhe, Germany
<b>Paraformaldehyde</b>	Powder	0335.2	Carl Roth	Karlsruhe, Germany
<b>Penicillin/ Streptomycin</b>	10.000 U/mL / 10.000 µg/mL	A 2213	Biochrom GmbH	Berlin, Germany
<b>Penicillin/ Streptomycin</b>	10.000 U/mL / 10.000 U/mL	DE17-602E	Lonza Group Ltd	Basel, Swiss
<b>Phenol-red free MEM</b>	-	51200046	ThermoFisher	Waltham, MA, USA
<b>Propidium iodide</b>	1,0 mg/mL in H <sub>2</sub> O	P4864-10ML	Sigma-Aldrich	Darmstadt, Germany
<b>Protease-peptone</b>	Powder	HP32.1	Carl Roth	Karlsruhe, Germany
<b>RPMI-1640 without glutamine</b>	-	BE12-167F	Lonza Group Ltd	Basel, Swiss
<b>Sakura Finetek™ Tissue Tek optimum cutting temperature (O.C.T.) compound</b>	-	12351753	ThermoFisher	Waltham, MA, USA
<b>Sodium pyruvate</b>	Powder	L0473	Biochrome	Berlin, Germany
<b>Tetracyclin hydrochloride</b>		T7660-5G	Sigma-Aldrich	Darmstadt, Germany
<b>Tris</b>	Powder	AE15.2	Carl Roth	Karlsruhe, Germany
<b>Tri-sodium citrate x 2H<sub>2</sub>O</b>	Powder	12125	Grüssing	Filsum, Germany
<b>Triton X-100</b>	-	1.08603.1000	Merck KGaA	Darmstadt, Germany
<b>Trypanblau</b>	0,4% (v/v)	K940-100ML	VWR International GmbH	Darmstadt, Germany
<b>TWEEN® 20</b>	-	P1379-100ML	Sigma-Aldrich	Darmstadt, Germany
<b>Wasser, sterile filtered</b>		W3500-100mL	Sigma-Aldrich	Darmstadt, Germany

**Water, cell culture grade**

W3500-100mL

Sigma-Aldrich

Darmstadt,  
Germany

---

## 10.5. Accessories

Material	Modell	Order no.	Manufacturer	Location
Cell Culture Dish	100/20 mm	664970	Greiner Bio-One	Frickenhausen, Germany
Cell culture Plates	6-Well	604181	Greiner Bio-One	Frickenhausen, Germany
	12-Well	606180		
	24-Well	607180		
	48-Well	760180		
Cell strainer	pluriStrainer Mini, 20 µm	43-10020-60	pluriSelect Life Science UG&Co.KG	Leipzig, Germany
Cell strainer	Easy Strainer 70 µm	542070	Greiner Bio-One	Frickenhausen, Germany
Centrifuge-Tube	15 mL	188271	Greiner Bio-One	Frickenhausen, Germany
	50 mL	227270		
Cryogenic Storage Vials	1.2 mL (Free-standing)	479-1254	VWR International GmbH	Darmstadt, Germany
ELISA plates	96 Well	ALEXADI-80-0144	VWR International GmbH	Darmstadt, Germany
MICROPLATE, 96 WELL	96 Well	655101	Greiner Bio-One	Frickenhausen, Germany
Micro reaction tube	1.5 mL	72.690.001	Sarstedt AG & Co. KG	Nümbrecht, Germany
Micro reaction tube	2 mL	0030 120.094	Eppendorf AG	Hamburg, Germany
Pipette tips	0.5 – 20 µL	732024	Brand GmbH + Co. KG	Wertheim, Germany
	2 – 20 µL	732028		
	50 – 100 µL	732012		
Pipette (Serological)	1 mL	604181	Greiner Bio-One	Frickenhausen, Germany
	5 mL	606180		
	10 mL	607180		
	25 mL	760180		
Silicone tubing	VMQ; 3 mm 1 mm	-	Deutsch & Neumann	Berlin, Germany
Syringe Filter	0.2 µm Celluloseacetate	514-0061	VWR International GmbH	Darmstadt, Germany
Syringe (Injekt® Solo; Luer)	20 mL	4606205V	B. Braun SE	Melsungen, Germany
Wipes	Kimtech	115-2074	VWR International GmbH	Darmstadt, Germany

## 10.6. Devices and Equipment

Device	Modell	Manufacturer	Location
<b>Autoclave (Table)</b>	3850 EL	Systec GmbH	Linden, Germany
<b>Autoclave (Standing)</b>	V150	Systec GmbH	Linden, Germany
<b>Automated Cell counter</b>	LUNA-FLTM Dual Fluorescence Cell counter	Logos Biosystems	Gyeonggi-do, South Korea
<b>Single CellSorter Sorter</b>	Modular System at the AG Weig	CELLSORTER Biotechnology Innovations	Budapest, Hungary
<b>Centrifuge</b>	Sorvall LYNX6000	Thermo Scientific (Thermo Fisher Scientific)	Waltham, Massachusetts, USA
<b>Centrifuge</b>	Multifuge 3 S-R	Heraeus	Hanau, Germany
<b>Centrifuge</b>	Biofuge pico	Heraeus	Hanau, Germany
<b>CO<sub>2</sub> Incubator</b>	BBD 6220	Thermo Scientific (Thermo Fisher Scientific)	Waltham, Massachusetts, USA
<b>CO<sub>2</sub> Incubator</b>	Thermo Forma Direct Heat CO <sub>2</sub> Incubator Model 311	Thermo Scientific (Thermo Fisher Scientific)	Waltham, Massachusetts, USA
<b>Cryogenic Cell Bank</b>	Cryo 200	Thermo Electron Corporation	Waltham, Massachusetts, USA
<b>Dishwasher</b>	Professional G 7883	Miele & Cie. KG	Güterslohe, Germany
<b>Flow cytometer</b>	Cytomics FC500	Beckmann Coulter GmbH	Krefeld, Germany
<b>Freezer (-20 °C)</b>	Liebherr Comfort	Liebherr-International AG	Bulle, Switzerland
<b>Freezing container</b>	Mr. Frosty	Thermo Scientific (Thermo Fisher Scientific)	Waltham, Massachusetts, USA
<b>Fridge (4 °C)</b>	Liebherr profi line	Liebherr-International AG	Bulle, Switzerland
<b>Gel-Electrophoresis-Chamber</b>	40-1214	Peqlab (VWR International GmbH)	Darmstadt, Germany
<b>Gel-Electrophoresis-Voltage-supply</b>	E835	Consort bvba	Turnhout, Belgium
<b>Glas-Beaker</b>	50 mL; 100 mL; 250 mL	Eppendorf AG	Hamburg, Germany
<b>Glas-Bottles</b>	100 mL; 250 mL; 500 mL; 1 L; 2 L	Eppendorf AG	Hamburg, Germany
<b>Heat-Block</b>	ThermoMixer F1.5	Eppendorf AG	Hamburg, Germany
<b>Laminar Flow Hood</b>	Mobilien W90 Variolab Typ SWB	Waldner	Wangen, Germany
<b>Magnetic stirrer</b>	RCT basic	IKA®-Werke GmbH & CO. KG	Staufen, Deutschland
<b>Membrane-Vakuum Pump</b>	AP 04	Hettich Benelux B.V.	Geldermalsen, Netherlands
<b>Microscope (Inverse)</b>	Primovert with Axiocam 105 color	Carl Zeiss Microscopy Deutschland GmbH	Oberkochen, Germany
<b>Microscope (Inverse)</b>	CKX41	Olympus	Hamburg, Germany
<b>Millipore water supply</b>	Synergy Water Purification System	Merck Millipore (Merck KGaA)	Darmstadt, Germany

<b>Minishaker</b>	MS2	IKA®-Werke GmbH & CO. KG	Staufen, Germany
<b>Orbital Shaker</b>	Noctua K30	Thermo Scientific (Thermo Fisher Scientific)	Waltham, Massachusetts, USA
<b>Pipette controller</b>	-	Integra Biosciences	Zizers, Switzerland
<b>Pipette</b>	Research plus 0.5 – 10 µL 2 – 20 µL 10 – 100 µL 20 – 200 µL 100 – 1000 µL	Eppendorf AG	Hamburg, Germany
<b>Pipette (Multichannel)</b>	Transferpette S-12 20 – 200 µL	Brand GmbH + Co. KG	Wertheim, Germany
<b>pH-Meter</b>	SevenCompact	Mettler-Toledo	Columbus, Ohio, USA
<b>Plate reader</b>	GENios Pro	Tecan Group AG	Männedorf, Switzerland
<b>Microvolume UV-Vis Spectrophotometer</b>	NanoDrop™	Thermo Scientific (Thermo Fisher Scientific)	Waltham, Massachusetts, USA
<b>Rotator</b>	SB2	Stuart	Stone, UK
<b>Scale (analytical)</b>	E01140	Ohaus	Nänikon, Schweiz
<b>Scale (Laboratory)</b>	BP 2100 S	Sartorius	Göttingen, Germany
<b>Shaking flask</b>	100 mL; 250 mL; 500 mL; 1 L; 2 L	Schott	Mainz, Germany
<b>Standard Resin (clear resin)</b>	V4	Formlabs	Somerville, Massachusetts, USA
<b>Storage Tank for Liquid Nitrogen</b>	CS 200 SK	Cryo Anlagenbau GmbH	Wilnsdorf, Germany
<b>Syringe Pump</b>	KDS model 100	KD Scientific	Holliston, Massachusetts, USA
<b>Ultra-Low Temperature Freezer</b>	HERAfreeze™ (- 80 °C)	Thermo Scientific (Thermo Fisher Scientific)	Waltham, Massachusetts, USA
<b>UV-Lamp for sterilisation</b>	VL 215 G	Thermo Scientific (Thermo Fisher Scientific)	Waltham, Massachusetts, USA
<b>Waterbath</b>	WB20	P-D Industriegesellschaft GmbH	Wilsdruff, Germany



## 10.7. Software

Software	Function	Version	Producer	Location
<b>CellSorter_7</b>	Cell Sorting	13.04.2021	CELLSORTER Biotechnology Innovations	Budapest, Hungary
<b>Citavi</b>	Writing	6.3.0.0	Swiss Academic Software	Wädenswill, Switzerland
<b>ClueGO database</b>	Analysis of RNA <sub>seq</sub>	13.05.2021	Apps. cytoscape.org	Online
<b>COMETSCORE™</b>	Analysis of COMET assay	2.0.0.38	RexHoover.com	Online
<b>Cytoscape</b>	Analysis of RNA <sub>seq</sub>	3.9.0	cytoscape.org	Online
<b>FlowJo</b>	FC-Data- Analyses	v 10.5.0	Tree Star, Inc.	Ashland, Oregon, USA
<b>Fusion 360</b>	CAD		Autodesk	Santa Clara, California, USA
<b>Inkscape</b>	Rendering	1.0.1	open-source	
<b>Microsoft Office</b>	Writing, Data curation	MicrosoftOffice 365	Microsoft	Redmond, Washington, USA
<b>OmicsBox</b>	Analysis of RNA <sub>seq</sub>	2.0.36	BioBam Bioinformatics S.L.	Valencia, Spain
<b>Origin 2022</b>	Data curation, Plotting	9.9.0.225 (Lehre)	OriginLab Corporation	Northampton, Massachusetts, USA
<b>PreForm</b>	Slicer		Formlabs	Somerville, Massachusetts, USA
<b>smart.servier</b>	Illustrater		Servier	Online
<b>Xfluor</b>	Plate-Reading	V4.53	Tecan	Männedorf, Switzerland
<b>Zenlite</b>	Microscope- Imaging	blue3.0	Carl Zeiss AG	Oberkochen, Germany

## 11. List of publications

### *Exclusive first authorship*

**Völkl, M.**; Jérôme, V.; Weig, A.; Jasinski, J.; Meides, N.; Strohmriegl, P.; Scheibel, T.; Freitag, R. (2022): Pristine and artificially-aged polystyrene microplastic particles differ in regard to cellular response. In: *Journal of hazardous materials* 435, Artikel 128955, S. 1–13. DOI: 10.1016/j.jhazmat.2022.128955.

### *Shared first authorship*

Ramsperger, A. F. R. M.; Jasinski, J.; **Völkl, M.**; Witzmann, T.; Meinhart, M.; Jérôme, V. Kretschmer, W. P.; Freitag, R.; Senker, J.; Fery, A.; Kress, H.; Scheibel, T.; Laforsch, C. (2022): Supposedly identical microplastic particles substantially differ in their material properties influencing particle-cell interactions and cellular responses. In: *Journal of hazardous materials* 425, Artikel 127961, S. 1–14. DOI: 10.1016/j.jhazmat.2021.127961.

Riedl, S. A. B.; **Völkl, M.**; Holzinger, A.; Jasinski, J.; Jérôme, V.; Scheibel, T.; Feldhaar, H.; Freitag, R. (2022): In vitro cultivation of primary intestinal cells from *Eisenia fetida* as basis for ecotoxicological studies. In: *Ecotoxicology (London, England)* 31 (2), S. 221–233. DOI: 10.1007/s10646-021-02495-2.

Rudolph, J.; **Völkl, M.**; Jérôme, V.; Scheibel, T.; Freitag, R. (2021): Noxic effects of polystyrene microparticles on murine macrophages and epithelial cells. In: *Scientific reports* 11 (1), Artikel 15702, S. 1–16. DOI: 10.1038/s41598-021-95073-9.

Jasinski, J.; **Völkl, M.**; Hahn, J.; Jérôme, V.; Freitag, R.; Scheibel, T. (2023): Polystyrene microparticle distribution after ingestion by murine macrophages. In: *Journal of hazardous materials* 457, Artikel 131796, S. 1–12. DOI: 10.1016/j.jhazmat.2023.131796.

### *Co-authorship*

Jasinski, J.; Wilde, M. V.; **Völkl, M.**; Jérôme, V.; Fröhlich, T.; Freitag, R.; Scheibel, T. (2022): Tailor-Made Protein Corona Formation on Polystyrene Microparticles and its Effect on Epithelial Cell Uptake. In: *ACS applied materials & interfaces* 14 (41), S. 47277–47287. DOI: 10.1021/acsami.2c13987.

Müller, A. K.; Brehm, J.; **Völkl, M.**; Jérôme, V.; Laforsch, C.; Freitag, R.; Greiner, A. (2022): Disentangling biological effects of primary nanoplastics from dispersion paints' additional compounds. In: *Ecotoxicology and environmental safety* 242, Artikel 113877, S. 1–9. DOI: 10.1016/j.ecoenv.2022.113877.

Zhang, Y.; Paul, T.; Brehm, J.; **Völkl, M.**; Jérôme, V.; Freitag, R.; Laforsch, C.; Greiner, A.: Role of Residual Monomers in the Manifestation of (Cyto)toxicity by Polystyrene Microplastic Model Particles (2023). In: *Environmental Science & Technology* 57, S. 9925-9933. DOI: doi.org/10.1021/acs.est.3c01134.

### *Completed manuscripts as shared first authorship*

**Völkl, M.**; Mondellini, S.; Schwarzer, M.; Jasinski, J.; Jérôme, V.; Scheibel, T.; Laforsch, C.; Freitag, R.: Trophic transfer between unicellular protists: Microplastic accumulation in *Amoeba proteus* through *Tetrahymena pyriformis* and *Paramecium caudatum*

**Völkl, M.**; Ritschar, S.; Ramsperger, A. F. R. M. ; Jasinski, J.; Jérôme, V.; Scheibel, T.; Laforsch, C.; Freitag, R.: Analysis of Microplastic in 3D Cell Spheroids

Jasinski, J.; **Völkl, M.**; Wilde, M.; Jérôme, V.; Fröhlich, T.; Freitag, R.; Scheibel, T.: Cellular effects of different polymer microparticles on murine cells

## 12. References

- [1] **Geyer, R.**; Jambeck, J. R.; Law, K. L. (2017), "Production, use, and fate of all plastics ever made", *Sci. Advan.*, 3. Article e1700782, pp. 1–6, DOI: 10.1126/sciadv.1700782.
- [2] **Thompson, R. C.**; Olsen, Y.; Mitchell, R. P.; Davis, A.; Rowland, S. J.; John, A. W. G.; McGonigle, D.; Russell, A. E. (2004), "Lost at sea: where is all the plastic?", *Science*, 304, p. 838, DOI: 10.1126/science.1094559.
- [3] **Provencher, J. F.**; Covernton, G. A.; Moore, R. C.; Horn, D. A.; Conkle, J. L.; Lusher, A. L. (2020), "Proceed with caution: The need to raise the publication bar for microplastics research", *Sci. Total Environ.*, 748. Article 141426, pp. 1–7, DOI: 10.1016/j.scitotenv.2020.141426.
- [4] **Frias, J. P. G. L.**; Nash, R. (2019), "Microplastics: Finding a consensus on the definition", *Mar. Pollut. Bull.*, 138, pp. 145–147, DOI: 10.1016/j.marpolbul.2018.11.022.
- [5] **An, L.**; Liu, Q.; Deng, Y.; Wu, W.; Gao, Y.; Ling, W. in *Microplastics in Terrestrial Environments*, Springer, Cham, 2020, pp. 143–159.
- [6] **Meides, N.**; Menzel, T.; Poetzschner, B.; Löder, M. G. J.; Mansfeld, U.; Strohriegel, P.; Altstaedt, V.; Senker, J. (2021), "Reconstructing the Environmental Degradation of Polystyrene by Accelerated Weathering", *Environ. Sci. Technol.*, 55, pp. 7930–7938, DOI: 10.1021/acs.est.0c07718.
- [7] **Kiran, B. R.**; Kopperi, H.; Venkata, M. S. (2022), "Micro/nano-plastics occurrence, identification, risk analysis and mitigation: challenges and perspectives", *Rev. Environ. Sci. Biotechnol.*, 21, pp. 169–203, DOI: 10.1007/s11157-021-09609-6.
- [8] **Hamid, S. F.**; Mehran Sanam, B.; Norkhairiyah, A.; Norkhairah, A.; Priya, M.; Agamuthu, P. (2018), "Worldwide distribution and abundance of microplastic: How dire is the situation?", *Waste Manag. Res.*, 36, pp. 873–897, DOI: 10.1177/0734242X18785730.
- [9] **Zhang, Y.**; Kang, S.; Allen, S.; Allen, D.; Gao, T.; Sillanpää, M. (2020), "Atmospheric microplastics: A review on current status and perspectives", *Earth. Sci. Rev.*, 203. Article 103118, pp. 1–15, DOI: 10.1016/j.earscirev.2020.103118.
- [10] **Triebkorn, R.**; Braunbeck, T.; Grummt, T.; Hanslik, L.; Huppertsberg, S.; Jekel, M.; Knepper, T. P.; Kraus, S.; Müller, Y. K.; Pittroff, M.; Ruhl, A. S.; Schmieg, H.; Schür, C.; Strobel, C.; Wagner, M.; Zumbülte, N.; Köhler, H.-R. (2019), "Relevance of nano- and microplastics for freshwater ecosystems: A critical review", *Trends Anal. Chem.*, 110, pp. 375–392, DOI: 10.1016/j.trac.2018.11.023.
- [11] **Wagner, M.**; Scherer, C.; Alvarez-Muñoz, D.; Brennholt, N.; Bourrain, X.; Buchinger, S.; Fries, E.; Grosbois, C.; Klasmeier, J.; Marti, T.; Rodriguez-Mozaz, S.; Urbatzka, R.; Vethaak, A. D.; Winther-Nielsen, M.; Reifferscheid, G. (2014), "Microplastics in freshwater ecosystems: what we know and what we need to know", *Environ. Sci. Eur.*, 26, pp. 1–9, DOI: 10.1186/s12302-014-0012-7.
- [12] **Palmer, J.**; Herat, S. (2021), "Ecotoxicity of Microplastic Pollutants to Marine Organisms: a Systematic Review", *Water. Air Soil Pollut.*, 232, pp. 1–21, DOI: 10.1007/s11270-021-05155-7.
- [13] **Sharma, S.**; Chatterjee, S. (2017), "Microplastic pollution, a threat to marine ecosystem and human health: a short review", *Environ. Sci. Pollut. Res.*, 24, pp. 21530–21547, DOI: 10.1007/s11356-017-9910-8.
- [14] **Du, S.**; Zhu, R.; Cai, Y.; Xu, N.; Yap, P.-S.; Zhang, Y.; He, Y.; Zhang, Y. (2021), "Environmental fate and impacts of microplastics in aquatic ecosystems: a review", *RSC Advan.*, 11, pp. 15762–15784, DOI: 10.1039/d1ra00880c.
- [15] **Eltemsah, Y. S.**; Bøhn, T. (2019), "Acute and chronic effects of polystyrene microplastics on juvenile and adult *Daphnia magna*", *Environ. Pollut.*, 254. Article 112919, pp. 1–9, DOI: 10.1016/j.envpol.2019.07.087.
- [16] **Klein, K.**; Piana, T.; Lauschke, T.; Schweyen, P.; Dierkes, G.; Ternes, T.; Schulte-Oehlmann, U.; Oehlmann, J. (2021), "Chemicals associated with biodegradable microplastic drive the toxicity to the freshwater oligochaete *Lumbriculus variegatus*", *Aquat. Toxicol.*, 231. Article 105723, pp. 1–10, DOI: 10.1016/j.aquatox.2020.105723.

- [17] **Schwarzer, M.**; Brehm, J.; Vollmer, M.; Jasinski, J.; Xu, C.; Zainuddin, S.; Fröhlich, T.; Schott, M.; Greiner, A.; Scheibel, T.; Laforsch, C. (2022), "Shape, size, and polymer dependent effects of microplastics on *Daphnia magna*", *J. Haz. Mat.*, 426. Article 128136, pp. 1–9, DOI: 10.1016/j.jhazmat.2021.128136.
- [18] **Xia, X.**; Sun, M.; Zhou, M.; Chang, Z.; Li, L. (2020), "Polyvinyl chloride microplastics induce growth inhibition and oxidative stress in *Cyprinus carpio* var. larvae", *Sci. Total Environ.*, 716. Article 136479, pp. 1–8, DOI: 10.1016/j.scitotenv.2019.136479.
- [19] **Xu, E. G.**; Cheong, R. S.; Liu, L.; Hernandez, L. M.; Azimzada, A.; Bayen, S.; Tufenkji, N. (2020), "Primary and Secondary Plastic Particles Exhibit Limited Acute Toxicity but Chronic Effects on *Daphnia magna*", *Environ. Sci. Technol.*, 54, pp. 6859–6868, DOI: 10.1021/acs.est.0c00245.
- [20] **Nabi, G.**; Ahmad, S.; Ullah, S.; Zada, S.; Sarfraz, M.; Guo, X.; Ismail, M.; Wanghe, K. (2022), "The adverse health effects of increasing microplastic pollution on aquatic mammals", *J. King Saud Univ. Sci.*, 34. Article 102006, pp. 1–10, DOI: 10.1016/j.jksus.2022.102006.
- [21] **Charlton-Howard, H. S.**; Bond, A. L.; Rivers-Auty, J.; Lavers, J. L. (2023), "'Plasticosis': Characterising macro- and microplastic-associated fibrosis in seabird tissues", *J. Haz. Mat.*, 450. Article 131090, pp. 1–12, DOI: 10.1016/j.jhazmat.2023.131090.
- [22] **Qiao, R.**; Mortimer, M.; Richter, J.; Rani-Borges, B.; Yu, Z.; Heinlaan, M.; Lin, S.; Ivask, A. (2022), "Hazard of polystyrene micro- and nanospheres to selected aquatic and terrestrial organisms", *Sci. Total Environ.*, 853. Article 158560, pp. 1–16, DOI: 10.1016/j.scitotenv.2022.158560.
- [23] **van Raamsdonk, L. W. D.**; van der Zande, M.; Koelmans, A. A.; Hoogenboom, R. L. A. P.; Peters, R. J. B.; Groot, M. J.; Peijnenburg, A. A. C. M.; Weesepeel, Y. J. A. (2020), "Current Insights into Monitoring, Bioaccumulation, and Potential Health Effects of Microplastics Present in the Food Chain", *Foods*, 9, pp. 1–28, DOI: 10.3390/foods9010072.
- [24] **Jiang, B.**; Kauffman, A. E.; Li, L.; McFee, W.; Cai, B.; Weinstein, J.; Lead, J. R.; Chatterjee, S.; Scott, G. I.; Xiao, S. (2020), "Health impacts of environmental contamination of micro- and nanoplastics: a review", *Environ. Health Prev. Med.*, 25. Article 29, pp. 1–15, DOI: 10.1186/s12199-020-00870-9.
- [25] **Kraas, C.**; Bauske, B., "Mikroplastik in der Umwelt", can be found under <https://www.wwf.de/fileadmin/fm-wwf/Publikationen-PDF/WWF-Hintergrundpapier-Mikroplastik.pdf>, 2020.
- [26] **Cox, K. D.**; Covernton, G. A.; Davies, H. L.; Dower, J. F.; Juanes, F.; Dudas, S. E. (2019), "Human Consumption of Microplastics", *Environ. Sci. Technol.*, 53, pp. 7068–7074, DOI: 10.1021/acs.est.9b01517.
- [27] **Amato-Lourenço, L. F.**; Carvalho-Oliveira, R.; Júnior, G. R.; Dos Santos Galvão, L.; Ando, R. A.; Mauad, T. (2021), "Presence of airborne microplastics in human lung tissue", *J. Haz. Mat.*, 416. Article 126124, pp. 1–6, DOI: 10.1016/j.jhazmat.2021.126124.
- [28] **Schwabl, P.**; Köppel, S.; Königshofer, P.; Bucsics, T.; Trauner, M.; Reiberger, T.; Liebmann, B. (2019), "Detection of Various Microplastics in Human Stool: A Prospective Case Series", *Ann. Intern. Med.*, 171, pp. 453–457, DOI: 10.7326/M19-0618.
- [29] **Leslie, H. A.**; van Velzen, M. J. M.; Brandsma, S. H.; Vethaak, A. D.; Garcia-Vallejo, J. J.; Lamoree, M. H. (2022), "Discovery and quantification of plastic particle pollution in human blood", *Environ. Int.*, 163. Article 107199, pp. 1–8, DOI: 10.1016/j.envint.2022.107199.
- [30] **Ragusa, A.**; Svelato, A.; Santacroce, C.; Catalano, P.; Notarstefano, V.; Carnevali, O.; Papa, F.; Rongioletti, M. C. A.; Baiocco, F.; Draghi, S.; D'Amore, E.; Rinaldo, D.; Matta, M.; Giorgini, E. (2021), "Plasticenta: First evidence of microplastics in human placenta", *Environ. Int.*, 146. Article 106274, pp. 1–8, DOI: 10.1016/j.envint.2020.106274.
- [31] **González-Acedo, A.**; García-Recio, E.; Illescas-Montes, R.; Ramos-Torrecillas, J.; Melguizo-Rodríguez, L.; Costela-Ruiz, V. J. (2021), "Evidence from in vitro and in vivo studies on the potential health repercussions of micro- and nanoplastics", *Chemosphere*, 280. Article 130826, pp. 1–7, DOI: 10.1016/j.chemosphere.2021.130826.
- [32] **Deng, Y.**; Zhang, Y.; Lemos, B.; Ren, H. (2017), "Tissue accumulation of microplastics in mice and biomarker responses suggest widespread health risks of exposure", *Sci. Rep.*, 7, p. 46687, DOI: 10.1038/srep46687.

- [33] **Hirt, N.**; Body-Malapel, M. (2020), "Immunotoxicity and intestinal effects of nano- and microplastics: a review of the literature", *Part. Fibre Toxicol.*, 17. Article 57, pp. 1–22, DOI: 10.1186/s12989-020-00387-7.
- [34] **Hou, B.**; Wang, F.; Liu, T.; Wang, Z. (2021), "Reproductive toxicity of polystyrene microplastics: In vivo experimental study on testicular toxicity in mice", *J. Haz. Mat.*, 405. Article 124028, pp. 1–11, DOI: 10.1016/j.jhazmat.2020.124028.
- [35] **Liang, B.**; Zhong, Y.; Huang, Y.; Lin, X.; Liu, J.; Lin, L.; Hu, M.; Jiang, J.; Dai, M.; Wang, B.; Zhang, B.; Meng, H.; Lelaka, J. J. J.; Sui, H.; Yang, X.; Huang, Z. (2021), "Underestimated health risks: polystyrene micro- and nanoplastics jointly induce intestinal barrier dysfunction by ROS-mediated epithelial cell apoptosis", *Part. Fibre Toxicol.*, 18. Article 20, pp. 1–19, DOI: 10.1186/s12989-021-00414-1.
- [36] **Yang, Y.-F.**; Chen, C.-Y.; Lu, T.-H.; Liao, C.-M. (2019), "Toxicity-based toxicokinetic/toxicodynamic assessment for bioaccumulation of polystyrene microplastics in mice", *J. Haz. Mat.*, 366, pp. 703–713, DOI: 10.1016/j.jhazmat.2018.12.048.
- [37] **Jin, Y.**; Lu, L.; Tu, W.; Luo, T.; Fu, Z. (2019), "Impacts of polystyrene microplastic on the gut barrier, microbiota and metabolism of mice", *Sci. Total Environ.*, 649, pp. 308–317, DOI: 10.1016/j.scitotenv.2018.08.353.
- [38] **Pauwels, K.**; Herman, P.; van Vaerenbergh, B.; Thi, C. D. D.; Berghmans, L.; Waeterloos, G.; van Bockstaele, D.; Dorsch-Häsler, K.; Sneyers, M. (2007), "Animal Cell Cultures: Risk Assessment and Biosafety Recommendations", *Appl. Biosaf.*, 12, pp. 26–38, DOI: 10.1177/153567600701200105.
- [39] **Zucco, F.**; Angelis, I. de; Testai, E.; Stammati, A. (2004), "Toxicology investigations with cell culture systems: 20 years after", *Toxicol. In Vitro*, 18, pp. 153–163, DOI: 10.1016/S0887-2333(03)00147-4.
- [40] **Pamies, D.**; Hartung, T. (2017), "21st Century Cell Culture for 21st Century Toxicology", *Chem. Res. Toxicol.*, 30, pp. 43–52, DOI: 10.1021/acs.chemrestox.6b00269.
- [41] **Revel, M.**; Roman, C.; Châtel, A. (2021), "Is cell culture a suitable tool for the evaluation of micro- and nanoplastics ecotoxicity?", *Ecotoxicology*, 30, pp. 421–430, DOI: 10.1007/s10646-021-02355-z.
- [42] **Aderem, A.**; Underhill, D. M. (1999), "Mechanisms of phagocytosis in macrophages", *Annu. Rev. Immunol.*, 17, pp. 593–623, DOI: 10.1146/annurev.immunol.17.1.593.
- [43] **Champion, J. A.**; Mitragotri, S. (2006), "Role of target geometry in phagocytosis", *PNAS*, 103, DOI: 10.1073/pnas.0600997103.
- [44] **Champion, J. A.**; Walker, A.; Mitragotri, S. (2008), "Role of particle size in phagocytosis of polymeric microspheres", *Pharm. Res.*, 25, pp. 1815–1821, DOI: 10.1007/s11095-008-9562-y.
- [45] **Lee, H. J.**; Woo, Y.; Hahn, T. W.; Jung, Y. M.; Jung, Y. J. (2020), "Formation and Maturation of the Phagosome: A Key Mechanism in Innate Immunity against Intracellular Bacterial Infection", *Microorganisms*, 8. Article 1298, pp. 1–22, DOI: 10.3390/microorganisms8091298.
- [46] **Sadat, S. M. A.**; Jahan, S. T.; Haddadi, A.; Sams M. A. Sadat; Sheikh Tasnim Jahan; Azita Haddadi (2016), "Effects of Size and Surface Charge of Polymeric Nanoparticles on in Vitro and in Vivo Applications", *J. Biomater. Nanobiotechnol.*, 7, pp. 91–108, DOI: 10.4236/jbnb.2016.72011.
- [47] **Danaei, M.**; Dehghankhold, M.; Ataei, S.; Hasanzadeh Davarani, F.; Javanmard, R.; Dokhani, A.; Khorasani, S.; Mozafari, M. R. (2018), "Impact of Particle Size and Polydispersity Index on the Clinical Applications of Lipidic Nanocarrier Systems", *Pharmaceutics*, 10, pp. 1–17, DOI: 10.3390/pharmaceutics10020057.
- [48] **Conner, S. D.**; Schmid, S. L. (2003), "Regulated portals of entry into the cell", *Nature*, 422, pp. 37–44, DOI: 10.1038/nature01451.
- [49] **Augustine, R.**; Hasan, A.; Primavera, R.; Wilson, R. J.; Thakor, A. S.; Kevadiya, B. D. (2020), "Cellular uptake and retention of nanoparticles: Insights on particle properties and interaction with cellular components", *Mater. Today Commun.*, 25. Article 101692, pp. 1–19, DOI: 10.1016/j.mtcomm.2020.101692.

- [50] **Kettler, K.**; Veltman, K.; van de Meent, D.; van Wezel, A.; Hendriks, A. J. (2014), "Cellular uptake of nanoparticles as determined by particle properties, experimental conditions, and cell type", *Environ. Toxicol. Chem.*, 33, pp. 481–492, DOI: 10.1002/etc.2470.
- [51] **Fröhlich, E.** (2012), "The role of surface charge in cellular uptake and cytotoxicity of medical nanoparticles", *Int. J. Nanomedicine*, 7, pp. 5577–5591, DOI: 10.2147/IJN.S36111.
- [52] **Sadauskas, E.**; Wallin, H.; Stoltenberg, M.; Vogel, U.; Doering, P.; Larsen, A.; Danscher, G. (2007), "Kupffer cells are central in the removal of nanoparticles from the organism", *Part. Fibre Toxicol.*, 4, pp. 1–7, DOI: 10.1186/1743-8977-4-10.
- [53] **Wang, Z.-Y.**; Burlak, C.; Klaunig, J. E.; Kamendulis, L. M. (2014), "Development of a cytokine-producing immortalized murine Kupffer cell line", *Cytokine*, 70, pp. 165–172, DOI: 10.1016/j.cyto.2014.07.251.
- [54] **Gordon, S.**; Martinez-Pomares, L. (2017), "Physiological roles of macrophages", *Pflugers Arch. : Eur. J. Phys.*, 469, pp. 365–374, DOI: 10.1007/s00424-017-1945-7.
- [55] **Kowalski, W. J.**; Bahnfleth, W. P.; Whittam, T. S., *Filtration of airborne microorganisms: Modeling and prediction*, 1999.
- [56] **Attia, M. F.**; Anton, N.; Akasov, R.; Chipper, M.; Markvicheva, E.; Vandamme, T. F. (2016), "Biodistribution and Toxicity of X-Ray Iodinated Contrast Agent in Nano-emulsions in Function of Their Size", *Pharm. Res.*, 33, pp. 603–614, DOI: 10.1007/s11095-015-1813-0.
- [57] **Shang, L.**; Nienhaus, K.; Nienhaus, G. U. (2014), "Engineered nanoparticles interacting with cells: size matters", *J. Nanobiotechnol.*, 12, pp. 1–11, DOI: 10.1186/1477-3155-12-5.
- [58] **Davies, S. P.**; Reynolds, G. M.; Stamataki, Z. (2018), "Clearance of Apoptotic Cells by Tissue Epithelia: A Putative Role for Hepatocytes in Liver Efferocytosis", *Front. Immunol.*, 9. Article 44, pp. 1–15, DOI: 10.3389/fimmu.2018.00044.
- [59] **Kamakura, R.**; Raza, G. S.; Prasannan, A.; Walkowiak, J.; Herzig, K. H. (2020), "Dipeptidyl peptidase-4 and GLP-1 interplay in STC-1 and GLUTag cell lines", *Peptides*, 134. Article 170419, DOI: 10.1016/j.peptides.2020.170419.
- [60] **Shah, B.**; Kona, S.; Gilbertson, T. A.; Nguyen, K. T. (2011), "Effects of poly-(lactide-co-glycolide) nanoparticles on electrophysiological properties of enteroendocrine cells", *J. Nanosci. Nanotechnol.*, 11, pp. 3533–3542, DOI: 10.1166/jnn.2011.3802.
- [61] **Schrade, A.**; Mailänder, V.; Ritz, S.; Landfester, K.; Ziener, U. (2012), "Surface roughness and charge influence the uptake of nanoparticles: fluorescently labeled pickering-type versus surfactant-stabilized nanoparticles", *Macromol. Biosci.*, 12, pp. 1459–1471, DOI: 10.1002/mabi.201200166.
- [62] **Musyanovych, A.**; Dausend, J.; Dass, M.; Walther, P.; Mailänder, V.; Landfester, K. (2011), "Criteria impacting the cellular uptake of nanoparticles: a study emphasizing polymer type and surfactant effects", *Acta Biomater.*, 7, pp. 4160–4168, DOI: 10.1016/j.actbio.2011.07.033.
- [63] **Lowick, J. H.**; James, A. M. (1957), "The electrokinetic properties of *Aerobacter aerogenes*; a comparison of the properties of normal and crystal violet-trained cells", *Biochem. J.*, 65, pp. 431–438, DOI: 10.1042/bj0650431.
- [64] **Ramsperger, A. F. R. M.**; Narayana, V. K. B.; Gross, W.; Mohanraj, J.; Thelakkat, M.; Greiner, A.; Schmalz, H.; Kress, H.; Laforsch, C. (2020), "Environmental exposure enhances the internalization of microplastic particles into cells", *Sci. Adv.*, 6. Article eabd1211, pp. 1–9, DOI: 10.1126/sciadv.abd1211.
- [65] **Cao, X.**; Han, Y.; Li, F.; Li, Z.; McClements, D. J.; He, L.; Decker, E. A.; Xing, B.; Xiao, H. (2019), "Impact of protein-nanoparticle interactions on gastrointestinal fate of ingested nanoparticles: Not just simple protein corona effects", *NanoImpact*, 13, pp. 37–43, DOI: 10.1016/j.impact.2018.12.002.
- [66] **Lundqvist, M.**; Stigler, J.; Elia, G.; Lynch, I.; Cedervall, T.; Dawson, K. A. (2008), "Nanoparticle size and surface properties determine the protein corona with possible implications for biological impacts", *PNAS*, 105, pp. 14265–14270, DOI: 10.1073/pnas.0805135105.

- [67] **Saavedra, J.**; Stoll, S.; Slaveykova, V. I. (2019), "Influence of nanoplastic surface charge on eco-corona formation, aggregation and toxicity to freshwater zooplankton", *Environ. Pollut.*, 252, pp. 715–722, DOI: 10.1016/j.envpol.2019.05.135.
- [68] **Shannahan, J. H.**; Lai, X.; Ke, P. C.; Podila, R.; Brown, J. M.; Witzmann, F. A. (2013), "Silver nanoparticle protein corona composition in cell culture media", *PloS one*, 8. Article e74001, 1-10, DOI: 10.1371/journal.pone.0074001.
- [69] **Tenzer, S.**; Docter, D.; Kuharev, J.; Musyanovych, A.; Fetz, V.; Hecht, R.; Schlenk, F.; Fischer, D.; Kiouptsi, K.; Reinhardt, C.; Landfester, K.; Schild, H.; Maskos, M.; Knauer, S. K.; Stauber, R. H. (2013), "Rapid formation of plasma protein corona critically affects nanoparticle pathophysiology", *Nature Nanotech*, 8, pp. 772–781, DOI: 10.1038/nnano.2013.181.
- [70] **Partikel, K.**; Korte, R.; Mulac, D.; Humpf, H.-U.; Langer, K. (2019), "Serum type and concentration both affect the protein-corona composition of PLGA nanoparticles", *Beilstein J. Nanotechnol.*, 10, pp. 1002–1015, DOI: 10.3762/bjnano.10.101.
- [71] **Rudolph, J.**; Völkl, M.; Jérôme, V.; Scheibel, T.; Freitag, R. (2021), "Noxic effects of polystyrene microparticles on murine macrophages and epithelial cells", *Sci. Rep.*, 11. Article 15702, pp. 1–16, DOI: 10.1038/s41598-021-95073-9.
- [72] **Vlácil, A.-K.**; Bänfer, S.; Jacob, R.; Trippel, N.; Kuzu, I.; Schieffer, B.; Grote, K. (2021), "Polystyrene microplastic particles induce endothelial activation", *PloS one*, 16. Article e0260181, 1-10, DOI: 10.1371/journal.pone.0260181.
- [73] **Hwang, J.**; Choi, D.; Han, S.; Choi, J.; Hong, J. (2019), "An assessment of the toxicity of polypropylene microplastics in human derived cells", *Sci. Total Environ.*, 684, pp. 657–669, DOI: 10.1016/j.scitotenv.2019.05.071.
- [74] **Aguilar-Guzmán, J. C.**; Bejtka, K.; Fontana, M.; Valsami-Jones, E.; Villezcás, A. M.; Vazquez-Duhalt, R.; Rodríguez-Hernández, A. G. (2022), "Polyethylene terephthalate nanoparticles effect on RAW 264.7 macrophage cells", *Micropl. & Nanopl.*, 2, pp. 1–15, DOI: 10.1186/s43591-022-00027-1.
- [75] **Florance, I.**; Ramasubbu, S.; Mukherjee, A.; Chandrasekaran, N. (2021), "Polystyrene nanoplastics dysregulate lipid metabolism in murine macrophages in vitro", *Toxicology*, 458. Article 152850, pp. 1–12, DOI: 10.1016/j.tox.2021.152850.
- [76] **Zhao, L.**; Shi, W.; Hu, F.; Song, X.; Cheng, Z.; Zhou, J. (2021), "Prolonged oral ingestion of microplastics induced inflammation in the liver tissues of C57BL/6J mice through polarization of macrophages and increased infiltration of natural killer cells", *Ecotoxicol. Environ. Saf.*, 227. Article 112882, pp. 1–8, DOI: 10.1016/j.ecoenv.2021.112882.
- [77] **Zhao, C.**; Xu, T.; He, M.; Shah, K. J.; You, Z.; Zhang, T.; Zubair, M. (2021), "Exploring the toxicity of the aged styrene-butadiene rubber microplastics to petroleum hydrocarbon-degrading bacteria under compound pollution system", *Ecotoxicol. Environ. Saf.*, 227. Article 112903, pp. 1–11, DOI: 10.1016/j.ecoenv.2021.112903.
- [78] **Wu, B.**; Wu, X.; Liu, S.; Wang, Z.; Chen, L. (2019), "Size-dependent effects of polystyrene microplastics on cytotoxicity and efflux pump inhibition in human Caco-2 cells", *Chemosphere*, 221, pp. 333–341, DOI: 10.1016/j.chemosphere.2019.01.056.
- [79] **Stock, V.**; Laurisch, C.; Franke, J.; Dönmez, M. H.; Voss, L.; Böhmert, L.; Braeuning, A.; Sieg, H. (2021), "Uptake and cellular effects of PE, PP, PET and PVC microplastic particles", *Toxicol. In Vitro*, 70. Article 105021, pp. 1–9, DOI: 10.1016/j.tiv.2020.105021.
- [80] **Stock, V.**; Böhmert, L.; Lisicki, E.; Block, R.; Cara-Carmona, J.; Pack, L. K.; Selb, R.; Lichtenstein, D.; Voss, L.; Henderson, C. J.; Zabinsky, E.; Sieg, H.; Braeuning, A.; Lampen, A. (2019), "Uptake and effects of orally ingested polystyrene microplastic particles in vitro and in vivo", *Arch. Toxicol.*, 93, pp. 1817–1833, DOI: 10.1007/s00204-019-02478-7.

- [81] **Stock, V.**; Böhmert, L.; Coban, G.; Tyra, G.; Vollbrecht, M.-L.; Voss, L.; Paul, M. B.; Braeuning, A.; Sieg, H. (2022), "Microplastics and nanoplastics: Size, surface and dispersant - What causes the effect?", *Toxicol. In Vitro*, 80. Article 105314, pp. 1–11, DOI: 10.1016/j.tiv.2022.105314.
- [82] **Lu, L.**; Wan, Z.; Luo, T.; Fu, Z.; Jin, Y. (2018), "Polystyrene microplastics induce gut microbiota dysbiosis and hepatic lipid metabolism disorder in mice", *Sci. Total Environ.*, 631-632, pp. 449–458, DOI: 10.1016/j.scitotenv.2018.03.051.
- [83] **Liu, S.**; Wu, X.; Gu, W.; Yu, J.; Wu, B. (2020), "Influence of the digestive process on intestinal toxicity of polystyrene microplastics as determined by in vitro Caco-2 models", *Chemosphere*, 256. Article 127204, pp. 1–9, DOI: 10.1016/j.chemosphere.2020.127204.
- [84] **Liang, S.**; Luo, Y.; Yi, J.; Feng, L.; Xu, M.; Yao, R., *Toxicity of microplastics and plastic additive co-exposure in liver Disse organoids from healthy donors and patient-derived induced pluripotent stem cells*, 2022.
- [85] **Li, S.**; Shi, M.; Wang, Y.; Xiao, Y.; Cai, D.; Xiao, F. (2021), "Keap1-Nrf2 pathway up-regulation via hydrogen sulfide mitigates polystyrene microplastics induced-hepatotoxic effects", *J. Haz. Mat.*, 402. Article 123933, pp. 1–11, DOI: 10.1016/j.jhazmat.2020.123933.
- [86] **Li, S.**; Ma, Y.; Ye, S.; Tang, S.; Liang, N.; Liang, Y.; Xiao, F. (2021), "Polystyrene microplastics trigger hepatocyte apoptosis and abnormal glycolytic flux via ROS-driven calcium overload", *J. Haz. Mat.*, 417. Article 126025, pp. 1–13, DOI: 10.1016/j.jhazmat.2021.126025.
- [87] **Rubio, L.**; Barguilla, I.; Domenech, J.; Marcos, R.; Hernández, A. (2020), "Biological effects, including oxidative stress and genotoxic damage, of polystyrene nanoparticles in different human hematopoietic cell lines", *J. Haz. Mat.*, 398. Article 122900, pp. 1–8, DOI: 10.1016/j.jhazmat.2020.122900.
- [88] **Paul, M. B.**; Stock, V.; Cara-Carmona, J.; Lisicki, E.; Shopova, S.; Fessard, V.; Braeuning, A.; Sieg, H.; Böhmert, L. (2020), "Micro- and nanoplastics - current state of knowledge with the focus on oral uptake and toxicity", *Nanoscale Adv.*, 2, pp. 4350–4367, DOI: 10.1039/d0na00539h.
- [89] **Brachner, A.**; Fragouli, D.; Duarte, I. F.; Farias, P. M. A.; Dembski, S.; Ghosh, M.; Barisic, I.; Zdzieblo, D.; Vanoirbeek, J.; Schwabl, P.; Neuhaus, W. (2020), "Assessment of Human Health Risks Posed by Nano-and Microplastics Is Currently Not Feasible", *Int. J. Environ. Res. Public Health*, 17. Article 8832, pp. 1–10, DOI: 10.3390/ijerph17238832.
- [90] **Blackburn, K.**; Green, D. (2022), "The potential effects of microplastics on human health: What is known and what is unknown", *Ambio*, 51, pp. 518–530, DOI: 10.1007/s13280-021-01589-9.
- [91] **Yong, C. Q. Y.**; Valiyaveetil, S.; Tang, B. L. (2020), "Toxicity of Microplastics and Nanoplastics in Mammalian Systems", *Int. J. Environ. Res. Public Health*, 17. Article 1509, pp. 1–24, DOI: 10.3390/ijerph17051509.
- [92] **Shi, Q.**; Tang, J.; Liu, R.; Wang, L. (2022), "Toxicity in vitro reveals potential impacts of microplastics and nanoplastics on human health: A review", *Crit. Rev. Environ. Sci. Technol.*, 52, pp. 3863–3895, DOI: 10.1080/10643389.2021.1951528.
- [93] **Rubio, L.**; Marcos, R.; Hernández, A. (2020), "Potential adverse health effects of ingested micro- and nanoplastics on humans. Lessons learned from in vivo and in vitro mammalian models", *J. Toxicol. Environ. Health B Crit. Rev.*, 23, pp. 51–68, DOI: 10.1080/10937404.2019.1700598.
- [94] **Rozman, U.**; Kalčíková, G. (2022), "Seeking for a perfect (non-spherical) microplastic particle - The most comprehensive review on microplastic laboratory research", *J. Haz. Mat.*, 424. Article 127529, pp. 1–17, DOI: 10.1016/j.jhazmat.2021.127529.
- [95] **Weis, J. S.**; Palmquist, K. H. (2021), "Reality Check: Experimental Studies on Microplastics Lack Realism", *Appl. Sci.*, 11. Article 8529, pp. 1–16, DOI: 10.3390/app11188529.
- [96] **Banerjee, A.**; Shelper, W. L. (2021), "Micro- and nanoplastic induced cellular toxicity in mammals: A review", *Sci. Total Environ.*, 755. Article 142518, DOI: 10.1016/j.scitotenv.2020.142518.
- [97] **Kurtz-Chalot, A.**; Villiers, C.; Pourchez, J.; Boudard, D.; Martini, M.; Marche, P. N.; Cottier, M.; Forest, V. (2017), "Impact of silica nanoparticle surface chemistry on protein corona formation and consequential interactions with biological cells", *Mater. Sci. Eng. C*, 75, pp. 16–24, DOI: 10.1016/j.msec.2017.02.028.



- [98] **Palaniappan, S.**; Sadacharan, C. M.; Rostama, B. (2022), "Polystyrene and Polyethylene Microplastics Decrease Cell Viability and Dysregulate Inflammatory and Oxidative Stress Markers of MDCK and L929 Cells In Vitro", *Expos. Health.*, 14, pp. 75–85, DOI: 10.1007/s12403-021-00419-3.
- [99] **Schirinzì, G. F.**; Pérez-Pomeda, I.; Sanchís, J.; Rossini, C.; Farré, M.; Barceló, D. (2017), "Cytotoxic effects of commonly used nanomaterials and microplastics on cerebral and epithelial human cells", *Environ. Res.*, 159, pp. 579–587, DOI: 10.1016/j.envres.2017.08.043.
- [100] **Rubin, A. E.**; Sarkar, A. K.; Zucker, I. (2021), "Questioning the suitability of available microplastics models for risk assessment - A critical review", *Sci. Total Environ.*, 788. Article 147670, pp. 1–12, DOI: 10.1016/j.scitotenv.2021.147670.
- [101] **Gewert, B.**; Plassmann, M. M.; MacLeod, M. (2015), "Pathways for degradation of plastic polymers floating in the marine environment", *Environ. Sci. Process Impacts*, 17, pp. 1513–1521, DOI: 10.1039/c5em00207a.
- [102] **Syranidou, E.**; Karkanorachaki, K.; Amorotti, F.; Franchini, M.; Repouskou, E.; Kaliva, M.; Vamvakaki, M.; Kolvenbach, B.; Fava, F.; Corvini, P. F.-X.; Kalogerakis, N. (2017), "Biodegradation of weathered polystyrene films in seawater microcosms", *Sci. Rep.*, 7. Article 17991, pp. 1–12, DOI: 10.1038/s41598-017-18366-y.
- [103] **Liu, P.**; Shi, Y.; Wu, X.; Wang, H.; Huang, H.; Guo, X.; Gao, S. (2021), "Review of the artificially-accelerated aging technology and ecological risk of microplastics", *Sci. Total Environ.*, 768. Article 144969, pp. 1–11, DOI: 10.1016/j.scitotenv.2021.144969.
- [104] **Liu, P.**; Zhan, X.; Wu, X.; Li, J.; Wang, H.; Gao, S. (2020), "Effect of weathering on environmental behavior of microplastics: Properties, sorption and potential risks", *Chemosphere*, 242. Article 125193, DOI: 10.1016/j.chemosphere.2019.125193.
- [105] **Huang, Y.**; Ding, J.; Zhang, G.; Liu, S.; Zou, H.; Wang, Z.; Zhu, W.; Geng, J. (2021), "Interactive effects of microplastics and selected pharmaceuticals on red tilapia: Role of microplastic aging", *Sci. Total Environ.*, 752. Article 142256, pp. 1–15, DOI: 10.1016/j.scitotenv.2020.142256.
- [106] **Zou, W.**; Xia, M.; Jiang, K.; Cao, Z.; Zhang, X.; Hu, X. (2020), "Photo-Oxidative Degradation Mitigated the Developmental Toxicity of Polyamide Microplastics to Zebrafish Larvae by Modulating Macrophage-Triggered Proinflammatory Responses and Apoptosis", *Environ. Sci. Technol.*, 54, pp. 13888–13898, DOI: 10.1021/acs.est.0c05399.
- [107] **Wang, Q.**; Wangjin, X.; Zhang, Y.; Wang, N.; Wang, Y.; Meng, G.; Chen, Y. (2020), "The toxicity of virgin and UV-aged PVC microplastics on the growth of freshwater algae *Chlamydomonas reinhardtii*", *Sci. Total Environ.*, 749. Article 141603, pp. 1–7, DOI: 10.1016/j.scitotenv.2020.141603.
- [108] **Wang, C.**; Xian, Z.; Jin, X.; Liang, S.; Chen, Z.; Pan, B.; Wu, B.; Ok, Y. S.; Gu, C. (2020), "Photo-aging of polyvinyl chloride microplastic in the presence of natural organic acids", *Water Res.*, 183. Article 116082, DOI: 10.1016/j.watres.2020.116082.
- [109] **Guimarães, A. T. B.**; Estrela, F. N.; Pereira, P. S.; Andrade Vieira, J. E. de; Lima Rodrigues, A. S. de; Silva, F. G.; Malafaia, G. (2021), "Toxicity of polystyrene nanoplastics in *Ctenopharyngodon idella* juveniles: A genotoxic, mutagenic and cytotoxic perspective", *Sci. Total Environ.*, 752. Article 141937, pp. 1–12, DOI: 10.1016/j.scitotenv.2020.141937.
- [110] **Yu, X.**; Lang, M.; Huang, D.; Yang, C.; Ouyang, Z.; Guo, X. (2022), "Photo-transformation of microplastics and its toxicity to Caco-2 cells", *Sci. Total Environ.*, 806. Article 150954, DOI: 10.1016/j.scitotenv.2021.150954.
- [111] **Zhu, K.**; Jia, H.; Sun, Y.; Dai, Y.; Zhang, C.; Guo, X.; Wang, T.; Zhu, L. (2020), "Enhanced cytotoxicity of photoaged phenol-formaldehyde resins microplastics: Combined effects of environmentally persistent free radicals, reactive oxygen species, and conjugated carbonyls", *Environ. Int.*, 145. Article 106137, pp. 1–8, DOI: 10.1016/j.envint.2020.106137.
- [112] **Jeon, S.**; Lee, D.-K.; Jeong, J.; Yang, S. I.; Kim, J.-S.; Kim, J.; Cho, W.-S. (2021), "The reactive oxygen species as pathogenic factors of fragmented microplastics to macrophages", *Environ. Pollut.*, 281. Article 117006, pp. 1–12, DOI: 10.1016/j.envpol.2021.117006.

- [113] **Stepanenko, A. A.**; Dmitrenko, V. V. (2015), "Pitfalls of the MTT assay: Direct and off-target effects of inhibitors can result in over/underestimation of cell viability", *Gene*, 574, pp. 193–203, DOI: 10.1016/j.gene.2015.08.009.
- [114] **Ghasemi, M.**; Turnbull, T.; Sebastian, S.; Kempson, I. (2021), "The MTT Assay: Utility, Limitations, Pitfalls, and Interpretation in Bulk and Single-Cell Analysis", *Int. J. Mol. Sci.*, 22. Article 12827, pp. 1–30, DOI: 10.3390/ijms222312827.
- [115] **Ramsperger, A. F. R. M.**; Jasinski, J.; Völkl, M.; Witzmann, T.; Meinhart, M.; Jérôme, V.; Kretschmer, W. P.; Freitag, R.; Senker, J.; Fery, A.; Kress, H.; Scheibel, T.; Laforsch, C. (2022), "Supposedly identical microplastic particles substantially differ in their material properties influencing particle-cell interactions and cellular responses", *J. Haz. Mat.*, 425. Article 127961, pp. 1–14, DOI: 10.1016/j.jhazmat.2021.127961.
- [116] **Völkl, M.**; Jérôme, V.; Weig, A.; Jasinski, J.; Meides, N.; Strohhriegl, P.; Scheibel, T.; Freitag, R. (2022), "Pristine and artificially-aged polystyrene microplastic particles differ in regard to cellular response", *J. Haz. Mat.*, 435. Article 128955, pp. 1–13, DOI: 10.1016/j.jhazmat.2022.128955.
- [117] **Müller, A.-K.**; Brehm, J.; Völkl, M.; Jérôme, V.; Laforsch, C.; Freitag, R.; Greiner, A. (2022), "Disentangling biological effects of primary nanoplastics from dispersion paints' additional compounds", *Ecotoxicol. Environ. Saf.*, 242. Article 113877, pp. 1–9, DOI: 10.1016/j.ecoenv.2022.113877.
- [118] **Riedl, S. A. B.**; Völkl, M.; Holzinger, A.; Jasinski, J.; Jérôme, V.; Scheibel, T.; Feldhaar, H.; Freitag, R. (2022), "In vitro cultivation of primary intestinal cells from *Eisenia fetida* as basis for ecotoxicological studies", *Ecotoxicology*, 31, pp. 221–233, DOI: 10.1007/s10646-021-02495-2.
- [119] **Hesler, M.**; Aengenheister, L.; Ellinger, B.; Drexel, R.; Straskraba, S.; Jost, C.; Wagner, S.; Meier, F.; Briesen, H. von; Büchel, C.; Wick, P.; Buerki-Thurnherr, T.; Kohl, Y. (2019), "Multi-endpoint toxicological assessment of polystyrene nano- and microparticles in different biological models in vitro", *Toxicol. In Vitro*, 61. Article 104610, pp. 1–15, DOI: 10.1016/j.tiv.2019.104610.
- [120] **Forman, H. J.**; Zhang, H. (2021), "Targeting oxidative stress in disease: promise and limitations of antioxidant therapy", *Nat. Rev. Drug Discov.*, 20, pp. 689–709, DOI: 10.1038/s41573-021-00233-1.
- [121] **Turrens, J. F.** (2003), "Mitochondrial formation of reactive oxygen species", *J. Physiol.*, 552, pp. 335–344, DOI: 10.1113/jphysiol.2003.049478.
- [122] **Mittler, R.** (2017), "ROS Are Good", *Trends Plant Sci.*, 22, pp. 11–19, DOI: 10.1016/j.tplants.2016.08.002.
- [123] **Herb, M.**; Gluschnko, A.; Schramm, M. (2021), "Reactive Oxygen Species: Not Omnipresent but Important in Many Locations", *Front. Cell Dev. Biol.*, 9. Article 716406, pp. 1–12, DOI: 10.3389/fcell.2021.716406.
- [124] **Davies, K. J. A.** (2016), "Adaptive homeostasis", *Mol. Aspects Med.*, 49, pp. 1–7, DOI: 10.1016/j.mam.2016.04.007.
- [125] **Pizzino, G.**; Irrera, N.; Cucinotta, M.; Pallio, G.; Mannino, F.; Arcoraci, V.; Squadrito, F.; Altavilla, D.; Bitto, A. (2017), "Oxidative Stress: Harms and Benefits for Human Health", *Oxid. Med. Cell. Longev.*, 2017. Article 8416763, pp. 1–13, DOI: 10.1155/2017/8416763.
- [126] **Sies, H.**; Berndt, C.; Jones, D. P. (2017), "Oxidative Stress", *Annu. Rev. Biochem.*, 86, pp. 715–748, DOI: 10.1146/annurev-biochem-061516-045037.
- [127] **Winterbourn, C. C.**; Hampton, M. B. (2008), "Thiol chemistry and specificity in redox signaling", *Free Radic. Biol. Med.*, 45, pp. 549–561, DOI: 10.1016/j.freeradbiomed.2008.05.004.
- [128] **Wright, S. L.**; Kelly, F. J. (2017), "Plastic and Human Health: A Micro Issue?", *Environ. Sci. Technol.*, 51, pp. 6634–6647, DOI: 10.1021/acs.est.7b00423.
- [129] **Chen, X.**; Zhong, Z.; Xu, Z.; Chen, L.; Wang, Y. (2010), "2',7'-Dichlorodihydrofluorescein as a fluorescent probe for reactive oxygen species measurement: Forty years of application and controversy", *Free Radic. Res.*, 44, pp. 587–604, DOI: 10.3109/10715761003709802.

- [130] **Chung, S.**; Kim, S.-H.; Seo, Y.; Kim, S.-K.; Lee, J. Y. (2017), "Quantitative analysis of cell proliferation by a dye dilution assay: Application to cell lines and cocultures", *Cytometry Part A*, 91, pp. 704–712, DOI: 10.1002/cyto.a.23105.
- [131] **Begum, J.**; Day, W.; Henderson, C.; Purewal, S.; Cerveira, J.; Summers, H.; Rees, P.; Davies, D.; Filby, A. (2013), "A method for evaluating the use of fluorescent dyes to track proliferation in cell lines by dye dilution", *Cytom., : J. Int. Soc. Anal. Cytol.*, 83, pp. 1085–1095, DOI: 10.1002/cyto.a.22403.
- [132] **Lemieszek, M. B.**; Findlay, S. D.; Siegers, G. M. (2022), "CellTrace™ Violet Flow Cytometric Assay to Assess Cell Proliferation", *Methods Mol. Biol.*, 2508, pp. 101–114, DOI: 10.1007/978-1-0716-2376-3\_9.
- [133] **Riss, T.**; Niles, A.; Moravec, R.; Karassina, N.; Vidugiriene, J. in *Assay Guidance Manual [Internet]* (Eds.: T. Riss, A. Niles, R. Moravec, N. Karassina, J. Vidugiriene), Eli Lilly & Company and the National Center for Advancing Translational Sciences, 2019.
- [134] **Ostling, O.**; Johanson, K. J. (1984), "Microelectrophoretic study of radiation-induced DNA damages in individual mammalian cells", *Biochem. Biophys. Res. Commun.*, 123, pp. 291–298, DOI: 10.1016/0006-291x(84)90411-x.
- [135] **Lapuente, J. de**; Lourenço, J.; Mendo, S. A.; Borràs, M.; Martins, M. G.; Costa, P. M.; Pacheco, M. (2015), "The Comet Assay and its applications in the field of ecotoxicology: a mature tool that continues to expand its perspectives", *Front. Genet.*, 6, Article 180, pp. 1–20, DOI: 10.3389/fgene.2015.00180.
- [136] **Aydin, S.** (2015), "A short history, principles, and types of ELISA, and our laboratory experience with peptide/protein analyses using ELISA", *Peptides*, 72, pp. 4–15, DOI: 10.1016/j.peptides.2015.04.012.
- [137] **Merkley, S. D.**; Moss, H. C.; Goodfellow, S. M.; Ling, C. L.; Meyer-Hagen, J. L.; Weaver, J.; Campen, M. J.; Castillo, E. F. (2022), "Polystyrene microplastics induce an immunometabolic active state in macrophages", *Cell Biol. Toxicol.*, 38, pp. 31–41, DOI: 10.1007/s10565-021-09616-x.
- [138] **Coppack, S. W.** (2001), "Pro-inflammatory cytokines and adipose tissue", *PNS*, 60, pp. 349–356, DOI: 10.1079/pns2001110.
- [139] **Locati, M.**; Curtale, G.; Mantovani, A. (2020), "Diversity, Mechanisms, and Significance of Macrophage Plasticity", *Annu. Rev. Pathol.*, 15, pp. 123–147, DOI: 10.1146/annurev-pathmechdis-012418-012718.
- [140] **Sica, A.**; Mantovani, A. (2012), "Macrophage plasticity and polarization: in vivo veritas", *J. Clin. Investig.*, 122, pp. 787–795, DOI: 10.1172/JCI59643.
- [141] **Martinez, F. O.**; Gordon, S. (2014), "The M1 and M2 paradigm of macrophage activation: time for reassessment", *F1000 Prime Rep.*, 6, pp. 1–13, DOI: 10.12703/P6-13.
- [142] **Orecchioni, M.**; Ghosheh, Y.; Pramod, A. B.; Ley, K. (2019), "Macrophage Polarization: Different Gene Signatures in M1(LPS+) vs. Classically and M2(LPS-) vs. Alternatively Activated Macrophages", *Front. Immunol.* Article 1084, pp. 1–14, DOI: 10.3389/fimmu.2019.01084.
- [143] **Zhu, L.**; Zhao, Q.; Yang, T.; Ding, W.; Zhao, Y. (2015), "Cellular Metabolism and Macrophage Functional Polarization", *Int. Rev. Immunol.*, 34, pp. 82–100, DOI: 10.3109/08830185.2014.969421.
- [144] **Wang, L.-x.**; Zhang, S.-x.; Wu, H.-j.; Rong, X.-l.; Guo, J. (2019), "M2b macrophage polarization and its roles in diseases", *J. Leukoc. Biol.*, 106, pp. 345–358, DOI: 10.1002/JLB.3RU1018-378RR.
- [145] **Chatziioannou, E.**; Aydin, S. A.; Forchhammer, S.; Sinnberg, T.; Eigentler, T. (2022), "Makrophagen im Melanom – von molekularen Signalen zur therapeutischen Anwendung", *Dermatologie*, 73, pp. 915–928, DOI: 10.1007/s00105-022-05077-3.
- [146] **Zhang, Y.**; Choksi, S.; Chen, K.; Pobezinskaya, Y.; Linnoila, I.; Liu, Z. G. (2013), "ROS play a critical role in the differentiation of alternatively activated macrophages and the occurrence of tumor-associated macrophages", *Cell Res.*, 23, pp. 898–914, DOI: 10.1038/cr.2013.75.
- [147] **Gillooly, J. F.**; Hayward, A.; Hou, C.; Burleigh, J. G. (2012), "Explaining differences in the lifespan and replicative capacity of cells: a general model and comparative analysis of vertebrates", *Proc. Biol. Sci.*, 279, bin3976–3980, DOI: 10.1098/rspb.2012.1129.

- [148] **Kengla, C.**; Kidiyoor, A.; Murphy, S. V. in *Kidney Transplantation, Bioengineering and Regeneration*, Elsevier, **2017**, pp. 957–971.
- [149] **Li, Z.** in *Comprehensive Biotechnology*, Elsevier, **2019**, pp. 535–549.
- [150] **Verma, A.**; Verma, M.; Singh, A. in *Animal Biotechnology*, Elsevier, **2020**, pp. 269–293.
- [151] **Halappanavar, S.**; Mallach, G. (**2021**), "Adverse outcome pathways and in vitro toxicology strategies for microplastics hazard testing", *Curr. Opin. Toxicol.*, 28, pp. 52–61, DOI: 10.1016/j.cotox.2021.09.002.
- [152] **Jin, H.**; Yan, M.; Pan, C.; Liu, Z.; Sha, X.; Jiang, C.; Li, L.; Pan, M.; Li, D.; Han, X.; Ding, J. (**2022**), "Chronic exposure to polystyrene microplastics induced male reproductive toxicity and decreased testosterone levels via the LH-mediated LHR/cAMP/PKA/StAR pathway", *Part. Fibre. Toxicol.*, 19, pp. 1–17, DOI: 10.1186/s12989-022-00453-2.
- [153] **Jung, B.-K.**; Han, S.-W.; Park, S.-H.; Bae, J.-S.; Choi, J.; Ryu, K.-Y. (**2020**), "Neurotoxic potential of polystyrene nanoplastics in primary cells originating from mouse brain", *Neurotoxicology*, 81, pp. 189–196, DOI: 10.1016/j.neuro.2020.10.008.
- [154] **Zwollo, P.**; Quddos, F.; Bagdassarian, C.; Seeley, M. E.; Hale, R. C.; Abderhalden, L. (**2021**), "Polystyrene microplastics reduce abundance of developing B cells in rainbow trout (*Oncorhynchus mykiss*) primary cultures", *Fish Shellfish Immunol.*, 114, pp. 102–111, DOI: 10.1016/j.fsi.2021.04.014.
- [155] **Salimi, A.**; Alavehzadeh, A.; Ramezani, M.; Pourahmad, J. (**2022**), "Differences in sensitivity of human lymphocytes and fish lymphocytes to polyvinyl chloride microplastic toxicity", *Toxicol. Ind. Health*, 38, pp. 100–111, DOI: 10.1177/07482337211065832.
- [156] **Akhatova, F.**; Ishmukhametov, I.; Fakhrullina, G.; Fakhrullin, R. (**2022**), "Nanomechanical Atomic Force Microscopy to Probe Cellular Microplastics Uptake and Distribution", *Int. J. Mol. Sci.*, 23, pp. 1–12, DOI: 10.3390/ijms23020806.
- [157] **Feng, S.**; Duan, X.; Lo, P.-K.; Liu, S.; Liu, X.; Chen, H.; Wang, Q. (**2013**), "Expansion of breast cancer stem cells with fibrous scaffolds", *Integr. Biol.*, 5, pp. 768–777, DOI: 10.1039/c3ib20255k.
- [158] **Habanjar, O.**; Diab-Assaf, M.; Caldefie-Chezet, F.; Delort, L. (**2021**), "3D Cell Culture Systems: Tumor Application, Advantages, and Disadvantages", *Int. J. Mol. Sci.*, 22. Article 12200, pp. 1–35, DOI: 10.3390/ijms22212200.
- [159] **Shen, H.**; Cai, S.; Wu, C.; Yang, W.; Yu, H.; Liu, L. (**2021**), "Recent Advances in Three-Dimensional Multicellular Spheroid Culture and Future Development", *Micromachines*, 12, pp. 1–21, DOI: 10.3390/mi12010096.
- [160] **Justus, C. R.**; Leffler, N.; Ruiz-Echevarria, M.; Yang, L. V. (**2014**), "In vitro cell migration and invasion assays", *J. Vis. Exp.*, 88. Article e51046, pp. 1–8, DOI: 10.3791/51046.
- [161] **Marshall, J.** in *Cell Migration*, Humana Press, **2011**, pp. 97–110.
- [162] **Martins-Green, M.**; Petreaca, M.; Yao, M. in *Methods in Enzymology, volume 443* (Ed.: D. A. Cheres), Elsevier; Academic Press, Amsterdam, **2008**, pp. 137–153.
- [163] **Busch, M.**; B., G.; K., A. A. M.; Schins, R. F. (**2021**), "Investigations of acute effects of polystyrene and polyvinyl chloride micro- and nanoplastics in an advanced in vitro triple culture model of the healthy and inflamed intestine", *Environ. Res.*, 193. Article 110536, pp. 1–12, DOI: 10.1016/j.envres.2020.110536.
- [164] **Busch, M.**; Kämpfer, A. A. M.; Schins, R. P. F. (**2021**), "An inverted in vitro triple culture model of the healthy and inflamed intestine: Adverse effects of polyethylene particles", *Chemosphere*, 284. Article 131345, pp. 1–12, DOI: 10.1016/j.chemosphere.2021.131345.
- [165] **DeLoid, G. M.**; Cao, X.; Bitounis, D.; Singh, D.; Llopis, P. M.; Buckley, B.; Demokritou, P. (**2021**), "Toxicity, uptake, and nuclear translocation of ingested micro-nanoplastics in an in vitro model of the small intestinal epithelium", *Food Chem. Toxicol.*, 158. Article 112609, pp. 1–30, DOI: 10.1016/j.fct.2021.112609.

- [166] **Domenech, J.**; Hernández, A.; Rubio, L.; Marcos, R.; Cortés, C. (2020), "Interactions of polystyrene nanoplastics with in vitro models of the human intestinal barrier", *Arch. Toxicol.*, 94, pp. 2997–3012, DOI: 10.1007/s00204-020-02805-3.
- [167] **Qiao, J.**; Chen, R.; Wang, M.; Bai, R.; Cui, X.; Liu, Y.; Wu, C.; Chen, C. (2021), "Perturbation of gut microbiota plays an important role in micro/nanoplastics-induced gut barrier dysfunction", *Nanoscale*, 13, pp. 8806–8816, DOI: 10.1039/d1nr00038a.
- [168] **Shen, M.**; Zhang, Y.; Zhu, Y.; Song, B.; Zeng, G.; Hu, D.; Wen, X.; Ren, X. (2019), "Recent advances in toxicological research of nanoplastics in the environment: A review", *Environ. Pollut.*, 252, pp. 511–521, DOI: 10.1016/j.envpol.2019.05.102.
- [169] **Paul, M. B.**; Fahrenson, C.; Givélet, L.; Herrmann, T.; Loeschner, K.; Böhmert, L.; Thünemann, A. F.; Braeuning, A.; Sieg, H. (2022), "Beyond microplastics - investigation on health impacts of submicron and nanoplastic particles after oral uptake in vitro", *Micropl. & Nanopl.*, 2, pp. 1–19, DOI: 10.1186/s43591-022-00036-0.
- [170] **Zhang, M.**; Shi, J.; Huang, Q.; Xie, Y.; Wu, R.; Zhong, J.; Deng, H. (2022), "Multi-omics analysis reveals size-dependent toxicity and vascular endothelial cell injury induced by microplastic exposure in vivo and in vitro", *Environ. Sci.: Nano*, 9, pp. 663–683, DOI: 10.1039/D1EN01067K.
- [171] **Frost, T. S.**; Jiang, L.; Lynch, R. M.; Zohar, Y. (2019), "Permeability of Epithelial/Endothelial Barriers in Transwells and Microfluidic Bilayer Devices", *Micromachines*, 10, pp. 1–18, DOI: 10.3390/mi10080533.
- [172] **Hidalgo, I. J.**; Raub, T. J.; Borchardt, R. T. (1989), "Characterization of the human colon carcinoma cell line (Caco-2) as a model system for intestinal epithelial permeability", *Gastroenterology*, 96, pp. 1–14.
- [173] **Zhao, W.**; Han, L.; Bae, Y.; Manickam, D. S. (2019), "Lucifer Yellow - A Robust Paracellular Permeability Marker in a Cell Model of the Human Blood-brain Barrier", *J. Vis. Exp.* Article e58900, pp. 1–14, DOI: 10.3791/58900.
- [174] **Gunti, S.**; Hoke, A. T. K.; Vu, K. P.; London, N. R. (2021), "Organoid and Spheroid Tumor Models: Techniques and Applications", *Cancers*, 13. Article 874, pp. 1–17, DOI: 10.3390/cancers13040874.
- [175] **Decarli, M. C.**; Amaral, R.; Santos, D. P. D.; Tofani, L. B.; Katayama, E.; Rezende, R. A.; Silva, J. V. L. d.; Swiech, K.; Suazo, C. A. T.; Mota, C.; Moroni, L.; Moraes, Â. M. (2021), "Cell spheroids as a versatile research platform: formation mechanisms, high throughput production, characterization and applications", *Biofabrication*, 13. Article 032002, pp. 1–37, DOI: 10.1088/1758-5090/abe6f2.
- [176] **Jeong, Y.**; Tin, A.; Irudayaraj, J. (2022), "Flipped Well-Plate Hanging-Drop Technique for Growing Three-Dimensional Tumors", *Front. Bioeng. Biotechnol.*, 10. Article 898699, pp. 1–14, DOI: 10.3389/fbioe.2022.898699.
- [177] **Fu, J. J.**; Lv, X. H.; Wang, L. X.; He, X.; Li, Y.; Yu, L.; Li, C. M. (2021), "Cutting and Bonding Parafilm® to Fast Prototyping Flexible Hanging Drop Chips for 3D Spheroid Cultures", *Cell Mol. Bioeng.*, 14, pp. 187–199, DOI: 10.1007/s12195-020-00660-x.
- [178] **Wu, C.-G.**; Chiovaro, F.; Curioni-Fontecedro, A.; Casanova, R.; Soltermann, A. (2020), "In vitro cell culture of patient derived malignant pleural and peritoneal effusions for personalised drug screening", *J. Transl. Med.*, 18. Article 163, pp. 1–9, DOI: 10.1186/s12967-020-02331-x.
- [179] **Ishiguro, T.**; Ohata, H.; Sato, A.; Yamawaki, K.; Enomoto, T.; Okamoto, K. (2017), "Tumor-derived spheroids: Relevance to cancer stem cells and clinical applications", *Cancer Sci.*, 108, pp. 283–289, DOI: 10.1111/cas.13155.
- [180] **Ryu, N.-E.**; Lee, S.-H.; Park, H. (2019), "Spheroid Culture System Methods and Applications for Mesenchymal Stem Cells", *Cells*, 8, pp. 1–13, DOI: 10.3390/cells8121620.
- [181] **Hua, T.**; Kiran, S.; Li, Y.; Sang, Q.-X. A. (2022), "Microplastics exposure affects neural development of human pluripotent stem cell-derived cortical spheroids", *J. Haz. Mat.*, 435. Article 128884, DOI: 10.1016/j.jhazmat.2022.128884.

- [182] **Cheng, W.**; Li, X.; Zhou, Y.; Yu, H.; Xie, Y.; Guo, H.; Wang, H.; Li, Y.; Feng, Y.; Wang, Y. (2022), "Polystyrene microplastics induce hepatotoxicity and disrupt lipid metabolism in the liver organoids", *Sci. Total Environ.*, 806, DOI: 10.1016/j.scitotenv.2021.150328.
- [183] **Cheng, W.**; Zhou, Y.; Xie, Y.; Li, Y.; Zhou, R.; Wang, H.; Feng, Y.; Wang, Y. (2022), "Combined effect of polystyrene microplastics and bisphenol A on the human embryonic stem cells-derived liver organoids: The hepatotoxicity and lipid accumulation", *Sci. Total Environ.*, 854. Article 158585, DOI: 10.1016/j.scitotenv.2022.158585.
- [184] **Zeeshan, M.**; Murugadas, A.; Akbarsha, M. A. (2014), "Alternative model organisms for toxicity testing and risk assessment", *Contemp. Topics Life Sci.*, pp. 259–275.
- [185] **Jenner, R. A.**; Wills, M. A. (2007), "The choice of model organisms in evo–devo", *Nat. Rev. Genet.*, 8, pp. 311–314, DOI: 10.1038/nrg2062.
- [186] **Prokić, M. D.**; Gavrilović, B. R.; Radovanović, T. B.; Gavrić, J. P.; Petrović, T. G.; Despotović, S. G.; Faggio, C. (2021), "Studying microplastics: Lessons from evaluated literature on animal model organisms and experimental approaches", *J. Haz. Mat.*, 414. Article 125476, pp. 1–13, DOI: 10.1016/j.jhazmat.2021.125476.
- [187] **Mansano, A. S.**; Hisatugo, K. F.; Hayashi, L. H.; Regali-Selegim, M. H. (2014), "The importance of protozoan bacterivory in a subtropical environment (Lobo-Broa Reservoir, SP, Brazil)", *Braz. J. Biol.*, 74, pp. 569–578, DOI: 10.1590/bjb.2014.0081.
- [188] **Mansano, A. S.**; Moreira, R. A.; Pierozzi, M.; Oliveira, T. M. A.; Vieira, E. M.; Rocha, O.; Regali-Selegim, M. H. (2016), "Effects of diuron and carbofuran pesticides in their pure and commercial forms on *Paramecium caudatum*: The use of protozoan in ecotoxicology", *Environ. Pollut.*, 213, pp. 160–172, DOI: 10.1016/j.envpol.2015.11.054.
- [189] **Drago, C.**; Pawlak, J.; Weithoff, G. (2020), "Biogenic Aggregation of Small Microplastics Alters Their Ingestion by a Common Freshwater Micro-Invertebrate", *Front. Environ. Sci.*, 8. Article 574274, pp. 1–11, DOI: 10.3389/fenvs.2020.574274.
- [190] **Jeong, C.-B.**; Won, E.-J.; Kang, H.-M.; Lee, M.-C.; Hwang, D.-S.; Hwang, U.-K.; Zhou, B.; Souissi, S.; Lee, S.-J.; Lee, J.-S. (2016), "Microplastic Size-Dependent Toxicity, Oxidative Stress Induction, and p-JNK and p-p38 Activation in the Monogonont Rotifer (*Brachionus koreanus*)", *Environ. Sci. Technol.*, 50, pp. 8849–8857, DOI: 10.1021/acs.est.6b01441.
- [191] **Zheng, J.-L.**; Wang, D.; Chen, X.; Song, H.-Z.; Xiang, L.-P.; Yu, H.-X.; Peng, L.-B.; Zhu, Q.-L. (2022), "Nutritional-status dependent effects of microplastics on activity and expression of alkaline phosphatase and alpha-amylase in *Brachionus rotundiformis*", *Sci. Total Environ.*, 806. Article 150213, DOI: 10.1016/j.scitotenv.2021.150213.
- [192] **Athey, S. N.**; Albotra, S. D.; Gordon, C. A.; Monteleone, B.; Seaton, P.; Andrady, A. L.; Taylor, A. R.; Brander, S. M. (2020), "Trophic transfer of microplastics in an estuarine food chain and the effects of a sorbed legacy pollutant", *Limnol. Oceanogr. Letters*, 5, pp. 154–162, DOI: 10.1002/lol2.10130.
- [193] **Bermúdez, J. R.**; Metian, M.; Oberhänsli, F.; Taylor, A.; Swarzenski, P. W. (2021), "Preferential grazing and repackaging of small polyethylene microplastic particles ( $\leq 5 \mu\text{m}$ ) by the ciliate *Sterkiella* sp", *Mar. Environ. Res.*, 166. Article 105260, pp. 1–5, DOI: 10.1016/j.marenvres.2021.105260.
- [194] **Bulannga, R. B.**; Schmidt, S. (2022), "Uptake and accumulation of microplastic particles by two freshwater ciliates isolated from a local river in South Africa", *Environ. Res.*, 204. Article 112123, pp. 1–10, DOI: 10.1016/j.envres.2021.112123.
- [195] **Feng, J.**; Zhao, H.; Gong, X.; Xia, M.-C.; Cai, L.; Yao, H.; Zhao, X.; Yan, Z.; Li, Z.; Nie, H.; Ma, X.; Zhang, S. (2021), "In Situ Identification and Spatial Mapping of Microplastic Standards in *Paramecia* by Secondary-Ion Mass Spectrometry Imaging", *Anal. Chem.*, 93, pp. 5521–5528, DOI: 10.1021/acs.analchem.0c05383.
- [196] **Zhang, Y.**; Wang, J.; Geng, X.; Jiang, Y. (2021), "Does microplastic ingestion dramatically decrease the biomass of protozoa grazers? A case study on the marine ciliate *Uronema marinum*", *Chemosphere*, 267. Article 129308, pp. 1–8, DOI: 10.1016/j.chemosphere.2020.129308.

- [197] **Nisbet, B.** in *Nutrition and Feeding Strategies in Protozoa* (Ed.: B. Nisbet), Springer Netherlands, Dordrecht, **1984**, pp. 71–83.
- [198] **Conkle, J. L.**; Báez Del Valle, C. D.; Turner, J. W. (**2018**), "Are We Underestimating Microplastic Contamination in Aquatic Environments?", *J. Environ. Manage.*, 61, pp. 1–8, DOI: 10.1007/s00267-017-0947-8.
- [199] **Lindeque, P. K.**; Cole, M.; Coppock, R. L.; Lewis, C. N.; Miller, R. Z.; Watts, A. J. R.; Wilson-McNeal, A.; Wright, S. L.; Galloway, T. S. (**2020**), "Are we underestimating microplastic abundance in the marine environment? A comparison of microplastic capture with nets of different mesh-size", *Environ. Pollut.*, 265. Article 114721, pp. 1–12, DOI: 10.1016/j.envpol.2020.114721.
- [200] **Sivakumar, S.** (**2015**), "Effects of metals on earthworm life cycles: a review", *Environ. Monit. Assess.*, 187, pp. 1–16, DOI: 10.1007/s10661-015-4742-9.
- [201] **Bernard, F.**; Brulle, F.; Dumez, S.; Lemiere, S.; Platel, A.; Nessler, F.; Cuny, D.; Deram, A.; Vandebulcke, F. (**2015**), "Antioxidant responses of Annelids, Brassicaceae and Fabaceae to pollutants: a review", *Ecotoxicol. Environ. Saf.*, 114, pp. 273–303, DOI: 10.1016/j.ecoenv.2014.04.024.
- [202] **Garcia-Velasco, N.**; Gandariasbeitia, M.; Irizar, A.; Soto, M. (**2016**), "Uptake route and resulting toxicity of silver nanoparticles in Eisenia fetida earthworm exposed through Standard OECD Tests", *Ecotoxicology*, 25, pp. 1543–1555, DOI: 10.1007/s10646-016-1710-2.
- [203] **Chae, Y.**; An, Y.-J. (**2018**), "Current research trends on plastic pollution and ecological impacts on the soil ecosystem: A review", *Environ. Pollut.*, 240, pp. 387–395, DOI: 10.1016/j.envpol.2018.05.008.
- [204] **Cui, W.**; Gao, P.; Zhang, M.; Wang, L.; Sun, H.; Liu, C. (**2022**), "Adverse effects of microplastics on earthworms: A critical review", *Sci. Total Environ.*, 850. Article 158041, DOI: 10.1016/j.scitotenv.2022.158041.
- [205] **Ji, Z.**; Huang, Y.; Feng, Y.; Johansen, A.; Xue, J.; Tremblay, L. A.; Li, Z. (**2021**), "Effects of pristine microplastics and nanoplastics on soil invertebrates: A systematic review and meta-analysis of available data", *Sci. Total Environ.*, 788, pp. 1–13, DOI: 10.1016/j.scitotenv.2021.147784.
- [206] **Liwarska-Bizukojc, E.** (**2021**), "Effect of (bio)plastics on soil environment: A review", *Sci. Total Environ.*, 795. Article 148889, pp. 1–18, DOI: 10.1016/j.scitotenv.2021.148889.
- [207] **Maity, S.**; Pramanick, K. (**2020**), "Perspectives and challenges of micro/nanoplastics-induced toxicity with special reference to phytotoxicity", *Glob. Chang. Biol.*, 26, pp. 3241–3250, DOI: 10.1111/gcb.15074.
- [208] **Chen, Y.**; Liu, X.; Leng, Y.; Wang, J. (**2020**), "Defense responses in earthworms (*Eisenia fetida*) exposed to low-density polyethylene microplastics in soils", *Ecotoxicol. Environ. Saf.*, 187. Article 109788, pp. 1–6, DOI: 10.1016/j.ecoenv.2019.109788.
- [209] **Holzinger, A.**; Mair, M. M.; Lückner, D.; Seidenath, D.; Opel, T.; Langhof, N.; Otti, O.; Feldhaar, H. (**2022**), "Comparison of fitness effects in the earthworm *Eisenia fetida* after exposure to single or multiple anthropogenic pollutants", *Sci. Total Environ.*, 838. Article 156387, pp. 1–10, DOI: 10.1016/j.scitotenv.2022.156387.
- [210] **Jemec Kokalj, A.**; Dolar, A.; Drobne, D.; Škrlep, L.; Škapin, A. S.; Marolt, G.; Nagode, A.; van Gestel, C. A.M. (**2022**), "Effects of microplastics from disposable medical masks on terrestrial invertebrates", *J. Haz. Mat.*, 438. Article 129440, pp. 1–9, DOI: 10.1016/j.jhazmat.2022.129440.
- [211] **Liu, J.**; Qin, J.; Zhu, L.; Zhu, K.; Liu, Z.; Jia, H.; Lichtfouse, E. (**2022**), "The protective layer formed by soil particles on plastics decreases the toxicity of polystyrene microplastics to earthworms (*Eisenia fetida*)", *Environ. Int.*, 162. Article 107158, pp. 1–11, DOI: 10.1016/j.envint.2022.107158.
- [212] **Rodríguez-Seijo, A.**; da Costa, J. P.; Rocha-Santos, T.; Duarte, A. C.; Pereira, R. (**2018**), "Oxidative stress, energy metabolism and molecular responses of earthworms (*Eisenia fetida*) exposed to low-density polyethylene microplastics", *Environ. Sci. Pollut. Res.*, 25, pp. 33599–33610, DOI: 10.1007/s11356-018-3317-z.

- [213] **Diogène, J.**; Dufour, M.; Poirier, G. G.; Nadeau, D. (1997), "Extrusion of earthworm coelomocytes: comparison of the cell populations recovered from the species *Lumbricus terrestris*, *Eisenia fetida* and *Octolasion tyrtaeum*", *Lab. Anim.*, 31, pp. 326–336, DOI: 10.1258/002367797780596068.
- [214] **Hendawi, M.**; Sauv  , S.; Ashour, M.; Brousseau, P.; Fournier, M. (2004), "A new ultrasound protocol for extrusion of coelomocyte cells from the earthworm *Eisenia fetida*", *Ecotoxicol. Environ. Saf.*, 59, pp. 17–22, DOI: 10.1016/j.ecoenv.2003.07.015.
- [215] **Toupin, J.**; Marks, D. H.; Cooper, E. L.; Lamoureux, G. (1977), "Earthworm coelomocytes in vitro", *In Vitro*, 13, pp. 218–222, DOI: 10.1007/BF02615078.
- [216] **Lescoat, A.**; Ballerie, A.; Jouneau, S.; Fardel, O.; Vernhet, L.; Jegou, P.; Lecureur, V. (2019), "M1/M2 polarisation state of M-CSF blood-derived macrophages in systemic sclerosis", *Ann. Rheum. Dis.*, 78. Article e127, 1-2, DOI: 10.1136/annrheumdis-2018-214333.
- [217] **Huang, X.**; Li, Y.; Fu, M.; Xin, H.-B. (2018), "Activating THP1-derived macrophage in vitro", *Methods Mol. Biol.*, 1784, pp. 119–126, DOI: 10.1007/978-1-4939-7837-3\_12.
- [218] **Hoppst  dter, J.**; Seif, M.; Dembek, A.; Cavelius, C.; Huwer, H.; Kraegeloh, A.; Kiemer, A. K. (2015), "M2 polarization enhances silica nanoparticle uptake by macrophages", *Front. Pharmacol.*, 6. Article 55, pp. 1–12, DOI: 10.3389/fphar.2015.00055.
- [219] **Genin, M.**; Clement, F.; Fattaccioli, A.; Raes, M.; Michiels, C. (2015), "M1 and M2 macrophages derived from THP-1 cells differentially modulate the response of cancer cells to etoposide", *BMC cancer*, 15, pp. 1–14, DOI: 10.1186/s12885-015-1546-9.
- [220] **Binnemars-Postma, K. A.**; Ten, H. H. W.; Storm, G.; Prakash, J. (2016), "Differential uptake of nanoparticles by human M1 and M2 polarized macrophages: protein corona as a critical determinant", *Nanomedicine (London, England)*, 11, pp. 1–14, DOI: 10.2217/nnm-2016-0233.
- [221] **Ivanov, D. P.**; Grabowska, A. M. (2018), "In Vitro Tissue Microarrays for Quick and Efficient Spheroid Characterization", *SLAS Discov.*, 23, pp. 211–217, DOI: 10.1177/2472555217740576.
- [222] **Prescott, D. M.**; James, T. W. (1955), "Culturing of *Amoeba proteus* on *Tetrahymena*", *Exp. Cell Res.*, 8, pp. 256–258, DOI: 10.1016/0014-4827(55)90067-7.
- [223] **Gong, Q.**; Jiang, Y.; Pan, X.; You, Y. (2021), "Fractalkine aggravates LPS-induced macrophage activation and acute kidney injury via Wnt/ $\beta$ -catenin signalling pathway", *J. Cell. Mol. Med.*, 25, pp. 6963–6975, DOI: 10.1111/jcmm.16707.
- [224] **Oh, H.**; Park, S.-H.; Kang, M.-K.; Kim, Y.-H.; Lee, E.-J.; Kim, D. Y.; Kim, S.-I.; Oh, S. Y.; Na, W.; Lim, S. S.; Kang, Y.-H. (2020), "Asaronic Acid Inhibited Glucose-Triggered M2-Phenotype Shift Through Disrupting the Formation of Coordinated Signaling of IL-4R $\alpha$ -Tyk2-STAT6 and GLUT1-Akt-mTOR-AMPK", *Nutrients*, 12, pp. 1–18, DOI: 10.3390/nu12072006.
- [225] **Susnik, E.**; Taladriz-Blanco, P.; Drasler, B.; Balog, S.; Petri-Fink, A.; Rothen-Rutishauser, B. (2020), "Increased Uptake of Silica Nanoparticles in Inflamed Macrophages but Not upon Co-Exposure to Micron-Sized Particles", *Cells*, 9. Article 2099, pp. 1–17, DOI: 10.3390/cells9092099.
- [226] **Wu, X.**; Hollingshead, N.; Roberto, J.; Knupp, A.; Kenerson, H.; Chen, A.; Strickland, I.; Horton, H.; Yeung, R.; Soysa, R.; Crispe, I. N. (2020), "Human Liver Macrophage Subsets Defined by CD32", *Front. Immunol.*, 11. Article 2108, pp. 1–11, DOI: 10.3389/fimmu.2020.02108.
- [227] **Pajarinen, J.**; Kouri, V.-P.; J  msen, E.; Li, T.-F.; Mandelin, J.; Konttinen, Y. T. (2013), "The response of macrophages to titanium particles is determined by macrophage polarization", *Acta Biomater.*, 9, pp. 9229–9240, DOI: 10.1016/j.actbio.2013.06.027.
- [228] **Akilbekova, D.**; Philip, R.; Graham, A.; Bratlie, K. M. (2015), "Macrophage reprogramming: Influence of latex beads with various functional groups on macrophage phenotype and phagocytic uptake in vitro", *J. Biomed. Mater. Res. A*, 103, pp. 262–268, DOI: 10.1002/jbm.a.35169.
- [229] **Jasinski, J.**, *Intracellular co-localization of MPP with specific organelles*, July 2022.



- [230] **Errington, R. J.**; Brown, M. R.; Silvestre, O. F.; Njoh, K. L.; Chappell, S. C.; Khan, I. A.; Rees, P.; Wilks, S. P.; Smith, P. J.; Summers, H. D. (2010), "Single cell nanoparticle tracking to model cell cycle dynamics and compartmental inheritance", *Cell cycle*, 9, pp. 121–130, DOI: 10.4161/cc.9.1.10246.
- [231] **Brown, M. R.**; Summers, H. D.; Rees, P.; Chappell, S. C.; Silvestre, O. F.; Khan, I. A.; Smith, P. J.; Errington, R. J. (2010), "Long-term time series analysis of quantum dot encoded cells by deconvolution of the autofluorescence signal", *Cytom., : J. Int. Soc. Anal. Cytol.*, 77, pp. 925–932, DOI: 10.1002/cyto.a.20936.
- [232] **Lijster, T.**; Åberg, C. (2020), "Asymmetry of nanoparticle inheritance upon cell division: Effect on the coefficient of variation", *PLoS one*, 15. Article e0242547, 1-18, DOI: 10.1371/journal.pone.0242547.
- [233] **Walczak, P.**; Kedziorek, D. A.; Gilad, A. A.; Barnett, B. P.; Bulte, J. W. M. (2007), "Applicability and limitations of MR tracking of neural stem cells with asymmetric cell division and rapid turnover: the case of the shiverer dysmyelinated mouse brain", *Magn. Reson. Med.*, 58, pp. 261–269, DOI: 10.1002/mrm.21280.
- [234] **Carlton, J. G.**; Jones, H.; Eggert, U. S. (2020), "Membrane and organelle dynamics during cell division", *Nat. Rev. Mol. Cell. Biol.*, 21, pp. 151–166, DOI: 10.1038/s41580-019-0208-1.
- [235] **Thyberg, J.**; Moskalewski, S. (1998), "Partitioning of cytoplasmic organelles during mitosis with special reference to the Golgi complex", *Microsc. Res. Tech.*, 40, pp. 354–368, DOI: 10.1002/(SICI)1097-0029(19980301)40:5<354::AID-JEMT3>3.0.CO;2-R.
- [236] **Zhao, Y.**; Gorvel, J.-P.; Méresse, S. (2016), "Effector proteins support the asymmetric apportioning of Salmonella during cytokinesis", *Virulence*, 7, pp. 669–678, DOI: 10.1080/21505594.2016.1173298.
- [237] **Townley, H. E.**; Rapa, E.; Wakefield, G.; Dobson, P. J. (2012), "Nanoparticle augmented radiation treatment decreases cancer cell proliferation", *Nanomed.: Nanotechnol. Biol. Med.*, 8, pp. 526–536, DOI: 10.1016/j.nano.2011.08.003.
- [238] **Fang, D.**; Maldonado, E. N. (2018), "VDAC Regulation: A Mitochondrial Target to Stop Cell Proliferation", *Adv. Cancer Res.*, 138, pp. 41–69, DOI: 10.1016/bs.acr.2018.02.002.
- [239] **Tanifum, E. A.**; Devkota, L.; Ngwa, C.; Badachhape, A. A.; Ghaghada, K. B.; Romero, J.; Pautler, R. G.; Annapragada, A. V. (2018), "A Hyperfluorinated Hydrophilic Molecule for Aqueous 19F MRI Contrast Media", *Contrast Media Mol. Imaging.*, 2018. Article 1693513, pp. 1–8, DOI: 10.1155/2018/1693513.
- [240] **Mutzke, E.**; Chomyshyn, E.; Nguyen, K. C.; Blahoianu, M.; Tayabali, A. F. (2015), "Phagocytosis-coupled flow cytometry for detection and size discrimination of anionic polystyrene particles", *Anal. Biochem.*, 483, pp. 40–46, DOI: 10.1016/j.ab.2015.04.034.
- [241] **Calabrese, E. J.**; Mattson, M. P. (2017), "How does hormesis impact biology, toxicology, and medicine?", *NPJ Aging Mech. Dis.*, 3, pp. 1–8, DOI: 10.1038/s41514-017-0013-z.
- [242] **Gopi, I. K.**; Rattan, S. I. S. (2019), "Biphasic Dose-Response and Hormetic Effects of Stress Hormone Hydrocortisone on Telomerase-Immortalized Human Bone Marrow Stem Cells In Vitro", *Int. Hormesis Soc.*, 17. Article 1559325819889819, 1-9, DOI: 10.1177/1559325819889819.
- [243] **Decker, K.** (1990), "Biologically active products of stimulated liver macrophages (Kupffer cells)", *Eur. J. Biochem.*, 192, pp. 245–261, DOI: 10.1111/j.1432-1033.1990.tb19222.x.
- [244] **Wang, J. F.**; Komarov, P.; Groot, H. de (1993), "Luminol chemiluminescence in rat macrophages and granulocytes: the role of NO, O<sub>2</sub>·/H<sub>2</sub>O<sub>2</sub>, and HOCl", *Arch. Biochem. Biophys.*, 304, pp. 189–196, DOI: 10.1006/abbi.1993.1338.
- [245] **Hu, M.**; Palić, D. (2020), "Micro- and nano-plastics activation of oxidative and inflammatory adverse outcome pathways", *Redox Biol.*, 37. Article 101620, pp. 1–16, DOI: 10.1016/j.redox.2020.101620.
- [246] **Jasinski, J.**; Wilde, M. V.; Voelkl, M.; Jérôme, V.; Fröhlich, T.; Freitag, R.; Scheibel, T. (2022), "Tailor-Made Protein Corona Formation on Polystyrene Microparticles and its Effect on Epithelial Cell Uptake", *ACS Appl. Mater. Interfaces*, 14, pp. 47277–47287, DOI: 10.1021/acsami.2c13987.

- [247] **Lu, N.**; Sui, Y.; Ding, Y.; Tian, R.; Peng, Y.-Y. (2018), "Fibrinogen binding-dependent cytotoxicity and degradation of single-walled carbon nanotubes", *J. Mater. Sci.*, 29, pp. 1–8, DOI: 10.1007/s10856-018-6123-8.
- [248] **Wang, J.**; Zheng, X.; Zhang, H. (2019), "Exploring the conformational changes in fibrinogen by forming protein corona with CdTe quantum dots and the related cytotoxicity", *Spectrochim. Acta A Mol. Biomol.*, 220. Article 117143, pp. 1–6, DOI: 10.1016/j.saa.2019.117143.
- [249] **Withey, J. R.** (1976), "Quantitative analysis of styrene monomer in polystyrene and foods including some preliminary studies of the uptake and pharmacodynamics of the monomer in rats", *Environ. Health Perspect.*, 17, pp. 125–133, DOI: 10.1289/ehp.7617125.
- [250] **Erni-Cassola, G.**; Zadjelovic, V.; Gibson, M. I.; Christie-Oleza, J. A. (2019), "Distribution of plastic polymer types in the marine environment; A meta-analysis", *J. Haz. Mat.*, 369, pp. 691–698, DOI: 10.1016/j.jhazmat.2019.02.067.
- [251] **Koutnik, V. S.**; Leonard, J.; Alkidim, S.; DePrima, F. J.; Ravi, S.; Hoek, E. M. V.; Mohanty, S. K. (2021), "Distribution of microplastics in soil and freshwater environments: Global analysis and framework for transport modeling", *Environ. Pollut.*, 274. Article 116552, pp. 1–13, DOI: 10.1016/j.envpol.2021.116552.
- [252] **Sivakanthan, S.**; Rajendran, S.; Gamage, A.; Madhujith, T.; Mani, S. (2020), "Antioxidant and antimicrobial applications of biopolymers: A review", *Int. Food Res. J.*, 136. Article 109327, DOI: 10.1016/j.foodres.2020.109327.
- [253] **da Silva, D.**; Kaduri, M.; Poley, M.; Adir, O.; Krinsky, N.; Shainsky-Roitman, J.; Schroeder, A. (2018), "Biocompatibility, biodegradation and excretion of polylactic acid (PLA) in medical implants and theranostic systems", *Chem. Eng. J.*, 340, pp. 9–14, DOI: 10.1016/j.cej.2018.01.010.
- [254] **Hu, X.-M.**; Li, Z.-X.; Lin, R.-H.; Shan, J.-Q.; Yu, Q.-W.; Wang, R.-X.; Liao, L.-S.; Yan, W.-T.; Wang, Z.; Shang, L.; Huang, Y.; Zhang, Q.; Xiong, K. (2021), "Guidelines for Regulated Cell Death Assays: A Systematic Summary, A Categorical Comparison, A Prospective", *Front. Cell Dev. Biol.*, 9. Article 634690, pp. 1–28, DOI: 10.3389/fcell.2021.634690.
- [255] **Silva, M. T.** (2010), "Secondary necrosis: the natural outcome of the complete apoptotic program", *FEBS letters*, 584, pp. 4491–4499, DOI: 10.1016/j.febslet.2010.10.046.
- [256] **Choi, D.**; Bang, J.; Kim, T.; Oh, Y.; Hwang, Y.; Hong, J. (2020), "In vitro chemical and physical toxicities of polystyrene microfragments in human-derived cells", *J. Haz. Mat.*, 400. Article 123308, DOI: 10.1016/j.jhazmat.2020.123308.
- [257] **Choi, D.**; Hwang, J.; Bang, J.; Han, S.; Kim, T.; Oh, Y.; Hwang, Y.; Choi, J.; Hong, J. (2021), "In vitro toxicity from a physical perspective of polyethylene microplastics based on statistical curvature change analysis", *Sci. Total Environ.*, 752. Article 142242, pp. 1–11, DOI: 10.1016/j.scitotenv.2020.142242.
- [258] **Shi, X.**; Wang, X.; Huang, R.; Tang, C.; Hu, C.; Ning, P.; Wang, F. (2022), "Cytotoxicity and Genotoxicity of Polystyrene Micro- and Nanoplastics with Different Size and Surface Modification in A549 Cells", *Int. J. Nanomedicine.*, 17, pp. 4509–4523, DOI: 10.2147/IJN.S381776.
- [259] **Paget, V.**; Dekali, S.; Kortulewski, T.; Grall, R.; Gamez, C.; Blazy, K.; Aguerre-Chariol, O.; Chevillard, S.; Braun, A.; Rat, P.; Lacroix, G. (2015), "Specific uptake and genotoxicity induced by polystyrene nanobeads with distinct surface chemistry on human lung epithelial cells and macrophages", *PloS one*, 10. Article e0123297, 1–20, DOI: 10.1371/journal.pone.0123297.
- [260] **Roursgaard, M.**; Hezareh, R. M.; Schulte, J.; Karadimou, I.; Marinelli, E.; Møller, P. (2022), "Genotoxicity of Particles From Grinded Plastic Items in Caco-2 and HepG2 Cells", *Front. Public Health*, 10. Article 906430, pp. 1–15, DOI: 10.3389/fpubh.2022.906430.
- [261] **Sarma, D. K.**; Dubey, R.; Samarth, R. M.; Shubham, S.; Chowdhury, P.; Kumawat, M.; Verma, V.; Tiwari, R. R.; Kumar, M. (2022), "The Biological Effects of Polystyrene Nanoplastics on Human Peripheral Blood Lymphocytes", *Nanomaterials*, 12. Article 1632, pp. 1–10, DOI: 10.3390/nano12101632.

- [262] **Domenech, J.**; de, B. M.; Velázquez, A.; Pastor, S.; Hernández, A.; Marcos, R.; Cortés, C. (2021), "Long-Term Effects of Polystyrene Nanoplastics in Human Intestinal Caco-2 Cells", *Biomolecules*, 11. Article 1442, pp. 1–16, DOI: 10.3390/biom11101442.
- [263] **Zhu, K.**; Jia, H.; Zhao, S.; Xia, T.; Guo, X.; Wang, T.; Zhu, L. (2019), "Formation of Environmentally Persistent Free Radicals on Microplastics under Light Irradiation", *Environ. Sci. Technol.*, 53, pp. 8177–8186, DOI: 10.1021/acs.est.9b01474.
- [264] **Rosado, J. A.**; González, A.; Salido, G. M.; Pariente, J. A. (2002), "Effects of reactive oxygen species on actin filament polymerisation and amylase secretion in mouse pancreatic acinar cells", *Cell. Signal.*, 14, pp. 547–556, DOI: 10.1016/s0898-6568(01)00273-x.
- [265] **Valdivia, A.**; Duran, C.; San Martin, A. (2015), "The role of Nox-mediated oxidation in the regulation of cytoskeletal dynamics", *Curr. Pharm. Des.*, 21, pp. 6009–6022, DOI: 10.2174/1381612821666151029112624.
- [266] **Haider, M. S.**; Jaskani, M. J.; Fang, J. in *Biocontrol Agents and Secondary Metabolites*, Elsevier, 2021, pp. 347–382.
- [267] **Marchi, S.**; Giorgi, C.; Suski, J. M.; Agnoletto, C.; Bononi, A.; Bonora, M.; Marchi, E. de; Missiroli, S.; Patergnani, S.; Poletti, F.; Rimessi, A.; Duszynski, J.; Wieckowski, M. R.; Pinton, P. (2012), "Mitochondria-ROS crosstalk in the control of cell death and aging", *J. Signal Transduct.*, 2012. Article 329635, pp. 1–17, DOI: 10.1155/2012/329635.
- [268] **Zorov, D. B.**; Juhaszova, M.; Sollott, S. J. (2006), "Mitochondrial ROS-induced ROS release: an update and review", *Biochim. Biophys. Acta*, 1757, pp. 509–517, DOI: 10.1016/j.bbabi.2006.04.029.
- [269] **Visalli, G.**; Facciola, A.; Pruiti Ciarello, M.; Marco, G. de; Maisano, M.; Di Pietro, A. (2021), "Acute and Sub-Chronic Effects of Microplastics (3 and 10  $\mu$ m) on the Human Intestinal Cells HT-29", *Int. J. Environ. Res. Public Health*, 18. Article 5833, pp. 1–12, DOI: 10.3390/ijerph18115833.
- [270] **Frostegård, J.**; Ulfgrén, A.-K.; Nyberg, P.; Hedin, U.; Swedenborg, J.; Andersson, U.; Hansson, G. K. (1999), "Cytokine expression in advanced human atherosclerotic plaques: dominance of pro-inflammatory (Th1) and macrophage-stimulating cytokines", *Atherosclerosis*, 145, pp. 33–43, DOI: 10.1016/S0021-9150(99)00011-8.
- [271] **Green, T. R.**; Fisher, J.; Stone, M.; Wroblewski, B. M.; Ingham, E. (1998), "Polyethylene particles of a 'critical size' are necessary for the induction of cytokines by macrophages in vitro", *Biomaterials*, 19, pp. 2297–2302, DOI: 10.1016/s0142-9612(98)00140-9.
- [272] **Shanbhag, A. S.**; Jacobs, J. J.; Black, J.; Galante, J. O.; Glant, T. T. (1994), "Macrophage/particle interactions: effect of size, composition and surface area", *J. Biomed. Mater. Res.*, 28, pp. 81–90, DOI: 10.1002/jbm.820280111.
- [273] **Li, X.**; Bechara, R.; Zhao, J.; McGeachy, M. J.; Gaffen, S. L. (2019), "IL-17 receptor-based signaling and implications for disease", *Nat. Immunol.*, 20, pp. 1594–1602, DOI: 10.1038/s41590-019-0514-y.
- [274] **Li, Y.**; Duan, J.; Yang, M.; Li, Y.; Jing, L.; Yu, Y.; Wang, J.; Sun, Z. (2017), "Transcriptomic analyses of human bronchial epithelial cells BEAS-2B exposed to atmospheric fine particulate matter PM<sub>2.5</sub>", *Toxicol. In Vitro*, 42, pp. 171–181, DOI: 10.1016/j.tiv.2017.04.014.
- [275] **Osborn, L.**; Kunkel, S.; Nabel, G. J. (1989), "Tumor necrosis factor alpha and interleukin 1 stimulate the human immunodeficiency virus enhancer by activation of the nuclear factor kappa B", *PNAS*, 86, pp. 2336–2340, DOI: 10.1073/pnas.86.7.2336.
- [276] **Chen, B.**; Wu, Z.; Tian, M.; Feng, T.; Yuanwei, C.; Luo, X. (2020), "Effect of surface morphology change of polystyrene microspheres through etching on protein corona and phagocytic uptake", *J. Biomater. Sci. Polym. Ed.*, 31, pp. 2381–2395, DOI: 10.1080/09205063.2020.1813062.
- [277] **Gaylarde, C. C.**; Neto, J. A. B.; da Fonseca, E. M. (2021), "Paint fragments as polluting microplastics: A brief review", *Mar. Pollut. Bull.*, 162. Article 111847, DOI: 10.1016/j.marpolbul.2020.111847.
- [278] **Paruta, P.**; Pucino, M.; Boucher, J., *Plastic Paints the Environment*, 2022.

- [279] **Melgar Aguilar, A. E.**; Fagundes, A. P.; Macuvele, D. L. P.; Cesca, K.; Porto, L.; Padoin, N.; Soares, C.; Gracher Riella, H. **(2021)**, "Green Synthesis of Nano Hydroxyapatite: morphology variation and its effect on cytotoxicity against fibroblast", *Mater. Lett.*, 284. Article 129013, pp. 1–4, DOI: 10.1016/j.matlet.2020.129013.
- [280] **Jin, C.**; Liu, Y.; Sun, L.; Chen, T.; Zhang, Y.; Zhao, A.; Wang, X.; Cristau, M.; Wang, K.; Jia, W. **(2013)**, "Metabolic profiling reveals disorder of carbohydrate metabolism in mouse fibroblast cells induced by titanium dioxide nanoparticles", *J. Appl. Toxicol.*, 33, pp. 1442–1450, DOI: 10.1002/jat.2808.
- [281] **Jin, C.-Y.**; Zhu, B.-S.; Wang, X.-F.; Lu, Q.-H. **(2008)**, "Cytotoxicity of titanium dioxide nanoparticles in mouse fibroblast cells", *Chem. Res. Toxicol.*, 21, pp. 1871–1877, DOI: 10.1021/tx800179f.
- [282] **Lee, H.-S.**; Amarakoon, D.; Wei, C.-I.; Choi, K. Y.; Smolensky, D.; Lee, S.-H. **(2021)**, "Adverse effect of polystyrene microplastics (PS-MPs) on tube formation and viability of human umbilical vein endothelial cells", *Food Chem. Toxicol.*, 154. Article 112356, DOI: 10.1016/j.fct.2021.112356.
- [283] **Horst, A. K.**; Tiegs, G.; Diehl, L. **(2019)**, "Contribution of Macrophage Efferocytosis to Liver Homeostasis and Disease", *Front. Immunol.*, 10. Article 2670, pp. 1–13, DOI: 10.3389/fimmu.2019.02670.
- [284] **Chu, Z.**; Zhang, S.; Zhang, B.; Zhang, C.; Fang, C.-Y.; Rehor, I.; Cigler, P.; Chang, H.-C.; Lin, G.; Liu, R.; Li, Q. **(2014)**, "Unambiguous observation of shape effects on cellular fate of nanoparticles", *Sci. Rep.*, 4, pp. 1–9, DOI: 10.1038/srep04495.
- [285] **Streets, A. J.**; Wagner, B. E.; Harris, P. C.; Ward, C. J.; Ong, A. C. M. **(2009)**, "Homophilic and heterophilic polycystin 1 interactions regulate E-cadherin recruitment and junction assembly in MDCK cells", *J. Cell Sci.*, 122, pp. 1410–1417, DOI: 10.1242/jcs.045021.
- [286] **Shi, Y.**; Li, R.; Yang, J.; Li, X. **(2020)**, "No tight junctions in tight junction protein-1 expressing HeLa and fibroblast cells", *Int. J. Physiol. Pathophysiol. Pharmacol.*, 12, pp. 70–78.
- [287] **Zdilla, M. J.**; Hatfield, S. A.; McLean, K. A.; Cyrus, L. M.; Laslo, J. M.; Lambert, H. W. **(2016)**, "Circularity, Solidity, Axes of a Best Fit Ellipse, Aspect Ratio, and Roundness of the Foramen Ovale: A Morphometric Analysis With Neurosurgical Considerations", *Arch. Craniofac. Surg.*, 27, pp. 222–228, DOI: 10.1097/SCS.0000000000002285.
- [288] **Thoma, C. R.**; Zimmermann, M.; Agarkova, I.; Kelm, J. M.; Krek, W. **(2014)**, "3D cell culture systems modeling tumor growth determinants in cancer target discovery", *Adv. Drug Deliv. Rev.*, 69–70, pp. 29–41, DOI: 10.1016/j.addr.2014.03.001.
- [289] **Kenny, P. A.**; Lee, G. Y.; Myers, C. A.; Neve, R. M.; Semeiks, J. R.; Spellman, P. T.; Lorenz, K.; Lee, E. H.; Barcellos-Hoff, M. H.; Petersen, O. W.; Gray, J. W.; Bissell, M. J. **(2007)**, "The morphologies of breast cancer cell lines in three-dimensional assays correlate with their profiles of gene expression", *Mol. Oncol.*, 1, pp. 84–96, DOI: 10.1016/j.molonc.2007.02.004.
- [290] **Amaral, R. L. F.**; Miranda, M.; Marcato, P. D.; Swiech, K. **(2017)**, "Comparative Analysis of 3D Bladder Tumor Spheroids Obtained by Forced Floating and Hanging Drop Methods for Drug Screening", *Front. Physiol.*, 8. Article 605, pp. 1–15, DOI: 10.3389/fphys.2017.00605.
- [291] **Ahmad, K. A.**; Abdul Hassan, N.; Abdullah, M. E.; Bilema, M. A. M.; Usman, N.; Al Allam, Al Allam M.; Hainin, M. R. B. **(2019)**, "Image processing procedure to quantify the internal structure of porous asphalt concrete", *MMMS*, 15, pp. 206–226, DOI: 10.1108/MMMS-08-2017-0073.
- [292] **Anada, T.**; Fukuda, J.; Sai, Y.; Suzuki, O. **(2012)**, "An oxygen-permeable spheroid culture system for the prevention of central hypoxia and necrosis of spheroids", *Biomater.*, 33, pp. 8430–8441, DOI: 10.1016/j.biomaterials.2012.08.040.
- [293] **Sambale, F.**; Lavrentieva, A.; Stahl, F.; Blume, C.; Stiesch, M.; Kasper, C.; Bahnemann, D.; Scheper, T. **(2015)**, "Three dimensional spheroid cell culture for nanoparticle safety testing", *J. Biotechnol.*, 205, pp. 120–129, DOI: 10.1016/j.jbiotec.2015.01.001.
- [294] **Islam, M. A.**; Barua, S.; Barua, D. **(2017)**, "A multiscale modeling study of particle size effects on the tissue penetration efficacy of drug-delivery nanoparticles", *BMC systems biology*, 11, DOI: 10.1186/s12918-017-0491-4.

- [295] **Ferguson, R.**; Subramanian, V. **(2018)**, "Embryoid body arrays: Parallel cryosectioning of spheroid/embryoid body samples for medium through-put analysis", *Stem Cell Res.*, 28, pp. 125–130, DOI: 10.1016/j.scr.2018.02.003.
- [296] **Klicks, J.**; Maßlo, C.; Kluth, A.; Rudolf, R.; Hafner, M. **(2019)**, "A novel spheroid-based co-culture model mimics loss of keratinocyte differentiation, melanoma cell invasion, and drug-induced selection of ABCB5-expressing cells", *BMC cancer*, 19. Article 402, pp. 1–14, DOI: 10.1186/s12885-019-5606-4.
- [297] **Ritschar, S.**, *Degradation of agarose mould during embedding*. Personal communication, **June 2022**, Bayreuth.
- [298] **Gabriel, J.**; Brennan, D.; Elisseff, J. H.; Beachley, V. **(2019)**, "Microarray Embedding/Sectioning for Parallel Analysis of 3D Cell Spheroids", *Sci. Rep.*, 9. Article 16287, pp. 1–10, DOI: 10.1038/s41598-019-52007-w.
- [299] **Xie, P.**; Zhao, C.; Liang, X.; Huang, W.; Chen, Y.; Cai, Z. **(2020)**, "Preparation of Frozen Sections of Multicellular Tumor Spheroids Coated with Ice for Mass Spectrometry Imaging", *Anal. Chem.*, 92, pp. 7413–7418, DOI: 10.1021/acs.analchem.9b05812.
- [300] **Ritschar, S.**, *Thin sections of embedded spheroids*. Personal communication, **July 2022**.
- [301] **Ritschar, S.**; Schirmer, E.; Hufnagl, B.; Löder, M. G. J.; Römpf, A.; Laforsch, C. **(2022)**, "Classification of target tissues of *Eisenia fetida* using sequential multimodal chemical analysis and machine learning", *Histochem. Cell Biol.*, 157, pp. 127–137, DOI: 10.1007/s00418-021-02037-1.
- [302] **Schirmer, E.**; Ritschar, S.; Ochs, M.; Laforsch, C.; Schuster, S.; Römpf, A. **(2022)**, "MALDI mass spectrometry imaging workflow for the aquatic model organisms *Danio rerio* and *Daphnia magna*", *Sci. Rep.*, 12. Article 7288, pp. 1–11, DOI: 10.1038/s41598-022-09659-y.
- [303] **Jasinski, J.**, *Observation of interactions of MPP and macrophages inside spheroids*, **October 2022**.
- [304] **da Silva Brito, W. A.**; Mutter, F.; Wende, K.; Cecchini, A. L.; Schmidt, A.; Bekeschus, S. **(2022)**, "Consequences of nano and microplastic exposure in rodent models: the known and unknown", *Part. Fibre Toxicol.*, 19, pp. 1–24, DOI: 10.1186/s12989-022-00473-y.
- [305] **Jiang, X.**; Chang, Y.; Zhang, T.; Qiao, Y.; Klobučar, G.; Li, M. **(2020)**, "Toxicological effects of polystyrene microplastics on earthworm (*Eisenia fetida*)", *Environ. Pollut.*, 259. Article 113896, pp. 1–8, DOI: 10.1016/j.envpol.2019.113896.
- [306] **Irizar, A.**; Rivas, C.; García-Velasco, N.; Goñi de Cerio, F.; Etxebarria, J.; Marigómez, I.; Soto, M. **(2015)**, "Establishment of toxicity thresholds in subpopulations of coelomocytes (amoebocytes vs. eleocytes) of *Eisenia fetida* exposed in vitro to a variety of metals: implications for biomarker measurements", *Ecotoxicology*, 24, pp. 1004–1013, DOI: 10.1007/s10646-015-1441-9.
- [307] **Mast, S. O. (1947)**, "The food-vacuole in *Paramecium*", *Biol. Bull.*, 92, pp. 31–72.
- [308] **Mondellini, S.**, **Schwarzer, M.**, *Uptake of particles in *Paramecium caudatum**. Personal communication, **July 2022**.
- [309] **Klein, H. P.**; Köster, B.; Stockem, W. in *Cell Dynamics*, Springer, Vienna, **1988**, pp. 76–87.
- [310] **Prusch, R. D.**; Minck, D. **(1985)**, "Chemical stimulation of phagocytosis in *Amoeba proteus* and the influence of external calcium", *Cell Tissue Res.*, 242, pp. 557–564.
- [311] **Kłopotcka, W.**; Grębecka, L. **(1985)**, "Effects of bivalent cations on the initiation of Na-induced pinocytosis in *Amoeba proteus*", *Protoplasma*, 126, pp. 207–214, DOI: 10.1007/BF01281796.
- [312] **Chapman-Andresen, C.**; Holtzer, H. **(1960)**, "The Uptake of fluorescent albumin by pinocytosis in *Amoeba proteus*", *J. Biophys. Biochem. Cytol.*, 8, p. 288, DOI: 10.1083/jcb.8.1.288.
- [313] **Prusch, R. D.**; Britton, J. C. **(1987)**, "Peptide stimulation of phagocytosis in *Amoeba proteus*", *Cell Tissue Res.*, 250, pp. 589–593, DOI: 10.1007/BF00218951.

- [314] **La Fuente, I. M. de**; Bringas, C.; Malaina, I.; Fedetz, M.; Carrasco-Pujante, J.; Morales, M.; Knafo, S.; Martínez, L.; Pérez-Samartín, A.; López, J. I.; Pérez-Yarza, G.; Boyano, M. D. (2019), "Evidence of conditioned behavior in amoebae", *Nat. Commun.*, 10. Article 3690, pp. 1–12, DOI: 10.1038/s41467-019-11677-w.
- [315] **Ahn, T. I.**; Jeon, K. W. (1982), "Structural and biochemical characteristics of the plasmalemma and vacuole membranes in Amoebae", *Exp. Cell. Res.*, 137, pp. 253–268, DOI: 10.1016/0014-4827(82)90026-x.
- [316] **Fabra, M.**; Williams, L.; Watts, J. E. M.; Hale, M. S.; Couceiro, F.; Preston, J. (2021), "The plastic Trojan horse: Biofilms increase microplastic uptake in marine filter feeders impacting microbial transfer and organism health", *Sci. Total Environ.*, 797. Article 149217, pp. 1–9, DOI: 10.1016/j.scitotenv.2021.149217.
- [317] **Jeon, K. W.**; Bell, L.G.E. (1962), "Pseudopod and foodcup formation in *Amoeba proteus*", *Exp. Cell Res.*, 27, pp. 350–352, DOI: 10.1016/0014-4827(62)90243-4.
- [318] **Mast, S. O.**; Hahnert, W. F. (1935), "Feeding, Digestion, and Starvation in *Amoeba proteus* (Leidy)", *Physiol. Zool.*, 8, pp. 255–272, DOI: 10.1086/physzool.8.3.30151248.
- [319] **Shi, Y.**; Queller, D. C.; Tian, Y.; Zhang, S.; Yan, Q.; He, Z.; Wu, C.; Wang, C.; Shu, L. (2021), "The Ecology and Evolution of Amoeba-Bacterium Interactions", *Appl. Environ. Microbiol.*, 87. Article e01866-20, pp. 1–16, DOI: 10.1128/AEM.01866-20.
- [320] **Mondellini, S., Schwarzer, M.**, *Retention time of particles in Paramecium caudatum*. Personal communication, July 2022.
- [321] **Menzel, T.**; Weigert, S.; Gagsteiger, A.; Eich, Y.; Sittl, S.; Papastavrou, G.; Ruckdäschel, H.; Altstädt, V.; Höcker, B. (2021), "Impact of Enzymatic Degradation on the Material Properties of Poly(Ethylene Terephthalate)", *Polymers*, 13. Article 3885, pp. 1–13, DOI: 10.3390/polym13223885.
- [322] **Kawai, F.**; Kawabata, T.; Oda, M. (2019), "Current knowledge on enzymatic PET degradation and its possible application to waste stream management and other fields", *Appl. Microbiol. Biotechnol.*, 103, pp. 4253–4268, DOI: 10.1007/s00253-019-09717-y.
- [323] **Kannan, K.**; Vimalkumar, K. (2021), "A Review of Human Exposure to Microplastics and Insights Into Microplastics as Obesogens", *Front. Endocrinol.*, 12. Article 724989, pp. 1–19, DOI: 10.3389/fendo.2021.724989.
- [324] **Menzel, T.**; Meides, N.; Mauel, A.; Mansfeld, U.; Kretschmer, W.; Kuhn, M.; Herzig, E. M.; Altstädt, V.; Strohmriegel, P.; Senker, J.; Ruckdäschel, H. (2022), "Degradation of low-density polyethylene to nanoplastic particles by accelerated weathering", *Sci. Total Environ.*, 826. Article 154035, pp. 1–11, DOI: 10.1016/j.scitotenv.2022.154035.
- [325] **Rebelein, A.**; Int-Veen, I.; Kammann, U.; Scharsack, J. P. (2021), "Microplastic fibers — Underestimated threat to aquatic organisms?", *Sci. Total Environ.*, 777. Article 146045, pp. 1–16, DOI: 10.1016/j.scitotenv.2021.146045.

## Tabellarischer Lebenslauf

### Matthias Völkl

Anschrift: Emil Warburg Weg 36, 95447 Bayreuth  
Geboren: 24.01.1993 in Bayreuth  
Tel.: +49 157 83928071  
Email: MatzeVoelkl@gmx.de

---

### Bildungsweg

03/2019 – 03/2023

#### Promotion im Bereich Biotechnologie

Universität Bayreuth, Lehrstuhl Bioprozesstechnik  
„Application of cell cultivation in increasing complexity to  
analyse effects of microplastic *in vitro*“

10/2016 – 03/2019

#### Master - Biotechnologie und Chemische Verfahrenstechnik – Schwerpunkt

##### Bioprozesstechnik

Universität Bayreuth

10/2012 – 10/2016

#### Bachelor – Engineering Science

Universität Bayreuth

---

### Praxiserfahrung

08/2013 - 02/2019

#### Studentische Hilfskraft am Fraunhofer Institut für Silicatforschung

Teilverantwortlich für den Bereich „Zerstörungsfreie  
Prüftechnik“

Erstellen von Berichten in der industrierelevanten und  
auftragsorientierten Forschung

08/2011 – 07/2012

#### Freiwilliges soziales Jahr Bayrisches Rotes Kreuz

Stärkung der Sozialkompetenz

2011 – 2022

#### Fußballtrainer – Jugend und Herren

Teamfähigkeit und Teamführungs Kompetenzen

Organisationfähigkeit

---

### Sprachkenntnisse

Deutsch – Muttersprache

Englisch – fließend in Wort und Schrift